# Probing and Restoring disrupted thalamocortical interactions during Parkinson's disease and Essential tremor


Carolina Pimenta Pugsley dos Reis

A thesis submitted for the degree of

*Doctor of Philosophy*

Nuffield Department of Clinical Neurosciences

MRC Brain Network Dynamics Unit

University of Oxford & Wolfson College

August 2021

# i) Declaration

I, Carolina Reis, confirm that the work presented in this thesis is my own. Where information has been derived from other sources, I confirm that this has been indicated in the thesis.

Signed: Carolina Reis……

Date: 20th August 2021……

# ii) Acknowledgments

I must start by thanking Hayriye Cagnan. None of this would have been possible without her belief in me. I must also thank her for her patience, guidance and invaluable insights whilst always supporting my professional and personal development. My thanks extend to all past and present members of the fast-growing Cagnan lab, and in particular to Tim West whose passion for science has been truly inspiring.

A heartfelt thanks also goes to the members of the Brown, Tan and Bogacz labs. I very much looked forward to our daily lunches, random chats and thought-provoking conversations. They were a source of distraction and fun and made this journey a lighter one.

I would also like to express my appreciation to Peter Brown, Andrew Sharott, Abbey Holt, Peter Magill and Kouichi Nakamura for their support at crucial stages of this research.

None of this would have been possible without the financial support of the Medical Research Council and the hard work of all my study participants – your genuine interest in advancing clinical science always moved me and fostered my interest in research.

To my family a mere thank you will never be enough; I am truly grateful for your presence and love, now and always. I would also like to thank my dear friends Rebe, Ada and Vero, who have encouraged and supported me every step of the way.

To Dav, saying words are not enough to thank you is an understatement. Your endless patience, love, and support made me believe this was possible, even at the most unlikely times. I am truly grateful for having you beside me.

# iii) Abstract

Parkinson's disease (PD) and Essential Tremor (ET) are two movement disorders where impaired motor function can lead to severe disability. In conjunction with motor impairments, both disorders display augmented frequency-specific activity patterns across brain networks that converge at the thalamocortical (TC) level. In treating motor symptoms, the available therapies for PD and ET modulate these pathologically increased activity patterns. However, therapeutic interventions can also lead to the disruption of physiological brain activity and cause undesirable secondary effects. A major challenge delaying the development of selective neuromodulatory therapies is our limited understanding of the impact of neural activity on function and dysfunction. This thesis contributes to addressing this knowledge gap by probing the TC network dynamics that underlie aberrant synchrony in PD, and by exploring ways of restoring motor function in ET through temporally-specific perturbations of tremor-related TC interactions. By using a combination of tools that span from computational modelling, signal analysis and closed-loop stimulation algorithms we have found that: 1) transient events of high-power beta synchrony in PD are promoted by synaptic dynamics across the TC circuit; 2) the temporal patterning of beta activity in PD is mediated by unit and ensemble dynamic changes in TC temporal alignment; 3) phase-specific stimulation (Cagnan *et al.*, 2017*a*) can bring kinetic and postural tremor control in ET patients with stable tremor properties, and 4) closed-loop algorithms using online estimates of phase and amplitude to trigger median nerve stimulation might be more effective in yielding tremor suppression in ET patients. Overall, the findings of this thesis contribute to the fields of neuroscience and neurotechnology by deepening our understanding on the dynamics of pathological neural synchrony and shedding light on the key features underlying the efficacy of selective neuromodulatory therapies.

# iv) Contents

# v) List of Figures

# vi) List of tables

# vii) List of Supplementary Figures

# viii) List of Supplementary Tables

# ix) Abbreviations

| | |
|---|---|
| 6-OHDA | 6-Hydroxydopamine |
| ARC | Amplitude response curve |
| BG | Basal ganglia |
| BGTC | Basal ganglia-thalamocortical |
| BMC | Bayesian model comparison |
| BZ | Basal ganglia-recipient zone of the thalamus |
| CTC | Cerebello-Thalamocortical |
| CZ | Cerebellar-recipient zone of the thalamus |
| CV | Coefficient of variation |
| ECoG | Electrocorticography |
| EEG | Electroencephalography |
| EMG | Electromyography |
| ET | Essential tremor |
| fMRI | Functional magnetic resonance imaging |
| FXX-BMC | Fixed-effects Bayesian model comparison |
| GPe | Globus pallidus externus |
| GPi | Globus pallidus internus |
| HPβ | High-power beta |
| IQR | Interquartile range |
| LFP | Local Field Potential |
| LPβ | Low-power beta |
| MEG | Magnetoencephalography |

| | |
|---|---|
| MRI | Magnetic resonance imaging |
| NS | No stimulation |
| PEB | Parametric Empirical Bayes |
| PD | Parkinson’s disease |
| PSA | Posterior Subthalamic Area |
| PSI | Phase Synchrony Index |
| PSS | Phase-specific stimulation |
| RSS | Random-search stimulation |
| SD | Standard deviation |
| SEM | Standard error of the mean |
| SNc | Substantia nigra pars compacta |
| SNr | Substantia nigra pars reticulata |
| STN | Subthalamic nucleus |
| TC | Thalamocortical |
| ViM | Ventral intermediate thalamus |

# x) Publications incorporated into this thesis

Reis C, Sharott A, Magill PJ, van Wijk BCM, Parr T, Zeidman P, et al. Thalamocortical dynamics underlying spontaneous transitions in beta power in Parkinsonism. Neuroimage 2019; 193: 103–14.

Reis C, Arruda SB, Pogosyan A, Brown P, Cagnan H. Essential Tremor amplitude modulation by median nerve stimulation. Scientific Reports 2021; 11: 1–10.

**Other publication during the DPhil:**

Arruda SB, Reis C, Sermon JJ, Pogosyan A, Brown P, Cagnan H. Identifying and Modulating Distinct Tremor States through Peripheral Nerve Stimulation in Parkinsonian Rest Tremor. Journal of NeuroEngineering and Rehabilitation 2021; (under review)

# 1 General Introduction

This thesis explores the role of thalamocortical (TC) interactions in the emergence and disruption of pathologically augmented rhythmic activity patterns established in Parkinson's disease (PD) and Essential Tremor (ET). PD and ET are the two most common movement disorders, affecting about 0.02% and 0.9% of the population worldwide, respectively (Louis and Ferreira, 2010; James *et al.*, 2018). Both movement disorders display altered frequency-specific activity patterns across the TC circuit and other areas of the motor circuit in association with motor deficits. However, the mechanisms underlying the generation and propagation of pathological rhythms in PD and ET have not been fully characterised, and effective ways of selectively disrupting them have not been developed. Motivated by this, I have undertaken two fundamental and two translational research projects aimed at 1) creating a better understanding of how aberrant patterns of neural activity come about in PD and 2) testing the effectiveness of time-specific electrical stimulation approaches in disrupting the pathological rhythms of ET. More specifically:

- Project one tests the hypothesis that TC interactions contribute to the dynamic regulation of PD-related neural synchrony.

- Project two tests the hypothesis that transient events of high PD-related synchrony observed at the cortical level are distributed across downstream structures of the motor circuit and mediated by dynamic changes in cortico-subcortical temporal alignments.

- Project three tests the hypothesis that thalamic phase-specific Deep Brain Stimulation (DBS) is capable of yielding tremor relief in ET patients, regardless of state changes in the underlying motor circuit.

- Project four tests the hypothesis that temporally specific proprioceptive thalamic afferents triggered via median nerve stimulation can modulate ET tremor.

This introductory chapter summarises the network dynamics involved in PD and ET and the means of interacting with such dynamics via electrical stimulation approaches. I will start by discussing the TC interactions involved in healthy and diseased motor processes. Then I will focus on the disrupted TC communication during PD and ET, while summarising the known etiology, symptomology and associated neural correlates of each movement disorder. Next, I will outline means of modulating disrupted neural networks via electrical stimulation of the central and peripheral nervous system, i.e., via DBS and peripheral nerve stimulation. Lastly, I will review emerging real-time controllers for electrical stimulation used to achieve patient-specific stimulation and reflect on how temporally specific stimulation strategies might achieve symptom relief in a more efficient manner. I will conclude this chapter by addressing the aims of my thesis.

## 1.1 Thalamocortical dynamics during healthy motor behaviour

To better understand what diseased and treated states of the TC circuit entail, we must first appreciate its properties in health. Hence, this section commences with an overview of the anatomical organisation of the TC loop, and moves on to review the current views on how the TC loop and brain regions that project to it contribute to healthy motor control.

Cortex and thalamus are two interconnected brain regions which form both reciprocal and non-reciprocal loops (Jones, 1985). The thalamus is a paired structure located in the middle of the brain and acts as a central communication hub of the cerebral cortex, i.e., it facilitates information flow across different cortical areas and integrates peripheral and subcortical inputs converging onto the neocortex (Jones, 1985). How TC projections support cortical function is not well understood and has long been a key research area in fundamental neurosciences. There is however growing evidence that the thalamus does not solely relay information to the cortex but also has the capability of upregulating or downregulating the cortical, subcortical or peripheral inputs it receives before transmitting them to the cortex. A small overview of the literature on this issue is provided below; however, given the scope of this thesis, mainly the thalamic projecting systems related to motor control will be highlighted.

The thalamus is subdivided into various distinct nuclei which are involved in different processes, such as sensory, motor and limbic (see (Jones, 1985) for a detailed review on thalamic anatomy and functional connectivity). The ventral part of the thalamus is mainly comprised of a single nucleus which is made up of reticular cells. This nucleus does not project to cortex but instead sends GABAergic inhibitory inputs to different nuclei of the dorsal thalamus. Conversely, most thalamic nuclei contain ensembles of relay cells (known as relay nuclei) which are segregated in the dorsal part of the thalamus and send glutamatergic inputs to the cortex.

### Thalamic firing patterns

Thalamic neurons exhibit a wide range of activity from low to high frequencies (1–80 Hz) due to their intrinsic cell properties (Anderson and Turner, 1991; Pessiglione *et al.*, 2005). In addition to having the ability of firing in a tonic fashion, thalamic cells can also fire in bursts of low-threshold calcium spikes (LTS). LTS mediate highly synchronised brain states such as slow-wave sleep and are thought to promote synchrony across brain networks (Steriade *et al.*, 1993; Contreras, 2008).

An LTS burst occurs due to the presence of low voltage-activated channels (T-type calcium channels) in the soma and dendrites of the thalamic neurons, which trigger cell activation in response to an increased inhibitory or reduced excitatory drive, i.e., when the cell membrane is in a hyperpolarised state (Llinás and Jahnsen, 1982). When T-type calcium channels open, an increase in calcium conductance results in a low threshold conduction potential with approximately two to seven sodium action potentials upon its crest (Llinás and Jahnsen, 1982). T-type calcium channels then quickly inactivate and simultaneously, calcium-activated potassium channels activate, bringing the membrane back to a hyperpolarised state leading to another LTS burst. As each burst of LTS takes about 100-200ms to occur, the frequency of LTS busting is rather fixed and limited to frequencies between 5 and 10 Hz (Wang *et al.*, 1991). This is extremely different from the thalamic tonic firing mode which shows a fairly linear input-output relationship where firing rate and magnitude of the depolarising input are correlated. Conversely, LTS burst activity occurs in a nonlinear fashion, where burst firing is not influenced by the EPSPs but instead by an all-or-none neural event, the calcium spike (Sherman, 2017).

### Changes in neural activity of thalamic inputs during movement

In the context of motor function there are two key but distinct pathways which converge from deep structures to the motor cortex via the motor thalamus: the basal-ganglia-TC (BGTC) pathway, where Basal-Ganglia (BG) output nuclei (the Substantia Nigra Reticulata (SNr)) and Globus Pallidus Internus (GPi)) send GABAergic inputs to the ventrolateral anterior nucleus of the thalamus which in turn targets almost exclusively layer I of the motor cortex (mainly associative and premotor cortices) ; and the cerebello-TC (CTC) pathway where the cerebellum, namely the deep cerebellar nuclei, sends glutamatergic inputs to the ventrolateral posterior thalamus (also called ventral intermediate nucleus, ViM) which projects to layers 3-5 of the motor cortex (mainly to the primary motor cortex) (Anderson and DeVito, 1987; Arbuthnott *et al.*, 1990; Kuramoto *et al.*, 2011, 2015; Nakamura *et al.*, 2014).

These two pathways are relevant for this thesis due to their role in PD and ET, which will be discussed in depth in sections 1.2.1 and 1.2.2.

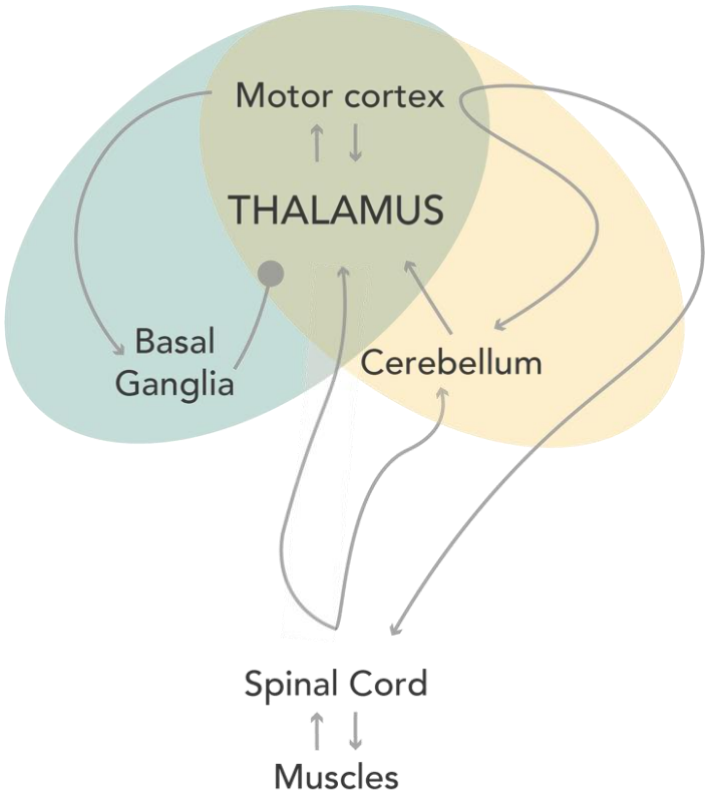


**Figure 1.1 - Diagram of the BGTC (green shade) and CTC (yellow shade) pathways of the motor circuit.** Excitatory and inhibitory projections are identified by the arrow and ball ended lines respectively.

Neural populations along both the BGTC and CTC pathways demonstrate movement-related changes in activity. In particular, motor cortical areas are known to change their spiking activity in association with both movement preparation (Porter and Lewis, 1975) and execution; the latter with movement parameters-related to movement force (Evarts, 1968), velocity (Georgopoulos, 1988) and orientation (Georgopoulos *et al.*, 1982). Changes in the activity of the BG-output are related to motor learning and motor execution. More specifically, the activity of the SNr changes before movement onset and during the reward period (i.e., movement-related reward) (Wichmann and Kliem, 2004; Nevet *et al.*, 2007; Fan *et al.*, 2012), while the GPi activity is similar to the cortical one in that it also is modulated according to movement kinematic parameters (Georgopoulos *et al.*, 1983; Anderson and Horak, 1985; Jaeger *et al.*, 1995; Turner and Anderson, 1997). The cerebellum, the other major subcortical input to the thalamus, also changes its spiking activity prior to movement onset (Ishikawa *et al.*, 2014) and is commonly thought to be implicated in movement coordination, error driven motor learning and has a temporal pattern generator function (Raymond *et al.*, 1996; Mauk *et al.*, 1997; Thier *et al.*, 2000; Ohyama and Mauk, 2001).

Lastly, neurons in the cerebellar and basal-ganglia recipient zones of the motor thalamus (named CZ and BZ throughout this thesis) also display significant changes in their firing rate and patterns before movement onset. The following section describes such changes with the aim of shedding light on the potential impact that motor thalamus has on motor behaviour.

## Spontaneous activity and Response of thalamus to inputs

### Changes in firing rate

Task-related changes in the motor thalamus are mainly characterised by an increase in tonic firing prior to movement onset (Strick, 1976; Donkelaar *et al.*, 1999; Kunimatsu and Tanaka, 2010; Goldberg *et al.*, 2012), although a decrease in firing and other patterns of activation have also been reported (Anderson and Turner, 1991; Bosch-Bouju *et al.*, 2014). Intriguingly, despite the anatomical segregation between BZ and CZ thalamus (highlighted in the previous section), the firing rates and movement-related activity of neurons from both areas of the thalamus have been reported to be extremely similar and seemingly indistinguishable (Anderson and Turner, 1991). While this observation has not been fully elucidated, as suggested in the review paper of Bosch-Bouju and colleagues (Bosch-Bouju *et al.*, 2013), it could potentially stem from common inputs that all areas of the motor thalamus receive from motor cortices and the thalamic reticular nucleus (Pare *et al.*, 1987; Hazrati and Parent, 1991).

There are several theories regarding the underlying mechanism through which the BG-BZ pathway communicates movement related information. The main theories are discussed below as they will provide a useful background for the interpretation of chapter 3, where I explore the spiking dynamics of neurons in the BG-output and BZ in relation to the cortex in the parkinsonian state.

BG-output nuclei (consisting of the internal segment of the pallidum (GPi) and the substantia nigra pars reticulata (SNr)) are composed of GABAergic neurons which are tonically active at rest (MacLeod *et al.*, 1980; Tanibuchi *et al.*, 2009) and increase their activity with movement onset (Deniau and Chevalier, 1985; Albin *et al.*, 1989; Chevalier and Deniau, 1990).

From a network perspective, depending on the input received by the BG-output nuclei, the firing rate of the thalamus is expected to be modulated in the opposite direction (Albin *et al.*, 1989; Alexander and Crutcher, 1990). Specifically, if receiving inputs from the striatum indirectly via the GPe and the Subthalamic Nucleus (STN) (which is Glutamatergic), neurons of the BG-output nuclei are expected to increase their firing rate and reinforce thalamic inhibition. Conversely, if receiving GABAergic inputs directly from the Striatum, BG-output neurons are expected to decrease their spiking, allowing for thalamic firing to occur. From this perspective, movement-related activity in BZ is thought to emerge from a "pause" in the tonic firing of BG-output neurons which will momentarily "release" BZ from inhibition (referred to as *disinhibition,* (Deniau and Chevalier, 1985; Chevalier and Deniau, 1990)). The disinhibition perspective relies on the assumption that firing patterns of BZ and BG-output neurons are inverse to each other at movement onset (Deniau and Chevalier, 1985; Albin *et al.*, 1989; Chevalier and Deniau, 1990; Nambu *et al.*, 1991; Hikosaka, 2007). This assumption has however been contradicted by various neurophysiological studies in behaving animals, where a co-activation of BG-output neurons and BZ neurons at movement onset has been observed (Inase *et al.*, 1996; Person and Perkel, 2005; Leblois *et al.*, 2009). One potential explanation for an increase in thalamic spiking in the presence of increased pallidal activity is the *rebound* mechanism. An increased BG-output firing leads to thalamic hyperpolarization and de-inactivation of thalamic low threshold T-type calcium channels, which in turn result in post-inhibitory rebound spikes during transient pauses in pallidal firing (Bosch-Bouju *et al.*, 2014; Kim *et al.*, 2017). Lastly, from studies showing that BG-output inactivation does not extinguish task-related activity in BZ (Inase *et al.*, 1996), and that pre-movement firing increases in the

BG-output lag behind those of BZ (Nambu *et al.*, 1991; Donkelaar *et al.*, 1999; Schwab *et al.*, 2020), the alternative perspective that thalamic activity is driven by cortical inputs and modulated by BG-outputs emerged (Goldberg *et al.*, 2012; Schwab *et al.*, 2020). This view has been further elaborated by Goldberg and colleagues, who have proposed that BZ activity is driven by excitatory cortical inputs but entrained to the interspike intervals of BG-output neurons (Goldberg *et al.*, 2013).

### Changes in firing pattern

Movement-related changes in neural activity do not always materialise as changes in firing-rate but can consist of changes in firing pattern. Patterned activity of single units can be difficult to detect but does become more evident when summed over multiple units (as shown in chapter 3, Figure **3.5**). Rhythmic patterns of spiking activity seem to be important for individual neurons to cooperate and indeed, there is evidence that coordinated activity patterns are important for binding cells into functionally coherent ensembles. For instance, within a pool of neurons projecting to the same muscle field, neurons changing their firing activity during specific phases of movement exhibited more synchronous spikes among themselves than with the remaining neurons (Jackson *et al.*, 2003). At a larger scale, synchronized ensemble activity of large populations of neurons give rise to the brain oscillations measured by Local Field Potentials (LFP), Magnetoencephalography (MEG) and Electrocorticography (EEG). Synchronisation is however not solely constrained to anatomically segregated neural populations ('local' synchrony), but can be extended to spatially distinct populations which exhibit coherent patterns of firing/oscillatory activity ('long-range' synchrony).

The presence of flexible 'local' and 'long-range' synchronisation patterns at beta (13-30Hz) and gamma frequencies (30-90Hz) in and across basal-ganglia- and cerebellar-TC pathways have been extensively described in association with movement-related behaviour (Pfurtscheller and Lopes Da Silva, 1999; Cassidy *et al.*, 2002; Courtemanche *et al.*, 2003; Paradiso *et al.*, 2004; Soteropoulos and Baker, 2006; Muthuraman *et al.*, 2012; Wijk *et al.*, 2012; Brücke *et al.*, 2013; Jenkinson *et al.*, 2013; Fischer *et al.*, 2017). Opposing functional roles have generally been attributed to beta and gamma oscillations: beta has been labelled as antikinetic because it suffers an attenuation prior to and during voluntary movement, and gamma has been labelled as prokinetic because it gets amplified at movement onset (for a review see (Brown, 2003)).
More recent studies have emphasized the importance of exploring the temporal dynamics of these oscillations to get a deeper understanding of the mechanisms subserving healthy motor

control. Following the observations by (Feingold *et al.*, 2015), levels of beta synchronisation observed in trial-averaged data, can be accurately described by the probability of observing short events of high-amplitude beta in a trial-by-trial basis. These events of high-amplitude beta are known as 'beta bursts' and are operationally identified by setting an arbitrary threshold to the envelope of the beta signal. Importantly, beta burst duration, rate, amplitude and timing seems to be implicated in different aspects of motor control, including reaction time, velocity and planning (Feingold *et al.*, 2015; Sherman *et al.*, 2016; Little *et al.*, 2019; Wessel, 2020).

## 1.2 Thalamocortical dynamics during diseased motor behaviour

### 1.2.1 Parkinson's disease

PD is a neurodegenerative movement disorder which results from a progressive loss of dopaminergic neurons in the substantia nigra pars compacta (SNc). Mainly characterised by resting tremor, rigidity, bradykinesia and postural instability (Jankovic, 2005), the first symptoms of PD usually occur at 50 years of age, when only around 20% of SNc dopaminergic cells remains intact (Sulzer and Surmeier, 2013). There are also non-motor complications in PD, which can in some cases (28% of patients in one study, (Witjas *et al.*, 2002)) cause a greater degree of disability than motor symptoms. These involve: cognitive impairment, autonomic dysfunction, sensory abnormalities, sleep disturbances, among others (review (Pfeiffer, 2016)).

Hitherto, the specific causes underlying neuronal degeneration in PD remain unknown. Also to date, a treatment which is capable of reversing the underlying causes of PD has not been approved for routine clinical use. Consequently, therapies available for PD focus on ameliorating symptoms. In the early stages, PD symptoms are pharmacologically targeted with medications that act to increase dopamine levels - these include dopamine replacement therapy (Levodopa), dopamine agonists (Apomorphine), monoamine oxidase-inhibitors or Catechol-O-methyl transferase-inhibitors.

As neuronal degeneration progresses and more severe stages of the disease are reached, medication efficacy decreases and severe side effects, such as dyskinesias, are observed (Obeso

*et al.*, 2000). At this stage, for patients experiencing significant functional disability, alternative surgical strategies such pallidotomy and thalamotomy (Lozano *et al.*, 1996; Giller *et al.*, 1998) or DBS targeting the STN or the GPi can be employed (Benabid *et al.*, 1991). Preferred over lesioning, given its reversible nature, DBS achieves an average reduction of PD symptoms of 50% (Kleiner-Fisman *et al.*, 2003; Volkmann *et al.*, 2009). Together, the decreased efficacy of long-term medication use, potential side-effects associated with irreversible lesioning (Krack *et al.*, 2019), and the high efficacy of DBS in the suppression of PD symptoms, have turned DBS into a key therapeutic technique for the clinical management of PD. The properties and mechanisms of action of DBS, as well as the exciting new developments that this therapeutical device is currently undergoing will be covered in sections 1.3.1 and 1.3.3, respectively.

#### 1.2.1.1 Pathological rhythms in Parkinson's disease

It is widely accepted that the loss of dopaminergic neurons in the SNc in PD leads to an imbalance of neural activity in brain regions involved with motor control. An early and still influential model on parkinsonism is the rate model (Albin *et al.*, 1989; DeLong, 1990). This model is based on the classic framework of BG organization, which attributes pro and anti-kinetic function to striatal direct and indirect pathways, respectively. More specifically, dopaminergic inputs from SNc to the striatum are integrated via D1 or D2 receptors and while activation of D1 neurons follows the direct pathway (striatum→GPi/SNr→thalamus→cortex) and leads to facilitation of movement initiation, activation of D2 neurons follows the indirect pathway (striatum→GPe→STN→GPi/SNr→thalamus→cortex) leading to difficulties in initiating movement (Alexander *et al.*, 1986). Critically, the gradual loss of dopaminergic neurons in the SNc during parkinsonism is thought to disrupt the balance that exists between these two pathways by promoting the indirect pathway (shown in blue in Figure **1.2**) over the direct one (shown in red in Figure **1.2**), resulting in the cardinal akinetic motor-symptoms of PD (Albin *et al.*, 1989).

Yet, based on an increasing number of neurophysiological studies in humans and animal models of disease that outlined how changes in overall firing rate were rather minimal when compared to emergence of a patterned activity (oscillatory activity) (Bergman *et al.*, 1994; Wichmann *et al.*, 1999; Starr *et al.*, 2005), a new perspective emerged – that abnormal motor behaviour in PD is driven by oscillatory and synchronous activity across the BGTC circuit.

The synchronous activity that is observed in the BGTC circuit during PD is the central theme of chapters 2 and 3 of this thesis. Hence, the sections that follow will briefly describe the properties of such oscillatory activity and how it relates to the cardinal symptoms of PD

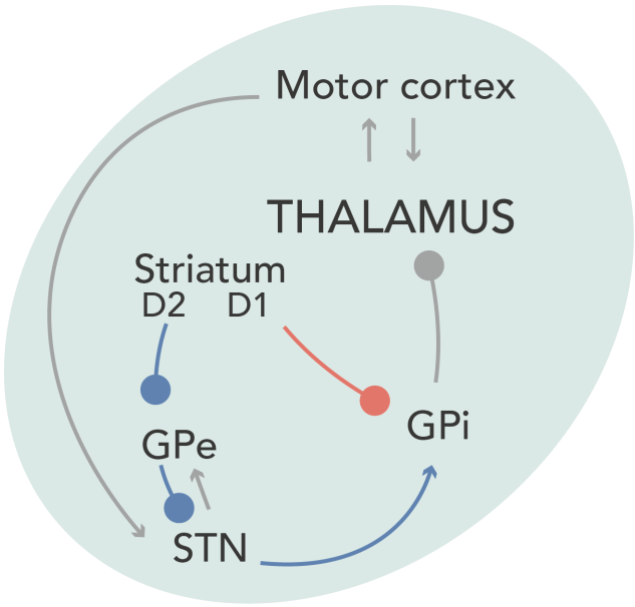


**Figure 1.2 - The direct and indirect pathways of the BGTC circuit.** Direct and indirect pathways are depicted in red and blue, respectively. Excitatory and inhibitory projections are identified by the arrow and ball ended lines, respectively.

### Beta oscillation in PD

Several studies have shown that in unmedicated PD patients, beta oscillations (13-30Hz), which are usually involved in healthy movement control (Engel and Fries, 2010; Jenkinson and Brown, 2011; Khanna and Carmena, 2015), become pathologically enhanced within and across regions of the BGTC (Brown *et al.*, 2001). Importantly, the strength of beta synchrony correlates with rigidity and bradykinesia and is reduced following dopamine replacement therapy and DBS when concurrent symptom relief is observed (Levy *et al.*, 2002; Brown, 2003; Silberstein *et al.*, 2005; Doyle Gaynor *et al.*, 2008; Kuhn *et al.*, 2008). How and where in the circuit beta band synchronisation originates remains a matter of debate.

At a network level, different structures, projections and parallel loops have been proposed to play a prominent role in the expression of beta activity, including: the motor cortex (Jensen *et al.*, 2005; Yamawaki *et al.*, 2008; Litvak *et al.*, 2011), the striatum (McCarthy *et al.*, 2011; Sharott *et al.*, 2017), the striatum-GPe loop (Corbit *et al.*, 2016; Crompe *et al.*, 2020), the

subthalamic-pallidal loop (Mallet *et al.*, 2008*a*; Cruz *et al.*, 2011; Tachibana *et al.*, 2011; Nevado-Holgado *et al.*, 2014; Cagnan *et al.*, 2015), the TC loop (Brazhnik *et al.*, 2016; Reis *et al.*, 2019) and an interplay between cortical and pallidal inputs to the STN (West *et al.*, 2020).

Beta oscillations exhibit fluctuations in their amplitude and are currently best described as 'beta bursts', as outlined above. Also in PD literature, a growing body of research has been focusing on how different beta burst metrics, such as burst rate, duration, amplitude and timing relate to motor performance (Tinkhauser *et al.*, 2017*a*, *b*; Deffains *et al.*, 2018; Lofredi *et al.*, 2019; Duchet *et al.*, 2020, He *et al.*, 2020*b*; Vinding *et al.*, 2020). Critically, it is presumed that an increased prevalence of long beta bursts over short beta bursts plays a critical role in Parkinson's and relates to the motor deficits observed in PD (Tinkhauser *et al.*, 2017*a*, *b*). This shift from an averaged description of beta power to characterisation of its intermittency, not only exposed the dynamic nature of beta synchrony but also corroborated the therapeutic mechanism underlying an innovative DBS strategy which has shown to be more efficient than the gold-standard continuous DBS. This experimental technique known as adaptive DBS (Little *et al.*, 2013, 2016*b*), uses an implanted electrode in the STN to monitor local beta power and deliver stimulation when an STN beta burst emerges. Employing methods which take into account the intermittent nature of beta oscillations, recent studies propose that instead of a local phenomenon, beta bursting in PD occurs across the basal-ganglia-cortical circuit (Tinkhauser *et al.*, 2018, Cagnan *et al.*, 2019*b*). In particular, in a recent study using concurrent electrophysiological recordings of multiple BG nuclei (STN, GPe and Striatum) and the motor cortex, beta bursting was found to be associated with a transient increase in coupling between cortical and subcortical regions which was presumably mediated by fast evolving (time scale of a burst) synaptic interactions (Cagnan *et al.*, 2019*b*). In order to complete the characterisation of the network dynamics underlying beta bursts, the third chapter of this thesis investigates whether similar neural events can be detected between the cortex and the BG-output nucleus (GPi) and the cortex and the thalamus.

So far, I have focused on describing the oscillatory dynamics linked to the PD symptoms of rigidity and bradykinesia. The following sections will move on to characterise the neural correlates and network dynamics associated with tremor in PD.

## Rhythmic activity at tremor frequencies in PD

Tremor and most specifically rest tremor, is a common symptom of PD; in a study which included 418 PD patients, tremor was present in about 88% of the cohort and rest tremor was the most common type of tremor (67%), followed by postural tremor (53%), and action tremor (51%) (Gupta and Kuo, 2018). Although to a lesser degree than rigidity and bradykinesia, rest tremor is also attenuated with dopaminergic medication (Dirkx *et al.*, 2017). A more effective therapeutic option for tremor control is DBS stimulation delivered to the STN, GPi or ViM (Benabid *et al.*, 1991; Wong *et al.*, 2019). This suggests that rest tremor in PD is mediated by a distributed network which involves the BGTC and the CTC circuits, rather than by local tremor pacemakers.

Early evidence supporting this view originates from deep brain recordings where units firing bursts at tremor-related frequencies (named "tremor cells") were found in the BG (specifically in the STN and the GPi, (Magnin *et al.*, 2000)) as well as in the ViM – the part of the thalamus that receives inputs from the cerebellum (Lenz *et al.*, 1994; Zirh *et al.*, 1998; Magnin *et al.*, 2000)). More recently, changes in functional and effective connectivity of the two circuits have been implicated in rest tremor. In an influential fMRI study, tremor-dominant PD patients showed increased functional connectivity between the ViM and other motor areas including, the motor cortex, cerebellum and globus pallidus, when compared with non-tremor PD patients (Zhang *et al.*, 2016). Moreover, tremor-related oscillatory activity in the motor cortex, cerebellum, and a diencephalic region (interpreted as the thalamus) has been detected via magnetoencephalography (Timmermann *et al.*, 2003). Using concurrent EMG and fMRI recordings, undulations in tremor severity have been shown to be positively correlated with rhythmic activity of the CTC circuit (Helmich *et al.*, 2011). Finally, the delivery of electrical stimulation at tremor frequencies to the motor cortex (Brittain *et al.*, 2013) and cerebellum (Brittain *et al.*, 2015*a*) using transcranial alternating current stimulation, and to the ViM and STN via DBS (Cagnan *et al.*, 2014), has been shown to entrain tremor, which again supports the existence of a broad tremor network.

What remains to be determined however, is the underlying mechanisms behind the emergence and propagation of rest tremor – how are the BGTC and CTC circuits causally linked? The dimmer-switch hypothesis suggests that PD tremor is triggered by the BG (GPi) and modulated by the CTC circuit (Helmich *et al.*, 2011, 2012). This hypothesis is based on fMRI recordings which have shown that while both the BGTC and CTC circuits display increased cerebral activity during tremor, only the latter exhibits activity changes in tandem with slow

modulations in tremor amplitude. Building on this hypothesis, a modelling study by the same group suggests that propagation of tremor from the GPi to the CTC circuit occurs via the motor cortex (Dirkx *et al.*, 2016).

### 1.2.2 Essential tremor

ET is one of the most common movement disorders with an estimated prevalence of between 0.5 and 4% of the population (Louis *et al.*, 1998). ET is predominantly characterised by postural and kinetic tremor but also includes some non-motor manifestations such as hearing loss, depression and anxiety, (Deuschl *et al.*, 1998; Tan *et al.*, 2005) . Although a genetic basis is commonly attributed to ET (50% of the ET patients inherit the condition in an autosomal dominant fashion (Louis and Ottman, 1996; Lorenz *et al.*, 2004)), the exact etiology remains elusive and thus hinders the development of effective and specific therapeutic approaches capable of supressing tremor. Patients suffering from ET are primarily treated with pharmacotherapy, typically demanding a trial-and-error approach to the prescription of anticonvulsants and beta-blockers. Because of their poor efficiency in treating tremor (suboptimal efficacy and frequent side-effects), about 56% of ET patients eventually discontinue the use of medication (Diaz and Louis, 2010; Deuschl *et al.*, 2011; Ondo, 2016). In more severe stages of ET, where patients face great functional disability, viable therapeutical options include thalamic ablation or thalamic neuromodulation via (low-intensity focused ultrasound or DBS) (Elble *et al.*, 2018). DBS delivered to the ViM or surrounding areas, provides a promising therapy for ET, given its reversible nature and high efficacy (up to 80% of tremor reduction) (Zhang *et al.*, 2010; Elble *et al.*, 2018; Lozano *et al.*, 2019). Surprisingly, the prevalence of ViM DBS implantation in ET patients is extremely low – with only 2% of patients undergoing DBS surgery according to data collected at an U.S. tertiary-referral centre over 5 years (Kestenbaum *et al.*, 2015). Factors that might help explain this underutilisation consist of risks inherent to any surgical intervention (haemorrhage and infection), ViM stimulation induced side-effects (dysarthria, poor verbal fluency and balance impairments), loss of clinical efficacy over time and its high cost (Zhang *et al.*, 2010; Baizabal-Carvallo *et al.*, 2014; Cury *et al.*, 2017; Fasano and Helmich, 2019).

Altogether, the poor efficacy of medication and the infrequent deployment of cutting-edge neuromodulatory techniques such as DBS, create a tangible demand for the development of novel therapies for ET to resolve the negative psychosocial impact that this neurological

disorder brings to those affected (Louis *et al.*, 2001; Lorenz *et al.*, 2011). The fifth chapter of this thesis contributes to the issue raised above, by employing a closed-loop median nerve stimulation paradigm and testing its impact on tremor severity of ET patients.

#### 1.2.2.1 Pathological rhythms in Essential tremor

A large part of this thesis is dedicated to finding efficient ways of disrupting pathological synchrony established in the TC circuit during ET and bring tremor relief to patients. Therefore, a brief summary of the characteristics of such synchrony and the current views on how it emerges is provided in this section.

From a network perspective, it is widely accepted that the CTC circuit is involved in the emergence of ET. Similar to PD, ET is also considered an oscillopathy since it is linked to aberrantly rhythmic neural activity. Although intermittent, several studies have shown, using measures of coherence, a synchronization between oscillations recorded from structures of the CTC circuit and tremulous muscles. In particular, the ViM is known to fire in a tonic but burst-like pattern which correlates with trembling activity observed at the periphery (Hua and Lenz, 2005) and the motor cortex displays oscillatory activity which is coherent with postural tremor (Muthuraman *et al.*, 2012). Furthermore, one study using magnetoencephalography and dynamic imaging of coherent sources beamformer as a localisation technique, was able to map a network of brain areas which resonated at tremor frequencies and the first harmonic (Schnitzler *et al.*, 2009). This network extended across contralateral primary motor cortex, premotor cortex, brainstem, thalamus, and ipsilateral cerebellum (Schnitzler *et al.*, 2009). Similarly, in an earlier fMRI study, the contralateral motor cortex and thalamus and bilateral cerebellum have shown increased activity during postural tremor (Bucher *et al.*, 1997). In addition to its widely accepted functional involvement in ET, a growing body of work suggests that the cerebellum also exhibits morphological changes during the disease. This has been shown in studies using advanced structural neuroimaging techniques, such as voxel-based morphometry (Pagan *et al.*, 2003; Daniels *et al.*, 2006; Benito-León *et al.*, 2009), as well as post-mortem studies where signs of pathology were identified in the cerebellum and brainstem (Rajput *et al.*, 2004; Louis *et al.*, 2007; Shill *et al.*, 2008). Whether these morphological alterations of the cerebellum reflect a primary progressive neurodegeneration in ET or a secondary effect similar to observed widespread oscillatory activity, is yet to be elucidated. One other key aspect of ET pathology that also remains to be uncovered, is the precise mechanism underlying the emergence and propagation of oscillatory activity in ET. One

hypothesis is highlighted by the research of Pedrosa and colleagues. The author has found that clusters of neurons in the cerebellar recipient zone of the thalamus and the oscillatory activity of trembling muscles are coherent in a spatially organised manner (Pedrosa *et al.*, 2012). Moreover, these muscle-specific clusters of tremor neurons in the motor thalamus comprise topographically indistinguishable pockets of cells which preferably mediate either efferent or afferent information (Lenz *et al.*, 1994). Using Granger causality on both EMG data and thalamic neural activity, Pedrosa and colleagues found that predominantly efferent pockets outnumbered afferent ones, suggesting that the emergence of ET tremor is centrally driven (Pedrosa *et al.*, 2018). Finally, different phases were associated with afferent and efferent connectivities resulting in different tremor amplitudes, suggesting that instantaneous tremor severity depends to a certain extend on the phase-relationship between afferent and efferent subpopulations (Pedrosa *et al.*, 2018).

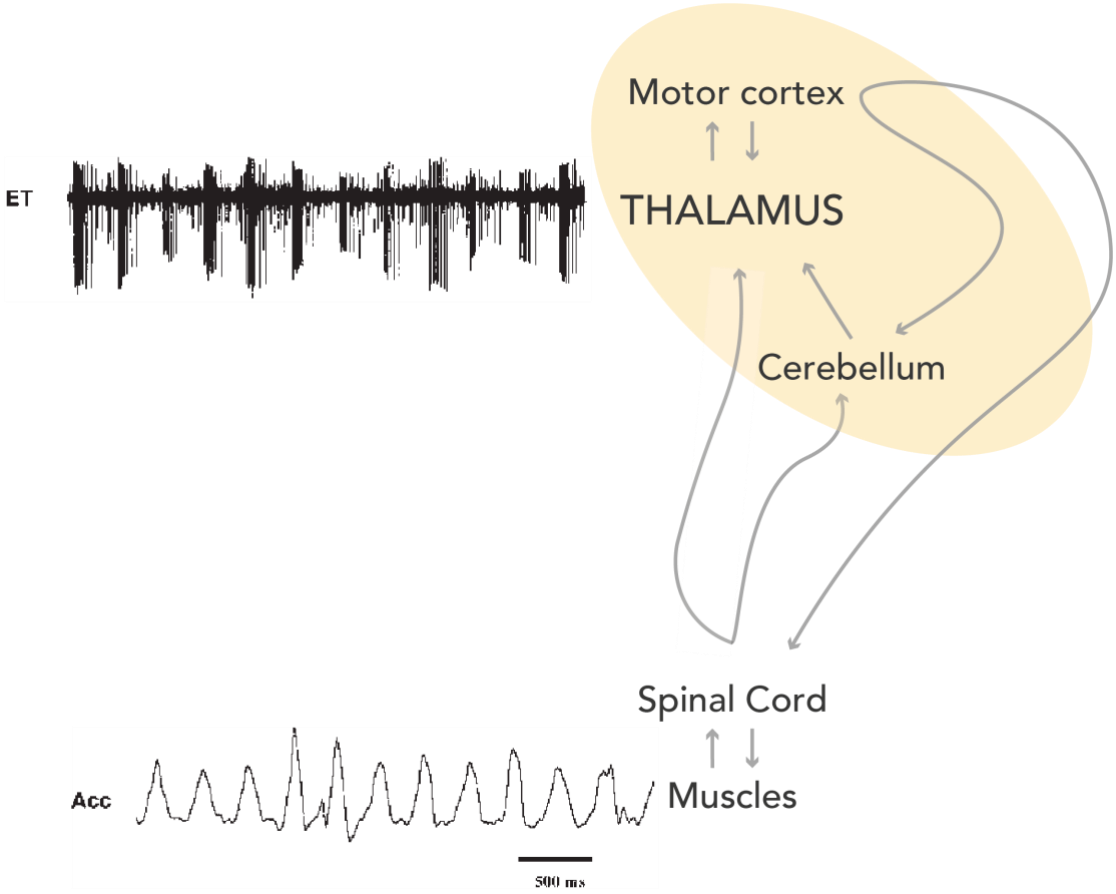


**Figure 1.3 - Thalamomuscular coherence in ET and the CTC pathway.** Thalamic tremor-related firing (trace labelled as ET) and accelerometery signal (labelled as Acc) were adapted from (Brodkey *et al.*, 2004).

## 1.3 Neuromodulation via electrical stimulation

In the previous sections of this chapter I have described the etiology, symptomology and associated neural correlates of PD and ET. In the following sections I will formally introduce some of the neuromodulatory strategies that can be employed to restore motor behaviour in these movement disorders.

### 1.3.1 Deep brain stimulation

DBS is an effective surgical treatment for movement disorders (Johnson *et al.*, 2008; Krack *et al.*, 2010), pain (Bittar *et al.*, 2005) and epilepsy (Fisher *et al.*, 2010; Laxpati *et al.*, 2014). DBS is most commonly used in movement disorders, where the delivery of electrical stimulation to key brain targets modulates pathological neural activity across the motor circuit and restores the motor performance of medically refractory patients who suffer from PD (Rodriguez-Oroz *et al.*, 2005; Benabid *et al.*, 2009), essencial tremor (ET) (Benabid *et al.*, 1991; Koller *et al.*, 2001; Elble *et al.*, 2018) and dystonia (Vidailhet *et al.*, 2005). Stimulation parameters, especially stimulation intensity, are adjusted in a patient-specific manner in order to achieve maximal clinical benefit, i.e., maximal symptom reduction with minimal side effects. Unlike the therapeutic range of stimulation parameters which is the same across movement disorders (130-180Hz frequency of stimulation, 30-150μs pulse width and 1-4V stimulation intensity), the targeted brain structure is specific to the brain networks thought to underly the disease and the patient's symptom profile.

DBS's reversible nature and efficacy in treating movement disorders has been a source of hope and inspiration for neurological and psychiatric conditions alike. This is supported by an ever-growing number of clinical trials investigating the use of DBS for the treatment of conditions such as Alzheimer's disease (Sankar *et al.*, 2015; Lozano *et al.*, 2016), Tourette's syndrome (Vandewalle *et al.*, 1999; Mink *et al.*, 2006; Kuhn *et al.*, 2008), obsessive-compulsive disorder (Nuttin *et al.*, 1999; Denys *et al.*, 2010; Kohl *et al.*, 2014), major depression (Mayberg *et al.*, 2005; Holtzheimer *et al.*, 2017) and addiction disorders (Müller *et al.*, 2013).

DBS does however show some limitations, including risks inherent to the surgical process itself, such as infection, haemorrhage and skin erosion, and postoperative complications such as stimulation-induced side effects. Side effects during high-frequency DBS are common

(reported by approximately half of the implanted patients) but mild in the majority of cases and usually reversible by reprogramming the stimulation settings (Koller *et al.*, 2001; Volkmann *et al.*, 2009). Stimulation-related adverse reactions are thought to emerge from the disruption of local physiological processes and/or spreading of the volume of tissue activated (VTA) to collateral areas surrounding the stimulation target, i.e., due to stimulation producing a larger VTA than that of the therapeutic target. The VTA itself is dependent on the contacts used for stimulation, stimulation intensity, type of return reference (larger spread if monopolar than bipolar) and properties of the surrounding tissue. Achieving an optimal match between the VTA and the surgical target relies heavily on our understanding of the mechanisms of action underlying high-frequency DBS, which, despite its widespread popularity are still not well understood. One overarching hypothesis is that DBS disrupts abnormal information flow (Chiken and Nambu, 2016); but how it achieves this and what the precise biophysical effects of stimulation on the target nucleus and surrounding nerve cells, remains unclear. Several contradictory hypotheses have been posited; some suggesting an inhibitory effect (Boraud *et al.*, 1996; Dostrovsky *et al.*, 2000; Milosevic *et al.*, 2018), and others proposing an excitatory effect (Hashimoto *et al.*, 2003; Maurice *et al.*, 2003) of DBS on the stimulated and downstream nuclei. Recent theoretical and experimental work reconcile the above by suggesting that high-frequency DBS induces both a suppression of intrinsic firing at the stimulated nucleus and an activation of the axons traversing in the vicinity of the stimulation electrode (Anderson *et al.*, 2003; McIntyre *et al.*, 2004; Li *et al.*, 2007). Activation of the passing fibres consequently leads to an inhibition or excitation of afferent and efferent brain regions depending on the type of projection (i.e., if they are GABAergic or glutamatergic).

A key characteristic of DBS is yet the possibility of recording neural activity (LFPs) from the deep structures of the brain. This has provided crucial insights into the pathophysiology of movement disorders since no other commonly used imaging methods are able to cover deep structures of the human brain with a comparable temporal and spatial resolution. Recordings are done via the implanted electrodes, and while traditionally the acquisition of LFPs could only be performed in a small time-window during surgery or shortly after when the DBS leads remained externalised, recent hardware advances such as the Medtronic Percept™, allow for LFP recordings to be acquired at any given time point for as long as needed (Gilron *et al.*, 2021).

In sum, DBS is an indispensable technique since it can be used to treat refractory neurological diseases and to investigate pathophysiological mechanisms underlying these disorders. Consequently, research across different fields is currently being carried out with the aim of mitigating the existing limitations of DBS. One example is the development of segmented electrodes which use 8 instead of 4 programable contacts to deliver directional DBS. Here, contacts of segmented electrodes are oriented to cover 3 different radial directions and yield greater control over the VTA. (Pollo *et al.*, 2014; Reker *et al.*, 2016). Another example is the development of DBS imaging software (Lead-DBS toolbox, (Horn and Kühn, 2015)) which allow for an accurate electrode localization in terms of personalized brain anatomy and its relationship to the achieved clinical effects. Finally, bidirectional implanted devices, i.e., devices with the capacity of sensing and stimulating, such as the Neuropace Responsive Neurostimulation system™ and Medtronic Activa PC+S™ and Percept™, have been recently developed to support the implementation of close-loop stimulation algorithms.

Unlike conventional DBS, which continuously stimulates the brain using fixed stimulation parameters not taking into account the fluctuations in disease or behavioural states of a patient (open-loop stimulation), closed-loop stimulation uses adaptive control algorithms which trigger stimulation in real-time when specific biomarkers of disease states are detected. This paradigm shift from a static to a dynamic neuromodulation is currently being researched using experimental algorithms which have so far shown promising (Little *et al.*, 2013, 2016*a*, *b*; Sun and Morrell, 2014; Rosa *et al.*, 2015; Malekmohammadi *et al.*, 2016; Cagnan *et al.*, 2017; Piña-Fuentes *et al.*, 2017; Velisar *et al.*, 2019). Section 1.3.3 of this chapter reviews the different real-time controllers that have been used to control electrical stimulation-based therapies.

### 1.3.2 Peripheral electrical stimulation

Treating symptoms of neurological diseases via stimulation of the peripheral nerves is not a new concept (Toglia and Izzo, 1985; Ridding *et al.*, 2000; Ben-Menachem, 2002; Mobbs *et al.*, 2007; Heo *et al.*, 2015). Since this thesis is focused on the modulation of disease circuits via electrical stimulation, I will solely focus on electrical stimulation paradigms which deliver electrical stimulation to peripheral nerves with the aim of modulating neural activity in networks (central and peripheral) that underlie motor control. For instance, peripheral electrical stimulation has been trialled in post-stroke patients with the aim of increasing excitability of the motor cortex via sensory input in order to facilitate cortical neural plasticity and recover

motor function (Ridding *et al.*, 1995; Conforto *et al.*, 2002; Peurala *et al.*, 2002; Charlton *et al.*, 2003; Kimberley *et al.*, 2004). In a recent study, the neuromuscular control and hand function of chronic stroke patients was significantly improved after 8 weeks of functional training followed by 40 minutes of electrical stimulation sessions (median nerve at the elbow, below motor threshold) compared to those of patients receiving 8 weeks of functional training followed by sham electrical stimulation (Pan *et al.*, 2018). Non-invasive therapies have also been widely explored in the context of tremor control, in conditions like dystonia, ET and PD (Pascual-Valdunciel *et al.*, 2021). Various protocols have been used across the literature (varying the targeted nerve, stimulation intensity, number of pulses, duty cycles, pulse width and frequency), and the effects of peripheral stimulation on supressing tremor have been heterogenous thus far (Munhoz *et al.*, 2003; Heo *et al.*, 2015; Pahwa *et al.*, 2019; Kim *et al.*, 2020). While the mechanism of action remain largely unknown, it is thought that the putative suppressive effects of peripheral nerve stimulation on tremor stem from driving sensory afferent inputs to the thalamus, so that abnormal rhythmic patterns across the TC circuit and other nodes of the motor circuit can be reversed (Hanajima *et al.*, 2004; Hernandez-Martin *et al.*, 2021). Chapter five of this thesis explores this idea in more detail by using a closed-loop and phase-specific electrical stimulation paradigm, where the modulatory effect of median nerve stimulation on tremor is assessed.

### 1.3.3 Real-time controllers for electrical stimulation-based therapies

Conventional electrical stimulation therapies operate in an open-loop manner by delivering stimulation according to pre-programmed settings which are blind to the underlying disease state. Conversely, adaptive stimulation algorithms adjust stimulation delivery in response to events which reflect fluctuations in patients' symptoms. This approach was applied in the experimental studies of chapters 4 and 5 and its characteristics, advantages and limitations are outlined below.

A critical challenge to closed-loop stimulation is precisely identifying events which can be used as real-time controllers for stimulation delivery, i.e., finding a reliable biomarker of the disease. An ideal biomarker is one which tightly correlates with symptom severity and is responsive to treatment (Little and Brown, 2012, Cagnan *et al.*, 2019*a*).

Different types of signals have been used as biomarkers, including healthy and pathological neural activity as well as peripheral measures. For instance, in ET where tremor emerges during goal-directed movements and ViM thalamus exhibits rhythmic activity patterns at tremor-related frequencies, various signals have been used to guide electrical stimulation timing. Examples include: DBS thalamic stimulation triggered by tremor states decoded from thalamic LFPs which led to a reduction of intention tremor by 90.5% (He *et al.*, 2020*a*); DBS thalamic stimulation triggered by upper limb motor activity detected via a cortical electrode, which achieved comparable levels of tremor suppression to those reached with conventional DBS (Opri *et al.*, 2020), and DBS thalamic stimulation triggered by tremor episodes measured via peripheral sensors, which supressed tremor up to 60% in single patient case-report (Herron *et al.*, 2017). Likewise, signals acting as control signals can range from unprocessed to heavily processed signals (for instance, phase values of a filtered tremor signal measured with a peripheral accelerometer or tremor related states decoded from LFP recordings). Stimulation strategies that require extensive processing of the raw neural data to yield a control signal typically result in high energy and processing cost which may pose a limitation for clinical translation. The number of processing steps (such as application of wavelet, fast Fourier and Hilbert transforms, or machine learning algorithms) will ultimately depend on the signal features that are under interest.

The most commonly used signal features for closed-loop stimulation are the amplitude and phase of frequency specific neural oscillations which correlate with symptoms of disease. Examples are the adaptive DBS (Little *et al.*, 2013) and Phase-dependent stimulation (McNamara *et al.*, 2020) strategies, which build on the well-established link between enhanced beta oscillations and severity of bradykinesia and rigidity in PD (Brown *et al.*, 2001; Kühn *et al.*, 2009). These two strategies use amplitude and phase of beta oscillations, respectively, to trigger stimulation to BG structures and reduce beta synchrony. The latter stimulation paradigm, where phase of cortical beta oscillations is tracked to deliver stimulation to the pallidum of 6-OHDA lesioned rats, successfully supressed beta oscillations and beta coupling in and across cortex and pallidum. Nonetheless, whether beta suppression gave rise to motor improvement was not shown in this study(McNamara *et al.*, 2020). Conversely, adaptive DBS which delivers intermittent stimulation to the STN of PD patients triggered by periods of excessively elevated STN beta oscillations, shows similar symptom improvement to that achieved with conventional DBS (Little *et al.*, 2013, 2016*a*; Rosa *et al.*, 2015; Meidahl *et al.*,

2017; Piña-Fuentes *et al.*, 2017), whilst using less energy and reducing stimulation-induced side effects (Little *et al.*, 2016*b*; Rosa *et al.*, 2017).

Most closed-loop strategies use pathological signals to guide stimulation in order to spare physiological oscillations and reduce stimulation-induced side-effects; however, innovative solutions are arising whereby, to mitigate stimulation-induced adverse effects, stimulation intensity is lowered when a side-effect related signal is detected. For instance, in PD, conventional STN DBS successfully eliminates levodopa-induced dyskinesias (Kim *et al.*, 2015). Paradoxically, in some cases, dyskinesias are induced by the stimulation itself (Baizabal-Carvallo and Jankovic, 2016). Building on the fact that dyskinesias and cortical narrow band gamma oscillations (60-90Hz) are positively correlated (Swann *et al.*, 2016), work by the Starr group has shown that adjusting stimulation intensity according to cortical gamma activity yields reduction of PD's cardinal symptoms without inducing dyskinesias (Swann *et al.*, 2018).

Despite various benefits associated with closed-loop stimulation, including enhanced efficacy, reduced side effects (Little *et al.*, 2016*b*; Piña-Fuentes *et al.*, 2017; Rosa *et al.*, 2017), increased battery life (Little *et al.*, 2016*a*; Cagnan *et al.*, 2017), and patient-specificity (Rosa *et al.*, 2015; Cagnan *et al.*, 2017), most studies have only tested these algorithms for a few hours. It is expected that with the new generation of bidirectional DBS stimulators, the acquisition of long stimulated datasets will be possible (Gilron *et al.*, 2021), and the full potential of this strategy will be critically evaluated.

### 1.3.4 Regulation of disease circuits via temporally specific approaches

As hinted throughout the introduction, neural oscillations play a crucial role in neural communication (Buzsáki and Draguhn, 2004). They are key for coordinating information transfer within and across regions and have been found to contribute to motor, sensory and cognitive processing (Engel and Singer, 2001; Buzsáki and Draguhn, 2004; Fries, 2015). More specifically, it has been suggested that the phase alignment between neural activities of different populations will dictate the efficacy of information flow (Fries, 2005). Building on this hypothesis, different aspects of brain function could be subserved by a specific phase alignment between oscillatory activities of brain regions or neural circuits. However, in order

for the brain to transition between different functional states, the alignment of neural activities must be flexible, allowing different channels of communication to open and close across the network. A loss of such flexibility is hypothesised to underly PD and ET (Cagnan *et al.*, 2014). Both movement disorders display excessive, frequency-specific synchronization of oscillations across the motor circuit that are associated with specific motor impairments (tremor in ET at around 4-7 Hz and rigidity and bradykinesia in PD at around 13-30 Hz). Previous literature suggests that an external perturbation of a neural oscillator can lead to advances or delays in the oscillator's phase depending on the precise timing at which an input is given (Ermentrout, 1996; Smeal *et al.*, 2010; Farries and Wilson, 2012). It has been further hypothesised that once the phase of an oscillator is modulated via stimulation, the temporal relationship between that same oscillator and oscillators in the downstream brain regions will be disrupted, thus shifting the network from a diseased to a healthy state (Cagnan *et al.*, 2015).

Recently developed closed-loop stimulation paradigms support this hypothesis by showing that both oscillatory activity and performance can be modulated depending on the phase at which stimulation had been delivered. For instance, phase-specific intracortical microstimulation of the cortical beta signal led to changes in beta amplitude and reaction-time (Peles *et al.*, 2020). In a different study closed loop stimulation delivered to a specific phase of theta oscillations in the hippocampus of freely behaving mice inhibited the dorsal CA1 and enhanced spatial navigation performance (Siegle and Wilson, 2014). Lastly, thalamic DBS delivered at a specific phase of tremor led to significant ET tremor relief by up to 87% (Cagnan *et al.*, 2017).

In sum, temporally specific stimulation approaches can be used to disrupt the specific phase-alignment that a given brain circuit assumes during a diseased state. The experimental work developed in chapters four and five of this thesis use a temporally specific stimulation approach to modulate the severity of tremor in ET patients. Chapter four delivered stimulation directly to the thalamus via DBS, whereas chapter five delivered stimulation to the median nerve to disrupt thalamic activity via afferent inputs. In both cases, stimulation was triggered at different phases of the peripheral tremor (measured via accelerometery) and phase-dependent effects on tremor severity were found.

## 1.4 Thesis objectives

In both PD and ET, the TC circuit exhibits excessive synchronization of neural oscillations in association with motor impairment. Mounting upon the potential role that TC connectivity might have for flexible motor control, in this thesis I set out to answer the following questions:

1. Can fast synaptic TC dynamics help to explain the modulation of beta oscillations in PD? If so, are such dynamics circumscribed to inter-regional connections or do they involve local circuitries as well?

2. Does local synchronisation emerge simultaneously across the BG-output, motor thalamus and cortex? Are high beta oscillatory events mediated by changes in the temporal relationship between subcortical and cortical beta activities?

3. Given that temporal stimulation of the thalamus can in some cases restore motor behaviour in ET patients, how resilient is this strategy to state changes of the underlying motor circuit? Will this strategy be equally efficient during kinetic tremor?

4. Can motor behaviour in ET be restored by temporally specific proprioceptive thalamic afferency triggered via median nerve stimulation?

To address each question, four different projects have been implemented. These are reported in detail in this thesis as four chapters (chapter 2 to 5, inclusively). The first two chapters consist of fundamental research projects which aim to deepen our understanding about the mechanism underlying the emergence and propagation of beta oscillatory activity in PD – chapter 2 by employing theoretical methods of TC interactions and 3 while analysing archival neurophysiological data from the TC circuit. The third and fourth chapters of this thesis consist of translational studies where tremor recordings were acquired and harnessed to manipulate the CTC tremor networks of ET patients in real-time – either centrally with DBS or peripherally with median nerve stimulation (chapter 4 and 5 respectively). As three inherently different methods have been applied throughout this thesis, a general methods section will not be provided. Instead, the specific methods will be outlined as part of the methods section of each chapter.

# 2 Thalamocortical dynamics underlying spontaneous transitions in beta power in Parkinsonism

## 2.1 Introduction

In order to communicate in a behaviour-specific manner, neural populations must adapt their degree of rhythmic synchronization accordingly (Fries, 2015). In its normative physiological state, the BGTC circuit exhibits transient (de-) synchronization in the beta frequency band (13–30 Hz) activity during motor control (Pfurtscheller and Lopes Da Silva, 1999; Cassidy *et al.*, 2002; Foffani *et al.*, 2005; Tsang *et al.*, 2012; Zaepffel *et al.*, 2013). Conversely, during PD, the BGTC circuit displays increased beta oscillatory activity within and across its different nodes. Importantly, when parkinsonian motor deficits, such as rigidity and bradykinesia, are attenuated with pharmacological (Levodopa) or neuromodulatory interventions (DBS or optogenetics), a reduction in synchronization is observed in the beta-frequency band in brain recordings from patients (Brown, 2001; Levy *et al.*, 2002; Priori *et al.*, 2004; Silberstein *et al.*, 2005; Kuhn *et al.*, 2008; Eusebio *et al.*, 2009), as well as from other animal models of the disease, such as the 1-methyl-4-phenyl-1,2, 3,6-tetrahydropyridine treated non-human primate models of PD (Heimer *et al.*, 2006; Nambu and Tachibana, 2014) and the 6-hydroxydopamine (6-OHDA)-lesioned rat model of PD (Sharott *et al.*, 2005; Gradinaru *et al.*, 2009).

Despite being traditionally described as a sustained event when averaged over seconds (Lopez-Azcarate *et al.*, 2010; Brittain and Brown, 2014), excessive synchrony in the beta band (i.e. beta power), primarily manifests as intermittent events of high beta power or “beta bursts” (Little *et al.*, 2012; Feingold *et al.*, 2015; Sherman *et al.*, 2016, Tinkhauser *et al.*, 2017*a*). Operationally, beta bursts are commonly defined as epochs of beta oscillations that surpass a certain threshold  and while their presence has been quantified in physiological (Feingold *et al.*, 2015; Sherman *et al.*, 2016) and pathological neural activity, in PD the probability of long beta bursts has been positively correlated with PD motor symptom severity (Tinkhauser et al., 2017; Little et al., 2012).

From a neuronal network perspective, several studies have proposed that altered BG-output leads to excessive beta synchrony and motor impairments in PD (Bevan *et al.*, 2002; Terman *et al.*, 2002; Holgado *et al.*, 2010; McCarthy *et al.*, 2011). Employing Dynamic Causal Modelling (DCM) (Friston *et al.*, 2003), a framework for specifying, fitting and comparing mathematical models of neural circuitry, Moran et al. (2011) and Marreiros et al. (2013) indicated modulation of the hyperdirect pathway and of the projection from the STN to the GPe as potential mechanisms for beta power enhancement in dopamine-depleted states.

Some experimental studies, on the other hand, support the role of cerebral cortex in the generation and modulation of beta oscillations (Jensen *et al.*, 2005; Fogelson *et al.*, 2006; Yamawaki *et al.*, 2008; Sharott *et al.*, 2018). This perspective has motivated the consideration of cortical interlaminar interactions in the regulation of beta power. In the healthy state, the generation and modulation of beta oscillations has been investigated using DCM (Bhatt *et al.*, 2016), revealing a link between a set of laminar specific interactions within the primary motor cortex and the enhancement/suppression of beta power evoked by movement. Using a theoretical model, Sherman et al. (2016) suggested that high beta power events in the physiological state emerge through cortical laminar interactions conditioned by temporal characteristics of the distal and proximal synaptic drives in the neocortex.

Motivated by these studies, we hypothesized that in the Parkinsonian state an alteration of interlaminar and laminar-specific connectivity in the TC loop contributes to the mechanisms generating the parkinsonian spectral profile. We focused on the TC loop due to the anatomical and functional characteristics of this network: 1) the cortex is an optimal target for non-invasive therapeutic techniques such as TMS and TACS (Barker *et al.*, 1985; Cantello *et al.*, 2002; Kobayashi and Pascual-Leone, 2003; Herrmann *et al.*, 2013); 2) the thalamus is the only BGTC node projecting directly to cortex, allowing for the integration of information from subcortical structures to the motor cortex (Wise and Donoghue, 1986; Brazhnik *et al.*, 2016) and 3) cortex and thalamus establish a reciprocal relationship (Hooks *et al.*, 2013), which is thought to play a key role in physiological and pathological sensory and motor computations (Sherman and Guillery, 2009).

In PD, where motor impairments are the cardinal symptoms, understanding the synaptic dynamics and organization of the TC circuit could potentially shed light on pathophysiological mechanisms. Accordingly, we used cross spectral density (CSD) – DCM (Moran *et al.*, 2009,

2011) with a neural mass model of the TC loop (van Wijk *et al.*, 2018) to characterize its contribution to spontaneous beta power fluctuations observed in the motor cortex of 6-OHDA-lesioned Parkinsonian rats.

## 2.2 Methods

### 2.2.1 Electrophysiological recordings in Parkinsonian rats

The spectral data used in this study consisted of motor cortex field potentials (electrocorticograms) recorded in 36 urethane-anesthetized rats rendered Parkinsonian by unilateral 6-OHDA lesions of midbrain dopaminergic neurons. To record electrocorticogram (ECoG) data, a steel screw electrode was implanted over the right somatosensory-motor cortex ipsilateral to the 6-OHDA lesion and referenced to a steel screw electrode implanted over the ipsilateral cerebellar hemisphere. Electrophysiological recordings were carried out 21-42 days after surgery for the induction of 6-OHDA lesions, thus allowing for changes in the BGTC circuit to stabilize. For detailed descriptions of electrode implantation, anaesthesia, surgical induction of 6-OHDA lesions and related procedures, please refer to (Mallet *et al.*, 2008*b*, *a*; Sharott *et al.*, 2017). Only ECoG recordings made during periods of spontaneous 'cortical activation' were considered in this study due to the resemblance of its neural patterns to those found across the BG circuit of unmedicated PD patients (Mallet *et al.*, 2008*b*). All experimental procedures were carried out on adult male Sprague-Dawley rats (Charles River, Margate, UK) and were conducted in accordance with the Animals (Scientific Procedures) Act, 1986 (UK).

### 2.2.2 Data processing

All operations described in this section were performed in Matlab 2017a /2018a. Recordings were downsampled to 1000 Hz from 16000 Hz. To characterize the spontaneous beta power fluctuations typically observed in PD, we defined two conditions based on instantaneous beta power – condition one being Low-Power Beta (LPβ) and condition two being High-Power Beta (HPβ). Subsequent dynamic causal modelling was applied on selected data-features (i.e., timeseries) that were representative of the two conditions.

To extract the beta power envelope, we applied a second order band-pass Butterworth filter with cut-off frequencies at 15-35Hz to the ECoG recording and extracted its absolute amplitude

using the Hilbert transform. Each envelope was then divided into non-overlapping epochs of 500 msec. The two conditions were subsequently derived from a relative threshold applied to the area under the envelope across the 500msec epochs: (1) LPβ epochs consisted of segments whose envelope area fell below the 5th percentile of the envelope area observed across all epochs, and (2) HPβ epochs consisted of segments whose envelope area was above the 95th percentile of the envelope area observed across all epochs (Figure **2.1**). 5th and 95th percentile thresholds were determined per dataset. From each recording, we randomly selected 5 epochs per condition. This number corresponds to the minimum number of epochs found in either of the two conditions across all recordings. A detailed comparison between the above threshold and more conventional ones can be found in the Supplementary material (Supplementary Figure S1).

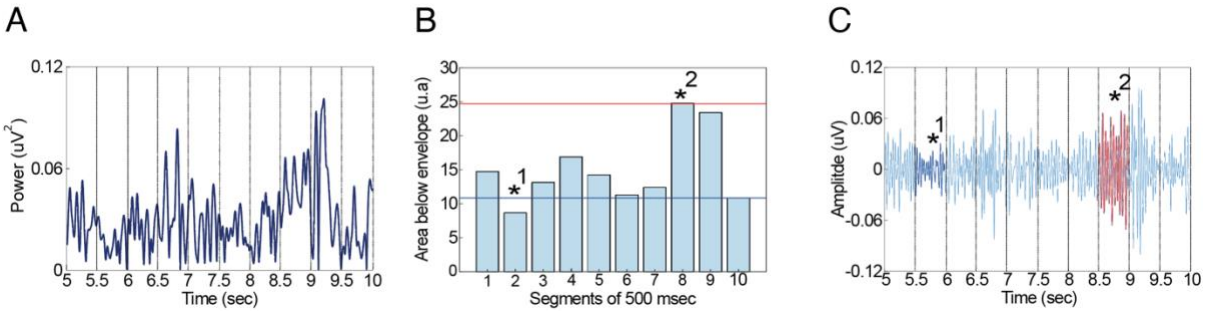


**Figure 2.1 - Extraction of low- and high-power beta features isolated from ECoG data.** Panel A shows the segmentation of the ECoG beta envelope into 500 msec epochs (5 seconds as an example). Panel B depicts the area under the envelope for each epoch. If an epoch had an area under the curve below the 5th percentile of the area under the envelope observed across all epochs (blue line), it was classified as LPβ (*1); if above the 95th percentile of the area observed under the envelope across all epochs (red line), it was classified as HPβ (*2). Both thresholds were determined per dataset. Epochs in between the two percentiles were not considered. Panel C shows the corresponding LPβ (dark blue) and HPβ (red) epochs in the ECoG signal filtered at 15-35 Hz.

## 2.2.3 Dynamic Causal Modelling (DCM)

DCM for cross spectral density is used to infer the hidden (neuronal) states (z) and synaptic parameters (θ) that generate spectral features of observed data (u) (Moran *et al.*, 2009, 2011). Hidden states and unknown parameters cannot be observed directly but can be estimated under a generative or forward model. This model comprises a biophysical neural mass model and the spectral composition of neural and channel noise (Moran *et al.*, 2008*b*). The neural mass model is expressed in terms of a differential equation with the following form:

$$\dot{z} = f(z, u, \theta) \qquad \text{(Equation 2.1)}$$

The neural mass model (f), together with a likelihood model mapping hidden states to observed measurements, constitutes a generative model; namely, a probabilistic mapping between neural fluctuations and the spectral content of observed activity. Using a Bayesian framework, DCM estimates the (posterior) probability density over the synaptic parameters, which are the most likely value of the hidden parameters, given the observed data (Moran *et al.*, 2011). The generative (neural mass) model calls on its biophysical parameters to describe the evolution of voltages (v) and currents (i) in each subpopulation of neurons (Jansen and Rit, 1995). In addition to estimating the posterior density over model parameters (e.g., synaptic connection strengths and the amplitude of neuronal fluctuations), DCM also provides an estimate of the evidence for a particular model or network architecture implicit in the generative model. This allows one to compare different models or hypotheses using Bayesian model comparison. A complete description of the mathematical framework that underwrites DCM can be found in Moran et al., 2013.

**Neural mass model of the Thalamocortical circuit**

A neural mass model of the TC circuit was created comprising two formally distinct neural mass models of the motor cortex and the thalamus using the new generic framework for DCM (van Wijk *et al.,* 2018) (Figure **2.2**). Here, we adopted the motor cortex microcircuit (MMC) model developed by Bhat and colleagues (2016) and coupled it to a model of the thalamus, based on thalamic anatomical literature (Douglas and Martin, 2004; Shepherd and Grillner, 2010). As with previous models of the sensory cortex, and incorporating the work of Yamawaki et al., 2014, Bhat and colleagues (2016) used 3 excitatory subpopulations (neuronal ensembles consisting of "superficial", "middle" and "deep" pyramidal cells located in the supragranular, granular and infragranular cortical layers, respectively) and one common inhibitory subpopulation (inhibitory interneurons) to model the primary motor cortex. In the MMC model, the coupling between these subpopulations (GABAergic or glutamatergic synapses) is tailored according to synaptic characteristics of the primary motor cortex: a reciprocal connection between superficial and middle pyramidal cells (Yamawaki *et al.*, 2014), a reciprocal connection between superficial and deep pyramidal cells (Weiler *et al.*, 2008; Anderson *et al.*, 2010; Hooks *et al.*, 2013; Yamawaki and Shepherd, 2015), a reciprocal connection between each of the three pyramidal subpopulations and the common inhibitory subpopulation (Fino *et*

*al.*, 2013), and a cell type specific self-inhibitory connection (Yoshimura and Callaway, 2005; Bastos *et al.*, 2012). The self-inhibitory connections aim to capture laminar-specific inhibition, mediated by local inhibitory neurons (Kätzel *et al.*, 2011). For further discussion on recurrent inhibitory connections in the context of the canonical microcircuit model, please refer to (Auksztulewicz and Friston, 2015).

In this study, the thalamus was modelled using an excitatory subpopulation (neuronal group of thalamic relay cells) and an inhibitory subpopulation (neuronal group of thalamic reticular cells) (Shepherd and Grillner, 2010) that were connected as follows: a reciprocal connection between relay and reticular cells and a self-inhibitory connection of reticular cells (Shu and McCormick, 2002). Although we acknowledge that there are distinct thalamic nuclei (i.e., neuronal ensembles receiving afferents from different brain regions (Sherman and Guillery, 2009) the thalamus was modelled here as a single neuronal mass model. An important extension of the current work would be to subdivide the motor thalamus (ventral anterior, ventral lateral and ventral medial nuclei in rodents) into input zones that receive GABAergic drive from the BG and glutamatergic drive from the cerebellum (Kuramoto *et al.*, 2011; Nakamura *et al.*, 2014).

To model the extrinsic synaptic interactions between the motor cortex and thalamus we used two corticothalamic projections from deep pyramidal cells to thalamic relay cells and thalamic reticular cells (Bourassa *et al.*, 1995; Jones, 2001). Although the thalamus is thought to project to all layers of the cortex (Hooks *et al.*, 2013) and the ventromedial nucleus (VM) of the motor thalamus has been shown via immunochemistry studies to project mainly to layers I and II of the motor and anterior cingulate cortices (Arbuthnott *et al.*, 1990; Clascá *et al.*, 2012; Kuramoto *et al.*, 2015), it is not clear which TC projections are important in modulating beta power. To resolve this, we considered different models to test the impact of including different connections on model evidence (Figure **2.3**). Operationally, the difference between within-structure (intrinsic) connections and between-structures connections (extrinsic), relies on their propagation delay parameters (

Table **2.1**). Aiming to bring bio-plausibility to the TC neural mass model architecture, here the propagation delays of extrinsic connections (TC and corticothalamic projections) were set to 8msec while the propagation delays of intrinsic dynamics (intracortical and intrathalamic connections) were set to 1msec.

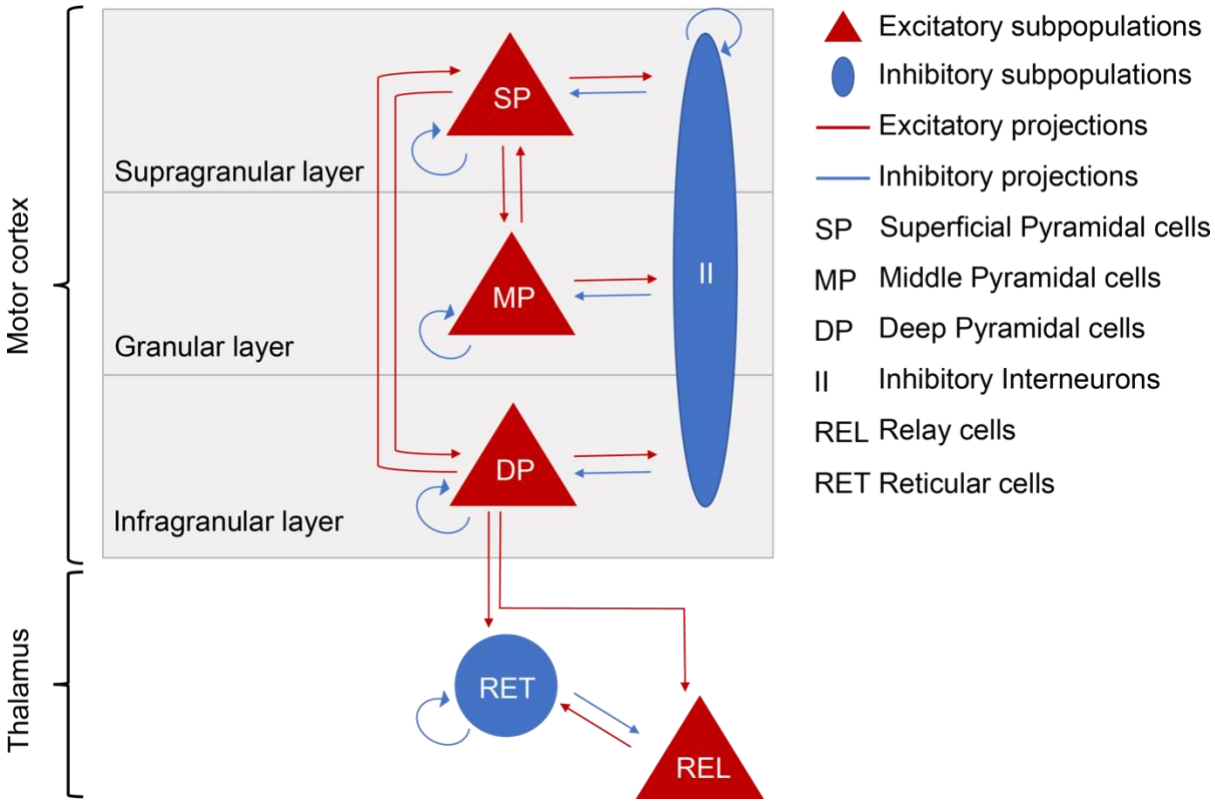


**Figure 2.2– Sources, subpopulations and synaptic projections of a TC loop neural mass model.** The top part of the diagram describes the first source - motor cortex and its subpopulations: superficial pyramidal cells (SP) in the supragranular layer, middle pyramidal cells (MP) in the granular layer, deep pyramidal cells (DP) in the infragranular layer and, inhibitory interneurons (II) as a common inhibitory subpopulation to the 3 cortical laminae. Intrinsic synaptic connections among the above subpopulations comprise a reciprocal connection between superficial and middle pyramidal cells, a reciprocal connection between superficial and deep pyramidal cells, a reciprocal connection between each of the three pyramidal subpopulations and the inhibitory subpopulation and finally, a self-inhibitory connection to each cortical node. The bottom part of the diagram depicts the thalamus and its subpopulations: reticular thalamic cells (RET) as the inhibitory subpopulation of the thalamus and relay cells (REL) as the excitatory subpopulation of the motor thalamus. Intrinsic synaptic connectivity of the thalamus comprises a reciprocal connection between relay and reticular cells and self-inhibitory connection of reticular cells. As corticothalamic extrinsic connections, deep pyramidal cells were considered to send afferents to both relay and reticular subpopulations, while the model space for TC projections is described in section 0 and illustrated in Figure **2.3** (top panel).

### Neural dynamics

In DCM, neural dynamics (i.e., fluctuations in voltages and currents) at the subpopulation level are described by two key operations (Equation 2.2): a convolution operator and an output

operator (Moran *et al.*, 2007). The convolution operator transforms presynaptic inputs (firing rate) into postsynaptic membrane potentials based on a synaptic impulse response function, which considers the nature of the synapse (i.e., excitatory or inhibitory).

The output operator consists of a non-linear function that converts the postsynaptic membrane potentials into a firing rate to be relayed to another subpopulation. This is conveyed through a sigmoid function $S$ which captures the membrane sensitivity and firing threshold of each subpopulation. Furthermore, the shape of the sigmoid function (slope) measures the efficacy of a presynaptic ensemble to generate output. This output is additionally scaled by the synaptic coupling strength as illustrated by the following generic second order differential equation:

$$\ddot{v}_j^a = \left(\gamma_k^a S(v_k^a) + \lambda_m^b S\left(v_m^b\right) + I - 2\dot{v}_j^a - \frac{v_j^a}{T_j^a}\right)/T_j^a \qquad \text{(Equation 2.2)}$$

Here, the averaged membrane potential $v$ of the subpopulation $j$ in the source $a$ is influenced by subpopulations of the same source with synaptic strength $\gamma$ and subpopulations from different sources with synaptic strength $\lambda$. Intrinsic synapses $\gamma$ show a positive synaptic strength if glutamatergic and negative synaptic strength if GABAergic. $S$ denotes the sigmoid function above and $T$ the subpopulation-specific membrane time constant. Endogenous fluctuations or input, $I$ is modelled as a mixture of white and pink noise and drives middle pyramidal cells and thalamic relay cells. The rationale for modelling afferent input to both the motor cortex and thalamus (as opposed to restricting the model to thalamic input) rests on the fact that both motor cortex and thalamus receives input from other (unmodelled) components of the motor system. Examples here include inputs from supplementary motor areas and premotor cortex to primary motor cortex (Jones *et al.*, 1975) and inputs from BZ and CZ to motor thalamus (Kuramoto *et al.*, 2011; Nakamura *et al.*, 2014).

In this study, we used DCM for cross spectral density (Moran *et al.*, 2009, 2011), where the data generated by a model of neural hidden states are expressed as cross spectra in channel space (ECoG screw electrodes). In the context of electrophysiological recordings, the mapping between neural states and observed signals is achieved by a gain function - unlike EEG/MEG data where an electromagnetic forward model is used. Contribution of each neural population to the cortical output is weighted according to parameter J (Table **2.1**- contributing states: [Superficial, Middle and Deep Pyramidal populations] - [0.6 0.2 0.2]) scaled by observation gain L (Table **2.1**- [1]). A detailed description of the transformation from state space to the

frequency domain can be found in (Friston *et al.*, 2012) (pages 442 and 443; section "From models to kernels": equations 5-7).
A summary of the parameters described in this section and their prior values are shown in

Table **2.1**. Prior values were based on previous DCM studies (Bhatt *et al.*, 2016) and optimized for our study.

### Model inversion

In DCM, model inversion iteratively tunes the model's parameters to optimize the fit of the predicted electrophysiological data to the observed data. Using a standard (variational) Bayesian scheme, model inversion uses priors to constrain the search of parameter space to explain the observed spectral features of electrophysiological data. When fitting the data (i.e., inverting the model), the optimization of model parameters uses a variational Laplace scheme to minimize a (free energy) bound on (negative) log model evidence. This free energy approximation to model evidence is subsequently used for model comparison (Friston and Stephan, 2007; Friston *et al.*, 2007).

In brief, model evidence is the (marginal) likelihood of observing data given a model, $p(y|m)$. It reflects a balance between accuracy (goodness of fit between predicted and observed spectral densities) and complexity (divergence between prior and posterior parameter estimates) (Stephan et al., 2010). This balance depends upon the expected precision of the observed data. Given the high signal to noise ratio in the data obtained using the electrocorticographic recording method, the expected precision of observed data was assumed to be high (with a log precision of 12). At this stage, LPβ was set as our baseline condition (with prior expectations optimized to best explain its spectral features). Condition-specific effects (B parameters) on both extrinsic (between-regions) and intrinsic (within-regions) coupling strengths (Moran *et al.*, 2007) were used to explain periods of HPβ. In other words, we estimated the changes in synaptic efficacy required to move from a low-power beta condition to a high-power beta condition.

| Parameters | Description | Prior means (μ) | Log-scaling parameters ($\pi, \sigma^2$) |
|---|---|---|---|
| $\gamma^{mmc}_{1...14}$ | Synaptic coupling strengths motor cortex [Hz] | [800 800 800 800 800 400 800 800 400 200 400 800 800 400] | 0, 1/16 |
| $T^{mmc}_{1...4}$ | Time constant [msec] of cell populations motor cortex: [MP, SP, II, DP] | [8 8 8 8] | 0, 1/16 |
| $\gamma^{tcr}_{1...3}$ | Synaptic coupling strengths motor thalamus [Hz] | [800 800 800] | 0, 1/64 |
| $T^{tcr}_{1...2}$ | Time constants [msec] cell populations thalamus: [RET; REL] | [8 8] | 0, 1/64 |
| $\lambda_{1...4}$ | Extrinsic connections strengths: [CT and TC] [Hz] | [800 800 800 800] | 0, 1/16 |
| $B_{1...8}$ | Condition-specific effects (on coupling strengths): | [0] | 0, 1/8 |
| $R^{mmc}$ | Slope sigmoidal function: | 2/3 | 0, 1/32 |
| $R^{tcr}$ | Slope sigmoidal function: | 2/3 | 0, 1/16 |
| $d_{1...2}$ | Intrinsic delays [msec]: [within MMC; within THAL] | [1] | 0,0 |
| $D_{1...2}$ | Extrinsic delays [msec]: [from MMC to THAL; from THAL to MMC] | [8] | 0,0 |
| $\alpha_c, \beta_c$ | Channel unspecific observation noise | [0 0] | 0, 1/128 |
| $\alpha_s, \beta_s$ | Channel specific observation noise | [0 0] | 0, 1/128 |
| $L$ | Observation gain | [1] | 0, 64 |
| $J$ | Contributing states: [SP, MP, DP] | [0.6 0.2 0.2] | 0, 1/16 |
| $hE$ | Log-precision of observed data | 12 | 0, 1/32 |

**Table 2.1 - Prior expectations set for the parameters of the baseline condition (LPβ).** CT - corticothalamic projections; TC - TC projections; MMC – motor microcircuit; THAL - thalamus; SP - superficial pyramidal cells; MP - middle pyramidal cells; DP – deep pyramidal cells.

### 2.2.4 Bayesian Model Comparison and parameters analysis

A set of models were implemented which varied according to 2 factors: i) the laminar-specificity of TC projections that generate beta oscillations, and ii) the changes in synaptic connectivity within the TC loop (intrinsic and/or extrinsic) required to induce a transition from a LPβ condition to a HPβ condition.

The first factor comprised 9 families (types) of models. These models had identical intrinsic and corticothalamic connections as described in section 2.2.3 - Neural mass model of the thalamocortical circuit and illustrated in Figure **2.2** but differed in the laminar targets of TC afferents: 1) superficial pyramidal cells; 2) middle pyramidal cells; 3) deep pyramidal cells; 4) superficial plus middle pyramidal cells; 5) middle plus deep pyramidal cells; 6) superficial plus deep pyramidal cells; 7) superficial pyramidal cells plus inhibitory interneurons; 8) middle pyramidal cells plus inhibitory interneurons and 9) deep pyramidal cells plus inhibitory interneurons (Figure **2.3**, top panel). It should be noted that the model where the thalamus projects to all three layers of the cortex has not been included in our model space however would be a relevant hypothesis to test in future studies.

The second factor comprised 16 families of models that varied in the set of connections that could show condition specific effects. For each one of the 9 architectures in the first factor, we explored condition specific effects by including or not the following features: intracortical modulatory synapses; intrathalamic modulatory synapses and extrinsic (between cortex and thalamus) modulatory synapses (Figure **2.3**, bottom panel). There were therefore 9 x 16=144 candidate models in total.

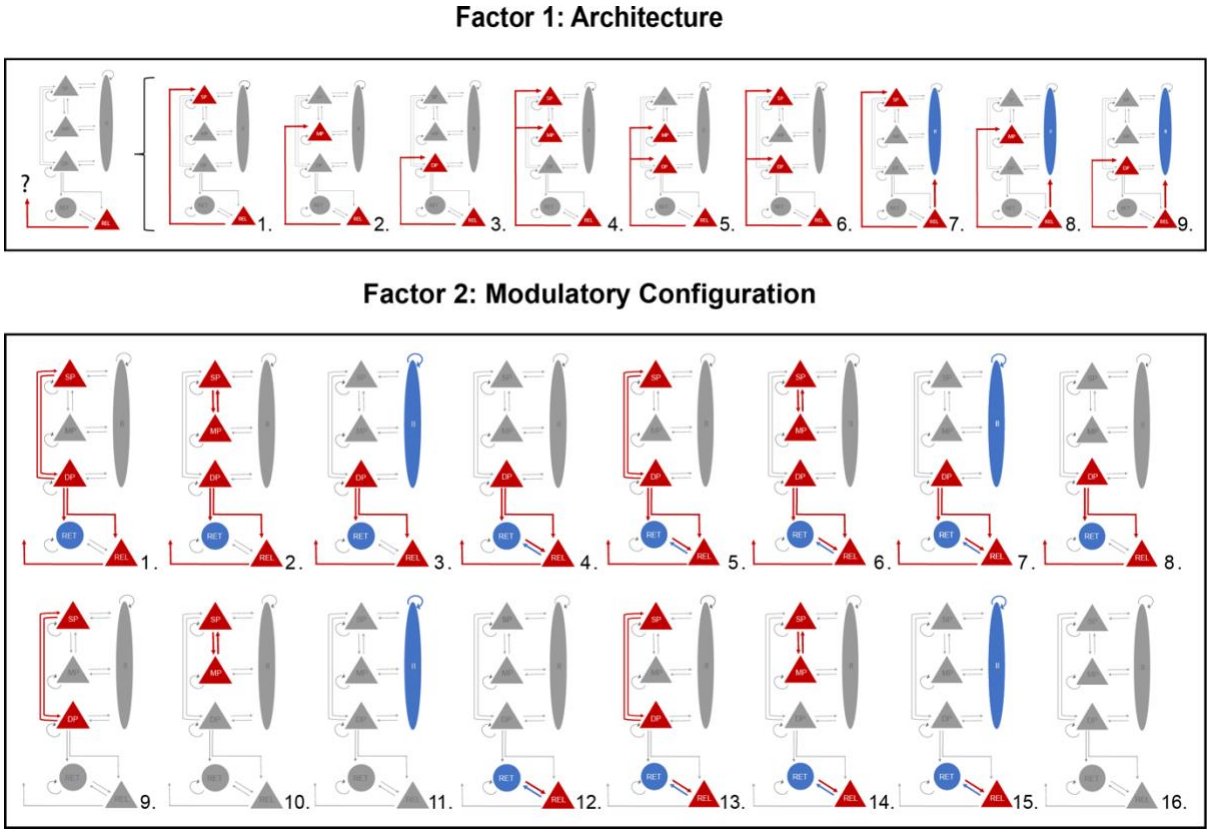


**Figure 2.3 – Competing models of the TC circuit as described by factors 1 and 2 (9 architectures times 16 modulatory configurations).** The diagram on the top (factor 1: architecture) describes the 9 families of models constructed to elucidate which TC projections are the most plausible explanation for the generation of beta oscillations - where (1.- 3.) accounts for a singular projection from thalamus to motor cortex; (4.- 6.) accounts for two afferents to two excitatory subpopulations of the motor cortex, and (7.- 9.) accounts for a combined projection to one excitatory subpopulations and the common inhibitory subpopulation. To disclose the synaptic modulation (intrinsic and/or extrinsic) responsible for an enhancement of beta power, the models on the bottom (factor 2: modulatory configuration) feature 16 different modulatory configurations, under each of the 9 architectures described above. The first eight set of connections (1.-8.) entail extrinsic and intrinsic synaptic modulation (except for model 8, with no intrinsic modulation) and the second eight set of connections (9.-16.) considers intrinsic modulation only. Of note, model 16. features the null hypothesis that neither extrinsic nor intrinsic connections change to explain condition specific changes in cortical beta power (i.e., enhancement of beta). Legend for SP, MP, DP, II, REL, RET and colour scheme are described in Figure **2.2**.

Bayesian Model Comparison (BMC) was used to determine the model with the highest log-model evidence among the models described above (Stephan et al., 2010). We then characterised the parameters of the winning model at the group level using Parametric Empirical Bayes (PEB) (Friston *et al.*, 2015). In brief, PEB uses a hierarchical model, where the parameters from each subject's DCM are summarized by a posterior density (the expected connectivity strength and posterior covariance). Random effects at the between subject level are similarly inferred to inform the group-level parameter estimates. This means that PEB

allows for estimation of fixed and random effects in an optimal fashion; implicitly reducing the influence of "outlier subjects" on the posterior density at the group level. Note that in Bayesian inference, (unstandardized) effect sizes are available explicitly in terms of posterior expectations and Bayesian credible intervals (Standardized effect sizes such as correlations are replaced by differences in model evidence – implicit in Bayesian model comparison). Here, only a subset of parameters was taken to the group level and assumed to exhibit random effects: synaptic coupling strength of intrinsic and extrinsic connections (G and A parameters in the DCM respectively); condition-specific effects on coupling strength (B parameters) and the time constants of subpopulations (T).

# 2.3 Results

## 2.3.1 Model Selection

The model with the highest evidence for the transition from LPβ epochs to HPβ epochs (Figure **2.4**) was that with i) an architecture featuring TC projections from the REL-DP and REL-II in cortex and ii) modulatory changes in: intrinsic connections at the cortical level between SP-MP; intrinsic connections at the thalamic level, between REL-RET; corticothalamic extrinsic connections from DP-REL and DP-RET and TC connections from REL-DP and REL-II (Figure **2.5**). The set of differential equations explaining the neural dynamics of the winning model can be found in the Supplementary Materials (Supplementary Figure S3). The winning model shows a free energy difference (i.e., log Bayes factor) of approximately 6 from the next closest model (Supplementary Figure S2). This corresponds to very high evidence for the winning model, in relation to alternative explanations.

Using fixed-effects Bayesian Model Comparison (FFX-BMC) to make inferences at the family level, the architecture with thalamic projections to DP and II showed the highest evidence across subjects (Figure **2.5**A). Similarly, the condition specific effects in the reciprocal connection between SP-MP, REL-RET and DP-REL plus connections from DP-RET and REL-II had the highest posterior probability (Figure **2.5**B). These results confirm our hypothesis that both the laminar-specificity of extrinsic connectivity and intrinsic connections are key elements underlying the modulation of oscillatory activity in the beta band.

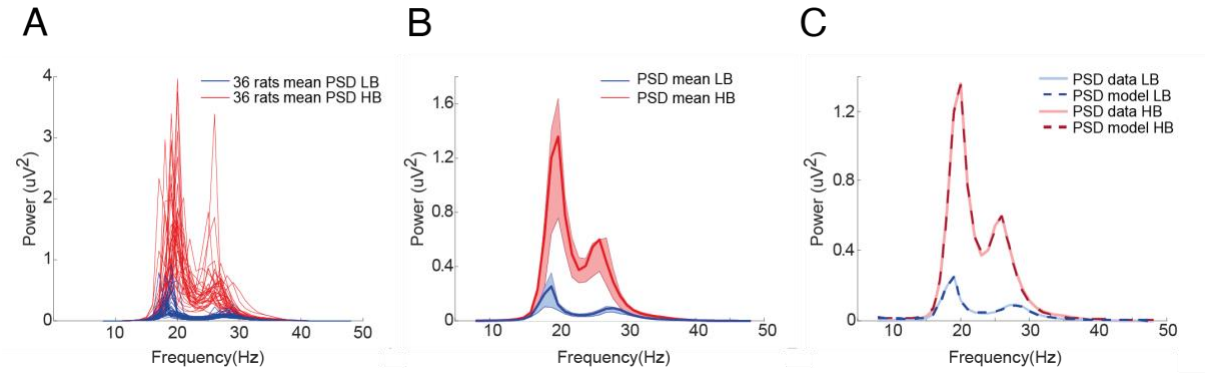


**Figure 2.4 – Observed and expected power spectral densities (PSD).** Panel A shows the spectral features to be explained by a DCM: Red lines depict the mean HPβ spectral densities and blue lines the mean LPβ spectral densities from each of the 36 rats. Panel B depicts the group mean of HPβ spectral densities in red and LPβ spectral densities in blue. Respective variabilities (75th and 25th percentiles of the mean spectra) denoted in light red and light blue. Panel C illustrates the goodness of the fits between mean data spectral densities and spectral densities generated by the winning model. The full red line shows the mean of HPβ data and the dark red dashed line the HPβ spectra estimated by the winning model (correlation coefficient, r=0.9997). The full dark blue line refers to the mean of LPβ data and the dark blue dashed line to the LPβ spectra produced by the winning model (correlation coefficient, r=0.9957).

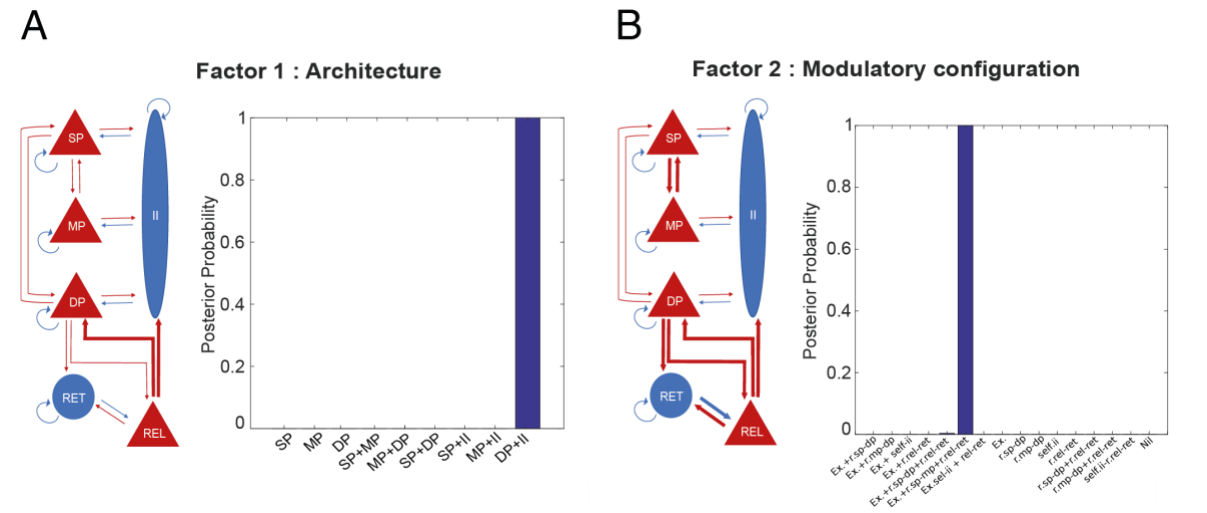


**Figure 2.5 – Schematic and posterior probability of the winning model selected via FFX-BMC.** The Diagram and bar plot in panel A refer to the architecture of the winning model (Figure **2.3**, Factor 1: Architecture, number 9). These results suggest that a TC projection to the deep pyramidal cells and cortical inhibitory subpopulation (in thick lines) were crucial for the generation of beta oscillations and that this effect was consistently observed across subjects (posterior probability of 1). The Diagram and bar plot in panel B indicate the modulatory connections of our winning model (Figure **2.3**, Factor 2: Modulatory configuration, number 6). The diagram shows the set of connections as thick lines to have a higher likelihood (compared to the homologous 15) of inducing the power spectral changes observed (beta enhancement). These being: a reciprocal connection between superficial and middle pyramidal subpopulations, reciprocal connection between thalamic relay and reticular subpopulation and a reciprocal extrinsic connection between deep pyramidal cells and thalamic relay cells, an extrinsic

connection from deep pyramidal cells to thalamic reciprocal cells and from thalamic relay cells to cortical inhibitory interneurons. The bar plot shows a posterior probability greater than 0.99 for the modulatory configuration described above and a negligible posterior probability of approximately 0.004 for a modulatory configuration which assumed the same modulatory characteristics as the winning model except for the intrinsic synaptic mechanisms of the motor cortex; i.e., presenting an intracortical modulation via reciprocal connections between superficial and deep pyramidal cells instead of reciprocal connections between superficial and middle pyramidal cells. (Ex.- extrinsic connections, r. - reciprocal connections, sp. - superficial pyramidal cells, mp. - middle pyramidal cells, dp. - deep pyramidal cells, ii.- inhibitory interneurons, rel. – relay cells and ret. – reticular cells).

## 2.3.2 Parameter analysis

The results from our second level analysis (PEB modelling of A,G,B and T parameters at the group level) suggest that the transition from LPβ state to HPβ state is induced by i) an increase in synaptic strength in connections from relay cells to inhibitory interneurons, relay cells to deep pyramidal cells, middle pyramidal cells to superficial pyramidal cells and relay to reticular cells; plus ii) a reduction of synaptic strength in connections from superficial to middle pyramidal cells, deep pyramidal to both relay and reticular cells and from reticular to relay cells (Figure **2.6**B). Additionally, from the posterior distribution of our B parameters we assessed the effect size of each modulatory connection on the enhancement of beta – illustrated in the bar plot below (Figure **2.6**A).

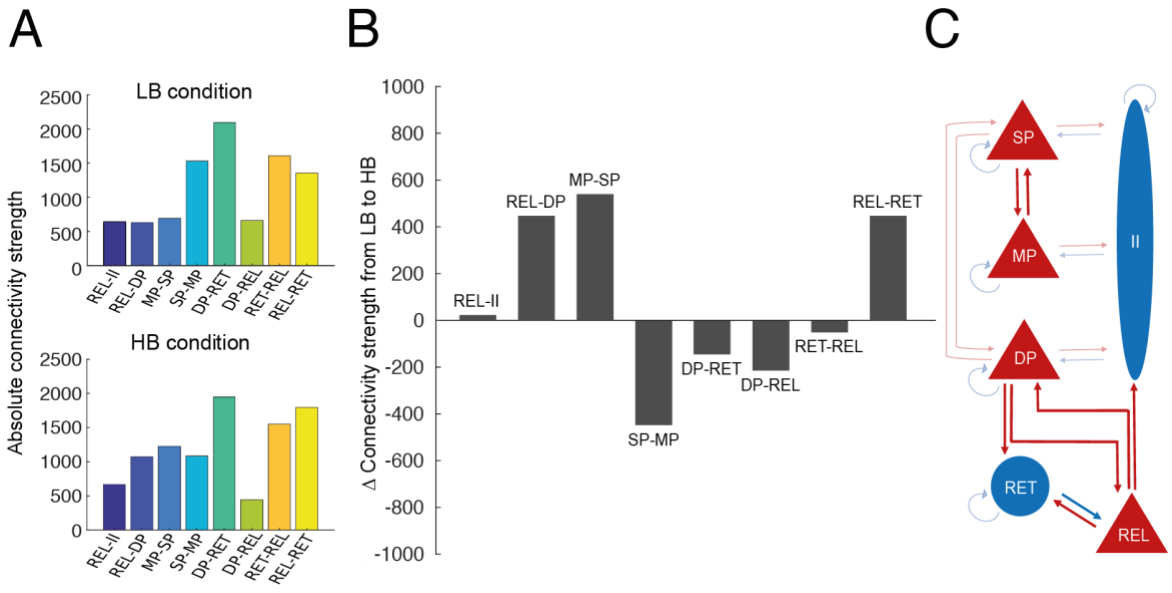


**Figure 2.6 – Average modulatory effect of B parameters (condition-specific parameters) obtained via Parametric empirical Bayes analysis (Friston *et al.*, 2015).** The two bar plots on panel A illustrate the absolute connection strength of each modulatory connection in the low-power (*LB condition)* and high-power (*HB condition*) beta conditions. The bar plot in panel C shows how connectivity strength of B parameter changed at the group level in order to induce an increase of beta power. Negative values

of change indicate a reduction in connectivity strength and positive values an increase. The anatomy of these connections is illustrated in the diagram on panel C.

Considering the connections that showed the greatest change to explain beta enhancement: REL-DP, MP-SP and REL-RET; we further analysed, via forward modelling, the impact of simultaneous alteration of the above connection strengths on the magnitude of beta power. As such, we aimed to characterize the contribution of these three parameters to the gradual transition between the two states – low- and high-power beta. To do so, we have effectively replaced the MP-SP and REL-DP posteriors with values between -1 and 1, while fixing posteriors of the intrinsic connection REL-RET to be weakly or strongly coupled (-1 versus 1), and plotted the summed beta spectral output (15-35Hz) normalised by the summed beta spectral output (15-35Hz) in the baseline condition (i.e., LPβ). This post hoc simulation allows us to characterize the selective effect of specific connections on the expression of cortical beta power level. Figure **2.7**A, suggests that when the intrinsic thalamic connection from relay to reticular cells have low levels of coupling strength, HPβ appears abruptly as the coupling strength from middle to superficial pyramidal cells is increased. This emergence of beta is modulated by the gradual change in coupling strength from thalamic relay cells to deep pyramidal cells, where reduced coupling leads to higher levels of beta.

On the other hand, Figure **2.7**B, suggests that when the connectivity from relay to reticular cells is high, a concurrent increase in the coupling from both relay to deep pyramidal cells and middle to superficial pyramidal cells is required to achieve beta power enhancement. In short, the level of cortical beta depends on the magnitude of excitatory inputs to both superficial and deep pyramidal.

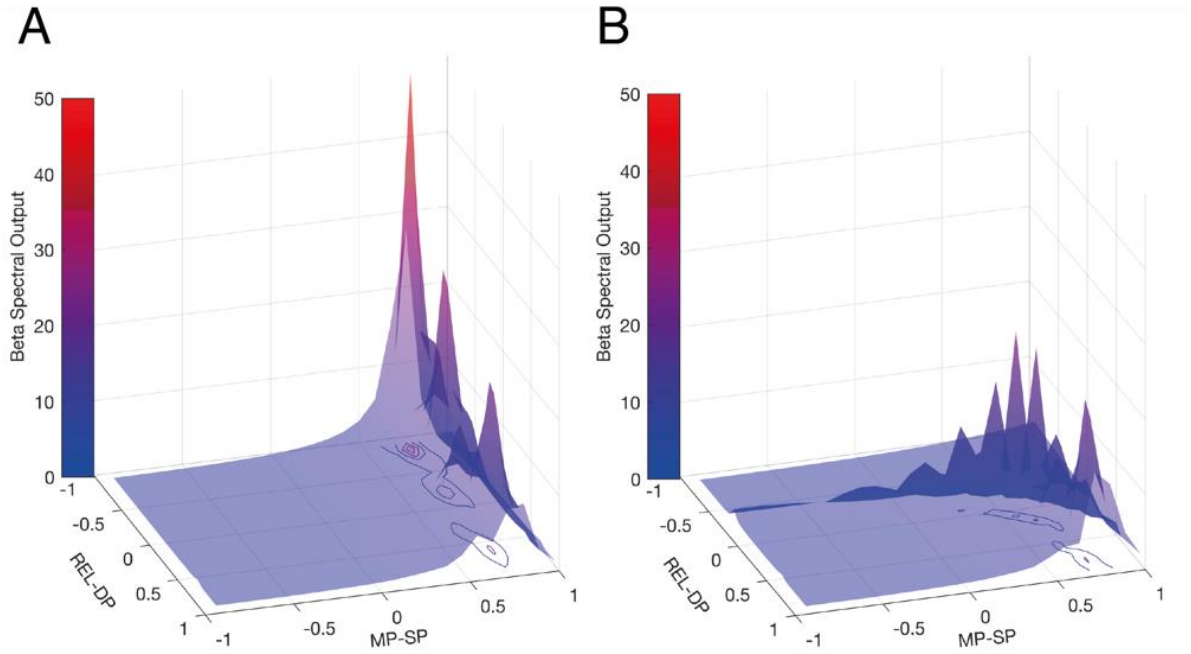


**Figure 2.7- Exploration of parameters space of connections with the greatest effect on beta enhancement.** Panel A shows the impact of changing the coupling strength of MP-SP and REL-DP on the beta spectral output, when the coupling between REL-RET is weak. Here, although an increase in synaptic strength from MP-SP is enough to generate relatively high levels of beta spectral output, the connection from REL-DP seems to have a modulatory effect, i.e., the weaker the extrinsic coupling between relay and deep pyramidal cells the higher the beta spectral output. Panel B considers a (constantly) strong coupling between REL-RET with the same changes in coupling strength between MP-SP and REL-DP. This time, we observe that an increase in beta is achieved with a concurrent strengthening of both MP-SP and REL-DP connections. In both plots, axis x and y denote a reduced connectivity strength when values are between -1 and 0 and an increased connectivity strength when values are between 0 and 1 for connections from middle pyramidal cells to superficial pyramidal cells and from relay cells to deep pyramidal cells respectively. Axis Z and colormap depict the magnitude of beta power.

We additionally explored the spectral output of each subpopulation of our TC neural mass model, by rerunning the winning model and changing the observational parameters to a single population (J=[1]). We observed that all nodes generated spectral curves within the beta band during both conditions and increased their power from condition one (LPβ) to two (HPβ) as expected. Please note that the plotted curves represent the source-space activity, which has been estimated separately for each data set (Figure **2.8**).

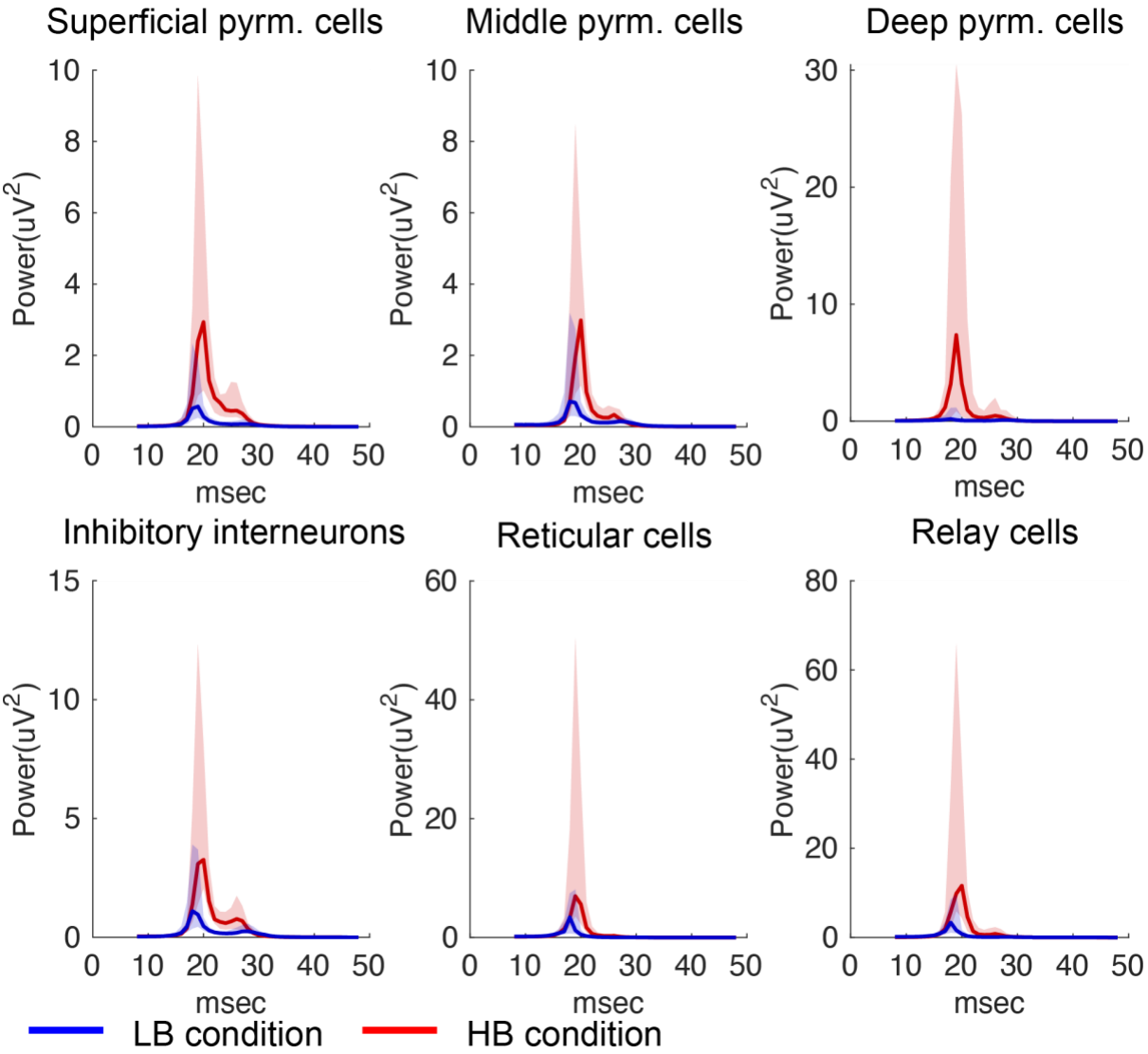


**Figure 2.8 – Spectral output of subpopulations at LPβ and HPβ.** All neural groups (in cortex and thalamus) have generated spectral responses within the beta band in both conditions as expected. Together with an increase in power a small increase in frequency peak of approximately 1-2 Hz is also apparent – when comparing the output generated in condition 1 (LPβ, *LB* in the figure legend) with condition 2 (LPβ, *HB* in the figure legend). Full curves represent the median spectral output across the 36 animals and shaded regions refer to the 25th and 75th percentiles.

## 2.4 Discussion

In this chapter we aimed to identifying the network mechanisms that contribute to the dynamic regulation of beta synchrony in the parkinsonian motor cortex. Focusing on the TC loop of the BGTC circuit, we have employed DCM to identify a model of TC interactions that offers plausible substrates for the transient enhancement of cortical beta. Our study suggests two core features of the TC circuit that may underwrite the genesis of beta oscillations in the

parkinsonian state: 1) laminar specific TC projections; and 2) modulation of synaptic strength across all network levels (i.e., within and between structures).

In-vivo studies of the BGTC circuit suggest that alterations in the firing rate across the direct and indirect pathways are responsible for the motor impairments observed in PD (Smith *et al.*, 1998; Nambu, 2004). Similarly, in-silico simulations of the BGTC circuit propose that an altered coupling from the STN to GPe, and strengthening of the hyperdirect pathway play an important role in the enhancement of beta synchrony following chronic dopamine depletion (Moran *et al.*, 2011; Marreiros *et al.*, 2013). Our study complements the literature on PD, while exploring two novel concepts: i) laminar-specific dynamics within the motor circuit as a putative mechanism for the spontaneous modulation of beta power and ii) short-term synaptic processes, i.e., transient alterations in effective connectivity to be responsible for the spontaneous and intermittent nature of beta power observed in Parkinsonian time-series.

To model different levels of beta synchrony, we extracted LPβ epochs and HPβ epochs from motor cortex ECoG recordings acquired from urethane-anesthetized rodents rendered Parkinsonian by 6-OHDA lesions. This rodent model, in both anaesthetized and behaving state, is useful in capturing the chronic dopamine depletion that is common to 'late stage' PD, and has been widely used for studies of the mechanisms by which excessive beta synchrony arises and propagates within the BGTC circuit in Parkinsonism. (Degos *et al.*, 2009; Avila *et al.*, 2010; Nevado-Holgado *et al.*, 2014; Abdi *et al.*, 2015; Brazhnik *et al.*, 2016).

We have used DCM in this study since it allows for the quantification of effective connectivity changes underlying transient modulations in cortical beta power. Bhatt et al., 2016 have previously employed DCM to link interlaminar dynamics within the motor cortex to the modulation of beta activity, evoked by movement. Fitting MEG data from healthy subjects to a neural mass model of the motor cortex, Bhat and colleagues reported that the increase in beta power observed due to the transition from grip to rest was induced by an increase in the extrinsic input applied to deep and superficial layers of the cortex. Our study suggests that beta power enhancement in Parkinsonism can be attributed to an increase in excitatory inputs to SP and DP; specifically from MP and thalamic relay cells, respectively – and a concomitant reduction of excitatory input from SP to MP. In addition, our results highlight the importance of intrinsic interactions in the thalamus for beta power modulation as the excitatory projection from the thalamic relay cells to reticular cells also contributes to cortical beta enhancement (Figure **2.6**).

Similarly, focusing on cortical intrinsic dynamics, Sherman et al., 2016 used a computational model to generate transient high beta power events (i.e., beta bursts), which were temporally identical to those observed in the somatosensory and frontal cortices in the physiological state. Two circuit features have been proposed as crucial for the generation of beta bursts: 1) a drive from the lemniscal thalamus to the proximal dendrites of the pyramidal neurons and inhibitory interneurons in L2/3 and L5 (via the granular layer) and 2) a strong drive from the nonlemniscal thalamus to the distal dendrites of the pyramidal neurons and inhibitory interneurons found in supragranular and infragranular layers.

It should be noted that due to the nature of the neural mass models employed in this study, we were not able to model detailed dendritic dynamics that contribute to the generation and modulation of neural activity in the beta band. This way, instead of accounting for variable propagation delays for inputs arriving to distal and proximal dendrites, here we have assumed fixed conduction delays for all within-region connections (1ms) and between-regions projections (8ms). Such creates a distinction between the excitatory input received by the superficial pyramidal cells versus those received by the deep pyramidal cells and the common inhibitory population; since the latter are attributed to extrinsic projections from thalamus, these are inherently modelled with longer conduction delays. Nonetheless, our results relate to the observations made in Sherman et al., 2016, given that comparable circuitry mechanisms yielded similar oscillatory effects. In other words, both studies propose that laminar specific glutamatergic inputs to the motor cortex must occur at two temporally separate instances in order to achieve high-power beta oscillatory activity.

Furthermore, it is worth noting that alternative models of the TC circuit showing thalamic projections to both the superficial and deep layers of the motor cortex (i.e., all models with architecture number 6, shown in Figure **2.3**), had lower model evidence than the winning model. Possibly because, unlike the winning model, simultaneous projections from thalamic relay cells to superficial and deep layers do not allow for a differentiation in input delays. Detailed analysis of the parameter space on gradual beta increase, opposed to a transition from extremely low to extremely high- power beta, further corroborated that the intrinsic (shorter delay) input from middle to superficial cells should have high levels of synaptic strength – together with the extrinsic (longer delay) input from the thalamic relay to deep pyramidal cells – to explain an up-regulation of beta synchrony when the coupling from thalamic relay to reticular is strong. (Figure **2.7**B). Nevertheless, taking both scenarios into account – strong vs

weak connectivity from relay cells to reticular cells - projections to superficial pyramidal cells via middle pyramidal cells must assume a moderate coupling strength to avoid a ramping up of beta synchrony at the cortical level; highlighting a potential substrate that could be targeted in order to control and modulate cortical beta.

An important difference between Sherman et al., 2016 and our study stems from the assumptions made on thalamic activity patterns. Sherman et al., 2016 posit that thalamic activity should be in the alpha band to drive beta bursts in the somatosensory and frontal cortices. However, in our study, thalamic neurons exhibited activity in the beta band during both low- and high-power conditions (Figure **2.8**). Our results are supported by recent experimental work showing a substantial and coherent enhancement of beta activity (30-36Hz) in the motor thalamus and motor cortex of behaving 6-OHDA-lesioned rats (Brazhnik *et al.*, 2016). There is also evidence of aberrant beta synchrony in the thalamus of unmedicated PD patients (Kempf *et al.*, 2009).Taken together, these results emphasise that thalamic neural activity in the beta band is likely to be a contributing circuit feature for the generation of aberrant beta synchronization in PD, and highlight a functional coupling between the thalamus and deep layers of the motor cortex.

### 2.4.1 Limitations and Future Directions

We would like to highlight that in DCM, "winning model" is a relative terminology. Winning model is effectively the most plausible model to generate the observed data among the set of models tested. As indeed there are plenty of configurations a neural mass model can assume (here 144 were tested) , DCM is only a robust method if used as a hypothesis-driven approach (Stephan et al., 2010).

Finally, an interesting extension of this study would involve using a conductance based neural mass model of the TC circuit to investigate in detail the intrinsic neurotransmitter dynamics underlying beta enhancement in the parkinsonian TC circuit. While convolution-based models are useful in explaining the "macroscopic mechanisms" underlying a given data set, such as network architecture and effective connectivity; conductance-based models would capture the dynamics of intrinsic ion channel mediators, such as Glutamaergic and GABAergic receptors (refer to Moran et al., 2013). This could be extremely interesting given the modulatory role that GABA-A is thought to exert over beta oscillations (Jensen *et al.*, 2005; Yamawaki *et al.*, 2008; Hall *et al.*, 2010; Brazhnik *et al.*, 2016).

## 2.5 Conclusion

A broadly accepted postulate concerning healthy and Parkinsonian states of the BGTC circuit is that they exhibit differential patterns of synchronization at beta frequencies (Gatev *et al.*, 2006; Hammond *et al.*, 2007; Brittain and Brown, 2014). While exaggerated beta synchronization has been associated with more frequent high power beta bursts in PD (Little *et al.*, 2013, Tinkhauser *et al.*, 2017*a*), healthy states seem to manifest as an adequate proportion of high beta events and therefore a flexible motor behaviour (Feingold *et al.*, 2015; Sherman *et al.*, 2016). Following this reasoning, a recognition of the mechanisms adopted by the BGTC network to regulate beta spectral undulations is vital to better understand healthy and diseased states; and consequently, inform novel therapeutic strategies. Here, using DCM, we highlight a set of synaptic alterations in the TC loop that elucidate how the transitions of beta synchrony from low to high levels might occur in PD. We provide a new perspective for the effective coupling of the Parkinsonian TC network, where a fine regulation of temporally different inputs to specific laminae of the motor cortex may underlie the spontaneous and transient variability in oscillatory neural activity in the beta band across the circuit.

# 3 Temporal dynamics of cortico-subcortical interactions in experimental Parkinsonism

## 3.1 Introduction

In PD, loss of dopamine is associated with pathologically enhanced beta (13-30Hz) oscillations across the BGTC network (Mallet *et al.*, 2008*b*; Jenkinson and Brown, 2011; Devergnas *et al.*, 2014; Brazhnik *et al.*, 2016, Cagnan *et al.*, 2019*b*). This is thought to drastically impair the information coding capacity of the motor circuit, leading to debilitating motor symptoms such as rigidity and bradykinesia (Murer *et al.*, 2002; Cruz *et al.*, 2009; Tinkhauser *et al.*, 2018; Khawaldeh *et al.*, 2020). Disruption of beta synchrony, evidenced by a drop in beta power at individual nodes of the BGTC network, and suppression of coherence between nuclei, is observed in most PD patients when treated with levodopa (Brown *et al.*, 2001; Levy *et al.*, 2002; Priori *et al.*, 2004; Silberstein *et al.*, 2005; Weinberger *et al.*, 2006) or high-frequency DBS (Kühn *et al.*, 2006; Eusebio *et al.*, 2011; Wang *et al.*, 2018). Recent studies have revealed that beta synchronization, in both diseased (Tinkhauser *et al.*, 2017*a*; Torrecillos *et al.*, 2018, Cagnan *et al.*, 2019*b*) and healthy states (Feingold *et al.*, 2015; Lundqvist *et al.*, 2016; Sherman *et al.*, 2016; Little *et al.*, 2019; Zich *et al.*, 2020), is best depicted by transient bursts of enhanced beta activity (β-bursts). Accordingly, in PD is the rate and duration of β-bursts that seems to positively correlate with the severity of PD motor symptoms (Tinkhauser *et al.*, 2017*a*, *b*; Vinding *et al.*, 2020). This recent shift in perspective, from averaged beta power to the presence of episodic beta bursts, has been leading many to investigate the transient network dynamics underlying β-bursts in order to uncover the most efficient way of interacting with this synchronous state (Tinkhauser *et al.*, 2018, Cagnan *et al.*, 2019*b*; Reis *et al.*, 2019; West *et al.*, 2020, 2021). It has been shown that alongside brief increases in the cortical beta power (cortical β-bursts), there is a transient increase in phase and amplitude synchrony between the STN and cortex of PD patients (Tinkhauser *et al.*, 2018, Cagnan *et al.*, 2019*b*). This is recapitulated when analysing single unit and neural ensemble recordings of the striatum, GPe and the STN of the 6-OHDA lesioned rat model of PD (Cagnan *et al.*, 2019*b*). The aforementioned studies do however lack a temporal characterisation of beta dynamics across the output nuclei of the BGTC circuit: the BG-output nucleus – Substantia Nigra reticulata

(SNr) and the part of the motor thalamus which receives projections from the SNr and projects back to the cortex (BZ).

Given the prominent role that the motor thalamus seems to play on the emergence and maintenance of cortical beta oscillations during PD (Brazhnik *et al.*, 2016; Reis *et al.*, 2019; West *et al.*, 2020), we hypothesised that analogously to what has been described across different BG nodes, transient modulation of beta within the SNr and the BZ, and beta coupling between the subcortical regions and cortex, occur alongside with cortical beta bursting. Accordingly, in this chapter, we interrogated the temporal dynamics of neuronal activity in the SNr and its afferent thalamic region, in the context of cortical beta bursting. To this end, we have used archival neural ensemble and single unit activity from the SNr and BZ thalamus, recorded simultaneously with frontal Electrocorticogram (ECoG) signals from 7 urethane-anaesthetised 6-OHDA lesioned rats (Nakamura el al., unpublished).

# 3.2 Methods

## 3.2.1 Recordings from Parkinsonian Rats

6-OHDA lesions of midbrain dopamine neurons were induced unilaterally in 7 rats (175–250 g), as previously detailed (Mallet *et al.*, 2008*a, b*, 2012; Abdi *et al.*, 2015). Lesions were assessed 14–16 days after the 6-OHDA injection using apomorphine (Schwarting and Huston, 1996*b*), and were considered successful when animals made ≥80 net contraversive rotations in 20 minutes (Abdi *et al.*, 2015). Electrophysiological recordings were acquired from the frontal cortex, BZ thalamus and SNr, ipsilateral to 6-OHDA lesions in anesthetized rats 21–51 days after surgery.

ECoG recordings were acquired with a 1 mm-diameter screw above the frontal (somatic sensory-motor) cortex and referenced to a screw implanted above the ipsilateral cerebellum (Mallet *et al.*, 2012; Abdi *et al.*, 2015). Simultaneous extracellular recordings of unit activity and wideband signals (0.1–6,000 Hz) were made from various sites in the BZ thalamus (5 rats; 97 recordings) and SNr (4 rats; 199 recordings) using silicon probes (NeuroNexus). Following electrophysiological recordings, only thalamic neurons were juxtacellularly labelled with neurobiotin as described elsewhere (Sharott *et al.*, 2012; Doig *et al.*, 2014; Nakamura *et al.*,

2014). Unit activity, wide band signals and the ECoG were sampled at 17.9 kHz and posteriorly downsampled to 1000Hz.

Data was visually inspected so that only epochs of spontaneous 'cortical activation' would be selected for analysis. Activated brain states in the urethane-anaesthetised 6-OHDA rat consist of an important model to study parkinsonism where patterns of neural activity resemble those observed in recordings from awake and unmedicated PD patients (Mallet *et al.*, 2008*b*).

### 3.2.2 Data Processing

Recordings were analysed using custom-written software in MATLAB. From the silicon probe recordings, the following two types of signals were extracted:

**BUA**

Background-unit activity (BUA) is a continuous signal which represent ensemble spiking activity of neurons in the vicinity of the recording contact. BUA was extracted from the silicon probe recordings, after high-pass filtering the wide-band probe signal at 300Hz using a third-order Butterworth filter and removing large-amplitude spikes. To remove large-amplitude spikes, a threshold at mean + 4 SD of the recording was set, and a 4-ms segment around each threshold crossing was removed to be replaced by a randomly selected part of the recording that did not contain any spiking activity (Moran *et al.*, 2008*a*). Following the removal of spikes, the data was rectified, and low-pass filtered at 300 Hz using a third-order Butterworth filter. BUA activity in the beta frequency band (BUAβ) was derived by filtering (second-order Butterworth filter) the BUA activity ±5Hz around the frequency of highest coherence with the frontal ECoG within the beta frequency band (15 to 35 Hz).

**SUA**

Single-unit activity (SUA) was extracted from the band-pass filtered (500 to 6,000 Hz) wide-band probe signals following standard "spike sorting" procedures (Mallet *et al.*, 2008*b*), such as template matching, principal component analysis, and supervised clustering (Spike2). Only units with a distinct refractory period in the interspike interval (ISI) histograms (<1% of all ISIs were <2 ms) were classified as single units.

### ECoG and BUA spectral analysis

Power and coherence of cortical and subcortical signals were calculated (Figure **3.1**) using a Fast Fourier Transform (FFT) size of 1000 (i.e., frequency resolution of 1Hz) and 50% of overlap of FFT windows. For power spectra, each individual power spectrum between 1-80Hz was normalised to the sum of the total power. To ensure that the computed changes in beta dynamics were not spurious, ECoG/BUA pairs were included in for further analysis only if the summed coherence between 15 and 35 Hz was greater than 10% of the total coherence from 1 to 500 Hz. These were 55/97 BZ contacts and 79/119 contacts in the SNr. Next, cortical and subcortical signals were filtered ±5 Hz around the beta peak coherence between each pair of ECoG/BUA recordings, using a second-order Butterworth filter.

### β-burst definition

β-bursts were derived from the frontal ECoG and subcortical BUAs (BZ and SNr). β-bursts were defined as segments where the instantaneous beta amplitude of these signals surpassed the 75th percentile across the entire recording for at least 1 beta cycle (i.e., 50 ms) (Tinkhauser *et al.*, 2017*b*, 2018) . β-burst onset and offset consisted of the first and last points of the $75^{th}$ percentile threshold crossing, respectively and were adjusted to the nearest 0° (within ±30 ms of the threshold crossing). Phase adjustment of β-burst was done across all analyses so that neural events locked to the cortical beta could be detected. Instantaneous beta amplitude and phase were derived from the magnitude and phase of the Hilbert transform, respectively. Finally, β-bursts were divided into short and long according to their duration, unless otherwise stated. β-bursts were considered short if their duration was longer than 50 ms but shorter than the median duration of all β-bursts for a given recording, and considered long if their duration was longer than the median duration of all β-bursts for a given recording.

To assess whether the observed beta dynamics at the ensemble level were preserved with a different burst definition, we have recomputed BUA analyses using the $55^{th}$ and $95^{th}$ amplitude percentile threshold to define beta bursts. Results are shown in the Supplementary Figure S4 for BUA BZ.

### 3.2.3 Assessing beta dynamics at the neural ensemble level

**Modulation of BUA β amplitude**

To assess whether subcortical beta gets modulated during cortical β-bursting, we first computed the magnitude of the Hilbert transformed ECoGβ and BUAβ signals. Next, the BUAβ envelope was aligned to the ECoG β-burst onset, defined according to the 75th percentile crossing and normalised with respect to the median BUAβ envelope -500 ms prior the onset of β-burst. Changes in beta activity were statistically tested using a cluster-based nonparametric statistics (detailed in section 3.2.5). Results of this analysis are shown on Figure **3.2**A and Figure **3.2**B.

**β-burst overlaps**

To investigate whether cortical and subcortical signals concurrently displayed high beta power activity, β-burst overlap was calculated between the ECoG and subcortical BUAs from the BZ and SNr, separately. For a pair of cortico-subcortical signals, β-bursts were first identified for the cortical and subcortical recording as defined above, i.e., as events where the instantaneous beta amplitude exceeded the $75^{th}$ percentile of the amplitude calculated across the entire recording. Next, the two time-series were discretised according to the position of a given point relative to a β-burst, i.e., a 1 was assigned to points inside a burst, and a 0 to those outside a burst. By adding the two discretised time-series we then calculated the percentage duration of overlapping bursts relative to the total burst duration in the ECoG (%OVL). This normalisation accounted for the total burst duration variation across rats.

β-burst overlaps between ECoG/BZ and ECoG/SNr were compared to the percentage duration of overlap achieved by chance (%OVL due to chance) (Tinkhauser *et al.*, 2018). For each of the discretised time-series of a given pair, a breaking point was randomly selected across the length of the signal and the two segments were shuffled. The %OVL was calculated for these shuffled discretised signals. This procedure was repeated 100 times and the average across iterations yielded the %OVL due to chance for that given pair. While this iterative process preserves beta burst properties (number and duration), it excludes any biologically driven overlap between bursts and keeps only those due to chance. Results from this analysis are shown on Figure **3.2**C and Figure **3.2**D.

### Modulation of BUAβ-ECoGβ phase-locking

To assess whether the phase relationship between cortical and subcortical beta gets modulated during ECoG β-bursting, the instantaneous phase of both signals was first derived from the Hilbert transform of the beta band-pass filtered ECoG and BUAs in the beta band. Next, phase alignment (ϕj) was calculated by subtracting the instantaneous phase of the BUAβ from that of the ECoGβ. Phase alignment values were corrected to be within ± π and their consistency was calculated by computing the Phase Synchrony Index (PSI) along two different dimensions: across bursts (Figure **3.3**A and 3.3C) and in time (Figure **3.3**B and 3.3D). PSI in time was computed by dividing the burst period (±500 ms around the β-burst onset), into 50 ms-overlapping windows which advanced every 1 ms, and deriving the PSI for each window using Equation 3.1 (N=number of samples corresponding to 50 ms). With this analysis we were interested in capturing the average temporal evolution of cortico-subcortical synchronization during each individual burst, irrespective of changes in the cortico-subcortical phase relationship across bursts. Conversely, to measure the consistency of phase differences across bursts (which might be compromised by two signals having different frequencies across different bursts), PSI across bursts was computed by deriving PSI at a given time point across all β-bursts using Equation 3.1 (N=number of β-bursts).

$$PSI = \left| \left( \sum_{j=1}^{j=N} \exp^{-i\phi_j} \right) \right| / N \qquad \text{(Equation 3.1)}$$

For both analyses, PSI values from each BUAβ/ECoGβ recording pair were first z-scored and then averaged across different pairs. Periods of significant phase-locking modulation between BUAβ /ECoGβ were determined using a cluster-based nonparametric statistical test (explained in section 3.2.5).

### Analysis of phase slips in the cortico-subcortical phase alignment

To investigate whether discontinuities in the beta subcortico-cortical phase alignment were related to the emergence of stable synchronization, we first computed the phase alignment between the two signals. This was done by subtracting the Hilbert-transformed-derived instantaneous phase of the BUAβ from that of the ECoGβ. Phase alignment between each recording pair (BUA and ECoG) was next unwrapped, differentiated and z-scored. Unwrapped phase alignment values showing either a positive derivative greater than 1.96 (z score) or a negative derivative less than -1.96 (z score) were labelled as a phase slip. Next, a binary time

series was created by setting phase slips to 1 and the remaining samples to 0. Transformed time series from each BUA/ECoG pair were then averaged across recording pairs for the 25 longest β-bursts and smoothed using a moving average filter of length 10 ms (Figure **3.4**A). To evaluate how consistent phase-slips were across bursts, data was collapsed across the 25 longest β-bursts, and the overall probability of phase slips occurring 200 ms prior to the reference point was compared to that 200 ms after using a paired t-test (Figure **3.4**B).

To better understand the functional role of phase-slips, we evaluated the cortico-subcortical phase stability around a phase slip by assessing the angular difference between cortico-subcortical phase-alignments across 50 ms epochs found 1) before a phase slip and after a burst onset 2) right after a phase slip and after a burst onset (Figure **3.4**C). For this analysis phase-slips used as reference were those with an index that was the closest to burst onset (i.e., within -200 to 0 msec).

### 3.2.4 Assessing beta dynamics at the unit level

In this set of analyses, ECoG signals were band-pass filtered from 15 and 35Hz with a second order Butterworth filter and only units which were significantly locked to the ECoG β signal (Rayleigh test, alpha = 0.05) were included for further analysis.

#### Burst-triggered averaging of spiking activity

To explore whether the firing properties of subcortical neurons got modulated by cortical beta bursting, we first transformed the spiking activity of BZ thalamus and the SNr units into a binary time series where the peak point in each spike was set to 1. This binary signal was convolved with a Gaussian (SD of 25ms), and divided into segments centred on the onset of each ECoG β-burst (±200ms). The burst-triggered spiking activity of each unit was computed by z-scoring the average of the centred data segments. Only units whose burst-triggered spiking activity had a peak above 1.96 (z score) were included on the grand average (Figure **3.5**A). To discern between phase-driven modulation and that evoked by slower changes in firing rate, the absolute beta amplitude of burst-triggered spiking activities aligned to adjusted ECoG β-burst onsets were compared to that aligned to non-phase adjusted ECoG β-burst onsets (Figure **3.5**B). A cluster-based nonparametric statistical test (described on section 3.2.5) was used to determine when these two time-courses differed significantly.

#### Phase-locking analysis with a cycle-by-cycle resolution

To investigate whether the evolution of cortical β-bursting was associated with how single units lock to cortical β we looked at whether the vector-length and preferred phase at which a unit spikes relatively to the cortical beta, varied across beta cycles (5 cycles around ECoG β-burst onset). To this end, first the instantaneous phase and amplitude of the ECoG β signal were extracted via Hilbert transformation. Next, using the instantaneous ECoG β amplitude the onset of each ECoG β-burst was found according to the 75$^{th}$ percentile threshold method and adjusted to the nearest 0 degree. For each ECoG β-burst onset the 5 preceding and succeeding ECoG β cycles were identified and used as reference points for further analyses.

Lastly, ECoG β phase values corresponding to subcortical spiking activity were extracted in order to compute the vector length and mean angle of locking at each one of the 11 β cycles (5 cycles around the adjusted ECoG β-burst onset). To assess whether the vector length of BZ thalamic spiking and SNr spiking were significantly modulated by ECoG β cycle position with respect to ECoG β-burst onset, a Kruskal–Wallis ANOVA was used (alpha=0.025, using Bonferoni correction for number of neuron group). Results of this analysis are shown in Figure **3.6**.

### 3.2.5 Statistical analysis

#### Cluster-based nonparametric statistical test for statistical comparison of time series

Statistical difference between 2 time series (condition A - averaged data aligned to β-burst onset and condition B - averaged data aligned to random points) was determined using the ft_timelockstatistics function from the MATLAB tool-box FieldTrip. After computing a paired t test to compare condition A and condition B, clusters were defined according to neighbouring samples where the t value exceeded that corresponding to a pre-determined threshold ($p < 0.05$). Subsequently, t values inside these clusters were summed to yield a cluster-level t statistic. This procedure was repeated 2,000 times while randomly swapping labels between the 2 conditions. Clusters were labelled as significant if their summed t-statistic value exceeded 97.5% of the randomized distribution (i.e., the distribution of the maximal summed t-statistic values collated across the 2,000 random reassignments). This would correspond to an alpha level of 0.025, since we were interested in testing for both positive and negative differences.

# 3.3 Results

## 3.3.1 Beta dynamics of subcortical neural populations

In this study we describe the temporal evolution of beta dynamics across the output nuclei of the BGTC circuit (the SNr, and part of the thalamus that receives input from the BG) and motor cortex in experimental Parkinsonism. Using simultaneously recorded signals of the frontal cortex and subcortical regions (BZ thalamus and SNr) of urethane-anesthetised 6-OHDA lesion rats we investigated whether changes in amplitude and phase-locking between subcortical and cortical beta activity occurred alongside β-bursting. To address this, we first confirmed that cortical and subcortical signals of our urethane-anesthetised 6-OHDA lesioned rats presented synchronous beta oscillations. This is shown in Figure **3.1**, where the averaged power of subcortical and cortical signals plus the coherence across them shows a peak in the beta band.

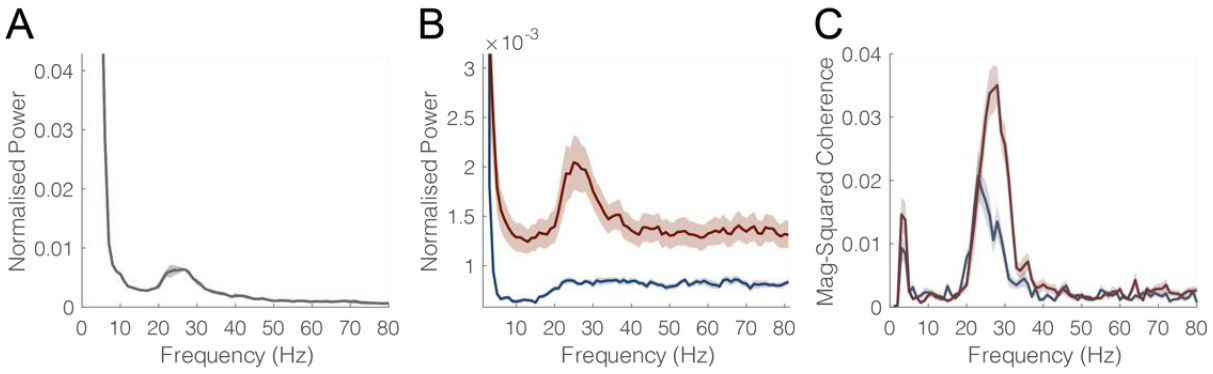


**Figure 3.1- Beta oscillatory profile of neural recordings in 7 urethane-anaesthetised 6-OHDA lesioned rats.** Panel A shows the averaged power spectrum of all frontal ECoG recordings (normalised to the total power). Panel B shows the averaged power spectrum of ensemble unit activity of the BZ thalamus (red) and SNr (blue). Panel C shows the averaged magnitude-squared coherence between ECoG/BZ recordings (red) and ECoG/SNr (blue). Shaded regions in the three panels denote the mean±SEM.

### Modulation of subcortical beta activity during cortical beta bursting

All our analyses have been performed relative to the onset of ECoG β-bursts, except in the few cases where the termination point of a burst was also used as a reference point (shown in Supplementary Figure S5). ECoG β-bursting was defined as any period where the instantaneous beta amplitude exceeded the 75th percentile derived from the entire recording for longer than 50 ms. Referencing our synchronization calculations to ECoG β-bursts allowed

us to descriptively compare how synchronous dynamics across the BG-output nucleus, its receiving parts of the thalamus and the cortex behaved in the experimental parkinsonian state. Using the β filtered BUAs and their envelopes, we first found that beta rhythms in both BZ and SNr were transiently modulated around the onset (Figure **3.2**A and B) and offset (Supplementary Figure S5B) of ECoG β-bursting. This transient modulation consisted of a modest (less than 10%) but significant increase in beta activity which occurred when aligning the data to both short β and long β-bursts (i.e., β-bursts with durations below and above the median duration of all β-bursts, respectively). Importantly, effects were significantly larger when data was aligned to β-bursts than when aligned to randomly selected points in the data (cluster based non-parametric analysis, described on section 3.2.5).

To further assess the temporal organisation of beta synchrony across the pathway, we computed the percentage of overlap between beta bursts (%OVL) derived from the ECoG, and the BZ and SNr BUA signals. Here %OVL was computed from bursting periods that co-occurred between pairs of cortical and subcortical signals, which were normalised to the total duration of β-bursting in the ECoG signal and statistically contrasted against percentage of overlap by chance (detailed in the methods section 3.2.3 - *β-burst overlaps*). ECoG β-bursting showed an average 14.9±3.5 %OVL with the BZ thalamus (Figure **3.2**C) and 15.1±3.1 %OVL with the SNr (Figure **3.2**D). Overlapping percentages in both cases were above chance level (%OVL by chance of 12.0±0.8 for BZ and 12.2±0.8 for SNr; $p<0.05$).

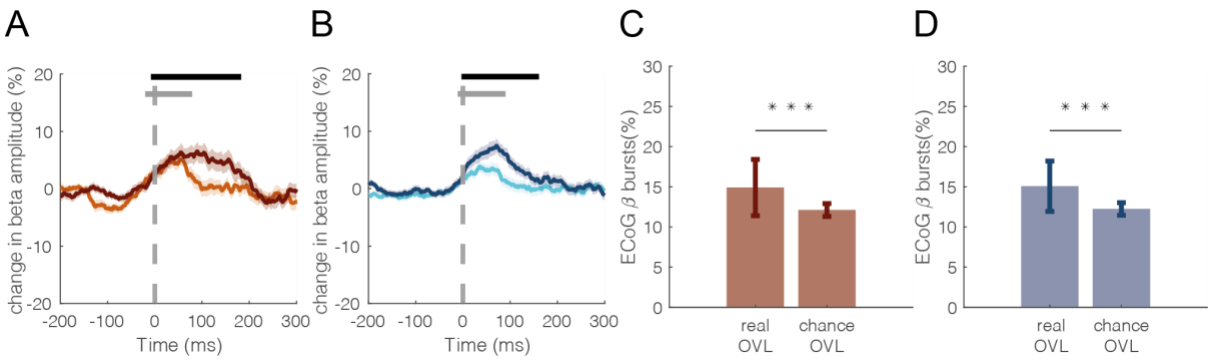


**Figure 3.2 - Significant and concurrent enhancement of beta activity in the cortical and subcortical regions.** Panel A shows the modulation of BZ BUAβ amplitude during both short (orange) and long (red) ECoG β-bursts. Periods of significant beta activity modulation with respect to the baseline (cluster-based analysis, $p<0.025$) are indicated with horizontal bars, with grey coding for short and black for long ECoG β-bursts. Panel B shows the same as A but for BUA recordings from the SNr. Shaded regions indicate median±SEM across all recordings made from each subcortical region. Panels B and C show the percentage of ECoG β-bursts that overlapped with BZ and SNr β-bursts, respectively.

The average percentage of overlapping β-bursts between cortical and subcortical regions (first bar) is contrasted with the averaged percentage of overlapping β-bursts occurring by chance (second bar). Error bars indicate mean±1SD. β-burst overlap between ECoG/BZ and ECoG/SNr is small (14.9±3.5 and 15.1±3.1) but significant ($p<0.001$, ***) in the experimental parkinsonian state.

### Subcortico-cortical beta phase-relationship

We have also explored the temporal dynamics of interregional beta synchrony by investigating the changes in phase coupling strength between ECoG/BZ and ECoG/SNr beta activity around ECoG β-bursting. To assess changes in phase coupling we used the phase synchrony index (PSI). PSI was computed using the phase alignment between the Hilbert transform-derived phases of cortico-subcortical signals across two dimensions: in time, with a moving window of 50 ms along each burst (-200 ms and +300 ms around the onset of a beta burst); and across bursts where PSI was calculated for each time point (-200 ms to +300 ms centred on the beta burst onset) across all cortical beta bursts.

In both cases, SNrβ/ECoGβ and BZβ/ECoGβ, we found periods of significant phase coupling modulation around ECoG β-bursting. This was true for both metrics (PSI in time, Figure **3.3**A and C, and PSI across bursts, Figure **3.3**B and D), where a transient increase in phase synchrony index occurred around the ECoG β-burst onset, and was terminated concurrently with the offset of ECoG β-bursts (Supplementary Figure S5C and D). Together the increase in PSI during and across ECoG β-bursts indicate that interregional synchronization is increased in individual bursts and that the conditions for such synchronisation, i.e., the cortico-subcortical phase differences, are stable across bursts.

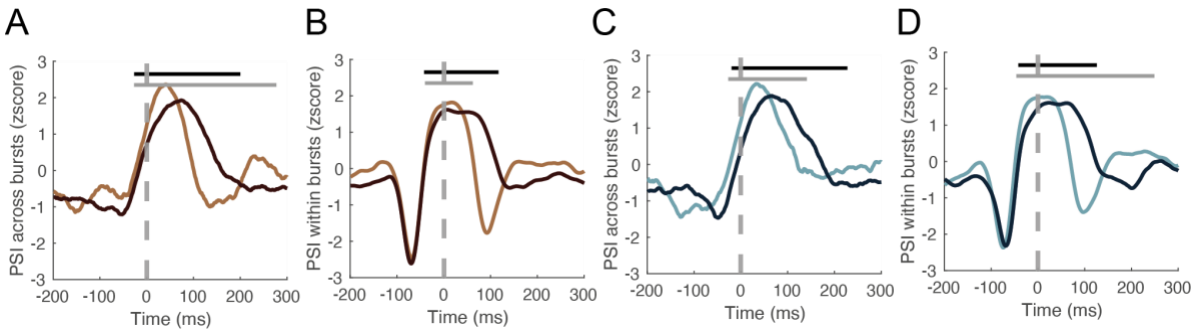


**Figure 3.3 – Transient enhancement of phase-coupling between ECoGβ and subcorticalβ is associated with ECoGβ-bursting.** The evolution of Phase Synchrony Index (PSI) across bursts (panel A) and across time (panel B) between ECoGβ and BZ BUAβ is shown during cortical β-bursts (short bursts in orange and long bursts in brown). PSI across bursts and in time between ECoGβ and SNr BUAβ when aligned to ECoGβ-bursting (aligned to short bursts in light blue and to long bursts in dark blue) is shown in panel C and D respectively. Modulation of PSI in the burst-aligned data was statistically compared to that aligned to random points in the data using a cluster-based analysis. Significant periods of PSI modulation ($p<0.025$) are indicated by horizontal bars where grey denotes short bursts and black indicates significant periods of long bursts. In all plots, the grey dashed line indicates onset of ECoGβ-bursting and the shaded regions indicate the median±SEM across recordings.

Complementary to this analysis, we looked into the probability of the phase alignment between subcortical-cortical regions suffering abrupt changes around the onset and offset of ECoG β-bursting. Figure **3.4**A shows the evolution of phase alignment in time (averaged within a 10ms window) for the 25 longest cortical bursts where the probability of observing an abrupt change in phase alignment (phase slip) is depicted in the inset colormap. Together with Figure **3.4**B, which looks at the average probability of a phase slip around beta bursts, abrupt changes in the alignment of subcortical-cortical beta activity show a higher likelihood of occurring before the onset of a cortical beta burst rather than during a cortical beta burst ($p<0.0001$).

Lastly, the top rose plots (Figure **3.4**C) show that the angular difference between preferred locking phases just before a phase slip and right after a β-burst onset is not consistent for BZ units (Rayleigh test, $p=0.59$) and tends to be out of phase for SNr units ($p=0.008$, angular difference of 180 degrees). Right after a phase slip occurs, the preferred angle at which units in both BZ and SNr regions lock to the ECoG beta, is the same as the angle inside a β-burst, i.e., there is a 0° phase difference between the preferred phase alignment of units to ECoG after the slip and during the burst (bottom rose plots on Figure **3.4**C, Rayleigh test, $p<0.0001$ both ECoG/BZ and ECoG/SNr).

Overall, these results suggest that after a phase slip, a relatively constant phase-relationship between SNr BUAβ/ECoGβ and BZ BUAβ/ECoGβ is established, creating the necessary conditions for beta activity to increase locally in both cortex and subcortical regions (Figure **3.2**A and B).

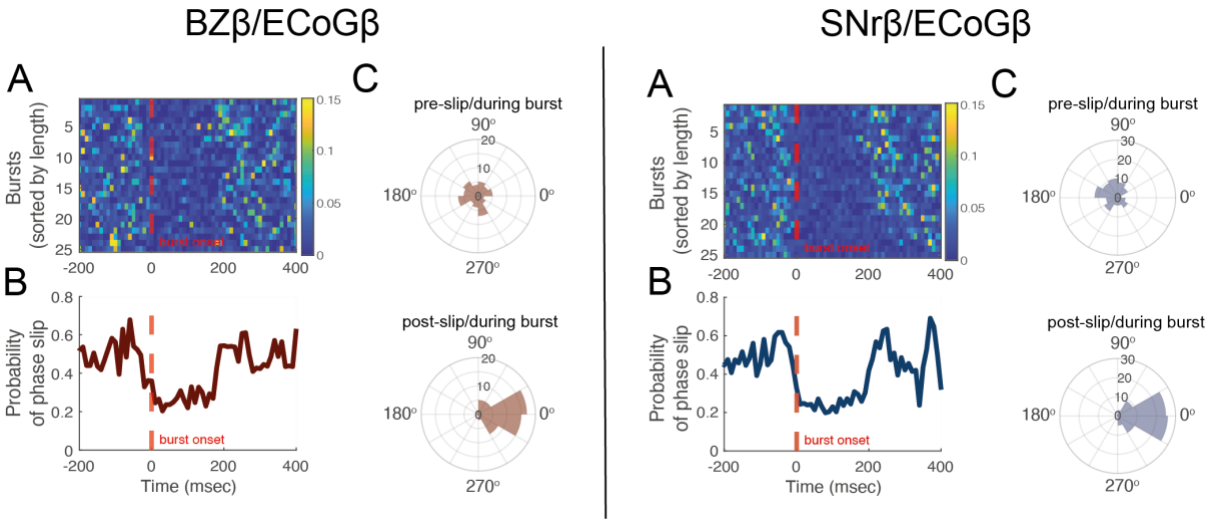


**Figure 3.4 - Abrupt changes in cortico-subcortical beta phase-alignment precedes the elevation of cortical beta amplitude above threshold levels.** Phase slips consisted of data points where the z-score difference between adjacent unwrapped ECoGβ and subcortical BUAβ phase alignment was greater than 1.96 or less than -1.96. Heat maps on panel A show the probability of observing phase slips between cortical beta and BZ thalamus beta ("BZβ/ECoGβ", left) and cortical beta and SNr beta ("SNrβ/ECoGβ", right) during the 25 longest cortical beta bursts. While abundant before onset of a burst, phase slips were scarce during bursts. Panel B corroborates this information by showing that across bursts there is a higher (averaged) probability of BZβ/ECoGβ (left, red) and SNrβ/ECoGβ (right, blue) phase slips occurring in the 200 ms prior to burst onset than in the 200 ms following burst onset ($p<0.0001$ for both cortico-subcortical phase alignments). Panel C shows that right after a phase slip (50 msec window), the established cortico-subcortical phase-alignment is identical to that observed inside a burst ("post-slip/during burst", Rayleigh test $p<0.0001$), whereas the angular differences between the cortico-subcortical phase-alignment found right before a phase slip and inside a burst diverge ("pre-slip/during burst", Rayleigh test, $p>0.05$ on BZβ/ECoGβ pairs only).

We further assessed beta dynamics with respect to beta bursts detected in the BZ or SNr, by recomputing all the analyses above. This is summarised in Supplementary Figure S6 and highlights that irrespective of the reference signal, dynamics characterised around a beta burst were consistent and hardly distinguishable.

Taken as a whole, the above results suggest that in experimental Parkinsonism, local and inter-regional changes in beta activity of the BG-output, the BG-recipient part of the thalamus and

the motor cortex occur simultaneously and in a temporally well-defined manner. As cortical beta amplitude surpasses it's 75$^{th}$ percentile and evolves in time, the instantaneous beta amplitude of subcortical neuronal ensembles (or cortical ones when the reference is subcortical) transiently increase by about 10% (Figure **3.2** and Supplementary Figure S6 right and left panels). These neural events are however immediately preceded by an abrupt reorganization of cortico-subcortico phase alignment, whereby the likelihood of subcortico-cortico phase-slips plummets, finally leading to a strengthening of phase coupling between ECoG and BUA beta (Figure **3.3**A).

### 3.3.2 Modulation of subcortical single unit locking properties to cortical beta

Action potentials from all single neurons in the BZ (firing rate= 20±9 spikes/sec) and ~46% of single units in the SNr (firing rate= 29±12spikes/sec), were significantly locked to ECoG β (15-35Hz) (Rayleigh test, $p < 0.05$, 10/10 BZ and 19/35 SNr). The preferred angle at which the BZ and SNr locked to cortical beta was 148$^{o}$ and 239$^{o}$, respectively. Further investigating whether the firing properties of these subcortical units were modulated during ECoGβ-bursts, we found that instead of a modulation in the firing rate, there was a modulation in the timing of action potentials. This was true for both BZ and SNr neurons, where a transient oscillatory firing pattern (with a period of around 50ms), emerged before and after the adjusted cortical β-burst onset (Figure **3.5**A). Despite of only including individual β-burst onset-triggered unit averages with a peak value above 1.96 (z-score) in our grand average, the firing rate evolution of BZ and SNr neurons showed a peak below 1.96 z-score (n=16 SNr; n=10 BZ) (Figure **3.5**B). When inspecting the alignment of peaks and troughs across individual onset-triggered unit averages in a greater detail, a jitter of a few milliseconds can be visually observed (example provided for BZ units in Supplementary Figure S7). This suggests that within our pool of BZ and SNr neurons, the preferred ECoG β angle at which these neurons locked was not exactly the same.

In both structures however, the beta content of these weakly phase-locked oscillatory events, was greater than those where unit averages were triggered from either non-phase adjusted ECoGβ-burst onsets or randomly selected points across the ECoG beta signal (Figure **3.5**B, cluster-based analysis, described on section 3.2.5).

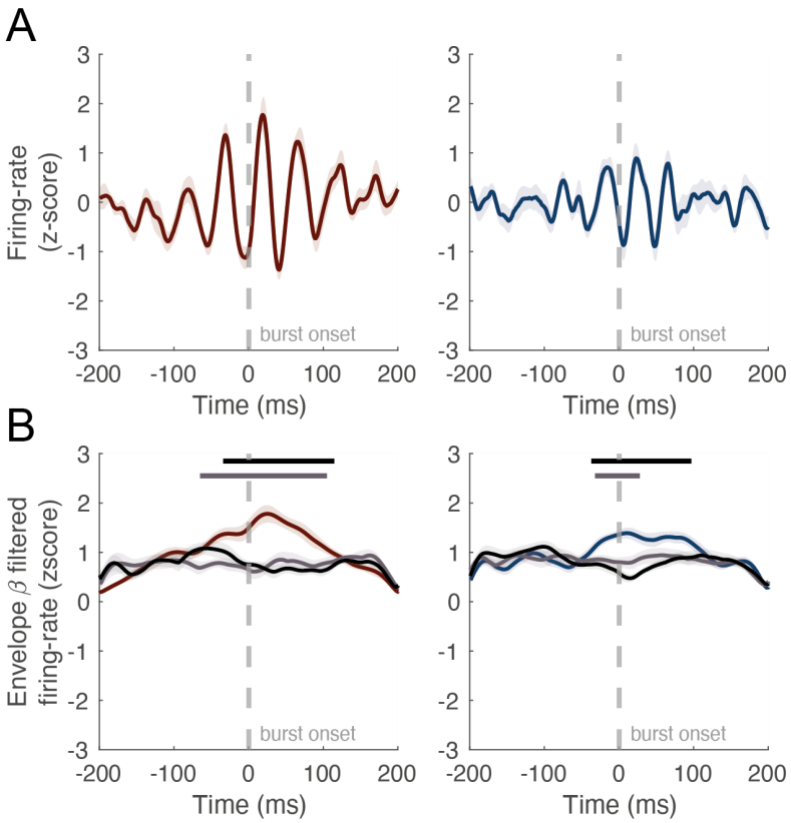


**Figure 3.5 - BZ and SNr units transiently phase-lock to ECoG β-bursts.** Panel A shows the mean z-scored firing rate of single units (unfiltered) in the BZ (left-hand side) and SNr (right-hand side) triggered at ECoGβ-bursts onset adjusted to the cortical beta 0 phase. Mean firing rate of single units in each region were also computed around non-adjusted ECoGβ-bursts onsets and around reference points randomly selected along the ECoGβ recording (n=1000). For each region, individual z-scored firing rates of single units triggered around the three reference points (adjusted onset, non-adjusted onset, baseline), were filtered in the beta band (band pass [15-35Hz], 2$^{nd}$ order Butterworth filter) and their absolute amplitude was computed using the Hilbert transform. Panel B compares the firing pattern evolution in the beta frequency of units in BZ (on the left-hand side, average in red) and SNr (on right-hand side, average in blue) when triggered by adjusted ECoGβ-bursts onset to those 1) triggered around non-adjusted ECoGβ-bursts onsets (in grey) and 2) triggered around random points (in black). Periods of significant firing pattern modulation in the beta band during ECoGβ-bursts are denoted for both BZ and SNr units by the horizontal lines (as detailed in section 3.2.5), colour-matched to the different conditions.

Having established that during ECoGβ-bursts the BZ and SNr units transiently phase-lock to the cortical beta, we aimed to explore the synchronisation conditions underlying this

observation. To this end, we computed the phase-locking properties between subcortical units and the cortical beta (vector length and preferred phase), as the amplitude of the ECoG β-burst evolved (over 10 beta cycles centred around ECoG β-burst onset). We found that phase-locking strength of SNr but not BZ subcortical units to cortical beta was significantly modulated by beta cycle progression (Figure **3.6**A, Kruskal–Wallis ANOVA, p=0.015 and p=0.659, respectively). Using a post hoc Dunn-Sidak test we found that the coupling of SNr units to the ECoG β one cycle prior to β-burst onset (cycle -1) was significantly larger than the one found at the cycle proceeding β-burst onset (cycle 1). It is possible that the non-significant results found for the locking of BZ units to the cortical beta were due to the amount of data available for this analysis (BZ units, n=10). A larger sample of BZ units would be necessary to confirm that indeed unlike the BG, BZ neurons do not show a significant modulation of locking strength over the time course of a β-burst.

Locking of subcortical spikes to cortical beta was maintained across several beta cycles and clustered around $142^{o}\pm43$SD and $255^{o}\pm64$SD in the case of BZ and SNr neurons, respectively (Figure **3.6**A). However, it is worth highlighting that locking of subcortical units to cortical beta was not consistent across all cycles. Cycles with significant locking across units ($p<0.05$, Rayleigh test) are indicated in Figure **3.6** with a full diamond shape and consisted of cycles -5, -1 and 1 to 5 for BZ and cycles -4, -2, 1 and 4, for SNr (cycle 0 contains the ECoG β-burst onset).

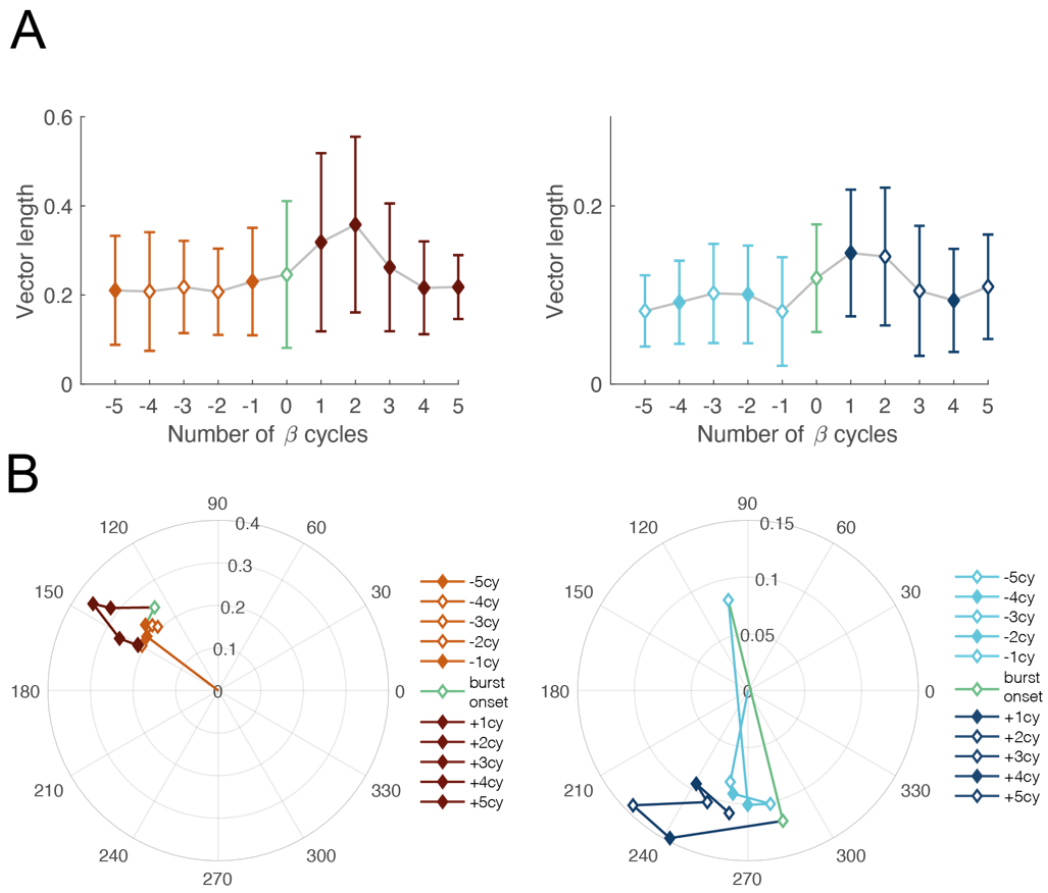


**Figure 3.6 - Phase-locking strength of SNr but not BZ units to cortical beta is significantly modulated by beta cycle progression.** Panel A shows the mean vector length ±1 SD (error bars) of the phase-locking of subcortical action potentials to the ECoG beta ±5 oscillation cycles around an ECoG β-burst onset (cycle 0) for units in the BZ (n=10, left hand side) and SNr (n=15, right hand side). Only the locking of SNr spikes to ECoG beta was significantly modulated across cycles (Kruskal–Wallis ANOVA, P = 0.015 SNr and p=0.659 BZ). Panel B displays the preferred locking angle of spikes (position on circle) of each neuron type (BZ on the left hand-side and SNr on the right-hand side) in each ECoG β cycle (±5 oscillation cycles). The distance at which each symbol is from the centre denotes the average vector length as shown in panel A. Filled diamond symbols denote cycles at which the preferred locking angle of spikes to cortical beta across the different units is uniform (p<0.05, Rayleigh test).

## 3.4 Discussion

We found that fluctuations in beta oscillatory activity within the substantia nigra reticulata, the motor thalamus and the somatosensory cortex of rats rendered parkinsonian, occur simultaneously and are preceded by abrupt changes in cortico-subcortical phase coupling. These results support the hypothesis that beta bursts emerge and evolve in a spatially and temporally segregated manner (Cagnan *et al.*, 2019*b*; Zich *et al.*, 2020), which is sustained by long-range coupling between structures of the motor circuit (Tinkhauser *et al.*, 2018, Cagnan

*et al.*, 2019*b*). Results from this chapter contribute to a more complete characterisation of the network dynamics underlying beta bursts, as until the present date, a temporal description of beta dynamics across the BG-output, its recipient nucleus in the motor thalamus and cortex has been lacking. From a translational perspective, this is important as it might shed light on how to interact with the emergence and propagation of aberrant synchrony more efficiently and consequently recover motor function in Parkinson's.

6-OHDA lesions induced an increased power and coherence around 25 Hz in the SNr, BZ thalamus and cortex. This is in good agreement with previous reports on the spectral properties of recordings from different BG nodes of the same disease model; namely the STN (Mallet *et al.*, 2008*b*, *a*), GPe (Mallet *et al.*, 2008*a*), and striatum (Sharott *et al.*, 2017). A temporal characterisation of this oscillatory biomarker across these different nodes of the BG was recently reported by Cagnan and colleagues, 2019. In that study, authors made use of spiking of single neuron, as well as population-level beta activities recorded from the striatum, STN, GPe of 6-OHDA lesioned rats and found a set of neural events which preceded the emergence of cortical beta bursts. These were, an abrupt increase in coupling strength between beta activities of the BG and ECoG, a transient shift of the preferred phase at which BG neurons locked to cortical β and a modulation of the firing pattern of BG single units. In this chapter we used a comparable data set (unit and ensemble neuronal activity recorded simultaneously with ECoG signals), and found that beta synchrony across the SNr, BZ thalamus and cortex was extremely similar to those described in the previous study. In particular, we found that when aligned to a burst, transient changes in subcortical beta activity were larger than spontaneous fluctuations observed in the baseline. Although consistent across bursts, this modulation seldomly corresponded to increases in beta amplitude above its 75th percentile – evidenced by a cortico-subcortical burst overlap of 15%. Likewise, at the single unit level, BZ and SNr neurons started firing in a temporally organized manner, assuming an oscillatory pattern in the beta frequency-band (~50ms/cycle), right before the cortical beta burst onset. Again, despite showing a beta profile larger than that in the baseline, transient spike-triggered averages showed a modest magnitude (peak<1.69 z-score). Assuming that the amplitude of oscillatory activity translates levels of local synchrony (Buzsáki *et al.*, 2012), the above observations suggest that at the time of beta bursting, local synchrony across the return pathway of the BGTC circuit increases simultaneously but not to similar levels.

Prominent in our results is the modulation of the phase-relationship between cortical and subcortical beta activities around the onset of high beta power cortical events. This is shown through a set of complementary analyses at the population and unit level. Our data suggests the following course of events: right before an increase in the cortical beta power surpasses the predetermined threshold, SNr and BZ thalamic units transiently lock their firing to cortical beta. At the population level, this is evidenced by a phase slip in the phase alignment between cortical and subcortical regions. After this abrupt reorganisation, the probability of phase slips decreases and the phase-relationship between regions stabilises until burst offset. This neural process creates the necessary conditions to temporarily strengthen the coupling between cortical and subcortical regions (shown by an increase in phase synchrony index), yielding an increase in synchrony (shown by local amplitude enhancement and coincidence of bursts above chance level). Importantly, similar to what is observed in other regions of the BG (Cagnan *et al.*, 2019*b*), the strength at which SNr units locked to cortical beta changed significantly as cortical bursts evolved, i.e., across -5 to +5 beta cycles from the adjusted cortical burst onsets (Kruskal–Wallis ANOVA, $P = 0.015$ SNr). Also, at the unit level the vector-length of phases at which SNr units lock to cortical beta right before a beta burst onset is significantly different from that succeeding it. This together with the fact that there is no significant locking across units at the cycle pre-burst, but there is significant locking on the cycle after, suggests once more that in a very short period of time subcortical spikes assume a specific phase alignment with respect to cortical rhythms. We believe that this early and significant alignment between the BZ-output and cortical beta activity might potentially mediate an enhancement of local synchrony and subsequent propagation across the network.

Across the entire dataset, most subcortical units were significantly locked to ECoG β (100% of BZ units and 46% SNr units, Rayleigh test, $p<0.05$), at 239º and 148º, for SNr and BZ neurons respectively. These mean angles match those reported by Brazhnik et al., 2016, where the locking of action potentials from the SNr and ventral medial thalamus (part of BZ thalamus) to cortical beta LFPs in 6-OHDA lesioned rats, were 269º and 122º (after shifting phase values by 180°, to match the polarity of our ECoG and their LFPs recordings), respectively in awake and behaving animals. The preferred locking angles for SNr and BZ units differed by 270 degrees, which corresponds to 21-50 msec in the beta band (15–35 Hz). This tallies well with the inhibitory nature of the nigrothalamic synapses and is in line with previous literature where the pause duration of BZ spiking immediately after optogenetic stimulation of SNr axons was found to be ≥ 20 ms (Edgerton and Jaeger, 2014). Indeed, it has been experimentally shown

that inhibitory inputs from the BZ-output to the motor thalamus are crucial for the maintenance of beta resonance across the circuit (Brazhnik *et al.*, 2016). In Brazhnik et al., 2016, the infusion of picrotoxin (a GABAA antagonist) and muscimol (a GABAA agonist) into the ventral medial thalamus (nucleus contained in BZ), induced opposite spectral and behavioural effects in the behaving parkinsonian rats. This is, while picrotoxin reduced beta power and coherence in and between the motor cortex and SNr while restoring the lesioned rats' ability to walk, muscimol led to an enhancement of the cortical–SNr local power and coherence (Brazhnik *et al.*, 2016). In our data, despite lacking simultaneous recordings from the SNr and BZ thalamus to assess changes in SNr-BZ coupling during cortical beta bursting, the fact that similar beta dynamics occur between SNr-cortex and BZ-cortex around cortical beta bursts, support the idea that motor thalamus is entrained by the BG at beta frequencies, which in turn maintains or even exacerbates beta synchrony at the cortical level.

A growing body of literature indicates that high incidence of long oscillatory events with high beta power at specific structures of the motor circuit correlates with the severity of motor deficits in PD (Tinkhauser *et al.*, 2017*a*, *b*; Deffains *et al.*, 2018; Vinding *et al.*, 2020). We found that, before an increase in local synchrony can be detected via amplitude thresholding, an abrupt change in phase alignment between regions occurs. This observation provides important insights into the pathophysiological mechanisms underlying PD, and has the potential to be harnessed into a novel stimulation strategy to improve the treatment of PD patients with DBS. Our results support the view that stimulation delivered to subcortical targets at a specific phase of the cortical beta would be sufficient to prevent the motor circuit from entering specific phase-alignments which facilitate the emergence of local and long-range beta synchronisation (McNamara *et al.*, 2020; West *et al.*, 2020). Feasibility of this strategy has been experimentally demonstrated in a recent study by McNamara and colleagues, whereby stimulation delivered to the GPe of 6-OHDA lesioned rats at a specific phase of the cortical beta, significantly reduced the network's beta power (McNamara *et al.*, 2020). With a similar rational, but this time employing computational methods (West *et al.*, 2021), West and colleagues went further and demonstrated that while stimulation delivered to the cortex according to a specific phase of the STN beta was capable of reducing beta power (increasing average inter-burst interval and reducing mean burst durations), the efficacy of this strategy proved to be highly dependent on the network state. This is, that both magnitude of beta suppression and the precise stimulation timing yielding optimal suppression depended on how strongly or loosely coupled specific subloops of the BGTC circuit were (West *et al.*, 2020).

### 3.4.1 Limitations and future directions

In the current study we have made use of archival data from the parkinsonian rat model obtained in the anaesthetized and cortically activated state (Nakamura *et al.*, 2021). While this model of PD has been vastly used to study beta oscillations, it does not allow us to interrogate the impact of transient local and interregional beta dynamics on motor behaviour. Building on evidence from previous studies showing a functional role of burst timing on motor performance (Torrecillos *et al.*, 2018; Little *et al.*, 2019; Lofredi *et al.*, 2019), an interesting extension of this chapter would consist of acquiring simultaneous recordings of different sites of the BGTC circuit from behaving 6-OHDA lesioned rats and investigate how the beta neural events described in this study influence motor performance on a trial-by-trial basis.

## 3.5 Conclusion

There is a vast amount of literature providing evidence of a link between excessive beta oscillatory activity and motor deficits in PD. Describing how and when, spatially distributed structures of the BGTC circuit overtly synchronize their neural activities in beta frequencies is crucial for uncovering the disease mechanisms of PD and guide stimulation strategies aimed at improving efficiency of therapeutic strategies. This chapter contributes to the above while showing that preceding the emergence of high-power beta oscillation, interareal communication between subcortical and cortical beta activities is abruptly and transiently modulated both at the population as well as the unit level.

# 4 Phase-specific Deep Brain Stimulation revisited: stable tremor drivers for stable tremor modulation

## 4.1 Introduction

Temporally coordinated neural activity, within and across brain regions, is essential for normal functioning of the brain (Engel and Singer, 2001; Buzsáki and Draguhn, 2004; Fries, 2015). Disruption of information flow across brain structures, which is implicated in many brain disorders, often results from hypo- or hyper-synchronised neural activity (Schnitzler and Gross, 2005; Uhlhaas and Singer, 2006; Brown, 2007). Therapeutical options that can reverse abnormal brain synchrony in oscillopathies such as ET and PD, range from pharmacological treatments, lesioning surgeries and high-frequency DBS (Benabid *et al.*, 1991; Brown, 2001; Rodriguez-Oroz *et al.*, 2005; Silberstein *et al.*, 2005; Kühn *et al.*, 2009; Elble *et al.*, 2018) . However, these therapies often induce widespread effects on the network, resulting in undesirable side-effects (Hariz *et al.*, 2008; Volkmann *et al.*, 2009; Castrioto *et al.*, 2011; Deuschl *et al.*, 2011; Ondo, 2016). To improve therapy and elucidate the role of neural oscillations in health and disease, state-of-the-art research now focuses on selectively controlling synchrony, i.e., in disrupting pathological and sparing physiological neural activity.

Among some of the recently developed approaches (see (Cagnan *et al.*, 2019*a*) for a review), delivering patterned DBS according to the temporal properties of the pathological neural activity in a closed-loop fashion, is an experimental strategy which has elegantly shown to be able to selectively manipulate synchronisation (Rosin *et al.*, 2011; Holt *et al.*, 2016; Cagnan *et al.*, 2017; Zanos *et al.*, 2018; Escobar Sanabria *et al.*, 2020; McNamara *et al.*, 2020; Peles *et al.*, 2020). By delivering stimulation at a specific phase of the underlying oscillatory activity, this strategy can either promote or disrupt intrinsic temporal dynamics, leading to an amplification or suppression of the targeted oscillation.

In ET, a neurological disease which affects up to 6.3% of the population above 65 years old (Louis *et al.*, 1998), an excessive synchronisation of the CTC circuit is thought to drive involuntary shaking of the limbs (Raethjen and Deuschl, 2012). Critically, thalamic neural activity closely matches the rhythmic limb acceleration in ET (Hua and Lenz, 2005; Schnitzler *et al.*, 2009). This presents a unique opportunity for guiding stimulation: tremor can be used to control stimulation and determine the stimulation pattern that can most efficiently alter thalamic neural activity and yield tremor modulation. Thalamic stimulation controlled by a specific timing limb acceleration was trialled in 2017 by Cagnan and colleagues with the objective of optimising the efficiency and efficacy of conventional DBS, i.e., using less energy, inducing fewer side effects and retaining or even enhancing the levels of tremor reduction. This work has successfully shown that for a subset of ET patients, phase-specific DBS could achieve similar levels of postural tremor reduction with respect to conventional high-frequency stimulation while using less than half of the energy. Whether when delivered bilaterally, this stimulation strategy leads to fewer stimulation induced-side effects, such as dysarthria and loss of balance, remains to be tested.

Patients diagnosed with ET almost exclusively suffer from action tremor, which can be divided into two subtypes: postural and kinetic tremor (Deuschl *et al.*, 1998). Hence, it is paramount that effects of phase-specific DBS on kinetic tremor are also tested before this strategy can be considered as a therapeutic option for patients suffering from ET. In line with the above, this chapter explores whether phase-specific DBS is capable of supressing not only postural but also kinetic tremor. To this end, the hand tremor of 4 ET patients was tracked using a triaxial accelerometer to trigger stimulation to the contralateral thalamus or surrounding areas at different timings, while patients were either holding a posture or drawing a spiral. Our results suggest that: 1) phase-locked stimulation can reduce both postural and kinetic tremor and 2) suppressive effects of phase-locked stimulation during intermittent posture (i.e., while holding a tremor inducing posture and sporadically resting hands on the lap for brief periods), are on average maintained for tremors with specific properties.

## 4.2 Methods

### 4.2.1 Participants

Six patients with ET were recruited for this study. The research project was approved by the local ethics committee in accordance with the Declaration of Helsinki and all patients gave their informed consent to take part in the study. Patients 2 and 5 were excluded from the study; the former due to an incompatibility between the patient's implanted stimulator (Medtronic Kinetra) and our interface device (Nexus-D2) for phase-locked stimulation, and the latter due to an insufficient level of tremor to perform the task. On the day of the experiment, a potential diagnosis of dystonic tremor (DT) was raised for patient 3 by the clinical team. Thereafter, the cohort of patients included in this study consisted of 3 ET patients and one ET/DT patient. Please see Table **4.1** for their clinical details.

### 4.2.2 Recordings

Participants were not asked to interrupt their therapeutic routine for this experiment. During the experiment, the most tremulous hand was visually assessed by asking the patient to assume a tremor provoking posture: extended arms straight ahead followed by folding of the forearms inwards so that both hands were pointed at each other at the level of the nose. Only the hand with the most prominent tremor was recorded by fixing a triaxial accelerometer (Biometrics Ltd, ACL300) on top of the metacarpophalangeal joint of the index finger. The triaxial signals from the accelerometer sensor were amplified using a Biometrics K800 and recorded using a 1401 amplifier (Cambridge Electronic Design) at a sampling rate of 10,417 kHz.

### 4.2.3 Experimental design

The experiment consisted of four conditions: 1) a No-Stimulation (NS) condition, 2) a Random-Search Stimulation (RSS) condition, 3) a Phase-Specific Stimulation (PSS) condition and 4) a High-Frequency Stimulation (HFS) condition. In all conditions tremor severity was recorded in the three axes while a motor task was performed. The two tasks consisted of holding a tremor provoking posture and continuously drawing spirals outwards and inwards. The triaxial signals were downsampled to 1000Hz for analysis.

The NS condition was performed with the aim of measuring the baseline tremor variability. It consisted of 2 trials during which the patients were asked to assume a tremor provoking posture for about 1 minute followed by 1 minute of resting with their hands placed on their lap and a subsequent 1 minute of spiral drawing. This amounted to 2 baseline postures and 2 baseline spirals. Trial epochs were derived from the hand movement, i.e., initiation and termination of either the tremor provoking posture or spiral drawing. To this end, we lowpass filtered the triaxial signal (third order Butterworth filter with a cut-off frequency of 2Hz) and visually inspected patients' hand position from the change in the DC offset of the accelerometer signal.

From the baseline recordings two key parameters were extracted: 1) the dominant tremor axis (x, y or z) to perform the RSS condition, and 2) the peak tremor frequency, which was kept fixed throughout the experiment. These features were determined from the power spectral densities of the triaxial signals from the posture hold task with a minimum frequency resolution of 0.5Hz (Spike 2, Cambridge Electronic Design).

During phasic-stimulation conditions (RSS and PSS), the accelerometer signal from the dominant tremor axis was band-pass filtered between 2-8Hz (Digitimer Neurolog N125/6). This bandpass filtered signal was used to estimate the tremor phase in real-time (based on the instantaneous zero crossings and the average tremor frequency estimated from the posture hold task of the NS condition). For each motor task, posture and spiral drawing, once the desired phase of stimulation was detected (one out of twelve phases equally spaced across the limb acceleration, as detailed below), a TTL pulse was sent to the implanted stimulator via Nexus-D2, closing the loop.

The RSS condition was performed to investigate the impact of different stimulation timings (12 phases) on tremor severity. The goal of this experimental step was to find for each individual and motor task, the stimulation phase inducing the largest tremor suppression among the 12 possible stimulation phases. To this end, the RSS condition consisted of 8 trials where patients were asked to assume the tremor provoking posture for 71 seconds, rest for approximately 1 minute, draw a spiral for 71 seconds and rest again for another minute. For each posture held or spiral drawn, 12 blocks of stimulation lasting 5 seconds each, with one second of stimulation interval, were delivered. Each 5 second stimulation block was delivered at a specific phase, randomly selected from 12 equally spaced phase values (i.e., 0-330

degrees with a 30-degree resolution). The order of stimulation phases across different trials was randomized to avoid an order effect. Stimulation duration at each phase (5-seconds) was dictated by a trade-off between the number of phases tested and patient fatigue.

The PSS condition was performed to determine the sustained effects of locking stimulation to the optimal phase for tremor suppression during posture holding and spiral drawing. The PSS condition consisted of 6 trials; three where patients were asked to intermittently hold the tremor provoking posture while one minute of stimulation was delivered continuously at the phase that yielded the largest tremor suppression in the RSS condition; and other three trials where patients were asked to draw a spiral for one minute continuously while stimulation was concurrently delivered at the phase affording maximum suppression during spiral drawing in the RSS condition. For the first three phase-locked stimulation trials, where patients held a posture, we have also asked patients to slowly tap on their laps with their hands and return to posture hold - referred from here onwards as *intermittent posture*. Tapping occurred approximately at 20 seconds and 40 seconds of stimulation and lasted on average 1300ms±800 SD (ranging from 500 to 2800 msec). PSS during spiral drawing was delivered for one minute while the patient continuously drew spirals outwards and inwards, with no interruptions. PSS during intermittent posture was only performed in half of the cohort (patients 2 and 4) and spiral drawing was performed by all but patient 1 (cf. Table **4.1**)

The HFS condition consisted of 1 minute posture holding and 1 minute spiral drawing with 1 minute of inter-trial interval and stimulation was delivered at the patient's clinical parameters (Table **4.1**).

### Dominant and Tracked Tremor Axis

In between the experimental conditions, the dominant tremor axis was updated so that the axis tracked for PSS would as much as possible correspond to the one with the largest excursion. The tremor axis tracked for the RSS condition, was the one showing the highest tremor peak while patients held a static posture during the NS condition. It should be noted that the dominant tremor axis derived from the NS posture hold was the one used for the RSS condition during both motor tasks. For all patients this was the Z axis. When stimulation was delivered continuously for approximately one minute at the optimal phase for tremor suppression (PSS condition), the axis to track was re-assigned to the one showing a higher count of stimulation blocks at which the tremor envelope was higher than the other envelopes during RSS posture

hold and spiral drawing, respectively (Figure **4.2**B and Figure **4.3**B). Shifts in the dominant tremor axis across conditions did not seem to compromise the phase accuracy of stimulation effects since tracked and dominant axes for each patient and at each motor task displayed a tight phase relationship during the RSS condition (Supplementary Figure S9, averaged PSI of 0.77 ± 0.06 SD and 0.72 ± 0.09 SD, for posture and spiral tasks, respectively). Please refer to Figure **4.1**, for a comprehensive diagram on the tracked axis updates.

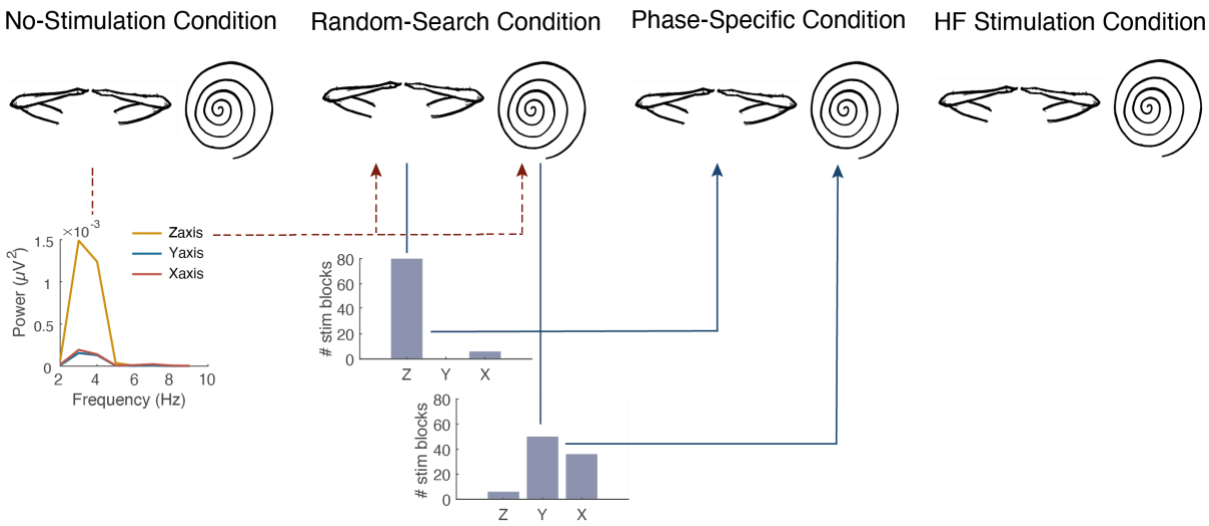


**Figure 4.1– Matching tracked to dominant axis across stimulation conditions.** Triaxial accelerometer signals were recorded during four conditions: No-Stimulation; Random-Search; Phase-Specific and High-Frequency (HF) stimulation conditions. During each condition patients alternated between two motor tasks: posture hold, where patients were asked to fold their forearms inwards so that both hands were pointed at each other at the level of the nose; and spiral drawing, where patients were asked to continuously draw over a spiral displayed on a digital tablet, outwards and inwards. The axis tracked during the RSS condition was the one with the highest power spectral density from the posture hold recorded in the No-Stimulation condition (inset Z axis depicted with the yellow line). Phase estimation was guided by the peak tremor frequency derived from the same power spectral density. After performing the RSS condition, the dominant tremor axis was re-evaluated (blue plot bars) for each motor task. The phase affording the maximum tremor suppression at the dominant tremor axis (here, Z for posture hold and Y for spiral) was next used to deliver PSS.

### DBS Stimulation Target

Stimulation was delivered either to the Posterior Subthalamic Area (PSA) or the Ventral Intermediate (ViM) thalamus, depending on the hospital site patients had their DBS implantation surgery performed. In both ET and DT, the ViM is considered as the gold-standard, whilst the PSA has emerged as an alternative target over the last decade. The PSA contains the zona incerta, fibre tracts connecting the cerebellum and internal segment of the

pallidum with the thalamus and is located ventral to the thalamus, posterior-medial to the STN and lateral to the red nucleus (Lévy *et al.*, 2020). Tremor control efficacy of this novel stimulation target has been tested and validated by various experimental studies (Plaha *et al.*, 2004; Blomstedt *et al.*, 2010); some of which report superior tremor suppression with PSA DBS than ViM (Herzog *et al.*, 2007; Blomstedt *et al.*, 2011; Xie *et al.*, 2012; Barbe *et al.*, 2018). Due to the small size of our cohort, phase-specific effects have not been separated according to the stimulation location.

| Patients | Diagnose | Meds | Stim target | Clinical parameters | Experimental parameters | Experimental conditions | PSS posture | PSS spiral |
|---|---|---|---|---|---|---|---|---|
| **1** | ET | N | PSA | 210µs, 2.5V, 120 Hz | 210µs, 3.5V | NS/HFS/RSS/NS | N | N |
| **2** | ET/DT | N | PSA | 60µs, 1.1V, 130Hz | 210µs, 1.7V | NS/RSS/PSS/ HFS | Y | Y |
| **3** | ET | Primidone Topiramate | PSA | 60µs, 1.3V, 130Hz | 210µs, 1.3V | NS/RSS/PSS/ HFS | N | Y |
| **4** | ET | N | ViM | 90µs, 3.3V, 130Hz | 210µs, 3.0V | HFS/NS/RSS/PSS | Y | Y |

**Table 4.1– Clinical information and stimulation parameters of patients included in the study.** ET = Essential Tremor; DT = Dystonic Tremor; PSA = Posterior Subthalamic Area; Clinical and experimental stimulation parameters: pulse width, amplitude and frequency; ViM = Ventral Intermediate Thalamus; NS = No-Stimulation; HFS = High-Frequency Stimulation; RSS= Random-Search Stimulation; PSS= Phase-Specific Stimulation; N = No; Y=Yes.

### 4.2.4 Data Processing

To avoid having stimulation effects confounded by different peripheral tremor manifestations, we have clustered the coefficients of the first principal component derived from filtered triaxial data in the NS and RSS conditions. It should be noted that each motor task was considered separately. Only a single patient (patient 2) exhibited two distinct tremor manifestations during both motor tasks. The NS and RSS data of patient 2 was hence reduced to the data points that belonged to the largest data cluster. Clustering analysis was not performed on the Phase-Specific Stimulation condition. In this experimental step, stimulation was delivered continuously for 1 minute to evaluate whether sustained phase-specific effects on tremor suppression could be observed and the number of trials was insufficient for the performance of

cluster analysis. Please refer to the Supplementary Materials - ***Cluster analysis*** for a detailed description.

### Quantification of change in tremor severity during random-search stimulation

Two amplitude response curves (ARCs) per patient were calculated to detect the stimulation phase affording maximum tremor suppression for each motor task during the RSS condition. These curves are shown in Figure **4.2**A for posture hold and Figure **4.3**A for spiral drawing and reflect the median change in tremor severity at the three tremor axes while stimulation was being delivered at 12 different and equally spaced phase values. To measure the change in tremor severity we first filtered the tremor signal using a second order Butterworth band-pass filter (cut-off frequency of ±2 Hz around the patient's peak tremor frequency) and computed the instantaneous tremor envelope using the Hilbert Transform. Next, for each stimulation block (5-seconds of stimulation at a certain phase), the average tremor severity found in the last second of stimulation (from the 4th-5th second) was normalised with respect to the average tremor severity during the one second prior to stimulation onset. A change in tremor severity of -1 indicates complete tremor suppression, 0 indicates no change in tremor amplitude and positive values indicate amplification of tremor. A diagram detailing the analysis pipeline to measure RSS effects can be found in chapter 5,
Figure **5.2**.

### Quantification of change in tremor severity while intermittently holding a posture during phase-specific stimulation

The impact of PSS on postural tremor was calculated for the three patients who completed this part of the experiment (patients 2 and 4, Table **4.1**). With this experimental task we aimed at further evaluating the efficacy of phase-specific DBS by quantifying phase-dependent suppression across a task where posture was interrupted by short periods of rest. To this end, we have averaged the tremor severity (envelope of the band-passed filtered tremor signal) across 3 seconds in 4 different occasions: 1) prior to stimulation onset; 2) prior to tapping; 3) following tapping and 4) prior to stimulation was turned off. Like the RSS condition, the impact of stimulation on tremor was measured as a change in tremor severity with respect to tremor severity immediately prior to stimulation onset. As such, we normalised the average tremor severity prior to tapping, following tapping and prior to stimulation offset with respect to the average tremor severity found 3 seconds prior to stimulation onset. This normalised measure

afforded once more a comprehensive scale where -1 indicates complete tremor suppression, 0 indicates no change in tremor and positive values indicate amplification of tremor. Results are shown per subject, per trial and for the three tremor axes (Figure **4.6**). The delineation of the beginning and end of tapping was achieved in a similar fashion to NS posture trials – by visually inspecting patients' hand position from the change in DC offset of the low pass filtered triaxial signals (third order Butterworth filter and cut-off frequency of 2Hz) (please refer to the Supplementary Figure S8 for an example of our visual assessment). Additionally, we have quantified how variable the dominant tremor axis of each patient was while using a moving window of one second across the recordings (Figure **4.6**, pie charts)

### Quantification of change in tremor severity while spiral drawing during phase-specific stimulation

The impact of PSS on kinetic tremor was calculated for the three patients who completed this part of the experiment (patients 2, 3 and 4, Table **4.1**). Unlike postural tremor where the voluntary drivers are fixed (i.e., muscles sustaining the posture), spiral drawing emerges from voluntary contributions which continuously evolve over time. Therefore, we have not measured stimulation effects as changes in the stimulated spiral with respect to tremor prior to stimulation onset. Instead, effects of PSS during spiral drawing were assessed by comparing the power spectra of tremor obtained in the NS, PSS and HFS conditions for each patient. PSD was calculated for each patient and for each condition separately using the Welch's method with a 1000-sample-long Hann window plus a 50% overlap size (i.e., frequency resolution of 1 Hz). Individual PSD curves were normalised to the sum of the total power between 100 and 500Hz. In order to mitigate the order effects that our results might have been subjected to, we have normalised every PSD curve to the power of the tremor peak (between 3 and 10Hz) of the concatenated data across all conditions (Figure **4.7**).

Lastly, we were interested in comparing the changes in tremor dynamics across stimulation conditions. To this end, we concatenated the tremor envelope derived from the Hilbert transformed band-pass filtered tremor data across conditions and took its $50^{th}$ percentile. For each condition we computed the amount of time patient's tremor was above or below this threshold. The duration of low tremor and bursts of tremor was averaged across patients per condition (Figure **4.8**A and B, respectively).

### 4.2.5 Statistical analysis

**Surrogate Distribution**

To determine whether modulation of postural and kinetic tremor severity during RSS was larger than the natural variability of tremor, the following analysis were performed using data from the NS condition. First the envelope of the tremor signal was computed using a Hilbert transform. Next, 50,000 5-second long segments (or less if patient's data was reduced to one cluster, see Supplementary Materials - *Cluster analysis*) were randomly selected and the normalised change in tremor severity was calculated. From this distribution, $x$ values were randomly selected and their median calculated ($x$ corresponding to the average number of stimulation blocks delivered at each phase for a given patient, to closely match the median change in tremor severity that created ARCs in the RSS condition). This was repeated 1,000,000 times leading to a surrogate distribution of spontaneous changes in tremor severity. Stimulation effects summarised by ARCs were then compared to the z-scores of this distribution after controlling for multiple comparisons using the Bonferroni method (n=12 phases, $\alpha$ =0.0021).

## 4.3 Results

With this study we aimed to explore the robustness of phase-specific DBS (Cagnan *et al.*, 2017) during different motor states. While phasic-stimulation has proven to be efficient in inducing clinically relevant symptom relief by disrupting the critical temporal relationships that are established during postural tremor in ET (Cagnan *et al.*, 2017), it remains unknown 1) if suppressive stimulation effects during postural tremor are maintained when posture is interrupted by short periods of rest and 2) whether phase-dependent suppressive effects can also be observed during kinetic tremor. By providing a thorough assessment of the spatial and temporal dynamics of tremor while stimulation was delivered at state-specific phases of tremor, we sought for a better understanding of the key features underlying phase-specific stimulation efficacy.

### 4.3.1 Effects of Random-Search Stimulation

**Phase-dependent stimulation effects are observed in postural tremor and not in kinetic tremor**

From the RSS condition, where stimulation was delivered 8 times for 5 seconds phase-locked to each one of the 12 possible phases, we first determined the consistency of stimulation's modulatory effects at each phase across the 8 trials. Despite only tracking the dominant tremor axis to deliver stimulation, the impact of stimulation on tremor severity was computed for all three axes (Z, Y, X). This is summarised by the ARCs shown in Figure **4.2**A, for stimulation blocks where patients were holding a posture, and Figure **4.3**A, for blocks where patients were drawing a spiral. Median changes in tremor severity for each patient at each motor task, axis and stimulated phase have been contrasted with respect to the corresponding surrogate distributions which summarised the spontaneous (unstimulated) changes in tremor severity (see section 0).

We found that during the posture hold, all ET patients, except for patient two (for whom a possible dystonic tremor diagnosis has been raised during the recording session), had at least one instance at which stimulation afforded significant tremor modulation (marked as red dots on Figure **4.2**A). During spiral drawing however, none of the 4 patients show statistically significant phase-dependent stimulation effects on tremor severity (Figure **4.3**A).

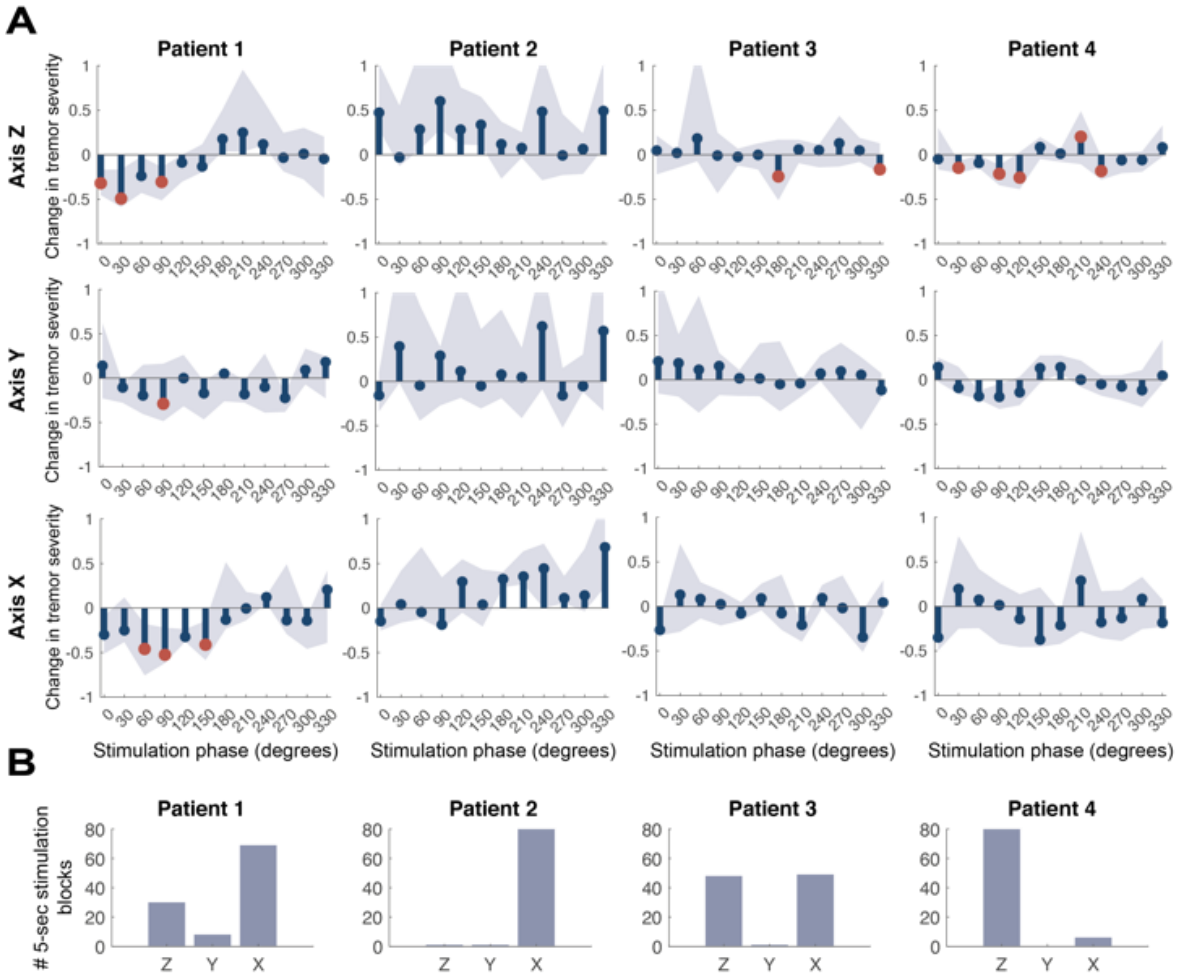


**Figure 4.2 – Effects of Random-Search Stimulation on postural tremor amplitude.** Blue stem plots in panel A show the amplitude response curves (ARCs) computed for each individual (columns) and each tremor axis (rows) during the posture hold task. ARCs summarise the median change in tremor severity at each stimulation phase, where 0 denotes no modulation of tremor severity, -1 indicates complete tremor suppression and positive values indicate tremor amplification. The shaded light blue area represents the 25th and 75th percentile of change in tremor severity (across RSS trials). Red dots indicate stimulation phases that yielded a significant modulation of tremor severity with respect to that found in the NS condition (section 0, $p<0.0021$). The histograms on panel B, show the count of stimulation blocks at which a given tremor axis had a larger tremor envelope than the remaining 2 axes – axis X, X, X, and Z, for patients 1 to 4. The axis with the highest number of counts and the phase yielding the largest tremor suppression were selected to control the delivery of continuous phase-locked stimulation in the subsequent experimental condition (the PSS condition).

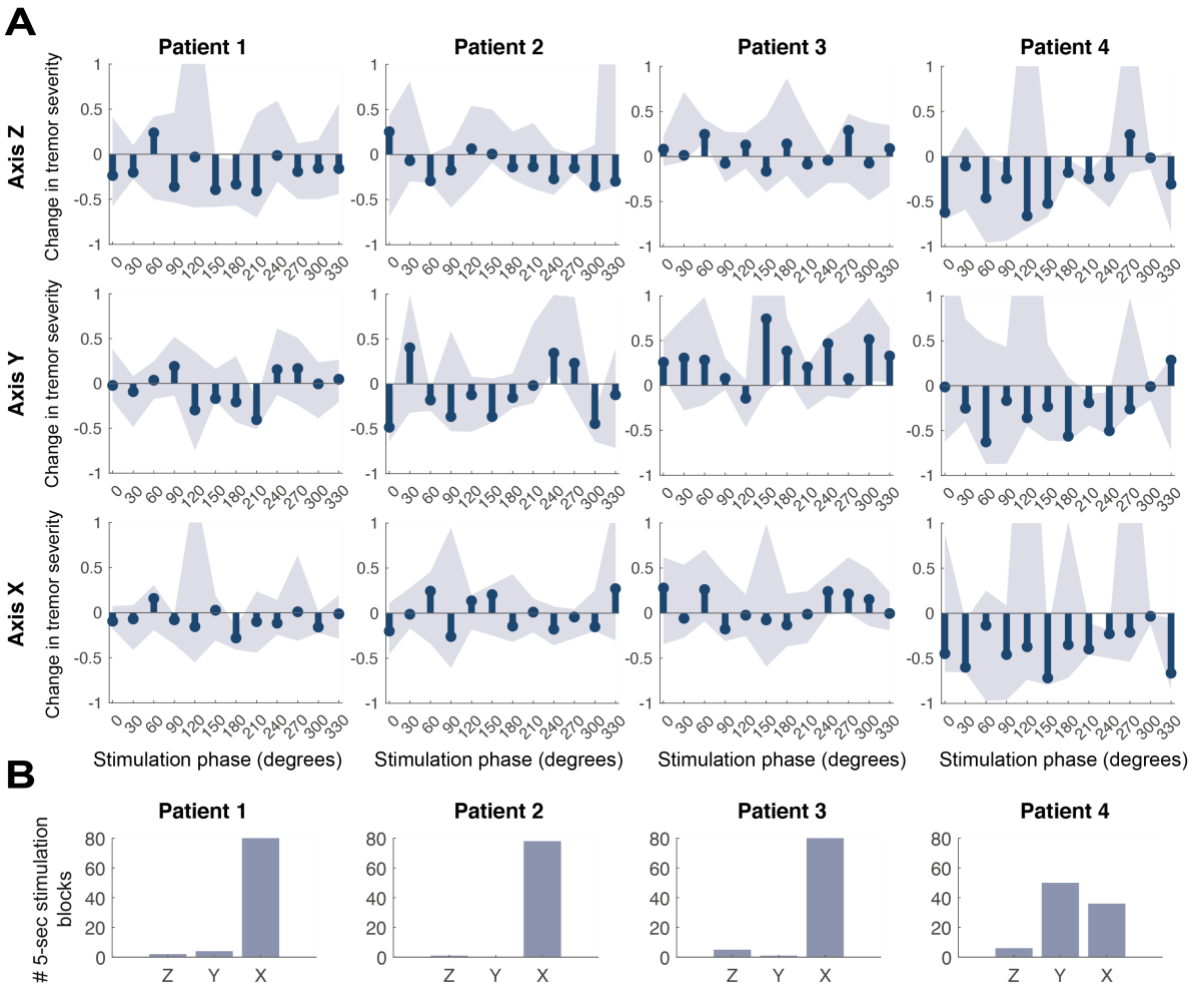


**Figure 4.3 - Effects of Random-Search Stimulation on kinetic tremor amplitude.** Blue stem plots in panel A show the amplitude response curves (ARCs) computed for each individual (columns) and each tremor axis (rows) during the spiral drawing task. ARCs summarise the median change in tremor severity at each stimulation phase, where 0 denotes no modulation of tremor severity, -1 indicates complete tremor suppression and positive values indicate tremor amplification. The shaded light blue area represents the 25th and 75th percentile of change in tremor severity (across trials, n=8). Red dots indicate stimulation phases that yielded a significantly larger modulation in tremor severity with respect to the no stimulation condition (section 0, $p<0.0021$). Of note, no significant changes in tremor severity were observed during the spiral task. The histograms on panel B, show the count of stimulation blocks at which a given tremor axis had a larger tremor envelope than the remaining 2 axes – axis X, X, X, and Y, for patients 1 to four. The axis with the highest number of counts and the phase yielding the largest tremor suppression were selected to control the delivery of continuous phase-locked stimulation in the subsequent experimental condition (the PSS condition).

### Phase-dependent modulation of postural tremor amplitude depends on the underlying resonant properties of tremor

RSS during posture hold impacted patients' tremor severity in a fairly heterogenous manner: for instance, Figure **4.2**A shows that while no significant phase-dependent tremor modulation was observed in patient 2, patient 1 showed significant phase-dependent tremor modulation at various phases across all three axes. Previous literature suggests that tremor oscillators can be more or less easily disrupted via external perturbations depending on the underlying resonant properties of each individual's tremor (Cagnan *et al.*, 2014, Brittain *et al.*, 2015*a*). This hypothesis proposes that tremors that present a narrower frequency band at which they naturally oscillate are more likely to show phase-specific amplitude modulation than those that oscillate at a wider range of frequencies. Here we investigate whether the inter-subject variability of stimulation effects during our RSS postural tremor condition is linked to such a mechanism. The resonant properties of each individual's tremor were summarised by individual frequency-amplitude profiles which arrange the instantaneous tremor amplitude according to the instantaneous frequency of tremor (Figure **4.4**B).

Our results indeed show a negative but not significant, correlation between stimulation effects and the coefficient of variation of tremor from the NS condition (Figure **4.4**C, r= – 0.73, p= 0.27). For this analysis, stimulation effects have been summarised as deviations of the largest suppressive effect in each individual ARC from tremor's natural variability levels (dashed line on Figure **4.4**A which was obtained as outlined in section 0); and the coefficient of variation (CV) of baseline tremor was calculated after fitting a Weibull to the individual frequency-amplitude tremor profiles (normalised to the individual median tremor amplitude).

$$CV = \frac{IQR}{median} \qquad \textit{(Equation 4.1)}$$

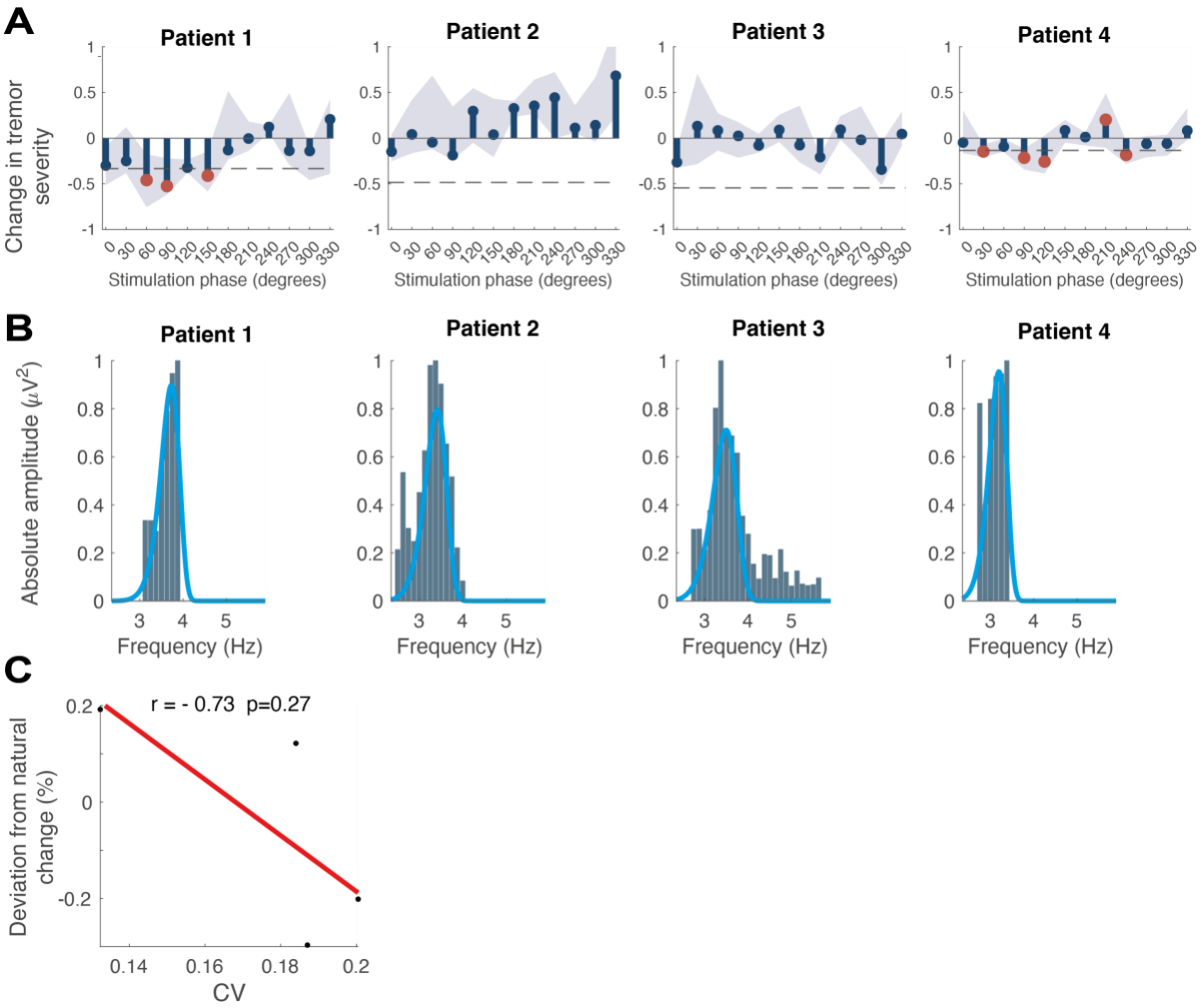


**Figure 4.4 - Stimulation effects are linked to the underlying tremor stability.** Panel A shows the posture hold ARC of each subject's dominant tremor axis. Dashed black lines depict the lower z-score threshold value for significance derived from the corresponding surrogate distribution (α=0.0021, Bonferroni corrected for multiple comparisons, n=12). Panel B describes how each patient's tremor severity at the dominant axis varies with the instantaneous and spontaneous fluctuations in tremor frequency. The overlaying blue lines show the Weibull fits from which the CV was calculated. Panel C correlates the deviation of the maximum level of suppression of each individual ARC from its corresponding significance threshold (panel A), with the coefficient of variation of a gaussian fitted to the tremor frequency-amplitude profiles (panel B). Results are suggestive of a strong link between consistent stimulation effects and stable tremor oscillators (r=-0.73), despite the small sample size of our cohort (p=0.27).

It is also worth highlighting the bidirectionality of stimulation effects in patient 4 (Figure **4.5**), where significant suppressive and amplifying effects were observed depending on the specific phase at which stimulation was delivered. This observation is in line with previous theoretical and experimental studies reporting that stimulation delivered in a precisely timed manner relative to the rhythmic control signal can act to either enhance or reduce the amplitude of oscillatory activity depending on the stimulation timing tested (Cagnan *et al.*, 2013, 2017; Witt

*et al.*, 2013; Holt and Netoff, 2014; Zanos *et al.*, 2018; Holt *et al.*, 2019; Escobar Sanabria *et al.*, 2020; McNamara *et al.*, 2020; Peles *et al.*, 2020; West *et al.*, 2020).

Since patient 4 was the one with the highest tremor severity across our cohort (Supplementary Table S2), it is unlikely that the lack of amplifying effects in the remaining patients can be explained by a potential ceiling effect. Taking this into account and given that patient four exhibits a stable postural tremor, we speculate that only oscillators that present very stable properties can be significantly modulated in both directions via temporally specific stimulation approaches.

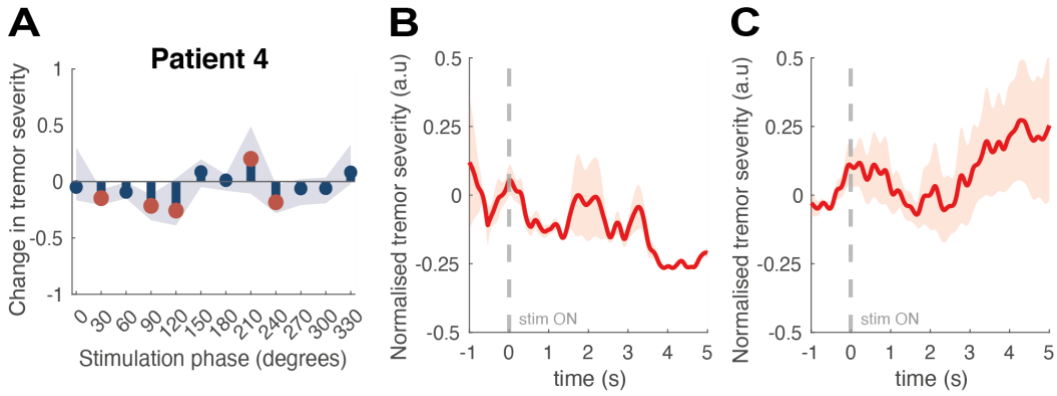


**Figure 4.5 – Bi-directional effects of Random-Search Stimulation on patient 4's postural tremor.** Panel A shows the ARC of patient 4 (blue stem plot) and the respective phases yielding significant tremor modulation (red dots). Panels B and C show the mean temporal evolution of the tremor envelope when stimulation was delivered for 5 seconds at the phase inducing the largest tremor suppression (120 degrees) and amplification (210 degrees), respectively. In both B and C panels, the tremor envelope has been normalised with respect to the average tremor envelope observed up to one second prior to stimulation onset and averaged across stimulation blocks (red line). The shaded red area represents the standard deviation across eight trials.

## 4.3.2 Effects of prolonged phase-specific stimulation

### Effects of phase-specific stimulation during intermittent posture

Five-second stimulation blocks at the optimal phase for suppression suggest that stimulation effects are, to a certain extent, dependent on the stability of the underlying tremor oscillators. Continuous stimulation delivered at the optimal phase for suppression suggests that also a spatial stability is necessary for sustained stimulation effects.

Prolonged stimulation at the optimal phase for postural tremor suppression was delivered while patients intermittently held a posture. Intermittent posture holding meant that the posture sustained during stimulation was sporadically interrupted by brief periods of rest where patients slowly tapped their hands on their lap. Tremor in ET is predominantly an action tremor, meaning that during rest, the involuntary shaking of patients' limbs stops. Because our paradigm relies on the presence of tremor to deliver stimulation, it is implied that during episodes of rest (tapping periods), the signal used to control stimulation is lost and stimulation is interrupted. The impact of brief interruptions in posture and stimulation prompted by tapping on tremor's severity modulation, is what we have investigated here.

PSS during intermittent posture was delivered at 0 degrees of the X axis for patient two and at 120 degrees of the Z axis for patient four, and yielded very distinct results. Patient 2 showed inconsistent stimulation effects (an average 14% change in tremor severity ± 35 SD) and frequent shifts in the dominant tremor axis from axis Z to axis X (67% in axis X and 34% in axis Z across all trials, Figure **4.6**A). We speculate that the variable stimulation effects observed in this patient might have been driven by the stimulation angle having opposite effects on these two axes (~50% amplification of Z tremor and ~15% suppression on X tremor, according to the ARCs in Figure **4.2**A). Conversely, in patient 4, PSS induced a continued suppression of postural tremor (-74% change in tremor severity ±14SD) and the dominant tremor axis was maintained throughout the task (97% in axis Z and 3% in axis X across trials). Together, these results suggest that under stable tremor dynamics, phase-specific stimulation is capable of providing constant tremor control.

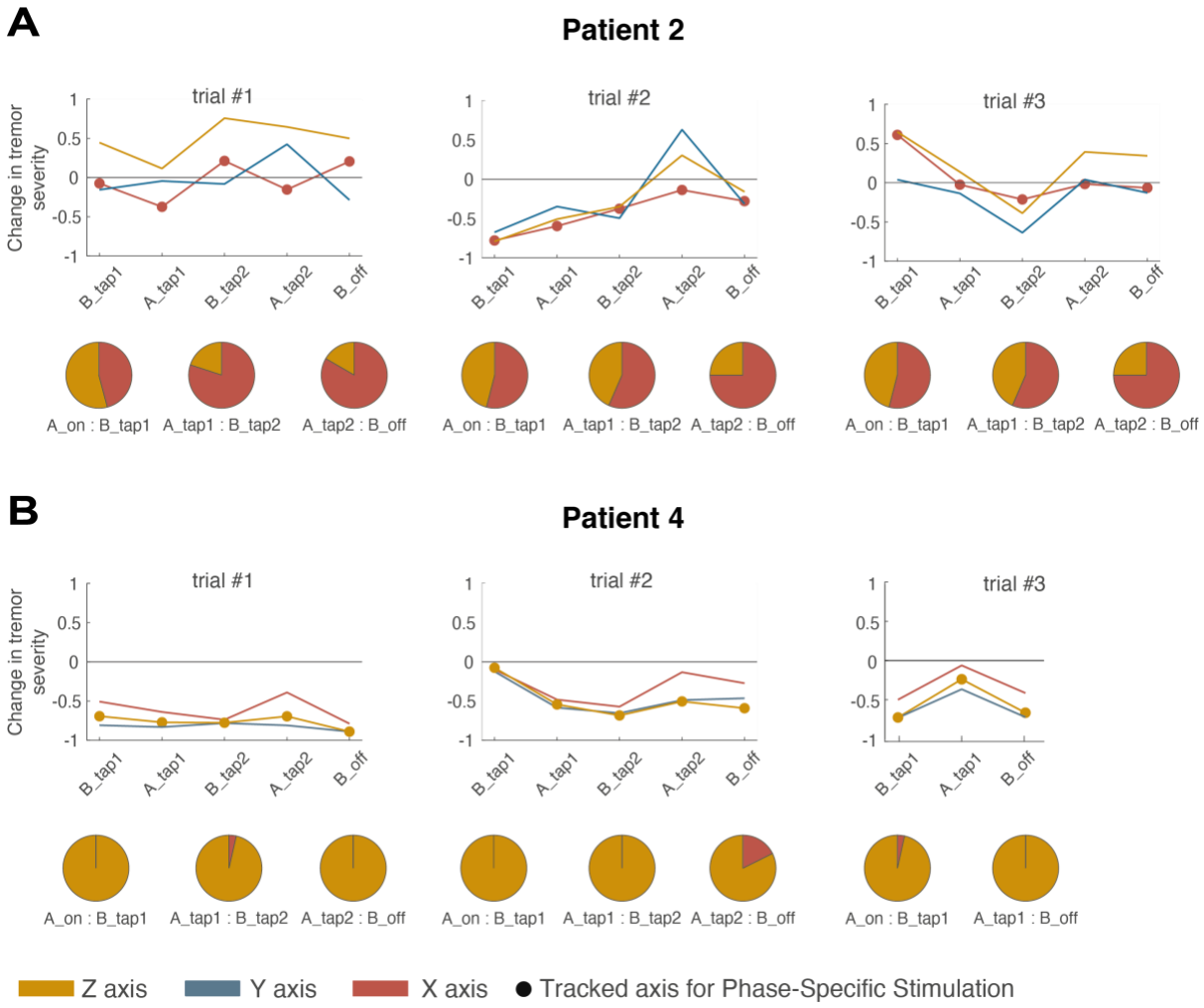


**Figure 4.6 - Consistency of stimulation effects are linked to stable contributions of independent oscillators.** The top row of each panel summarises the fluctuations in postural tremor severity for all the three axes at different instances of the intermittent posture task – before tapping the first time (*B_tap1*); after tapping the first time (*B_tap1*); before tapping the second time (*B_tap2*); after tapping the second time (*B_tap2*); and before stimulation is turned off (*B_off*). Change in tremor severity consists of a normalised measure of the averaged tremor severity at the five different instances of the task with regards to the average tremor severity before stimulation onset; a change in tremor severity with a positive value indicates tremor amplification, and a negative value indicates tremor suppression. Lines with dots denote the tremor axis being tracked to deliver phase-specific stimulation. The pie charts indicate dominant tremor axis as a ratio for a given epoch. The label *A_on*, indicates the time point after which stimulation was turned on.

### Effects of prolonged phase-specific stimulation during spiral drawing

During the PSS condition, stimulation was delivered at the phase that gave rise to the greatest tremor suppression in the individual ARCs (Figure **4.3**A). Comparing tremor power across conditions we found that tremor severity was the largest at NS, followed by PSS and HFS. Since in our protocol the PSS condition mostly followed the NS condition (refer to Table **4.1**), we tried to minimise the impact of a potential order effect by normalising each PSD by the

tremor power derived from the concatenated data across all conditions. This is shown in Figure **4.7**, together with an example of the individual spirals drawn on the digital tablet during each condition. These results suggest that PSS can reduce kinetic tremor severity (a tremor power change from NS of -57%±19 SD across patients) but not to the same degree as HFS (a tremor power change from NS of -97% ±3 SD across patients). Since stimulation was delivered at a phase which was not able to yield a significant tremor suppression during the RSS condition (Figure **4.3**A), we speculate that during spiral drawing, a phase-unspecific but systematic perturbation of the tremor network might be sufficient to induce tremor suppression.

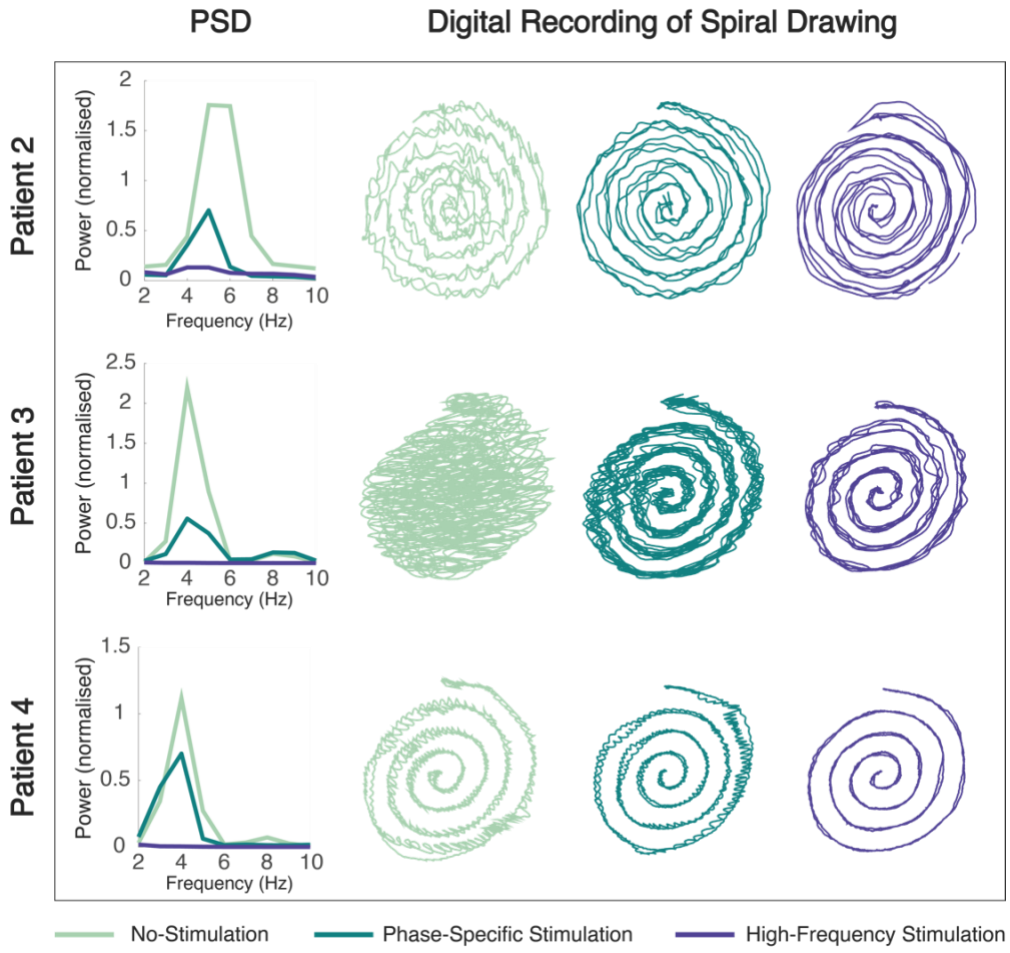


**Figure 4.7 – Tremor power across conditions during spiral drawing.** Normalised power spectra during No-Stimulation (in light green), Phase-Search Stimulation (in dark green) and High-Frequency Stimulation (in purple the stimulation) conditions are shown for patients 2, 3 and 4 on the left-hand side. Normalisation was performed in relation to the tremor power derived from concatenated data across all conditions. One digitised spiral per patient and condition is also shown, colour coded as per the inset legend.

How different stimulation conditions may influence tremor dynamics is summarised in Figure **4.8**. We observed that more frequent stimulation (NS → PSS → HFS) is characterised by longer periods of low amplitude tremor (amplitude below the median level of concatenated tremor severity) and shorter bouts of tremor rebound (amplitude above the median level of concatenated tremor severity). Since more frequent stimulation induces a larger suppressive effect (suggested by Figure **4.7**), we propose that greater control over kinetic tremor results from fewer and shorter bursts of tremor.

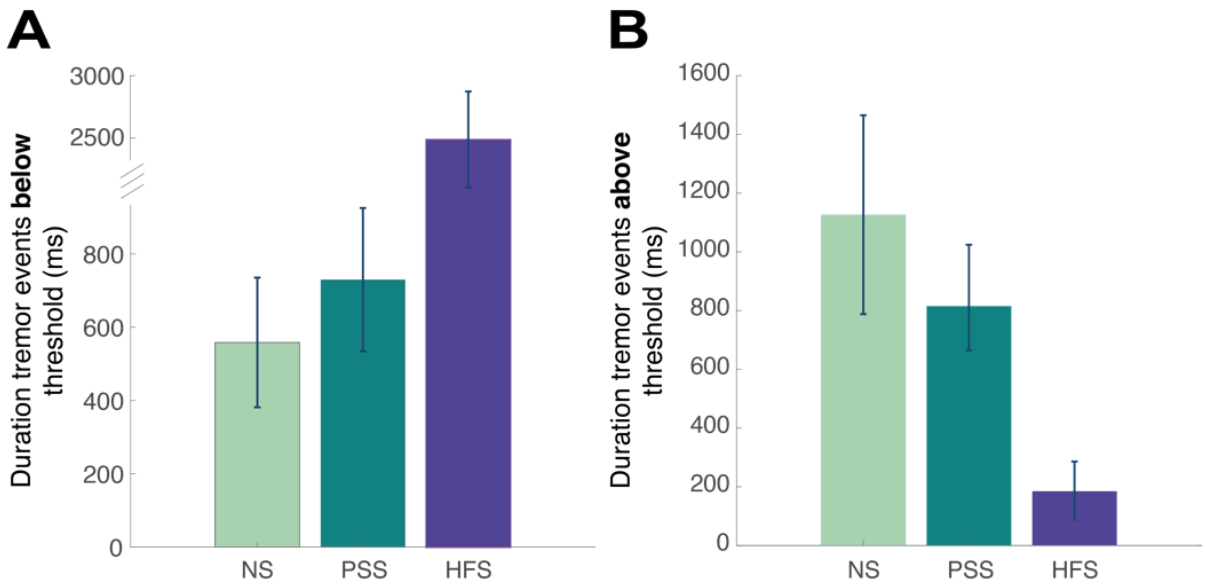


**Figure 4.8 - Amplitude dynamics of kinetic tremor across stimulation conditions.** Bar plots summarises the tremor dynamics underlying different stimulation conditions. Panels A and B show the average duration (in milliseconds) of tremor segments found below and above the 50th percentile of the concatenated tremor envelope across all conditions and suggest that from No-Stimulation (NS) → Phase-Specific Stimulation (PSS) → High-Frequency Stimulation (HFS)), there were increasingly longer epochs of low tremor amplitude and shorter episodes of tremor rebound. Error bars represent ± 1 SEM.

## 4.4 Discussion

The aim of this study was to further evaluate the effects of phase-specific DBS on ET. Here, we have tested the consistency of phase-dependent effects during intermittent posture holding and spiral drawing in 4 ET patients. We found that for selected patients with stable tremor characteristics, continued tremor suppression can be achieved by phase-locked stimulation despite brief interruptions in posture and stimulation. In addition, our results suggest that kinetic tremor during complex motor tasks such as spiral drawing can also be reduced via phase-specific DBS.

**Postural tremor reduction with Phase-Specific Stimulation**

Our results corroborate the findings reported by Cagnan et al., 2017 and show significant phase-dependent tremor suppression in a subset of cases in our cohort (3 out of 4 patients, as shown Figure **4.2**A). The negative correlation between the coefficient of variation of the frequency-amplitude profiles and the deviation of suppressive effects from spontaneous tremor fluctuations (r=- 0.73, Figure **4.4**C), also validates previous observations that patients who seem to benefit the most from phasic-stimulation are those whose tremor displays narrower resonant characteristics (Cagnan *et al.*, 2013, 2017, Brittain *et al.*, 2015*b*). From a mechanistic standpoint, this result suggests that less variable tremors (i.e., with narrower frequency-amplitude profiles) are more susceptible to disruption and therefore more easily manipulated. Furthermore, in certain cases this manipulation could have bidirectional effects (Zanos *et al.*, 2018; McNamara *et al.*, 2020). This was indeed the case for patient 4, where significant suppressive and amplifying stimulation effects were observed depending on the stimulation phase (Figure **4.4**A). For ET, there is no clinical utility for tremor amplification. However, in other conditions such as impulsivity, where decreased low frequency oscillations (2-8Hz) in the STN are linked to lower decision thresholds and frequent erroneous responses (Herz *et al.*, 2016), promoting low-frequency oscillations could potentially provide a viable therapeutic solution.

Prolonged stimulation at the optimal phase for postural tremor suppression was delivered to patients 2 and 4, while they intermittently held a posture. Suppressive phase-dependent effects were maintained across the entire task (i.e., even after tapping, when posture holding was resumed) for patient 4 (-74% change in tremor severity change from baseline ±14SD). We

speculate that maintenance of suppressive effects in this patient might have arisen from plastic effects induced by our stimulation paradigm, similar to those observed when phase-dependent stimulation was delivered to cortical beta oscillations (Zanos *et al.*, 2018). Future studies might consider prolonging the tapping period for more than couple of seconds, to determine for how long modulatory effects can be maintained. Alternatively, sustained tremor suppression during intermittent posture might have resulted from a random perturbation of the tremor network. With our system, stimulation is triggered as soon as the control signal is detected i.e., when both tremor amplitude and phase-tracking efficacy are expected to be very low. Hence phase-specific stimulation at this stage is thought to be equivalent to random periodic stimulation, which we believe if delivered before tremor can be fully established, might be sufficient to avoid a large tremor rebound.

Phase-locked stimulation during intermittent posture showed inconsistent effects in the other patient tested (patient 2). This result was however not surprising given the lack of significant stimulation effects during the RSS condition (Figure **4.2**A) and the wide frequency-amplitude profile derived from this patient's tremor (Figure **4.4**B). Another aspect that might help explain is the patient's tremor spatial dynamics (Figure **4.6**A). It is well known that the peripheral manifestation of tremor arise from an interaction between multiple competing central oscillators (Raethjen *et al.*, 2000; Pedrosa *et al.*, 2012). Hence, it is possible that an alteration in tremor's spatial manifestation is the outcome of a change in the weighted contribution of central tremorgenic oscillators. If this is indeed the case, in circumstances where the main tremor axis changes, a new temporal relationship between thalamic and limb tremor activity is likely to be established and the efficacy of phase-specific stimulation likely to be compromised.

On the day of the experiment, it was suggested that patient 2 may be exhibiting features suggestive of dystonic tremor. Dystonic tremor is known to be more variable (Panyakaew *et al.*, 2020), and less susceptible to external perturbations than ET (Cagnan *et al.*, 2017). It is worth mentioning that essential and dystonic tremor are often considered part of the same clinical spectrum and that for some patients a clear diagnostic delineation is never achieved (Elble, 2013).

In sum, our data suggests that effects of phase-specific stimulation on postural tremor can be maintained across motor state fluctuations, if the overall contribution of central tremor oscillators is relatively constant and if these oscillators display a narrow frequency-amplitude profile.

### Kinetic tremor reduction with Phase-Specific Stimulation

This study explores for the first time the impact of phase-specific DBS on kinetic tremor. Our results suggest that delivery of repetitive perturbations to the tremor network phase-locked to the peripheral tremor is capable of supressing kinetic tremor. However, we were unable to show phase-specificity of this effect.

How stimulation delivered at different phases of the tremor cycle affects kinetic and postural tremor was our first experimental question. To provide an answer, we have created the Random-Search Stimulation condition where patients performed each motor task (posture or spiral) 8 times, whilst 5-seconds of stimulation at each of the twelve possible phases was being delivered in a randomly selected order. The Random-Search condition and its impact on tremor was assessed in the same fashion for both posture and spiral so that phase dependent-effects could be compared across different motor states. Stimulation effects at each phase were calculated as an instantaneous change in tremor severity and significance tested against natural tremor variability found in the NS condition (section 0). While this method is very well suited to capture the impact of phasic stimulation on tremor during posture hold, the same may not be the case for spiral drawing.

Tremor in ET is an extremely volatile motor symptom, and its severity is modulated by different voluntary movements. Considering that tremor and voluntary movement pathways overlap (Hua and Lenz, 2005; Muthuraman *et al.*, 2012, 2018) and that with voluntary movement transient beta oscillations occur across the motor circuit (Pfurtscheller and Lopes Da Silva, 1999; Kühn *et al.*, 2004), movement can be considered as a competing oscillator which can transiently alter tremor output. Posture emerges from a constant voluntary motor drive, and hence phase-dependent effects of stimulation on tremor can be accurately assessed with instantaneous measurements. Spiral drawing, however, will have blocks of stimulation at the same phase falling at different instances of the spiral, where different voluntary drives will prevail, introducing noise and variability to our analysis. This has potentially obscured the

identification of effective stimulation phases during the RSS condition (spiral ARCs in Figure **4.3**A).

Nonetheless, prolonged phase-specific stimulation during spiral drawing was delivered at the phase showing maximal suppressive effects, and stimulation effects assessed by contrasting the power spectra of the tremor in this condition with respect to the power spectra of the remaining stimulation conditions (Herron *et al.*, 2017) – the NS and the HFS conditions. Across patients, the normalised tremor peaks found during phase-locked and high-frequency stimulation were 57%±19 SD and 97% ±3 SD smaller than that found in the NS condition. Our additional analysis on different stimulation conditions (Figure **4.8**) suggests that phase-specific stimulation improves tremor in a similar fashion to high-frequency stimulation, validating its therapeutic mechanism. Despite using normalised tremor measurements from data concatenated across the four conditions to mitigate a potential order effect in our experimental set up, the impact of phasic-stimulation on kinetic tremor must be validated in a larger cohort.

In sum, a clear delineation between stimulation effects and those simply induced by voluntary movement (or interactions between the two) comprises a great methodological challenge for trying to assess the impact of different stimulation parameters on tremor. Irrespective of phase-specificity of these effects, repetitive perturbations at the tremor frequency could yield kinetic tremor relief in all 3 patients tested.

### Feasibility of Phase-Specific DBS

The stimulation protocol employed in this chapter followed that developed by Cagnan et al., 2017, where the use of a peripheral sensor to drive central stimulation relies on the assumption that in ET a stable temporal relationship between thalamic neural activity and peripheral tremor exists (Marsden *et al.*, 2000; Schnitzler *et al.*, 2009; Pedrosa *et al.*, 2012, 2014).

By probing the network in a well-timed manner via DBS, this study provides insights into the underlying mechanisms of tremor. For certain subjects, during specific contexts, there is indeed a stable temporal relationship between thalamic neural activity and peripheral tremor which can be utilised to find when we can most efficiently perturb the system to achieve symptom relief (postural tremor suppression). Other patients exhibited higher frequency tolerance and intermittent central contributions, which lead to frequent changes in the network's intrinsic temporal dynamics. These changes, due to interactions with competing neural oscillators or

altered thalamic afferency from the periphery, cerebellum, cortex or BG for instance, influence the identification of the best timing to interact with these oscillators. In particular, in the context of spiral drawing, we speculate that phasic-stimulation was effective at disrupting tremor at certain instances and not so much at others – note in Figure **4.7** how the recorded spirals during the PSS condition are not homogeneous but show tremor emerging at specific areas of the spiral. Although theoretically plausible, our results suggest that with the current available methods, finding the optimal phase for each network state that patients may experience in everyday life is potentially too complex and computationally expensive.

### 4.4.1 Limitations and future directions

Our results were encouraging while showing for the first time how phase-specific stimulation can bring tremor relief during different motor states. Nevertheless, our cohort was small and heterogeneous and therefore replicating this study in a larger cohort is needed. One interesting extension of this study would entail monitoring patients' tremor at home before applying our stimulation paradigm. This would allow us to characterise patient-specific tremor variability during different motor states and potentially help delineate changes in tremor induced by external perturbation from those induced by endogenous inputs as well as interaction between the two.

## 4.5 Conclusion

Our findings suggest that phase-specific DBS is capable of supressing not only postural but also kinetic tremor in ET patients. While phase-specificity seems to be key to achieve tremor control in postural motor states, periodic phase-unspecific perturbations to the thalamus seem to be sufficient to yield tremor suppression during continuous movement. Moreover, this study suggests that for patients with stable tremor characteristics, continued tremor suppression can be achieved.

# 5 Essential Tremor amplitude modulation by median nerve stimulation

## 5.1 Introduction

Predominantly characterised by postural and kinetic tremor, ET is one of the most common movement disorders (Louis and Ferreira, 2010). Tremor in ET is often attributed to a malfunction of the CTC pathway, with activity in the cerebellar receiving areas of the thalamus coupled to patient's tremor (Hua and Lenz, 2005; Schnitzler *et al.*, 2009). Yet, the mechanism of tremor generation remains unclear, delaying advances in diagnostics (Brittain *et al.*, 2015*a*; di Biase *et al.*, 2017) and pharmacological treatment. Pharmacological treatments for tremor relief consist of a trial-and-error selection between anticonvulsants and beta-blockers. These show suboptimal efficacy and often induce side-effects (Deuschl *et al.*, 2011; Ondo, 2016). When pharmacological interventions are not effective, alternative surgical strategies can be employed for those individuals experiencing significant functional disability. Surgical therapies include thalamic ablation and neuromodulation of the ViM or surrounding targets – via DBS and more recently, low-intensity ultrasound (Elble *et al.*, 2018).

DBS is most commonly delivered continuously at high frequencies (>100Hz), inducing a significant reduction in tremor severity of about 80% (Zhang *et al.*, 2010; Elble *et al.*, 2018; Lozano *et al.*, 2019). Although highly effective, conventional high-frequency DBS has limitations. Among them are risks inherent to any surgical intervention (e.g. haemorrhage and infection), loss of efficacy over time (Fasano and Helmich, 2019), and side-effects mainly attributed to stimulation of brain areas adjacent to the target (Cagnan *et al.*, 2019*a*). In addition, DBS has a high cost and is resource-intensive in nature (Zhang *et al.*, 2010; Baizabal-Carvallo *et al.*, 2014; Cury *et al.*, 2017). These latter characteristics lead to inequality in terms of access to this therapy, in that it is almost exclusively provided to refractory patients with severe tremor in high-income countries (Jourdain and Schechtmann, 2014; Lozano *et al.*, 2019). Therefore, there is a need for non-invasive stimulation based technologies that might overcome the limitations of oral medication and invasive surgical strategies in order to address the negative psychosocial impact that ET brings to those affected (Louis *et al.*, 2001; Lorenz *et al.*, 2011).

There are two major approaches for ameliorating tremor using non-invasive stimulation. The first is to stimulate peripheral nerves or muscle end points with the aim of activating selected muscles at specific times or phases in the tremor cycle so that direct muscle responses serve to mechanically occlude the tremor (Prochazka *et al.*, 1992; Maneski *et al.*, 2011; Gallego *et al.*, 2013). The second approach involves the stimulation of peripheral nerves with the intention of evoking afferent activity that then interacts with either the central oscillators responsible for the tremor or with the local spinal circuits which relay tremor to the muscles (Hao *et al.*, 2013; Heo *et al.*, 2015; Dideriksen *et al.*, 2017; Pahwa *et al.*, 2019; Kim *et al.*, 2020). This too may require stimulation at specific instances of the tremor cycle, although stimulation need not elicit a direct muscle response. Here, we explore the second approach and aim to activate Group I muscle spindle afferents using median nerve stimulation phase-locked to patient's tremor. Thalamic inputs from this group of afferent fibers are localized near the border between the ViM and the Ventral Caudalis nucleus (Vc) (Vitek *et al.*, 1994; Hanajima *et al.*, 2004) – a thalamic region that overlaps with the optimal DBS target for tremor reduction(Milosevic *et al.*, 2018; Al-Fatly *et al.*, 2019). Stimulation of the median nerve at supramaximal intensity has been shown to drive spiking activity in the ViM and the Vc thalamic nuclei and to evoke very fast oscillatory activity (500-1500Hz) at the cortical level (Ohye and Narabayashi, 1979; Maendly *et al.*, 1981; Klostermann *et al.*, 1999; Hanajima *et al.*, 2004).

In recent years, phase-locked stimulation strategies have gained increasing attention due to their capacity to induce opposite behavioural effects when stimulation is delivered at different phases of an ongoing rhythm (Zanos *et al.*, 2018; Holt *et al.*, 2019; Escobar Sanabria *et al.*, 2020; McNamara *et al.*, 2020; Peles *et al.*, 2020). Nevertheless, to our knowledge all the previous experimental literature reporting bidirectional phase-dependent effects has emerged from stimulation protocols targeting specific brain structures but never peripheral ones. Motivated by the above and mounting upon the stable temporal relationship established between thalamic neural activity and postural tremor in ET (Marsden *et al.*, 2000; Schnitzler *et al.*, 2009; Pedrosa *et al.*, 2012, 2014), we hypothesised that driving thalamic afferent inputs via median nerve stimulation, phase-locked to patient's tremor, would modulate neural activity underlying tremor as evidenced by certain stimulation phases having tremor amplifying effects while others having suppressive effects. To test this hypothesis, 9 ET patients had median nerve stimulation delivered according to different phases of their hand tremor, captured via accelerometery (Cagnan *et al.*, 2013, 2017).

# 5.2 Methods

## 5.2.1 Participants

14 ET patients were recruited through the National Tremor Foundation. The research project was approved by the Health and Social Care Research Ethics Committee A of the Health Research Authority, National Health Service (NHS, UK) (HSC REC A) (reference number: 19/NI/0009) in accordance with the Declaration of Helsinki and all patients gave their informed consent to take part in the study. Based on the criteria outlined in the "Exclusion Criteria" section, five patients were excluded from the study and a total of 9 patients were included in the analysis (Table **5.1**).

**Exclusion criteria**

Only patients with a clinically significant tremor, consisting of a tremor severity above 0.2 $m/s^2$ according to the Bain and Findley tremor severity scale (Bain *et al.*, 1993), were included for further analyses. We also excluded subjects with inconsistent tremor (i.e., a tremor that waxed and waned during the tremor provoking posture) or tremor that was not sinusoidal as phase estimates would be unreliable. Both these scenarios led to too few or too many stimuli being delivered per block. To exclude these situations, only blocks of stimulation with a total number of stimuli between half the number of tremor cycles $[(\text{tremor's frequency peak} \times \text{block duration})/2]$ and double the number of tremor cycles $[(\text{tremor's frequency peak} \times \text{block duration}) \times 2]$ were included in the analysis. In four patients, these criteria led to less than half the trials for at least one phase value, consequently excluding the subject from further analysis. Lastly, the fifth patient excluded from this study was a patient who despite exhibiting a clinically relevant tremor at the time of the experiment (mean±SD, 2.07±0.71 $m/s^2$), was receiving bilateral thalamic DBS. In order not to confound the effects of our peripheral stimulation paradigm, we have excluded data from this patient.

**Peripheral-Stimulation Target**

Stimulation was delivered to the median nerve at the wrist level using an electrical peripheral-stimulator and a surface self-contained electrode with an adjustable strap that was tightly placed around the distal wrist. Intensity was gradually increased in steps of 0.5 mA from 2mA until a motor-threshold level was reached; i.e. until a twitch of the thumb could be visually

detected. For each TTL pulse sent to the peripheral stimulation device, a single pulse was delivered to the median nerve with a pulse width of 200msec. The average stimulation intensity was 9±2 mA. Stimulation sensation was assessed using the following Likert scale: "The stimulation was easily tolerated: A) Strongly disagree; B) Disagree; C) Neither agree nor disagree; D) Agree; E) Strongly agree". Results are given in Table **5.1**.

| Patients | Age, Sex | Age at onset | ET family history | Tremor reduction w/ alcohol | Tremor amplitude [$m/s^2$] | Medication | Stim Intensity [mA] | Tolerable stimulation |
|---|---|---|---|---|---|---|---|---|
| 1 | 65M | 60 | N | Y | 4.97±1.37 | Propranolol | 8 | Strongly agree |
| 2 | 67M | 52 | N | NA | 3.39±0.76 | Primidone | 9 | Strongly agree |
| 3 | 71M | <20 | Y | Y | 10.65±0.92 | N | 11 | Strongly agree |
| 4 | 67F | 14 | Y | Y | 1.81±0.52 | Propranolol Gabapentin | 9 | - |
| 5 | 72M | 69 | N | Y | 6.78±0.57 | N | - | Strongly agree |
| 6 | 84F | 56 | N | Y | 5.90±0.43 | Propranolol | 6 | Agree |
| 7 | 73M | 7 | Y | Y | 11.08±4.72 | N | 16 | Agree |
| 8 | 71M | 65 | Y | Y | 1.91±0.55 | Propranolol | 10 | Strongly agree |
| 9 | 64M | <15 | Y | Y | 2.02±0.18 | N | 7 | Strongly agree |

**Table 5.1 – Clinical information and stimulation parameters of patients included in the study.** Age and age at onset are in years. M = male; F = female; N = no; Y = yes; NA = not applicable as teetotal; - = missing observation. Tremor amplitude reflects the mean±SD tremor acceleration during the No-Stimulation condition.

### 5.2.2 Recordings

Participants were not asked to interrupt their therapeutic routine for this experiment. All patients included in this study presented tremor exclusively in one or both upper limbs, with the exception of patient number 1 who also exhibited a head tremor. During the experiment the most tremulous hand was visually assessed by asking the patient to assume a tremor provoking posture: extended arm straight ahead followed by folding of the forearms inwards so that both hands were pointed at each other at the level of the nose. Only the hand with the most prominent tremor was recorded by fixing a triaxial accelerometer (Biometrics Ltd, ACL300) on top of the metacarpophalangeal joint of the index finger. On the ipsilateral forearm, two Electromyograms (EMG) were placed on antagonist muscles responsible for the flexion and extension of the wrist (flexor carpi radialis and extensor carpi ulnaris muscles, respectively). In two out of 9 patients an additional EMG was placed over the thenar eminence which recorded abduction of the thumb during phasic-peripheral stimulation of the median nerve at supra-threshold intensity (Supplementary Figure S10 C). The triaxial signals from the accelerometer sensor were amplified using a Biometrics K800 and recorded and pre-processed using a 1401 amplifier and Spike2 software (Cambridge Electronic Design). EMG signals were recorded using a Digitimer D360 8 Channel Isolated Amplifier. The recording sampling rate for all signals was 10.417 kHz.

### 5.2.3 Experimental design

The experiment consisted of two conditions: 1) a No-Stimulation condition and 2) a Random-Search Stimulation condition. In both conditions tremor severity was recorded in the 3 axes while the tremor provoking posture was maintained.

The No-Stimulation (NS) condition was aimed at measuring the baseline tremor variability. It consisted of 2-5 trials where the patients were asked to assume the previously described tremor provoking posture for about 1 minute followed by 1 minute of resting with their hands on the lap. NS epochs were determined according to the hand movement initiating and finishing the tremor provoking posture. To this end, we used the low pass filtered triaxial signal (third order Butterworth filter with a cut-off frequency of 0.5Hz) and visually inspected patients' hand position from the change in DC offset of the accelerometer signal, with the exception of patient 6. For patient number 6 the instructed tremor provoking posture was not efficient in inducing tremor. As an alternative, the patient was tested with the forearm resting on a pillow whilst

flexing the wrist. NS trials for this patient were detected when the smoothed tremor envelope was above the average tremor severity in the NS condition for more than 10 seconds.

From the baseline recording two key parameters for the stimulation paradigm were determined: 1) the predominant tremor axis (x, y or z), and 2) tremor peak frequency. These features were determined using a power spectral analysis with a minimum frequency resolution of 0.5Hz (Spike 2, Cambridge Electronic Design).

During the Random-Search Stimulation (RSS) condition, the accelerometer signal from the predominant tremor axis was sent to a digital band-pass filter (Digitimer Neurolog N125/6) and filtered between 2-8Hz. This bandpass filtered signal was used to estimate the tremor phase in real time (based on the preceding zero crossing and the average tremor frequency estimated in the NS condition) and to control the peripheral stimulator. Once the desired phase of stimulation was detected (one out of twelve phases equally spaced across the limb acceleration, as detailed below), a TTL pulse was sent to the electrical-peripheral stimulator (Digitimer Constant Current Stimulator DS74), closing the loop.

The RSS condition consisted of 10 trials (except for one patient who, due to muscle fatigue, performed 7 trials) where patients were asked to assume the tremor provoking posture for 71 seconds and rest for approximately 1 minute in between trials. For each trial, 12 blocks of stimulation lasting 5 seconds each, with one second of inter-trial interval, were delivered. Each 5 second stimulation block was delivered at a specific phase, randomly selected from 12 possible equally spaced phase values (i.e., 0-330 degrees with a 30 degree resolution). The order of phase values across the trial was randomized to avoid an order effect in the results. Stimulation duration at each phase was dictated by a trade-off between the number of phases tested and patient fatigue since patients maintained the same tremor provoking posture as 12 blocks of 5-second-long stimulation was delivered to the median nerve. A previous study on phase-specific stimulation highlighted the importance of phase resolution since neighbouring phase values did not always induce significant changes in tremor severity (Cagnan *et al.*, 2017). Therefore, we opted to retain the same phase resolution in this study. By doing so, we inherently limited the duration of stimulation at each phase, potentially influencing the phase-dependent effect sizes. A schematic of our data collection and analysis pipeline is provided below in
Figure **5.2**.

## 5.2.4 Data processing

**Segregation of data according to tremor peripheral manifestations**

In order to analyse epochs of stimulated and unstimulated data with a peripherally comparable tremor manifestation, a PCA was performed in the triaxial filtered tremor data, followed by cluster division (k=2) using the Ward's method. Please refer to Figure **5.1** for an illustrative example of our cluster analysis and to the Supplementary Material - ***Cluster analysis*** for a more detailed description of this method. Overall, patients 2,7,8 and 9 exhibited two distinct tremor manifestations (i.e., tremor data well segregated into 2 clusters). For these specific patients, RSS and NS data was reduced to the data points allocated to the cluster with the largest percentage of samples in the RSS condition.

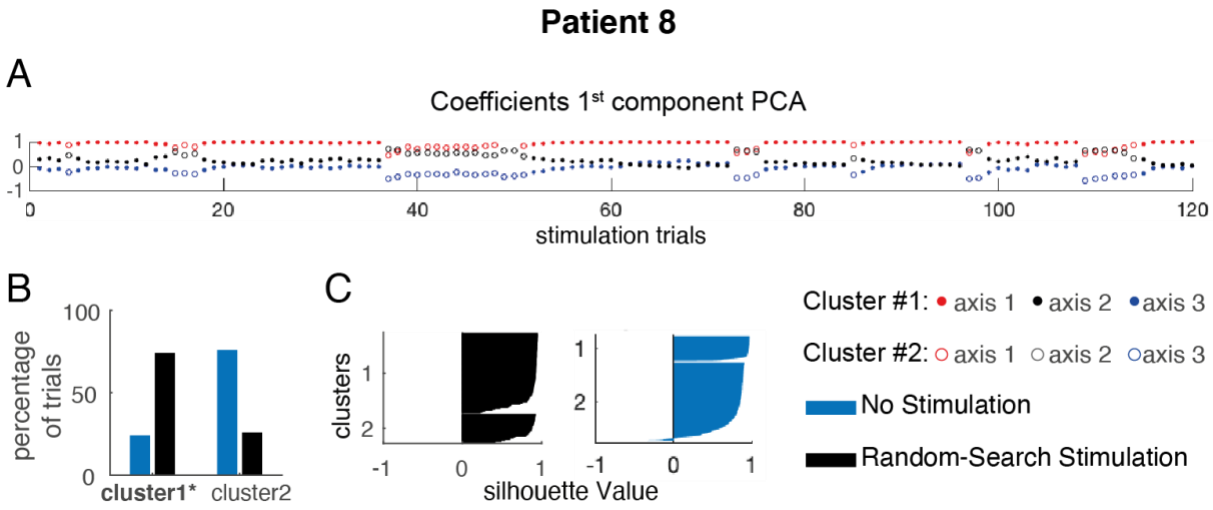


**Figure 5.1– Cluster analysis pipeline of tri-axial tremor data from patient 8.** A PCA was performed on the tri-axial tremor data merged data across NS and RSS conditions. Contributions from each axis to the first principal component were next allocated to one of two clusters using the Ward's method. Panel A illustrates how cluster representation changes over consecutive RSS runs. Panel B shows how cluster 1 was the one with the largest percentage of RSS trials (dark blue bar on cluster1*). Panel C displays a silhouette graphic representation of each cluster in each condition to qualitatively assess how well clustered the data is. In these graphs, a silhouette score (x axis) is attributed to every data point of each cluster (y axis) in each condition (RSS and NS on the left and right panels, respectively). Scores of 1 indicate similarity and scores of -1 dissimilarity of a given point to points of its own cluster compared points in another cluster. Since the average silhouette score of NS and RSS conditions was above 0.75 (our predefined threshold detailed in ***Cluster analysis***) , data of patient 8 was reduced to the data points found in cluster 1 (5-seconds segments of NS surrogate data, n=12,038/50,000 and 5-seconds segments of RSS data, n=89/120).

### Quantification of change in tremor severity during Random-Search Stimulation

ARCs were calculated to summarise stimulation effects. These curves show the median change in tremor severity observed during peripheral stimulation delivered at each tremor phases (n=12). To measure change in tremor severity we first filtered the tremor signal using a 2nd order Butterworth band-pass filter (cut-off frequency of ±2 Hz around the patient's tremor peak frequency) and obtained the evolution of the absolute amplitude (envelope/tremor severity) of the filtered tremor signal using the Hilbert Transform. Next, for each 5-second stimulation block, the average tremor severity found in the last second of stimulation (from the 4th-5th second) was normalised with respect to the average tremor severity during the one second prior to stimulation onset. This normalisation provides a comprehensive scale of stimulation effects where, -1 indicates complete tremor suppression, 0 indicates no change in tremor and positive values indicate amplification of tremor.

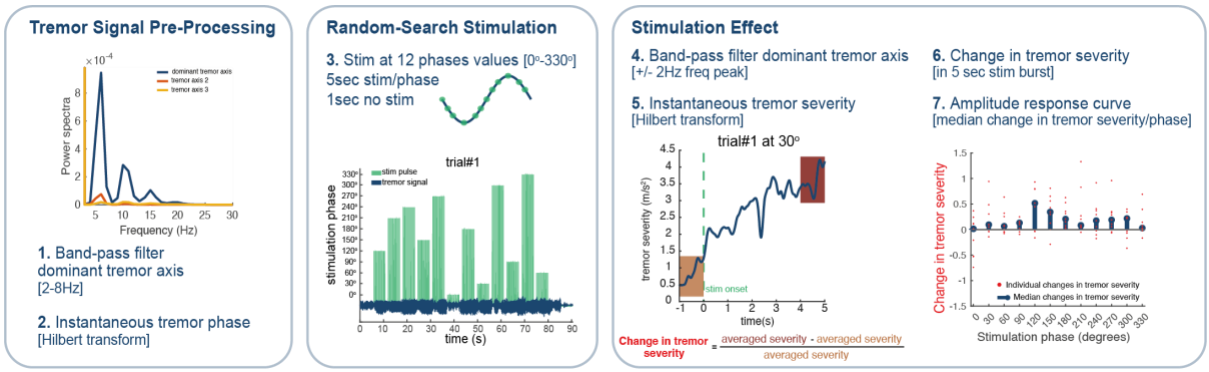


**Figure 5.2- Summary of data collection and analysis pipeline. Tremor Signal Pre-Processing**: unstimulated tremor signals were collected from the most tremulous hand using a triaxial accelerometer and the power spectral density of the three axes was computed. The dominant tremor axis was subsequently identified as the one with the largest power peak at the frequency of the tremor and bandpass-filtered between 2-8 Hz (1.) in order to have its phase extracted in real time (2.). **Random-Search Stimulation:** for 5 seconds, stimulation was locked to one of 12 randomly assigned phases from 0 to 330 degrees with a 30 degrees resolution (3.). **Stimulation Effect:** a Hilbert transform was then applied to the bandpass-filtered accelerometer signals (4. and 5.), from where the change in tremor severity within 5 second epochs was computed (6.). Lastly, ARCs were derived as the medians (blue stem plot) for all the changes (red dots) at a given phase (7.).

### Dependency of stimulation effects on tremor amplitude

The modulation of tremor across stimulation trials at a given tremor phase value need not be consistently suppressive or amplifying. For example, the direction of modulatory effects could be dependent on tremor amplitude at the time of stimulation. To test for this, we recomputed the individual ARCs after performing a median split of the data according to the averaged absolute tremor amplitude during the one second prior to stimulation onset. Similar to the stimulation effects analysis on the complete ARCs, changes in the two response curves (tremor

amplitude below or above the median at stimulation onset) were contrasted to those found during the NS condition.

### 5.2.5 Statistical analysis

To determine whether stimulation effects were significantly different from tremor spontaneous variability the following steps were applied to the data recorded in the NS condition. First, the envelope of the triaxial tremor signal during the NS condition was computed by Hilbert transforming the filtered triaxial tremor (2nd order Butterworth band-pass filter and cut-off frequency of ±2 Hz around the patient's tremor peak frequency). Next, 50,000 (or less if patient's data was reduced to one cluster; cf. section 5.2.4 - *Segregation of data according to tremor peripheral manifestations*) envelope segments of 5 seconds were randomly selected and the normalised change in tremor severity calculated. From this distribution, ten values were randomly selected and their median calculated (mimicking the median change in tremor severity across the 10 trials of stimulation that created ARCs). This was repeated 1,000,000 times leading to a surrogate distribution of spontaneous changes in tremor severity. Stimulation effects summarised by response curves were then compared to the z-scores of this distribution after controlling for multiple comparisons using the Bonferroni method (n=12 phases, alpha =0.0021).

Significance of the median split ARCs was achieved by splitting the initial NS distribution (n=50 000) according to the absolute tremor amplitude at the second preceding each of the randomly chosen 5-second epoch used to create the distribution. This procedure led to two distributions (n=25 000), from which in separate, 5 values were randomly selected and their median calculated, (mimicking the median change in tremor severity across the 5 trials of stimulation that created ARCs for low and high tremor). This was repeated 1,000,000 times leading to 2 final surrogate distributions of spontaneous changes in tremor severity from a low and high tremor baseline. Stimulation effects summarised by ARCs were then compared to the z-scores of their respective distributions after controlling for multiple comparisons using the Bonferroni method (n=12 phases, alpha =0.0021).

To test the significance of suppressive and amplifying effects of peripheral phasic-stimulation at the group level we have compared maximum suppression and amplification effects during RSS versus NS, using a Wilcoxon signed rank test (alpha =0.05). To this end, we first extracted from each individual ARC, both maximum suppression and amplification tremor values. These

were then compared to the 5$^{th}$ and 95$^{th}$ percentiles, of the most suppressive and amplifying effects found across NS ARCs, respectively. NS ARCs (n=1,000,000) were created by randomly drawing (with repetition), 12 values from the surrogate distribution of spontaneous changes in tremor severity (described at the beginning of this section). After finding the maximum spontaneous tremor amplification at each NS ARC, the 95$^{th}$ percentile was calculated and compared to the maximum tremor amplification observed during RSS. Likewise, maximum levels of tremor suppression derived from RSS ARCs were compared to the 5$^{th}$ percentile of maximum levels of spontaneous tremor suppression across NS ARCs.

To further characterise the impact of stimulation on tremor characteristics, a paired-wise t-test was used to compare the power at peak tremor frequency in the NS condition, to segments where stimulation was delivered and (1) amplification was observed, and (2) suppression was observed. Tremor data used for this calculation comprised all measured changes in tremor severity (amplifications and suppressions) and not only significant ones (Supplementary Figure S11).

# 5.3 Results

## 5.3.1 Within-subject modulation of tremor severity

Phase-specific stimulation of the median nerve can afford statistically significant modulation of tremor severity within subjects. In half of the cohort, change in tremor amplitude in the tracked axis during stimulation of the median nerve at a specific phase of the tremor was significantly higher than that observed spontaneously as demonstrated by individual ARCs. Stimulation phases at which a significant change in tremor severity was observed are depicted by red dots in Figure **5.3** (after controlling for multiple comparisons [n=12] with Bonferroni correction). Note that only two patients had their tremor significantly supressed by peripheral stimulation (patients 2 and 9). Our hypothesis that phase-locked median nerve stimulation would modulate neural activity underlying tremor as evidenced by certain stimulation phases having tremor amplifying effects while others having suppressive effects, could not be confirmed in 8/9 patients.

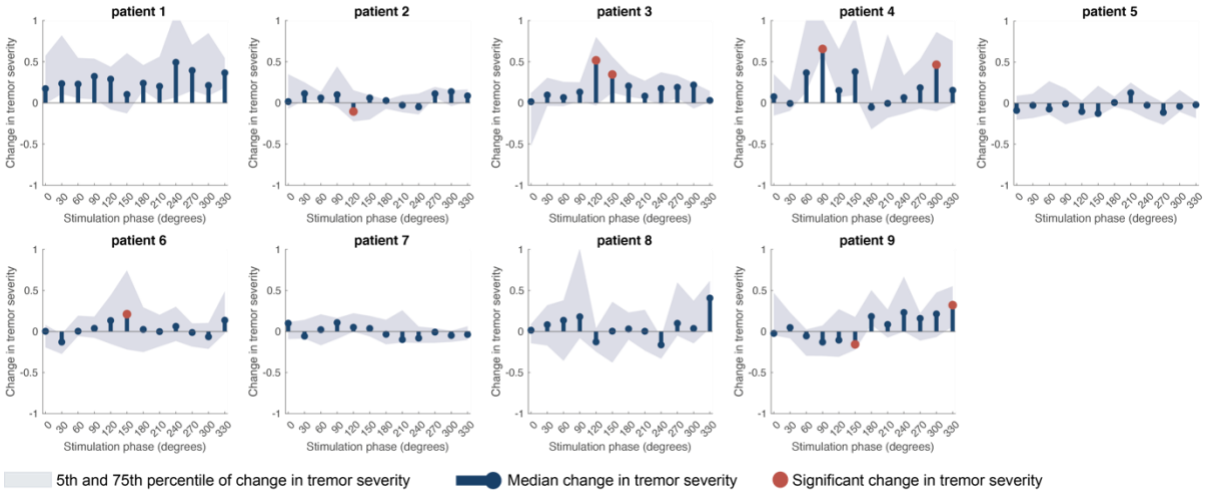


**Figure 5.3 - Patient-specific changes in tremor severity during Random-Search Stimulation.** The median change in tremor severity at the predominant (tracked) axis while stimulating at different phases of the tremor cycle (0-330°), is shown by the stem plots in dark blue (ARCs). Change in tremor severity has been normalised so that 0 denotes no modulation of tremor severity, -1 indicates complete tremor suppression and positive values indicate tremor amplification. The shaded light blue area represents the 25th and 75th percentile of change in tremor severity (across RSS trials). Red dots indicate phases at which stimulation induced modulation of tremor is beyond natural variability of tremor. Note that half of the cohort has at least one stimulation phase where effects were significant and that only patient 9 shows statistically significant bi-directional (i.e., phase-dependent amplification and suppression) stimulation effects.

Figure **5.3** summarises the changes in tremor severity at the tracked dominant tremor axis, as defined by the axis with the most prominent tremor signal in the RSS condition. However, tremor in other axes are also modulated by peripheral nerve stimulation. Across patients, axes and phases, peripheral stimulation induced significant changes in tremor amplitude in 22 instances - 2 significant suppressions and 20 significant amplifications. This result is above chance level (22>1.5, [no $significant\ effects$ > ($no\ patients \times no\ axes \times 0.05$)]), providing evidence that the delivery of stimulation to the median nerve in a phase-specific manner is capable of modulating tremor in a subset of patients.

## 5.3.2 Modulation of tremor severity at the group level

Phase-specific stimulation of the median nerve does not afford statistically significant modulation of tremor amplitude at the group level. Efficacy of phase-locked stimulation on tremor at the group level, was assessed by aligning individual ARCs to the stimulation phase which afforded the largest tremor suppression and amplification. While we have found a main effect of stimulation phase on tremor severity at the group level (Friedman's test applied to

ARCs realigned to the phase-affording maximum tremor amplification, P =0.0025, dF=11, and to ARCs realigned to the phase-affording maximum tremor suppression P=0.0072 ,dF=11, compared to no change or zero); changes on tremor severity induced by stimulation were not statistically different from those spontaneously achieved during no stimulation after aligning individual surrogate ARCs to spontaneously observed tremor amplification and suppression (p=0.702, tremor amplification and p=0.129, tremor suppression; Figure **5.4**).

Moreover, there were no significant differences in tremor power between experimental conditions and stimulation effects (Supplementary Figure S11). Tremor power at peak tremor frequency during peripheral stimulation, irrespective of phase-dependent effects (i.e., suppressive or amplifying), was not significantly different from tremor power when no stimulation was delivered (p= 0.901 and p= 0.793, respectively). Likewise, tremor power during tremor-amplifying stimulation was not significantly different from that when tremor suppression was observed (p= 0.723).

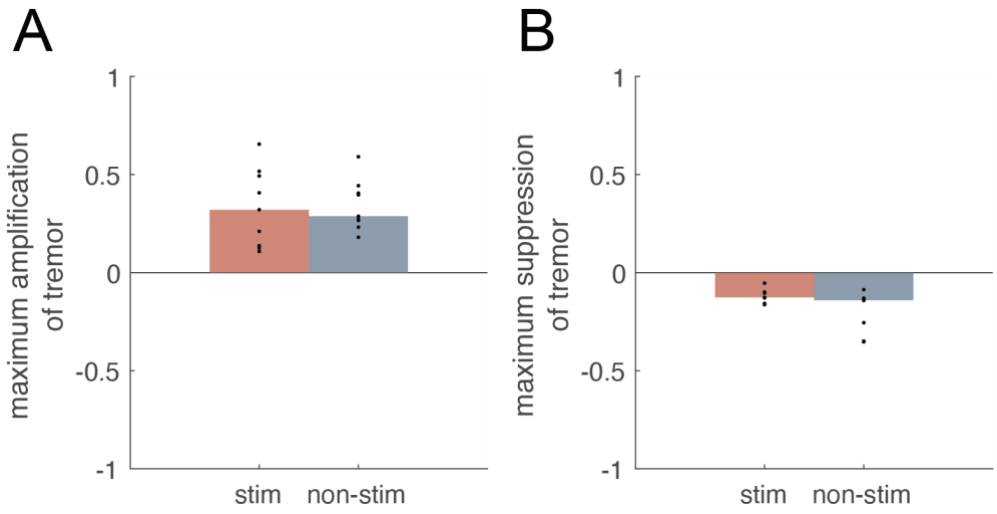


**Figure 5.4 - Group analysis of tremor modulation with peripheral stimulation.** Maximum amplification (panel A) and suppression (panel B) of tremor amplitude across patients during Random-Search Stimulation (*stim*, red bars) and No-Stimulation (*non-stim*, grey bars) conditions have been statistically compared using a Wilcoxon signed rank test (tremor amplification p=0.702 and tremor suppression p=0.129). Black dots indicate individual maximum changes in tremor severity and bars their median.

### 5.3.3 Dependency of stimulation effects on tremor amplitude

Phase-specific modulation of tremor amplitude is greater and significant when tremor is weaker. Segregating stimulation effects according to tremor severity at stimulation onset, reveals a link between the modulatory effect of phase-specific stimulation and spontaneous variability in tremor severity. For some patients, a high versus low amplitude tremor prior to stimulation delivery led to opposite effects at the same stimulation phase (amplification vs. suppression). In patient 6 (Figure **5.5**A), for example, when stimulating the median nerve at 210 degrees – if stimulation occurred when tremor amplitude was low, tremor became amplified; if delivered when tremor amplitude was high, stimulation supressed it. Tremor amplitude prior to stimulation delivery may be influenced by a carryover effect from previous stimulation epochs and spontaneous changes in tremor severity. Importantly, when taking instantaneous tremor amplitude into account, the overall number of phases leading to significant modulation of tremor increased from 8 to 12.

Contrasting the information contained in the individual amplitude median split ARCs, we found that the magnitude of stimulation effects, quantified as mean of absolute ARCs during low and high tremor amplitude, differed. This is shown in Figure **5.5**B where the absolute amplitude of stimulation effects is significantly higher when stimulation is delivered at low rather than high tremor amplitude ($p=0.004$). To account for a potential regression to the mean, the individual mean magnitude modulation (black dots in Figure **5.5**B) was obtained by averaging the absolute value of normalised low and high ARCs. Normalised ARCs were computed by subtracting the median changes in unstimulated tremor at each condition (epochs of tremor preceded by low and high tremor amplitude) from the respective low amplitude and high amplitude ARCs.

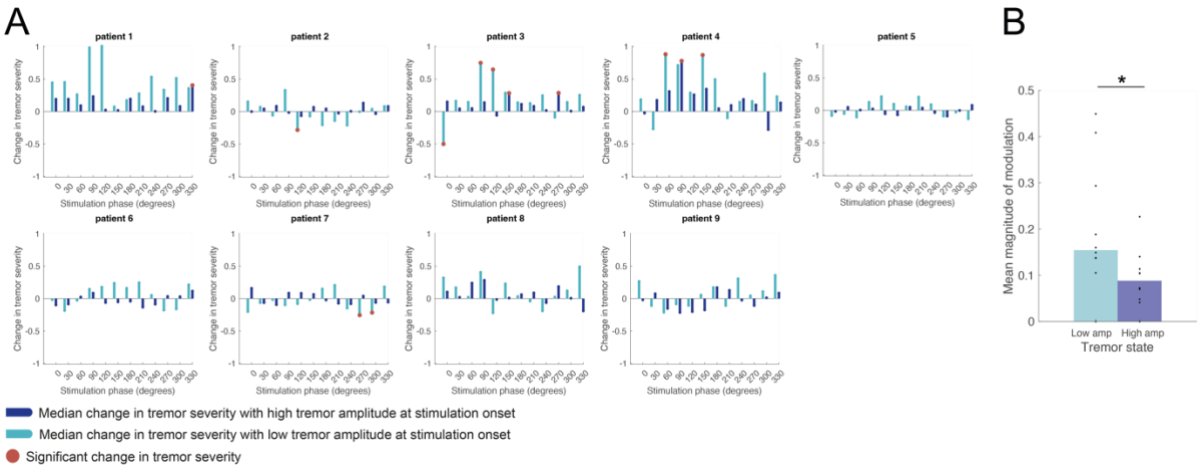


**Figure 5.5 - Individual stimulation effects during low and high tremor amplitude.** Panel A shows individual ARCs after dividing the data according to the tremor amplitude during the second prior to stimulation onset. Data are shown for the predominant (tracked) axis. Light blue bars corresponding to ARCs computed from stimulation blocks where tremor amplitude prior to stimulation was below the median tremor amplitude across the stimulation condition and dark blue bars where tremor amplitude prior to stimulation was above the median. For visualisation purposes low amplitude and high amplitude ARCs have been subtracted by the median change in tremor severity found in low and high unstimulated tremor distributions, respectively. Red dots indicate the phases at which stimulation induced a change in tremor severity significantly different to that observed naturally during similarly analysed unstimulated data. Panel B indicates that the mean (normalised) absolute effect size obtained by peripheral stimulation when delivered at spontaneously low tremor amplitude epochs (light blue) is significantly higher than when delivered at high tremor amplitude epochs (dark blue) (p=0.004).

## 5.4 Discussion

Most stimulation-based approaches for supressing tremor aim to disrupt excessive neural synchrony observed across the tremor network. The parameter space to achieve such disruption is vast and includes where (stimulation target), when (open or closed-loop) and how (invasive versus non-invasive, continuous or patterned stimulation) a perturbation to the tremorgenic network must be provided. Here, we deliver non-invasive electrical stimulation to the median nerve at motor-threshold intensity, in a patterned and closed-loop fashion in order to selectively modulate the central tremor drive. We observed a link between the modulatory effect of phase-specific stimulation and spontaneous variability in tremor severity, whereby delivered during spontaneously low tremor amplitude afforded more frequent phase-dependent modulation of tremor severity.

In ET, tremor severity fluctuates spontaneously over time. The rate and magnitude of this fluctuation is seldom structured and consistent across subjects (Cleeves and Findley, 1987; di Biase *et al.*, 2017). We accounted for this variability in several ways. First, we compared the median change in tremor severity at any given stimulation phase to spontaneous variations in tremor severity measured in the absence of stimulation as opposed to solely contrasting effects against a null distribution. Second, we ensured that effects of stimulation at different phases were assessed across epochs of relatively consistent posture by limiting the duration of stimulation at each phase. Third, by using a range of measures such as principal component analysis and cluster division, we analysed epochs of stimulated and unstimulated data with a comparable tremor manifestation peripherally. With these procedures we found that 5 seconds peripheral stimulation could elicit phase-dependent, albeit weak, effects on tremor severity.

These phase-specific effects were significantly greater than spontaneous fluctuations in tremor in more than half of our cohort (Figure **5.3**), however not present at the group level (Figure **5.4**). The latter potentially reflects limited phase-dependent effect sizes due to the stimulation duration at each phase (i.e., 5 seconds). Stimulation effects became clearer still when measuring the effect of stimulation while taking into account tremor severity right before stimulation onset. This enhanced the number of phases at which stimulation afforded significant changes in tremor amplitude (Figure **5.5**). Effects of peripheral stimulation delivered at a certain phase of limb acceleration would be depended on both, conduction delays of spindle afferents to the thalamus (Urasaki *et al.*, 1990; Hanajima *et al.*, 2004), and the subject specific relationship between limb acceleration and central tremor rhythms (Pedrosa *et al.*, 2018). As a result, the same phase derived from peripheral tremor may reflect different instances of central tremor activity across patients, giving rise to the variability in the precise stimulation phase that could elicit significant modulation in tremor severity (Figure **5.3** and Figure **5.5**).

In summary, these findings suggest that in some ET subjects, a fine modulation of tremor severity can be achieved via tolerable peripheral stimulation if both the phase and magnitude of the tremorgenic oscillator (measured here at the periphery with an accelerometer) are used to control stimulation delivery. In particular, we observed that modulation of tremor was greater if phasic-specific stimulation was applied when tremor amplitude was spontaneously low (Figure **5.5**B). A similar inverse relationship between the change in tremor severity due to stimulation and the absolute tremor severity has recently been proposed in a computational

work by Weerasinghe and colleagues (Weerasinghe *et al.*, 2019). In this computational study, the link between stimulation and tremor severity bore out if a set of properties were satisfied by the tremor oscillators such as the response of each oscillator to external perturbation having a specific form (Ermentrout, 1996). Patient specific variability in how tremor oscillators respond to external input and differences in coupling across the central and peripheral circuits could therefore strongly influence the individual response to phase-specific peripheral stimulation.

Nevertheless, tremor modulation when present, was small. We attribute this to several experimental factors. First, we used subject-specific motor-threshold as our stimulation intensity and delivered a single electrical pulse to the median nerve at each stimulation phase. This was motivated by our aim to evaluate the modulatory potential of easily tolerable peripheral stimulation. We speculate however, that these stimulation parameters were too weak to modulate thalamic neural activity and decouple the highly synchronised tremorgenic network sufficiently for clinical impact. That our stimulation intensity was weak is supported by the neurophysiological study performed by Hanajima and colleagues, where peripheral stimulation was delivered at 1.1-1.2 times the motor-threshold and yet only sparse changes in thalamic neural firing was reported (Hanajima *et al.*, 2004). It should be noted that, stimulation sensation could nonetheless lead to an interaction between tremor and arousal networks which in tandem with the weak but optimally timed proprioceptive afferent to the thalamus could further facilitate modulation of tremor severity (Dirkx *et al.*, 2020). In addition to stimulation intensity, the number of pulses delivered per tremor cycle (i.e. duty cycle) and stimulation frequency could play a critical role in stimulation efficacy as has been highlighted by a recent study where it has been shown that peripheral stimulation delivered to the radial nerve at 0 degrees with respect to tremor could yield 12-15% reduction in tremor severity (Kim *et al.*, 2020).

Second, stimulation location may have been sub-optimal. The choice of the median nerve at the wrist for stimulation was motivated by our aim to develop a convenient non-invasive therapeutic device that could bring tremor relief. A wristband that can supress tremor by sensing and stimulating according to patients' individual tremor characteristics would be extremely appealing. However, the peripheral manifestation of tremor has a fine somatotopic representation in the thalamus (Hua and Lenz, 2005; Pedrosa *et al.*, 2012), where even trembling muscles from the same limb are characterised by distinct tremor clusters (Pedrosa *et*

*al.*, 2012). Related afferent and efferent information is mediated by different thalamic cells (Hua and Lenz, 2005) which co-exist in the same tremor cluster (Pedrosa *et al.*, 2012, 2018), while the phase relationship between these cells determines tremor severity (Pedrosa *et al.*, 2018). Yet ET predominantly manifests at the hand through the out-of-phase activation of antagonist forearm muscles which control the flexion and extension of the wrist (Deuschl *et al.*, 1998). If tremor emerges and is controlled in a spatially organized manner, then the muscle twitch or orthodromic stimulation of thumb muscle proprioceptor afferents by median nerve stimulation may have had limited central effects on the tremor clusters underlying wrist dynamics (Hua and Lenz, 2005; Pedrosa *et al.*, 2012). Stimulation effects observed here might potentially stem not only from a phase-specific perturbation of central circuits but also of spinal ones; whereby an interaction between the afferent inputs and the descending signals might have coincided.

Lastly, it should also be noted that we only delivered stimulation at a particular phase of tremor for five seconds at a time, and thus any induced spike-timing dependent plasticity (Zanos *et al.*, 2018) will have been limited, if at all present. Instead, tremor amplitude modulation will have been predominantly down to the effect of stimulation in decreasing or increasing the period (i.e. instantaneous frequency) of the central tremor oscillator (Ermentrout, 1996; Smeal *et al.*, 2010). Particular phases of stimulation may pull the instantaneous frequency of the tremor away from or towards a given oscillator's resonance frequency, thereby modulating amplitude (Cagnan *et al.*, 2013, 2017). This effect may be diminished when tremor consists of several different independent tremor oscillators, as each may have its own sensitive phases. For a more precise evaluation of phase-dependent effects on different tremor oscillators, high-density electromyography (EMG) could be leveraged in the future. Unlike accelerometery which provides a composite measure, high-density surface EMGs can be used to sense and identify independent tremor oscillators through a complete spatial coverage of the upper-limb muscles displaying tremorgenic activity (Miller *et al.*, 2014). In this study, we opted for accelerometery as a control signal in order to minimise the amount of instrumentation needed to achieve close-loop peripheral stimulation, which may influence device use and compliance, and controlled for the compound nature of tremor using principal component analysis.

### 5.4.1 Limitations and future directions

The current study tested the hypothesis that phase-locked median nerve electrical stimulation is capable of driving thalamic afferent inputs and hence act to disrupt the central pathologic oscillatory resonance when delivered at a specific tremor phase. Due to the time constrains inherent to lab-based settings, we were only able to vary the tremor phase at which stimulation was triggered (n=12) and had to maintain stimulation parameters such as intensity, number of pulses and stimulation duration fixed. We believe that remote testing and potentially real-time parameter optimisation consist of near-future realities which will allow for a systematic exploration of different parameter combinations and their impact on the individual's symptoms, and lead to the development of more effective wearable devices for ET patients.

## 5.5 Conclusion

Our study provides useful insights into how to evaluate real-time and non-invasive strategies aimed at reducing tremor given its pronounced spontaneous variability. Our results suggest that motor-threshold peripheral stimulation is too weak to generate clinically useful tremor suppression, and although subtle significant amplitude modulation could be detected this tended to favour amplification. More frequent phase-dependent tremor modulation could be seen when spontaneous tremor amplitude prior to stimulation onset was taken into account, suggesting that a more sophisticated control policy that considered online estimates of not only tremor phase but also amplitude might be more effective in capturing and suppressing tremor in selected individuals.

# 6 General Discussion

To guide the general discussion that follows, a summary of the main results of this thesis is provided in the table below. These are displayed by chapter in conjunction with the respective research question posed at the beginning. Subsequently, I will focus on parallels between chapters while highlighting the important role of temporally specific communication for health, disease and therapeutical strategies.

| | Research questions | Main results |
|---|---|---|
| **2** | Can fast synaptic TC dynamics help explain the modulation of beta oscillations in PD? If so, are such dynamics circumscribed to inter-regional connections or do they involve local circuitries as well? | We found that a transition from low to high cortical beta power is promoted by changes in the synaptic strength of projections across the TC circuit.<br><br>These projections involve intracortical and intrathalamic circuitries as well as connections between thalamus and cortex.<br><br>The temporal distinction of laminar specific inputs to the motor cortex (delay of cortico-cortical vs thalami-cortical projections) was pinned-down as a key mechanism to achieve high levels of cortical beta synchrony. |
| **3** | Does local synchronisation emerge simultaneously across the BG-output, motor thalamus and cortex? Are high beta oscillatory events mediated by changes in the temporal relationship between subcortical and cortical beta activities? | We found that SNr and BZ beta activity is transiently increased during cortical beta bursts at the level of ensembles and single neurons.<br><br>Phase-locking between cortical/SNr and cortical/BZ ensemble signals follows the time course of cortical beta bursts<br><br>The onset of consistent phase-locking is preceded by abrupt phase slips in the alignment between cortical/SNr and cortical/BZ ensemble signals. |
| **4** | Given that temporal stimulation of the thalamus can in some cases restore motor behaviour in ET patients, how resilient is this strategy to state changes in the underlying motor circuit? Will this strategy be equally efficient during kinetic tremor? | Phase-specific DBS can suppress postural and kinetic tremor in ET patients.<br><br>We found that in ET patients with stable tremor characteristics, phase-specific DBS is capable of controlling postural tremor rebounds.<br><br>Phase-specificity is key to achieve postural tremor control.<br><br>Periodic phase-unspecific perturbations to the thalamus seem to be sufficient to yield kinetic tremor suppression. |
| **5** | Can motor behaviour in ET be restored by temporally specific proprioceptive thalamic afferency triggered via median nerve stimulation? | We found that delivery of single time-specific pulses to the median nerve tends to worsen rather than improve ET postural tremor.<br><br>Significant phase-dependent modulation becomes more evident if tremor amplitude is considered.<br><br>Modulation of tremor via thalamic proprioceptive afferency is more easily achieved during low levels of tremor synchrony. |

**Table 6.1– Summary of research questions and main results of each thesis chapter.**

## 6.1 The role of thalamocortical dynamics for the modulation of synchronisation in PD

This thesis tested the hypothesis that interactions between the thalamus and cortex contribute to the temporal patterning of beta oscillations in PD. Results from the two projects described in chapters 2 and 3 are supportive of this hypothesis while showing that the emergence of episodes of high beta synchrony are linked to: 1) a transient strengthening of delayed (extrinsic) inputs from thalamic relay cells to deep pyramidal cells and fast (intrinsic) inputs from middle pyramidal cells to superficial pyramidal cells, and 2) a dynamic adjustment of thalamic (and SNr's) phase alignment with respect to the cortex. For a critical interpretation of these results, I will first discuss the translational significance of these findings and then comment on our methodological choices.

### 6.1.1 Translational significance of the findings

Although not fully elucidated, there is strong evidence suggesting that excessive beta-rhythms observed in the BGTC circuit during untreated PD originate at the BG rather than the cortex or thalamus. More specifically, within the BG a common proposition is that beta emerges from the recurrent interactions between the STN and GPe (Bevan *et al.*, 2002; Terman *et al.*, 2002, Mallet *et al.*, 2008*a*; Holgado *et al.*, 2010; Cruz *et al.*, 2011; Tachibana *et al.*, 2011; Nevado-Holgado *et al.*, 2014; Cagnan *et al.*, 2015) or alternatively from the inhibitory processes within the GPe alone (Crompe *et al.*, 2020). The BGTC is highly interconnected and therefore activity of different nuclei and/or projections are thought to play a role in the propagation or even modulation of beta synchrony across the circuit. An example is the motor thalamus whose hyperactivity or silencing is capable of abolishing beta oscillations across the circuit (Brazhnik *et al.*, 2016).

While these mechanisms may help explain the propensity of the BGTC circuit to oscillate at beta frequencies, exactly which neural mechanisms control the temporal dynamics of beta are only now being explored. Recent literature indicates that beta burst dynamics such as the rate, duration and timing, are more informative metrics than average-estimates of beta amplitude when studying the relationship between beta and motor behaviour (Feingold *et al.*, 2015, Tinkhauser *et al.*, 2017*a*; Deffains *et al.*, 2018; Torrecillos *et al.*, 2018; Little *et al.*, 2019; Duchet *et al.*, 2020).

Crucially, a deep understanding of the transient nature of beta synchrony and its relevance for motor (dys-)function (Feingold *et al.*, 2015, Tinkhauser *et al.*, 2017*b*) has the important potential of shedding light on more naturalistic and effective ways of treating dysfunction than those currently available (Little *et al.*, 2013, 2016*b*, Tinkhauser *et al.*, 2017*a*). In turn, this has motivated an increasing number of studies, including this thesis, to focus on the intermittent neural processes underscoring time resolved beta dynamics (Tinkhauser *et al.*, 2018, Cagnan *et al.*, 2019*b*; Crompe *et al.*, 2020; West *et al.*, 2020).

This thesis focuses on the intermittent neural processes occurring at the TC level due to the reciprocal relationship that cortex and thalamus establish, the key anatomical position that the thalamus displays for BG-cortical communication, and the optimal position of cortex for non-invasive therapeutic techniques. Results from our DCM study (chapter 2) suggest that reducing the excitatory inputs to superficial or deep pyramidal cells of the cortex could potentially disrupt enhancement of cortical beta. Taking this into account, our findings could be leveraged into a potential stimulation strategy entailing an online, closed-loop stimulation of the cortex, where stimulation would be triggered as soon as the duration of a cortical beta burst would surpass a predetermined duration of bursts for that given patient. We propose a pre-clinical test of such a therapeutic strategy using animal models of PD and optogenetics since laminar specificity was featured in our model as an important aspect of cortical beta dynamics, and targeting a specific cortical layer or cell-type is not yet possible with the state-of-the-art non-invasive stimulation devices in humans (Underwood and Parr-Brownlie, 2021).

Through a variety of analyses summarised in chapter 3 we characterise neural events that dictate the temporal dynamics of beta synchronisation across the returning pathway of the CTCBG circuit. We consistently found that increased local synchrony is preceded by an abrupt discontinuity in the phase alignment between cortical/SNr and cortical/BZ beta oscillations, which temporarily stabilises while cortical beta amplitude is above a certain threshold and suffers a discontinuity again as cortical beta amplitude falls below the threshold. These temporal dynamics in cortical/subcortical beta alignment are consistent within and across bursts and have also been described in other nodes of the BG (Cagnan *et al.*, 2019*b*).

Slips in the phase of BG beta oscillations have been investigated before as a by-product of phase-locked stimulation of the STN in PD patients (Holt *et al.*, 2019). Authors of this study

found that significantly more phase slips would be observed immediately after stimulation at the preferred phase for beta suppression than in surrogates generated from unstimulated segments of the recording. Crucially, the number of stimulation-induced phase slips correlated with the levels of reduction in beta amplitude. Together, results from this study and chapter 3 of the present thesis, suggest that spontaneous or induced, phase slips do correlate with levels of modulatory effects upon local and inter-areal synchronisation.

Phase slips seem to play a critical role in the emergence (and termination) of transient events of high synchrony, which we know that if prolonged and in excess, drive disease symptoms (Tinkhauser *et al.*, 2017*b*). Hence, BZ or GPi stimulation at specific cortical beta phases, could potentially provide means of preventing BG or thalamic neurons from firing in a phase-locked regime which promotes beta bursts. To be harnessed into a closed-loop algorithm, ideal phase-dependent effects would necessarily have to involve a partial and not complete inhibition of beta bursts for the same reasons explained above (i.e., since short beta bursts are vital for healthy motor behaviour). In line with what is proposed here, suppression of cortical power in the beta band was observed in a seminal experimental study where stimuli were delivered at specific phases of the cortical beta to the BG (GPe) of behaving 6-OHDA hemi-lesioned rats (McNamara *et al.*, 2020). This study did not however include a behavioural assessment of stimulation effects. Hence, it is important that a simultaneous acquisition of behavioural and stimulation effects on neural activity is included in future explorations of subcortico-cortical phase-locked stimulation strategies for a better understanding of its therapeutic utility.

### 6.1.2 Methods and Data

Do interactions between the thalamus and cortex contribute to the temporal patterning of beta oscillations? To provide an answer to this question, I have used two sets of neurophysiological recordings from the PD rat model and estimated the effective and functional TC connectivity during a transition from low to high levels of cortical beta power. Why have we used these metrics of connectivity to assess TC interactions; how can we best measure low and high levels of local beta synchrony and how informative is the anaesthetised 6-OHDA lesioned rat model for the study of beta dynamics, are topics that I will be addressing below.

### Effective and functional connectivity

Previous studies on beta synchrony in the context of PD have mainly focused on determining how connectivity across the BGTC circuit, or loops of the circuit, change from untreated to treated PD states (Brown *et al.*, 2001; Moran *et al.*, 2011; Marreiros *et al.*, 2013; Kahan *et al.*, 2014; Brazhnik *et al.*, 2016). Here, building on the recently uncovered transient nature of beta activity and its functional relevance for motor behaviour (Feingold *et al.*, 2015, Tinkhauser *et al.*, 2017*a*; Torrecillos *et al.*, 2018; Little *et al.*, 2019), I have sought for a characterisation of within-disease TC interactions while looking at changes in TC connectivity linked to the emergence of beta bursting.

Interactions between brain structures can be divided into three types of connectivity (Friston, 2011): structural, which characterises the axonal projections across brain regions; functional, which describes statistical dependencies between brain regions, and effective, which estimates the causal influence that one region has on another. Taking advantage of the fact that both functional and effective connectivity can be directly estimated from neurophysiological recordings, I have leveraged both metrics and achieved a more complete description of TC interactions in the parkinsonian state.

In brief, using functional connectivity metrics I could identify changes in the statistical dependencies between the phase of beta activities in the BZ thalamus and in the cortex, as well as in the BG-output nucleus (SNr) and in the cortex, around periods of beta bursting. Despite not being able to explicitly determine which region is lagging or leading at the time cortical beta power becomes intermittently exaggerated, results from these analyses suggest that communication between down-stream structures from the BG are significantly increased when cortical beta is transiently enhanced.

In addition, analysing the effective connectivity of the TC circuit has allowed me to explore whether the way nodes of the TC network (i.e., different laminae of the cortex and nuclei of the thalamus) impact upon one another, can explain the transient amplification of cortical beta activity; and in particular, if there are some network projections that are more relevant than others for such modulation. Using DCM and a neural mass model of the thalamus and cortex, we have found that despite various connections across the loop (corticothalamic, thalamocortical, intracortical and intrathalamic) changing their coupling strength to promote an increase in cortical beta power, a temporal segregation of inputs to the cortex was identified

as crucial. Critically, a delayed input from thalamic relay cells to deep pyramidal cells and a fast input from middle pyramidal cells to superficial pyramidal cells were prominent features of our model for the evolution of cortical beta power to high levels.

Together these two studies contribute to a deeper knowledge on the intermittent nature of beta oscillations while 1) mapping out the TC synaptic dynamics underlying the generation of intermittent cortical high beta power and 2) describing the organisation that occurs across the network as beta bursts emerge.

### Measuring beta bursts

One of the aims of this thesis was to create a better understanding of the dynamic nature of beta synchrony in the PD state. Yet, how to best capture the temporal patterning of beta oscillations remains a rather arbitrary process. It has been proposed that a motor network displaying frequent short beta bursts, is healthier than one displaying frequent long beta bursts (Tinkhauser *et al.*, 2017*a*, *b*). Nevertheless, how to separate long from short bursts, as well as how to define bursts themselves is something that has not been empirically defined.

Bursts are usually identified by using a threshold, rather than an absolute cut off-value (Feingold *et al.*, 2015, Tinkhauser *et al.*, 2017*b*, *a*; Torrecillos *et al.*, 2018, Cagnan *et al.*, 2019*b*; Little *et al.*, 2019). In chapter 3, bursts were based on what previous studies exploring beta dynamics under parkinsonian states have used – i.e., defined at the 75th percentile crossing of the beta signal amplitude (Tinkhauser *et al.*, 2017*b*, *a*, 2018, Cagnan *et al.*, 2019*b*). Nevertheless, Supplementary Figure S4 suggests that results are preserved when using the $55^{th}$ and $95^{th}$ amplitude percentile as a threshold for burst definition.

Chapter 2 used a different definition of burst. In cross spectral density-DCM, the conditions upon which the inversion of our biophysical models occur are effectively spectral densities derived from segments of the data we are interested in studying. To be able to detect network dynamics linked to a transition from one condition to another, this method requires the two different conditions to have distinctively different power densities. Since this is not necessarily the case for the levels of beta power found within the segments preceding and following a single threshold, a different method was used for data selection. This consisted of a dual threshold on the cortical envelope. As a result, beta events with extreme beta power were obtained and labelled as low-power beta events if derived from data segments displaying an envelope with an area below the 5th percentile observed across the recording, and as high-

power beta events if derived from segments of data with an area above the 95th percentile observed across the recording (Figure **2.5**). Supplementary Figure S1 describes how beta power conditions in this specific chapter relate to beta bursts. In brief, data-segments labelled as high-power beta, contained more beta bursts (defined according to the 75$^{th}$ envelope percentile, but without a minimum duration of 50ms) than those labelled as low-power beta.

### 6-OHDA lesioned rats, anaesthetised and cortically activated

Animal models of PD aim to replicate both dopaminergic cell loss and motor impairments associated with PD. Moreover, they are crucial for preclinical research since new therapies developed to alleviate PD symptoms can be tested in such models. Recordings used in both chapters 2 and 3 were acquired from urethane-anesthetized rodents rendered parkinsonian by 6-OHDA lesions. The 6-OHDA lesioned rat is an extremely useful experimental model of PD, which has contributed important insights into the pathological mechanisms of the disease (Degos *et al.*, 2009; Avila *et al.*, 2010; Nevado-Holgado *et al.*, 2014; Abdi *et al.*, 2015; Brazhnik *et al.*, 2016; Crompe *et al.*, 2020).

The catecholamine neurotoxin 6-hydroxydopamine is a molecule that once injected causes degeneration of nerve terminals (and cell bodies but to a lesser degree) of both dopaminergic and noradrenergic neurons (Deumens *et al.*, 2002). The extension and selectivity of dopamine depletion varies with the site of injection; desipramine is often administrated before the 6-OHDA injections to minimize the uptake of 6-OHDA by noradrenergic neurons and achieve a higher selectivity of dopaminergic degeneration (Schwarting and Huston, 1996*a*). Recordings from this animal model of PD are often acquired in awake or anaesthetised states (Mallet *et al.*, 2008*b*, *a*; Avila *et al.*, 2010; Brazhnik *et al.*, 2016; Crompe *et al.*, 2020). During the awake state and episodes of spontaneous cortical activation in the anaesthetised state, recordings from the 6-OHDA rat's BGTC circuit display patterns of activity which are analogous to those observed in unmedicated PD patients (Mallet *et al.*, 2008*b*, *a*). This is at least true when contrasting the beta coherence and power spectra found in human and PD rat recordings; but the question remains whether the temporal pattering of beta oscillations in humans is comparable to that found in the rat model, and more specifically in the anaesthetised state. In the neurophysiological study by Cagnan and colleagues, phase-locking dynamics of cortico-subthalamic beta activity around cortical beta burst onset from recordings in PD patients and 6-OHDA lesioned rats under urethane-anaesthesia, were remarkably similar (Cagnan *et al.*, 2019*b*). Nevertheless, a recent study has reported that the mean beta burst duration, which

becomes shorter in the STN following levodopa administration and DBS in PD patients (Tinkhauser *et al.*, 2017*b*; Duchet *et al.*, 2020), is unchanged with STN lesioning or STN opto-inhibition in the urethane-anaesthetised 6-OHDA lesioned rat (Crompe *et al.*, 2020). Although this discrepancy might be partly due to altered mechanisms of action and network effects yielded by different interventions (DBS, levodopa, opto-inhibition and ablation), a thorough examination of beta dynamics across different nodes of the BGTC circuit, in different species and during different states of disease, is needed to confirm that animal models of PD are suitable for the study of beta dynamics.

## 6.2 The impact of thalamocortical dynamics on the modulation of ET tremor

An overarching hypothesis of this thesis was that modulation of pathological TC interactions could be achieved with temporally-specific stimulation approaches. To test this hypothesis, we have recruited patients suffering from ET and used the closed-loop phase-specific stimulation algorithm developed by Cagnan and colleagues in 2017, to deliver repetitive perturbations to the TC circuit and modulate tremor severity.

ET provides an excellent opportunity to investigate the role of TC interactions on motor behaviour. This is because ET's primary motor symptom, involuntary shaking of the upper limbs, reflects closely the underlying aberrant patterns of thalamic neural activity (Figure **1.3**). Building upon this observation, the phase-specific stimulation algorithm developed by (Cagnan *et al.*, 2017) uses accelerometery of the trembling limb to trigger repetitive thalamic perturbations at a specific timing of the peripheral tremor cycle. As a mechanism of action, this strategy proposes that for each patient there is a specific timing at which thalamic perturbations lead to a broad disruption of the tremor circuit's aberrant synchrony and result in tremor suppression.

Here, we delivered perturbations to the thalamus directly via deep brain stimulation (chapter 4) and indirectly via proprioceptive thalamic afferents triggered with median nerve stimulation (chapter 5). Our findings support our hypothesis while showing that phase-specific stimulation

aimed at central oscillators in the thalamus is capable of modulating tremor. Yet, our results were not always straightforward and raise various issues which are worth discussing.

In this last section of my general discussion, I will mainly focus on the common threads between the two last chapters and explore the key features underlying phase-specific stimulation efficacy.

### 6.2.1 Phase-specific stimulation efficacy and network states

It is thought that the stability of long-range synchronization across brain structures of a given network is dependent on the synaptic coupling of that same network. Although not directly, results from chapters 4 and 5 support this view by showing that consistent disruption of a specific phase alignment can only be maintained if the conditions from which this alignment emerged are kept close to constant.

Our findings from chapter 4 indicate that postural tremor can be supressed with phase-specific DBS if the following conditions hold: the frequency-range of tremor is narrow, and the spatial distribution of the central oscillators is stable. In broad terms, it is likely that both observations reflect dynamics of the underlying tremor network. Firstly, there is good evidence that the frequency at which neurons oscillate is in large parts determined by the inputs they receive (Hutcheon and Yarom, 2000). Hence, a wide frequency profile observed in some ET patients might potentially stem from a more complex tremor network, receiving more variable inputs. Secondly, because central oscillators consist of spatially segregated pockets of thalamic cells which oscillate coherently with specific tremulous muscles (Pedrosa *et al.*, 2012), we speculate that a change in the dominant tremor axis can potentially be linked back to a change in the tremor clusters dominating the tremor network. This will be discussed further towards the end of this chapter.

How the network state might interact with stimulation effects is further highlighted by the results from our peripheral stimulation. In chapter 5 we found that stimulation effects were linked to the amplitude of tremor at the time of stimulation onset. Similar to what has been predicted in a recent computational study (Weerasinghe *et al.*, 2019), we found that phase-specific stimulation had a greater effect on tremor severity if applied when the magnitude of

the targeted oscillation was low, i.e., when the underlying network was in a weakly coupled state.

These observations are suggestive that at each brain state, there are different connections, loops or even networks that prevail and interact with each other, leading to a new 'channel of communication' for optimal interaction. This idea has been well illustrated by a recent computational study showing that the amount by which in-silico cortical stimulation triggered by STN's beta phase could modulate STN's beta, was influenced by the underlying network's state (the strength of synaptic inputs to the STN) (West *et al.*, 2020). In a similar vein, a recent EMG/ fMRI study has reported that the amplification of PD tremor that occurs with cognitive load, is associated with a strengthening of connectivity between the cognitive control network and the cerebello-thalamo-cortical circuit (Dirkx *et al.*, 2020).

In the experimental examples provided above, different brain states were controlled for, and labelled as tremor being predominantly manifested at one versus multiple axes, low versus high tremor amplitude and rest versus high cognitive load. However, in real-life, i.e., outside a laboratory set up, as the brain transitions through different states (Baker *et al.*, 2014), the temporal relationships across different components of the diseased network are altered and so does the most efficient timing to interact with them.

Crucially, transitions to different states are also known to occur as a by-product of stimulation. This means that, even if effective in dampening the targeted disease biomarker, stimulation can lead to an amplification of other rhythmic activities within the circuit. For instance, in ET the prolonged delivery of stimulation to the ViM at an optimal phase of the peripheral tremor could lead to suppression of one tremor oscillator, but induce the emergence of another tremor oscillator with a different central frequency (supplementary section of (Cagnan *et al.*, 2017), Fig.S.7). Likewise, experimental and in silico phase-locked stimulation protocols aimed at reducing beta oscillations in PD, have reported that while phase-locked stimulation successfully induced suppression of low frequency beta rhythms, it concomitantly enhanced higher beta frequencies (Escobar Sanabria *et al.*, 2020; West *et al.*, 2020). This suggests that the high selectivity of closed-loop approaches can at times be too specific to achieve robust and continued stimulation benefits.

An important question arises: Is it feasible to map these spontaneous and stimulation-induced shifts in brain state and yield maximal clinical effects by adapting stimulation parameterisation accordingly? We speculate that despite challenging, online optimisation of stimulation parameters - including the relationship between brain states and optimal stimulation phase but also others such as amplitude - might be achieved in a near future through innovations in machine learning methods (Grado *et al.*, 2018).

### 6.2.2 Phase-specific stimulation efficacy and tremor variability

Chapters 4 and 5 of this thesis emphasise the importance of taking tremor variability into account to achieve a comprehensive assessment of the impact of experimental therapies. In brief, tremor variability, was used here to refer to how stable or unstable the peripheral tremor manifestation of a given patient is in either space, frequency and/or amplitude and was computed using different measures – including a PCA, cluster analysis and frequency-amplitude profiles.

A key message from such analyses was that tremors which are more variable are more difficult to tame. The idea that signal's variability is an important predictor of treatment outcome is not new (Cagnan et al., 2014, 2017), nor specific to tremor (Månsson et al., 2021); however, which variability metric best correlates with the underlying pathology and can best predict the overall outcome of a given treatment, is still a matter of debate. There are various metrics of tremor variability which have been put forward and proved to be useful in describing the underlying nature of tremor in different tremor conditions (Shaikh et al., 2008; Cagnan et al., 2014; di Biase et al., 2017; Vidailhet et al., 2017; Panyakaew et al., 2020; Nieuwhof et al., 2021). These metrics include the coefficient of variation (CV) of the tremor's frequency-amplitude profile, the Tremor Stability Index (TSI) and the Full Width Half-Maximum (FWHM). Here we have used the CV of patients' frequency-amplitude profiles as a proxy for the spectrum of frequencies at which a given tremor oscillates. This metric utilises the filtered tremor signal at the main tremor axis and creates a distribution of the average instantaneous amplitude at which tremor oscillates when exhibiting different instantaneous tremor frequencies (frequency-amplitude profile). To account for the non-parametric nature of our frequency-amplitude profile (Figure **4.4**B) a Weibull distribution is fitted to each frequency-amplitude profile and

its coefficient of variation computed as such: $\mathrm{CV} = \mathrm{IQR}/\mathrm{median}$. A similar, but less complex metric than ours is the FWHM, where the width of the tremor's spectrogram at half of the frequency peak is calculated. Indeed, when applying the FWHM to our data, similar results are found (Figure **6.1**A, middle panel) and a positive correlation between CV and FWHM is observed (Figure **6.1**B left panel). It would nonetheless be useful to compare the two metrics in a larger cohort in order to understand whether the increased resolution afforded by the CV of the amplitude-frequency profile allows for a more nuanced pathophysiological classification. The TSI is a widely used metric for tremor variability, which unlike the metrics above does not take into account the tremor amplitude (Brittain et al., 2015; di Biase et al., 2017). Instead, TSI measures how "jittery" the tremor (frequency) of a given patient is, i.e., how much tremor slows down or speeds up across tremor cycles. Computing the TSI for our tremor data and correlating it with stimulation effects shows once more a negative relationship (Figure **6.1**A, right panel); however, when correlating CV with TSI values, these do not seem to be related (Figure 6.1B, right panel). Once again, to thoroughly assess how the stability of tremor frequency over time and the span of tremor frequencies at which tremor oscillates relate to each other and whether they consist of different characteristics of the same oscillatory behaviour, TSI and CV would have to be compared in a larger cohort.

Lastly, despite of the metric used, tremor variability scores might change with the underlying motor state (postural versus kinetic tremor for example) and hence their predictive value might not be as informative and useful as previously thought (Panyakaew et al., 2020). Note for instance how the tremor profile of patient 3 becomes narrower from posture to spiral while patient 4's tremor profile becomes wider from posture to spiral (Figure **6.2**, middle and right panel panel). This way, I would advocate that using the FWHM measured from different commonly used clinical examinations on tremor, such as rest, finger-to-nose and writing, would consist of an objective and simple way of evaluating tremor and selecting patients for intervention studies. Using our experimental study as an example (Figure **6.2**), we hypothesize that the tremor of patient 1, whose variability is small and kept constant across posture and spiral motor states, would consist of an optimal tremor to apply phase-specific stimulation. Conversely, for patients 3 and 4, a hybrid stimulation strategy (Weerasinghe et al., 2019) would potentially prove to be more beneficial– this is, applying phase-locked stimulation during motor states yielding low tremor variability scores (spiral for patient 3 and posture for patient 4, for instance) and switching to high frequency stimulation whenever a motor states with high variability scores would emerge (posture for patient 3 and spiral for patient 4, for instance).

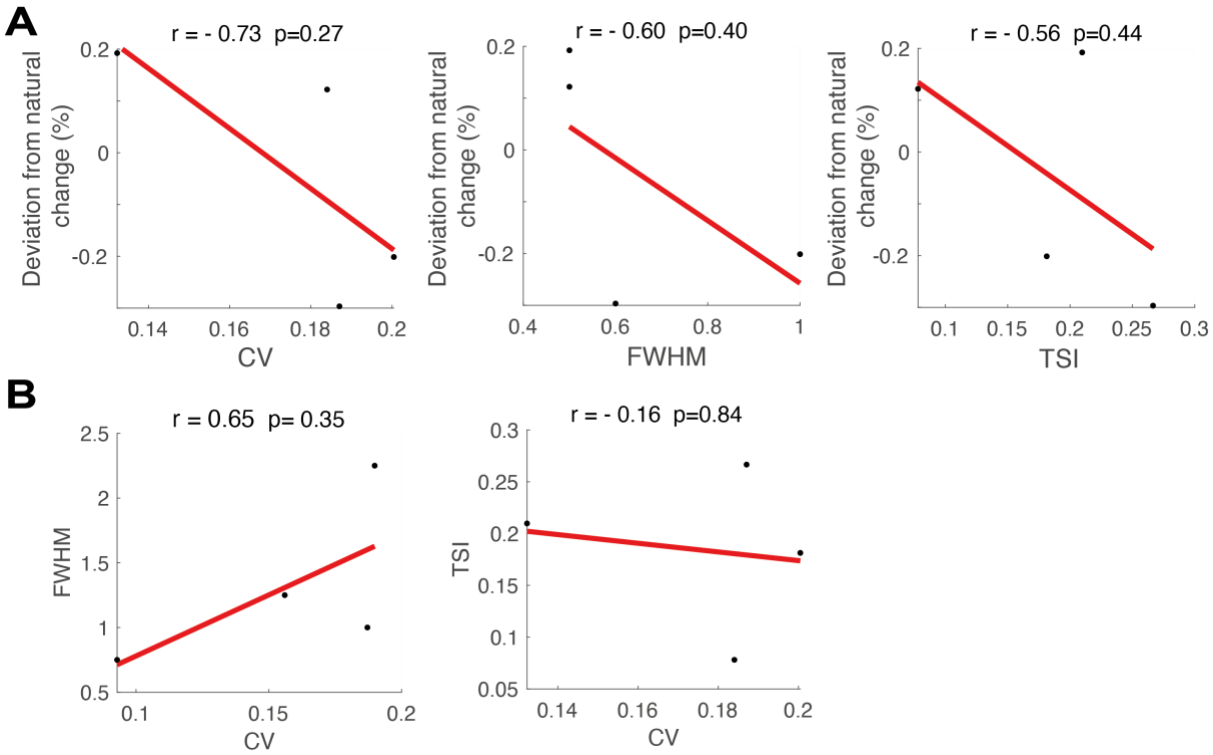


**Figure 6.1– Metrics of tremor variability.** Panel A shows the relationship between stimulation effects on postural tremor and different tremor metrics: coefficient of variability of tremor's frequency-amplitude profiles (CV, left), Full Width Half Maximum (FWHM, middle) and Tremor Stability Index (TSI, right). Note how all metrics of variability are negatively correlated with stimulation effects. Panel B shows how alternative metrics of tremor variability (FWHM and TSI) correlate to the metric used in this thesis (CV).

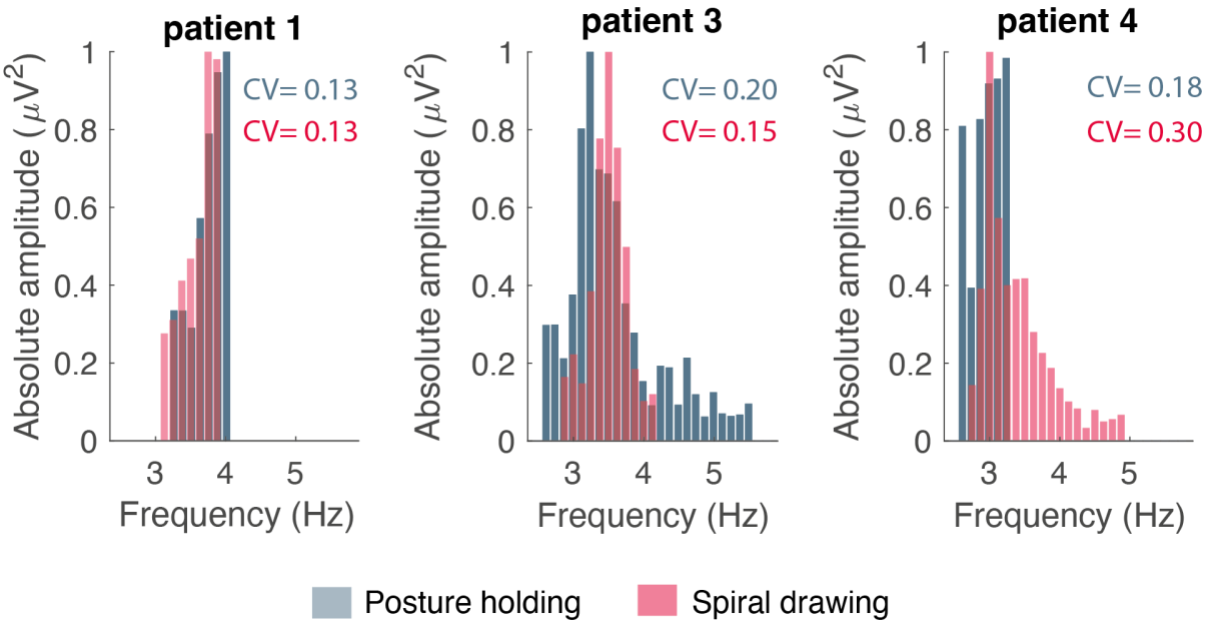


**Figure 6.2 – Spontaneous tremor behaviour during different motor state.** Histograms show the frequency-amplitude profile during unstimulated posture holding (in blue) and unstimulated spiral drawing (in red). The coefficient of variation (CV) of each frequency-amplitude profile is also provided and colour coded accordingly. Note while the tremor of patient 1 is kept stable across motor states, the tremor of patient 3 displays a stable behaviour during spiral drawing than posture holding and patient 4 shows a more stable tremor during posture holding compared to spiral drawing.

### 6.2.3 Phase-specific stimulation efficacy and stimulation target

One of the aims of this thesis was to test whether driving temporally specific proprioceptive thalamic afferents via median nerve stimulation could yield modulation of postural ET tremor in a similar fashion to phase-specific DBS. Despite the large variability in the cohorts (chapters 4 and 5, where phase-specific DBS and phase-specific median nerve stimulation were implemented, respectively), there are some commonalities and disparities across stimulation protocols that are worth noting here. As expected, the modulation of tremor severity was more consistent with phase-specific DBS than with phase-specific median nerve stimulation. Somewhat surprising however, was our finding that peripheral stimulation had an overall tendency to amplify rather than reduce tremor amplitude (Supplementary Figure S12). This difference in stimulation effects was also well depicted by the distinct profiles of ARCs (median tremor modulation per stimulated phase) obtained with the two stimulation paradigms. Phase response curves (PRCs) are commonly used to describe how periodically firing single

cells respond to stimulation (Lengyel *et al.*, 2005; Schultheiss *et al.*, 2010), and have also been used for neural ensembles by (Holt and Netoff, 2014), as a means to characterise how an oscillatory network responds to electrical stimulation. A distinction between type I and type II response curves is often used to describe spike time shifts caused by perturbations delivered at different times within the inter-spike interval: phase I describing unidirectional shifts in the spike times (either only delays or advances) which are irrespective of the input timing, and phase II consisting of bidirectional shifts, with advances occurring at certain input times and delays occurring at the remaining input times within a cycle (Hansel *et al.*, 1995; Ermentrout, 1996). In this thesis, amplitude response curves, (ARCs) are used to summarise the effects of phasic stimulation on tremor severity. ARCs follow the same rationale as phase response curves but describe how a given oscillator changes its amplitude (instead of phase), in response to a stimulus arriving at different timings (phases).

Unlike phase-specific DBS, phase-specific peripheral stimulation often led to a type I response curve, where unidirectional effects (consisting of an amplification) were observed (Figure **5.3**). Together with the observation that low tremor amplitude states allow for larger modulation of tremor severity following peripheral stimulation (Figure **5.5**B), we believe that driving a single thalamic afferent input by median nerve stimulation might more easily contribute to the generation of high synchrony (i.e., promoting tremor amplification), than to disrupt an already highly synchronised network (i.e., causing tremor reduction). Alternatively, amplifying effects might stem from a potential interaction between the delivered stimuli and peripheral circuitries, whereby stimuli are added to the descending tremor signals. Regardless of the underlying cause, the fact that median nerve stimulation mainly results in amplification suggests a potential dependency of stimulation effects on the perturbation location. This is something that has been observed for instance in PD tremor, where phase-dependent amplitude modulation of resting tremor is successfully attained with cortical stimulation (transcranial alternating current stimulation (Brittain *et al.*, 2013) but not with stimulation delivered to the thalamus or STN (Cagnan *et al.*, 2014).

### 6.2.4 Technical considerations for the implementation of phase-specific stimulation

Conventional high-frequency thalamic DBS is thought to bring clinically significant tremor relief to ET patients through inhibition of thalamic firing (Milosevic *et al.*, 2018). Phase-specific stimulation on the other hand focuses on achieving effective tremor control by finding the perfect timing at which brief bursts of stimulation delivered to the thalamus cause disruption in excessive rhythmic activity.

Previous studies highlight the necessity of consecutive and precise pluses to achieve significant amplitude modulation of the targeted oscillation. Evidence is provided by an offline analysis of phase-specific STN stimulation delivered at 8 different beta phases. That study reported that at least a quarter cycle stimulus precision is required to see modulation of beta amplitude and that an increased phase precision has the capacity to induce larger effect sizes (Holt *et al.*, 2019). Another phase-specific experimental paradigm found that effects of stimulation delivered at suppressive phases increased threefold from the first to the 5th pulse (Cagnan *et al.*, 2013), and similarly, results from chapter 4 show a 44% increase in suppressive effects from stimulation at the optimal phase for 5 seconds (~20 pulses) to approximately 30 seconds (~150 pulses).

A continuous temporal accuracy of triggered stimulation is dependent on two factors: how consistent the delay between phase detection and stimulation is, and how accurate online phase-estimation is over time. The former depends on the type of communication between sensor and neurostimulator and is likely to be of relevance in the future where communication between wearable devices and DBS will mainly rely on Bluetooth. Stability of online phase-estimation over time is expected to decline in two different contexts. First, when the frequency of the control signal changes and second, when the control signal displays low tremor amplitude. In our stimulation paradigm, online phase estimation is done based on the instantaneous zero crossings and the average tremor frequency estimated at the beginning of the experiment. Crucially, just like tremor amplitude, also tremor frequency is prone to suffer from spontaneous and stimulation-induced variations. This means that without an iterative update, an inaccurate estimation of phase-dependent modulatory effects upon tremor might occur. Second, while periods of low amplitude seem to decrease phase accuracy of the control signal (see supplementary figure S.4 in (Cagnan *et al.*, 2017)), this does not seem to pose a problem for

stimulation efficacy. A good example is the consistent phase-dependent tremor suppression observed in one of the two patients tested with phase-specific DBS during trials of intermittent posture (Figure **4.6**B). Here, as soon as posture was resumed (following a brief period of rest), a complete tremor rebound was prevented by what can be considered random-stimulation at the tremor frequency (given that the small amplitude of the remerging tremor cannot afford a reliable phase estimation). Unlike other control signals, peripheral tremor objectively captures symptom severity in ET. This means that while on the one hand low tremor amplitude is linked to a poor phase estimation (due to factors such as low signal to noise ratio), on the other hand low tremor amplitude is associated with low central synchrony which is mainly determined by a weakly coupled tremor circuit. From this it would follow that, random perturbation might be all that is needed to avoid tremor to re-emerge in a weakly coupled state. As previously proposed by Cagnan and colleagues, an interesting extension of our experimental stimulation strategy would consist of maintaining stimulation at the optimal phase for suppression continuously ON (i.e., even in the absence of tremor), while assessing if this would be sufficient to prevent a tremor rebound at the onset of postural and goal-directed movements. In moments of rest however, this alternative stimulation paradigm could nonetheless lead to the disruption of physiological synchronisation at theta frequencies and induce side effects.

### Implications of using accelerometery as a feedback signal

As described in the introductory chapter, there is a wide variety of signals that can be used as a feedback to control stimulation. The most commonly explored being local field potentials, either recorded directly from the stimulation electrode or alternatively from extra hardware such as electrocorticographic grids or strips implanted on the cortical surface. The first, despite being appealing due to the minimum surgical intervention and instrumentation needed for the implementation, has an important limitation which is the contamination of the sensing signal by stimulation artifacts. Stimulation artifacts can be more or less troublesome depending on the processing steps required to extract useful features from the signal to trigger stimulation. For instance, the adaptive DBS for PD which uses a control signal and stimulation at very distinct frequencies (13-30Hz and 130-180Hz, respectively), can efficiently overcome this issue using online filters (Little *et al.*, 2013). Conversely, delivering phasic stimulation to the thalamus while sensing the tremor-related activity directly from the stimulation electrode would prove extremely challenging (at least with the currently available analytical tools), since the frequency of interest of both signals is identical.

Our experiments worked around this issue by using an accelerometer to collect peripheral tremor activity and use its phase to drive a perturbation to the thalamus. Closing the loop with accelerometery, entails using an additional piece of hardware, which although risk free due to its non-invasive nature, does depend on patient compliance. Moreover, the translation of this stimulation protocol into a clinical application would most likely involve a Bluetooth communication between the peripheral accelerometer and stimulator. Adding to the potential suboptimal stimulation accuracy caused by inconsistent communication delays between phase detection and stimulation triggering (mentioned above), Bluetooth carries a security concern, due to having stimulation commands potentially intercepted by malware. The latter is however a general concern for future generations of adaptive deep brain stimulators which have as a promising feature the ability of downloading firmware upgrades, i.e., updating the current adaptive algorithm to more efficient ones (Khanna *et al.*, 2015).

Finally, in the specific case of tremor, on-demand stimulation triggered via peripheral sensors will necessarily follow the development of symptoms and will hence not be predictive. This means that our protocol acts not by preventing tremor to emerge but by trying to quickly abolish it as soon as it emerges. Nonetheless, it seems that no experimental closed-loop stimulation paradigm hitherto has managed to consistently trigger stimulation before tremor onset. Even in recent studies where the real-time controller for stimulation delivery is decoded from a central signal, stimulation delivery at therapeutic levels was mainly attained after tremor had already emerged. This is the case for example of studies by (He *et al.*, 2020*a*) and (Opri *et al.*, 2020), who have used thalamic and cortical signals, respectively, to decode voluntary movement and trigger thalamic high frequency stimulation. This is due to the necessary ramping up of stimulation amplitude from 0V to the therapeutic stimulation intensity, which is performed to avoid paraesthesia and ensure patients' safety and comfort. How fast the ramping up of stimulation can be, varies with the targeted tissue, stimulation parameters such as pulse width and therapeutic intensity, and patient-specific sensory threshold. When comparing the two adaptive approaches, triggered by a central or a peripheral signal, both may have a visible rebound of tremor before the therapeutic effects of stimulation kicks in. It is possible that high frequency stimulation at movement onset will prove to achieve more robust effects in supressing tremor than those by phase-specific stimulation given their different mechanisms of action.

### Measuring tremor with peripheral sensors

Finally, my last point of discussion is on the technical aspects of capturing tremor dynamics with peripheral sensors. In our stimulation paradigm, the sensed peripheral tremor is used to trigger stimulation (using its phase), and to assess stimulation effects (using its amplitude or power spectra). As such, the temporal and spatial resolution of the sensor used to record peripheral tremor, as well as the processing steps of the recorded signal are of great importance.

The spatial distribution of muscles displaying trembling activity is patient-specific and context-specific as shown in the previous two chapters. Using a triaxial accelerometer to capture these spatial dynamics has advantages and disadvantages which are discussed below.

Trembling muscles are known to oscillate coherently with specific ensembles of thalamic neurons, at tremor-related frequencies (Lenz *et al.*, 1994; Pedrosa *et al.*, 2012). It is precisely this relationship that we aim to track and selectively disrupt with our peripherally triggered DBS. However, not all trembling-muscle/central-cluster pairs are temporally aligned in the same fashion. This is for instance evidenced by Pedrosa and colleagues' study, where thalamic LFP/EMG coherent pairs showed different central frequencies (usually harmonics and sub-harmonics) (Pedrosa *et al.*, 2012). Intuitively, using EMG signals from antagonist trembling muscles would afford a more accurate estimation of the optimal phase for tremor suppression than the convoluted tremor signal measured with accelerometery. EMG is nonetheless limited by a potential sampling bias. Unlike accelerometery, EMG will only be able to capture changes in tremor in sampled muscles, running the risk of missing important spontaneous or stimulation-induced tremor dynamics.

Our closed-loop system allows us to simultaneously record the tremor signal in the x, y and z coordinates but requires us to choose only one of the three signals to control stimulation delivery. We attempted to mitigate this drawback by updating the tracked axis to the one displaying the largest tremor related acceleration across our experimental conditions. Still, as illustrated by the pie charts in Figure **4.6**A, this was not always sufficient. Hence, moving forward, our stimulation algorithm should include an iterative estimation of the main axis and tremor frequency, which as mentioned above might be achieved through future advances in machine learning methods. There is yet a simpler alternative, which despite having shown to be influenced by gravitational artifact, would spare us from having to select an axis to deliver stimulation. This would entail using the total acceleration as our controller signal and as the

signal upon which tremor effects would be measured. Total acceleration is given by the root of sum of square of each tremor axis. Reducing tremor to a single signal and using it to trigger stimulation could potentially be implemented in tasks like spiral drawing, where random-phase stimulation seems to be sufficient to reduce tremor. In other motor contexts where phase-specificity is key for tremor modulation (e.g., postural holding), I would expect that the weak trembling-muscle/central-cluster spatial resolution provided by this composite signal, would lead to less accurate estimations of the optimal phase and afford significantly smaller stimulation effects. Finally, using accelerometery in our stimulation paradigm yielded mechanistic insights regarding the efficacy of phase-specific DBS. By analysing tremor characteristics in the 3D space we were capable of dissecting some of the variability inherent to tremor of patients who were unresponsive to our stimulation.

By building on recent developments in DBS technology, an interesting extension of our work would entail using a chronic sensing and stim device (such as Percept from Medtronic) and directional electrodes to deliver phase-specific stimulation and as result uncover the natural and induced spatio-temporal dynamics of tremor.

## 6.3 Concluding remarks

Through the study and manipulation of pathological synchronisation at the TC level this thesis highlights how a better understanding of the dynamic nature of brain synchrony is key for the development of effective patient and context-specific therapeutic approaches. Since synchronisation within and across brain circuits is pertinent to virtually all realms of brain function, our findings do not solely concern to motor behaviour and the TC circuit, but might prove to be of great relevance for the treatment of other circuit disorders such as epilepsy, obsessive compulsive disorder, and Alzheimer's disease.

# 7 References


Abdi A, Mallet N, Mohamed FY, Sharott A, Dodson PD, Nakamura KC, et al. Prototypic and arkypallidal neurons in the dopamine-intact external globus pallidus. J Neurosci 2015; 35: 6667–88.

Al-Fatly B, Ewert S, Kübler D, Kroneberg D, Horn A, Kühn AA. Connectivity profile of thalamic deep brain stimulation to effectively treat essential tremor. Brain 2019; 142: 3086–98.

Albin RL, Young AB, Penney JB. The functional anatomy of basal ganglia disorders. Trends Neurosci 1989; 12: 366–75.

Alexander GE, Crutcher MD. Functional architecture of basal ganglia circuits: neural substrates of parallel processing. Trends Neurosci 1990; 13: 266–71.

Alexander GE, DeLong MR, Strick PL. Parallel organization of functionally segregated circuits linking basal ganglia and cortex. Annu Rev Neurosci 1986; VOL. 9: 357–81.

Anderson CT, Sheets PL, Kiritani T, Shepherd GMG. Sublayer-specific microcircuits of corticospinal and corticostriatal neurons in motor cortex. Nat Neurosci 2010; 13: 739–44.

Anderson ME, DeVito JL. An analysis of potentially converging inputs to the rostral ventral thalamic nuclei of the cat. Exp Brain Res 1987; 68: 260–76.

Anderson ME, Horak FB. Influence of the globus pallidus on arm movements in monkeys. III. Timing of movement-related information. J Neurophysiol 1985; 54: 433–48.

Anderson ME, Postupna N, Ruffo M, Marjorie E, Postupna N, Effects MR. Effects of high-frequency stimulation in the internal globus pallidus on the activity of thalamic neurons in the awake monkey. JNeurophysiol 2003; 89: 1150–60.

Anderson ME, Turner RS. Activity of neurons in cerebellar-receiving and pallidal-receiving areas of the thalamus of the behaving monkey. J Neurophysiol 1991; 66: 879–93.

Arbuthnott GW, MacLeod NK, Maxwell DJ, Wright AK. Distribution and synaptic contacts of the cortical terminals arising from neurons in the rat ventromedial thalamic nucleus. Neuroscience 1990; 38: 47–60.

Auksztulewicz R, Friston K. Attentional Enhancement of Auditory Mismatch Responses: a DCM/MEG Study. Cereb Cortex 2015; 25: 4273–83.

Avila I, Parr-Brownlie LC, Brazhnik E, Castañeda E, Bergstrom DA, Walters JR. Beta frequency synchronization in basal ganglia output during rest and walk in a hemiparkinsonian rat. Exp Neurol 2010; 221: 307–19.

Bain PG, Findley LJ, Atchison P, Behari M, Vidailhet M, Gresty M, et al. Assessing tremor severity. J Neurol Neurosurg Psychiatry 1993; 56: 868–73.

Baizabal-Carvallo JF, Jankovic J. Movement disorders induced by deep brain stimulation. Park Relat Disord 2016; 25: 1–9.

Baizabal-Carvallo JF, Kagnoff MN, Jimenez-Shahed J, Fekete R, Jankovic J. The safety and efficacy of thalamic deep brain stimulation in essential tremor: 10 years and beyond. J Neurol Neurosurg

Psychiatry 2014; 85: 567–72.

Baker AP, Brookes MJ, Rezek IA, Smith SM, Behrens T, Smith PJP, et al. Fast transient networks in spontaneous human brain activity. Elife 2014; 2014

Barbe MT, Reker P, Hamacher S, Franklin J, Kraus D, Dembek TA, et al. DBS of the PSA and the VIM in essential tremor. Neurology 2018; 91: e543–50.

Barker AT, Jalinous R, Freeston IL. Non-invasive magnetic stimulation of human motor cortex. Lancet (London, England) 1985; 1: 1106–7.

Bastos AM, Usrey WM, Adams RA, Mangun GR, Fries P, Friston KJ. Canonical Microcircuits for Predictive Coding. Neuron 2012; 76: 695–711.

Ben-Menachem E. Vagus-nerve stimulation for the treatment of epilepsy. Lancet Neurol 2002; 1: 477–82.

Benabid AL, Chabardes S, Mitrofanis J, Pollak P. Deep brain stimulation of the subthalamic nucleus for the treatment of Parkinson's disease. Lancet Neurol 2009; 8: 67–81.

Benabid AL, Pollak P, Hoffmann D, Gervason C, Hommel M, Perret JE, et al. Long-term suppression of tremor by chronic stimulation of the ventral intermediate thalamic nucleus. Lancet 1991; 337: 403–6.

Benito-León J, Alvarez-Linera J, Hernández-Tamames JA, Alonso-Navarro H, Jiménez-Jiménez FJ, Louis ED. Brain structural changes in essential tremor: Voxel-based morphometry at 3-Tesla. J Neurol Sci 2009; 287: 138–42.

Bergman H, Wichmann T, Karmon B, DeLong MR. The primate subthalamic nucleus. II. Neuronal activity in the MPTP model of parkinsonism. J Neurophysiol 1994; 72: 507–20.

Bevan MD, Magill PJ, Terman D, Bolam JP, Wilson CJ. Move to the rhythm: Oscillations in the subthalamic nucleus-external globus pallidus network. Trends Neurosci 2002; 25: 525–31.

Bhatt MB, Bowen S, Rossiter HE, Dupont-Hadwen J, Moran RJ, Friston KJ, et al. Computational modelling of movement-related beta-oscillatory dynamics in human motor cortex. Neuroimage 2016; 133: 224–32.

di Biase L, Brittain J-S, Shah SA, Pedrosa DJ, Cagnan H, Mathy A, et al. Tremor stability index: a new tool for differential diagnosis in tremor syndromes. Brain 2017; 140: 1977–86.

Bittar RG, Kar-Purkayastha I, Owen SL, Bear RE, Green A, Wang S, et al. Deep brain stimulation for pain relief: A meta-analysis. J Clin Neurosci 2005; 12: 515–9.

Blomstedt P, Sandvik U, Hariz MI, Fytagoridis A, Forsgren L, Hariz G-M, et al. Influence of age, gender and severity of tremor on outcome after thalamic and subthalamic DBS for essential tremor. Parkinsonism Relat Disord 2011; 17: 617–20.

Blomstedt P, Sandvik U, Tisch S. Deep brain stimulation in the posterior subthalamic area in the treatment of essential tremor. Mov Disord 2010; 25: 1350–6.

Boraud T, Bezard E, Bioulac B, Gross C. High frequency stimulation of the internal Globus Pallidus (GPi) simultaneously improves parkinsonian symptoms and reduces the firing frequency of GPi neurons in the MPTP-treated monkey. Neurosci Lett 1996; 215: 17–20.

Bosch-Bouju C, Hyland BI, Parr-Brownlie LC. Motor thalamus integration of cortical, cerebellar and

basal ganglia information: implications for normal and parkinsonian conditions. Front Comput Neurosci 2013; 7: 163.

Bosch-Bouju C, Smither RA, Hyland BI, Parr-Brownlie LC. Reduced Reach-Related Modulation of Motor Thalamus Neural Activity in a Rat Model of Parkinson's Disease. J Neurosci 2014

Bourassa J, Pinault D, Deschenes M. Corticothalamic projections from the cortical barrel field to the somatosensory thalamus in rats: a single-fibre study using biocytin as an anterograde tracer. Eur J Neurosci 1995; 7: 19–30.

Brazhnik E, McCoy AJ, Novikov N, Hatch CE, Walters JR. Ventral medial thalamic nucleus promotes synchronization of increased high beta oscillatory activity in the basal ganglia-thalamocortical network of the hemiparkinsonian rat. J Neurosci 2016; 36: 4196–208.

Brittain J-S, Cagnan H, Mehta AR, Saifee TA, Edwards MJ, Brown P. Distinguishing the Central Drive to Tremor in Parkinson's Disease and Essential Tremor. J Neurosci 2015; 35: 795–806.

Brittain JS, Brown P. Oscillations and the basal ganglia: Motor control and beyond. Neuroimage 2014; 85: 637–47.

Brittain JS, Cagnan H, Mehta AR, Saifee TA, Edwards MJ, Brown P. Distinguishing the central drive to tremor in Parkinson's disease and essential tremor. J Neurosci 2015; 35: 795–806.

Brittain JS, Probert-Smith P, Aziz TZ, Brown P. Tremor suppression by rhythmic transcranial current stimulation. Curr Biol 2013; 23: 436–40.

Brodkey JA, Tasker RR, Hamani C, Mcandrews MP, Dostrovsky JO, Lozano AM. Tremor cells in the human thalamus: differences among neurological disorders. 2004

Brown P. Dopamine dependency of oscillations between subthalamic nucleus and pallidum in Parkinson's disease. J Neurosci 2001; 21: 1033–8.

Brown P. Oscillatory nature of human basal ganglia activity: relationship to the pathophysiology of Parkinson's disease. Mov Disord 2003; 18: 357–63.

Brown P. Abnormal oscillatory synchronisation in the motor system leads to impaired movement. Curr Opin Neurobiol 2007; 17: 656–64.

Brown P, Oliviero A, Mazzone P, Insola A, Tonali P, Di Lazzaro V. Dopamine dependency of oscillations between subthalamic nucleus and pallidum in Parkinson's disease. J Neurosci 2001; 21: 1033–8.

Brücke C, Bock A, Huebl J, Krauss JK, Schönecker T, Schneider GH, et al. Thalamic gamma oscillations correlate with reaction time in a Go/noGo task in patients with essential tremor. Neuroimage 2013; 75: 36–45.

Bucher SF, Seelos KC, Dodel RC, Reiser M, Oertel WH. Activation mapping in essential tremor with functional magnetic resonance imaging. Ann Neurol 1997; 41: 32–40.

Buzsáki G, Anastassiou CA, Koch C. The origin of extracellular fields and currents-EEG, ECoG, LFP and spikes. Nat Rev Neurosci 2012; 13: 407–20.

Buzsáki G, Draguhn A. Neuronal oscillations in cortical networks. Science (80- ) 2004; 304: 1926–9.

Cagnan H, Brittain JS, Little S, Foltynie T, Limousin P, Zrinzo L, et al. Phase dependent modulation of tremor amplitude in essential tremor through thalamic stimulation. Brain 2013; 136: 3062–75.

Cagnan H, Denison T, McIntyre C, Brown P. Emerging technologies for improved deep brain stimulation. Nat Biotechnol 2019; 37: 1024–33.

Cagnan H, Duff EP, Brown P. The relative phases of basal ganglia activities dynamically shape effective connectivity in Parkinson's disease. Brain 2015; 138: 1667–78.

Cagnan H, Little S, Foltynie T, Limousin P, Zrinzo L, Hariz M, et al. The nature of tremor circuits in parkinsonian and essential tremor. Brain 2014; 137: 3223–34.

Cagnan H, Mallet N, Moll CKE, Gulberti A, Holt AB, Westphal M, et al. Temporal evolution of beta bursts in the parkinsonian cortical and basal ganglia network. Proc Natl Acad Sci U S A 2019; 116: 16095–104.

Cagnan H, Pedrosa D, Little S, Pogosyan A, Cheeran B, Aziz T, et al. Stimulating at the right time: phase-specific deep brain stimulation. Brain 2017; 140: 132–45.

Cantello R, Tarletti R, Civardi C. Transcranial magnetic stimulation and Parkinson's disease. Brain Res Brain Res Rev 2002; 38: 309–27.

Cassidy M, Mazzone P, Oliviero A, Insola A, Tonali P, Di Lazzaro V, et al. Movement-related changes in synchronization in the human basal ganglia. Brain 2002; 125: 1235–46.

Castrioto A, Lozano AM, Poon Y-Y, Lang A, Fallis M, Moro E. Ten-Year Outcome of Subthalamic Stimulation in Parkinson Disease. Arch Neurol 2011; 68: 1550.

Charlton CS, Ridding MC, Thompson PD, Miles TS. Prolonged peripheral nerve stimulation induces persistent changes in excitability of human motor cortex. J Neurol Sci 2003; 208: 79–85.

Chevalier G, Deniau JM. Disinhibition as a basic process in the expression of striatal functions. Trends Neurosci 1990; 13: 277–80.

Chiken S, Nambu A. Mechanism of Deep Brain Stimulation: Inhibition, Excitation, or Disruption? Neuroscientist 2016; 22: 313–22.

Clascá F, Rubio-Garrido P, Jabaudon D. Unveiling the diversity of thalamocortical neuron subtypes. Eur J Neurosci 2012; 35: 1524–32.

Cleeves L, Findley LJ. Variability in amplitude of untreated essential tremor. 1987

Conforto AB, Kaelin-Lang A, Cohen LG. Increase in hand muscle strength of stroke patients after somatosensory stimulation. Ann Neurol 2002; 51: 122–5.

Contreras D. The Role of T-Channels in the Generation of Thalamocortical Rhythms. CNS Neurol Disord - Drug Targets 2008; 5: 571–85.

Corbit VL, Whalen TC, Zitelli KT, Crilly SY, Rubin JE, Gittis AH. Pallidostriatal projections promote β oscillations in a dopamine-depleted biophysical network model. J Neurosci 2016; 36: 5556–71.

Courtemanche R, Fujii N, Graybiel AM. Synchronous, focally modulated beta-band oscillations characterize local field potential activity in the striatum of awake behaving monkeys. J Neurosci 2003; 23: 11741–52.

Crompe B de la, Aristieta A, Leblois A, Elsherbiny S, Boraud T, Mallet NP. The globus pallidus orchestrates abnormal network dynamics in a model of Parkinsonism. Nat Commun 2020 111 2020; 11: 1–14.

Cruz A V., Mallet N, Magill PJ, Brown P, Averbeck BB. Effects of dopamine depletion on network entropy in the external globus pallidus. J Neurophysiol 2009; 102: 1092–102.

Cruz A V, Mallet N, Magill PJ, Brown P, Averbeck BB. Effects of dopamine depletion on information flow between the subthalamic nucleus and external globus pallidus. J Neurophysiol 2011; 106: 2012–23.

Cury RG, Fraix V, Castrioto A, Pérez Fernández MA, Krack P, Chabardes S, et al. Thalamic deep brain stimulation for tremor in Parkinson disease, essential tremor, and dystonia. Neurology 2017; 89: 1416–23.

Daniels C, Peller M, Wolff S, Alfke K, Witt K, Gaser C, et al. Voxel-based morphometry shows no decreases in cerebellar gray matter volume in essential tremor. Neurology 2006; 67: 1452 LP – 1456.

Deffains M, Iskhakova L, Katabi S, Israel Z, Bergman H. Longer β oscillatory episodes reliably identify pathological subthalamic activity in Parkinsonism. Mov Disord 2018; 33: 1609–18.

Degos B, Deniau J-M, Chavez M, Maurice N. Chronic but not Acute Dopaminergic Transmission Interruption Promotes a Progressive Increase in Cortical Beta Frequency Synchronization: Relationships to Vigilance State and Akinesia. Cereb Cortex 2009; 19: 1616–30.

DeLong MR. Primate models of movement disorders of basal ganglia origin. Trends Neurosci 1990; 13: 281–5.

Deniau JM, Chevalier G. Disinhibition as a basic process in the expression of striatal functions. II. The striato-nigral influence on thalamocortical cells of the ventromedial thalamic nucleus. Brain Res 1985; 334: 227–33.

Denys D, Mantione M, Figee M, Van Den Munckhof P, Koerselman F, Westenberg H, et al. Deep brain stimulation of the nucleus accumbens for treatment-refractory obsessive-compulsive disorder. Arch Gen Psychiatry 2010; 67: 1061–8.

Deumens R, Blokland A, Prickaerts J. Modeling Parkinson's disease in rats: An evaluation of 6-OHDA lesions of the nigrostriatal pathway. Exp Neurol 2002; 175: 303–17.

Deuschl G, Bain P, Brin M. Consensus statement of the Movement Disorder Society on Tremor. Ad Hoc Scientific Committee. Mov Disord 1998; 13 Suppl 3: 2–23.

Deuschl G, Raethjen J, Hellriegel H, Elble R. Treatment of patients with essential tremor. Lancet Neurol 2011; 10: 148–61.

Devergnas A, Pittard D, Bliwise D, Wichmann T. Relationship between oscillatory activity in the cortico-basal ganglia network and parkinsonism in MPTP-treated monkeys. Neurobiol Dis 2014; 68: 156–66.

Diaz NL, Louis ED. Survey of medication usage patterns among essential tremor patients: Movement disorder specialists vs. general neurologists. Park Relat Disord 2010; 16: 604–7.

Dideriksen JL, Laine CM, Dosen S, Muceli S, Rocon E, Pons JL, et al. Electrical Stimulation of Afferent Pathways for the Suppression of Pathological Tremor. Front Neurosci 2017; 11: 178.

Dirkx MF, den Ouden H, Aarts E, Timmer M, Bloem BR, Toni I, et al. The cerebral network of parkinson's tremor: An effective connectivity fMRI study. J Neurosci 2016; 36: 5362–72.

Dirkx MF, Den Ouden HEM, Aarts E, Timmer MHM, Bloem BR, Toni I, et al. Dopamine controls Parkinson's tremor by inhibiting the cerebellar thalamus. Brain 2017; 140: 721–34.

Dirkx MF, Zach H, van Nuland AJ, Bloem BR, Toni I, Helmich RC. Cognitive load amplifies Parkinson's tremor through excitatory network influences onto the thalamus. Brain 2020; 143: 1498–511.

Doig NM, Magill PJ, Apicella P, Bolam JP, Sharott A. Cortical and thalamic excitation mediate the multiphasic responses of striatal cholinergic interneurons to motivationally salient stimuli. J Neurosci 2014; 34: 3101–17.

Donkelaar P van, Stein JF, Passingham RE, Miall RC. Neuronal Activity in the Primate Motor Thalamus During Visually Triggered and Internally Generated Limb Movements. https://doi.org/101152/jn1999822934 1999; 82: 934–45.

Dostrovsky JO, Levy R, Wu JP, Hutchison WD, Tasker RR, Lozano AM. Microstimulation-induced inhibition of neuronal firing in human globus pallidus. J Neurophysiol 2000; 84: 570–4.

Douglas RJ, Martin KA. Neuronal circuits of the neocortex. Annu Rev Neurosci 2004; 27: 419–51.

Doyle Gaynor LMF, Kühn AA, Dileone M, Litvak V, Eusebio A, Pogosyan A, et al. Suppression of beta oscillations in the subthalamic nucleus following cortical stimulation in humans. Eur J Neurosci 2008; 28: 1686–95.

Duchet B, Ghezzi F, Weerasinghe G, Tinkhauser G, Kühn AA, Brown P, et al. Average beta burst duration profiles provide a signature of dynamical changes between the ON and OFF medication states in Parkinson's disease. bioRxiv 2020: 2020.04.27.064246.

Edgerton JR, Jaeger D. Optogenetic activation of nigral inhibitory inputs to motor thalamus in the mouse reveals classic inhibition with little potential for rebound activation [Internet]. Front Cell Neurosci 2014; 8[cited 2021 Mar 30] Available from: https://pubmed.ncbi.nlm.nih.gov/24574972/

Elble R. Defining Dystonic Tremor. Curr Neuropharmacol 2013; 11: 48–52.

Elble RJ, Shih L, Cozzens JW. Surgical treatments for essential tremor. Expert Rev Neurother 2018; 18: 303–21.

Engel AK, Fries P. Beta-band oscillations-signalling the status quo? Curr Opin Neurobiol 2010; 20: 156–65.

Engel AK, Singer W. Temporal binding and the neural correlates of sensory awareness. Trends Cogn Sci 2001; 5: 16–25.

Ermentrout B. Type I Membranes, Phase Resetting Curves, and Synchrony. Neural Comput 1996; 8: 979–1001.

Escobar Sanabria D, Johnson LA, Yu Y, Busby Z, Nebeck S, Zhang J, et al. Real-time suppression and amplification of frequency-specific neural activity using stimulation evoked oscillations. Brain Stimul 2020; 13: 1732–42.

Eusebio A, Pogosyan A, Wang S, Averbeck B, Gaynor LD, Cantiniaux S, et al. Resonance in subthalamo-cortical circuits in Parkinsons disease. Brain 2009; 132: 2139–50.

Eusebio A, Thevathasan W, Doyle Gaynor L, Pogosyan A, Bye E, Foltynie T, et al. Deep brain stimulation can suppress pathological synchronisation in parkinsonian patients. J Neurol Neurosurg Psychiatry 2011; 82: 569–73.

Evarts E V. Relation of pyramidal tract activity to force exerted during voluntary movement. J Neurophysiol 1968; 31: 14–27.

Fan D, Rossi MA, Yin HH. Mechanisms of action selection and timing in substantia nigra neurons. J Neurosci 2012; 32: 5534–48.

Farries MA, Wilson CJ. Biophysical basis of the phase response curve of subthalamic neurons with generalization to other cell types. J Neurophysiol 2012; 108: 1838–55.

Fasano A, Helmich RC. Tremor habituation to deep brain stimulation: Underlying mechanisms and solutions. Mov Disord 2019; 34: 1761–73.

Feingold J, Gibson DJ, DePasquale B, Graybiel AM. Bursts of beta oscillation differentiate postperformance activity in the striatum and motor cortex of monkeys performing movement tasks. Proc Natl Acad Sci U S A 2015; 112: 13687–92.

Fino E, Packer AM, Yuste R. The logic of inhibitory connectivity in the neocortex. Neuroscientist 2013; 19: 228–37.

Fischer P, Pogosyan A, Cheeran B, Green AL, Aziz TZ, Hyam J, et al. Subthalamic nucleus beta and gamma activity is modulated depending on the level of imagined grip force. Exp Neurol 2017; 293: 53–61.

Fisher R, Salanova V, Witt T, Worth R, Henry T, Gross R, et al. Electrical stimulation of the anterior nucleus of thalamus for treatment of refractory epilepsy. Epilepsia 2010; 51: 899–908.

Foffani G, Bianchi AM, Baselli G, Priori A. Movement-related frequency modulation of beta oscillatory activity in the human subthalamic nucleus. J Physiol 2005; 568: 699–711.

Fogelson N, Williams D, Tijssen M, Van Bruggen G, Speelman H, Brown P. Different functional loops between cerebral cortex and the subthalmic area in parkinson's disease. Cereb Cortex 2006; 16: 64–75.

Fries P. A mechanism for cognitive dynamics: Neuronal communication through neuronal coherence. Trends Cogn Sci 2005; 9: 474–80.

Fries P. Rhythm for Cognition: Communication Through Coherence. Neuron 2015; 88: 220–35.

Friston K, Mattout J, Trujillo-Barreto N, Ashburner J, Penny W. Variational free energy and the Laplace approximation. Neuroimage 2007; 34: 220–34.

Friston K, Zeidman P, Litvak V. Empirical Bayes for DCM: A Group Inversion Scheme. Front Syst Neurosci 2015; 9: 1–10.

Friston KJ. Functional and effective connectivity: a review. Brain Connect 2011; 1: 13–36.

Friston KJ, Bastos A, Litvak V, Stephan KE, Fries P, Moran RJ. DCM for complex-valued data: Cross-spectra, coherence and phase-delays. Neuroimage 2012; 59: 439–55.

Friston KJ, Harrison L, Penny W. Dynamic causal modelling. Neuroimage 2003; 19: 1273–302.

Friston KJ, Stephan KE. Free-energy and the brain. Synthese 2007; 159: 417–58.

Gallego JÁ, Rocon E, Belda-Lois JM, Pons JL. A neuroprosthesis for tremor management through the control of muscle co-contraction. J Neuroeng Rehabil 2013; 10: 36.

Gatev P, Darbin O, Wichmann T. Oscillations in the basal ganglia under normal conditions and in movement disorders. Mov Disord 2006; 21: 1566–77.

Georgopoulos AP. Neural integration of movement: role of motor cortex in reaching. FASEB J 1988; 2: 2849–57.

Georgopoulos AP, DeLong MR, Crutcher MD. Relations between parameters of step-tracking movements and single cell discharge in the globus pallidus and subthalamic nucleus of the behaving monkey. J Neurosci 1983; 3: 1586–98.

Georgopoulos AP, Kalaska JF, Caminiti R, Massey JT. On the relations between the direction of two-dimensional arm movements and cell discharge in primate motor cortex. J Neurosci 1982; 2: 1527–37.

Giller CA, Dewey RB, Ginsburg MI, Mendelsohn DB, Berk AM. Stereotactic pallidotomy and thalamotomy using individual variations of anatomic landmarks for localization. Neurosurgery 1998; 42: 56–65.

Gilron R, Little S, Perrone R, Wilt R, de Hemptinne C, Yaroshinsky MS, et al. Long-term wireless streaming of neural recordings for circuit discovery and adaptive stimulation in individuals with Parkinson's disease. Nat Biotechnol 2021: 1–8.

Goldberg JH, Farries MA, Fee MS. Integration of cortical and pallidal inputs in the basal ganglia-recipient thalamus of singing birds. J Neurophysiol 2012; 108: 1403–29.

Goldberg JH, Farries MA, Fee MS. Basal ganglia output to the thalamus: still a paradox. Trends Neurosci 2013; 36: 695–705.

Gradinaru V, Mogri M, Thompson KR, Henderson JM, Deisseroth K. Optical deconstruction of parkinsonian neural circuitry. Science 2009; 324: 354–9.

Grado LL, Johnson MD, Netoff TI. Bayesian adaptive dual control of deep brain stimulation in a computational model of Parkinson's disease. PLoS Comput Biol 2018; 14: e1006606.

Gupta D, Kuo S-H. Prevalence and patterns of rest, postural and action tremor in drug-naïve Parkinson's disease (P2.066). Neurology 2018; 90

Hall SD, Yamawaki N, Fisher AE, Clauss RP, Woodhall GL, Stanford IM. GABA(A) alpha-1 subunit mediated desynchronization of elevated low frequency oscillations alleviates specific dysfunction in stroke - A case report. Clin Neurophysiol 2010; 121: 549–55.

Hammond C, Bergman H, Brown P. Pathological synchronization in Parkinson's disease: networks, models and treatments. Trends Neurosci 2007; 30: 357–64.

Hanajima R, Chen R, Ashby P, Lozano AM, Hutchison WD, Davis KD, et al. Very Fast Oscillations Evoked by Median Nerve Stimulation in the Human Thalamus and Subthalamic Nucleus. J Neurophysiol 2004; 92: 3171–82.

Hansel D, Mato G, Meunier C. Synchrony in excitatory neural networks. Neural Comput 1995; 7: 307–37.

Hao MZ, He X, Kipke DR, Lan N. Effects of electrical stimulation of cutaneous afferents on corticospinal transmission of tremor signals in patients with Parkinson's disease. In: International IEEE/EMBS Conference on Neural Engineering, NER. 2013. p. 355–8

Hariz MI, Rehncrona S, Quinn NP, Speelman JD, Wensing C. Multicenter study on deep brain stimulation in Parkinson's disease: An independent assessment of reported adverse events at 4 years. Mov Disord 2008; 23: 416–21.

Hashimoto T, Elder CM, Okun MS, Patrick SK, Vitek JL. Stimulation of the subthalamic nucleus changes the firing pattern of pallidal neurons. J Neurosci 2003; 23: 1916–23.

Hazrati LN, Parent A. Contralateral pallidothalamic and pallidotegmental projections in primates: an anterograde and retrograde labeling study. Brain Res 1991; 567: 212–23.

He S, Debarros J, Khawaldeh S, Pogosyan A, Mostofi A, Baig F, et al. Closed-loop DBS triggered by real-time movement and tremor decoding based on thalamic LFPs for essential tremor. In: 2020 42nd Annual International Conference of the IEEE Engineering in Medicine & Biology Society (EMBC). IEEE; 2020. p. 3602–5

He S, Everest-Phillips C, Clouter A, Brown P, Tan H. Neurofeedback-linked suppression of cortical B bursts speeds up movement initiation in healthy motor control: A double-blind sham-controlled study. J Neurosci 2020; 40: 4021–32.

Heimer G, Rivlin-Etzion M, Bar-Gad I, Goldberg JA, Haber SN, Bergman H. Dopamine replacement therapy does not restore the full spectrum of normal pallidal activity in the 1-methyl-4-phenyl-1,2,3,6-tetra-hydropyridine primate model of Parkinsonism. J Neurosci 2006; 26: 8101–14.

Helmich RC, Hallett M, Deuschl G, Toni I, Bloem BR. Cerebral causes and consequences of parkinsonian resting tremor: A tale of two circuits? Brain 2012; 135: 3206–26.

Helmich RC, Janssen MJR, Oyen WJG, Bloem BR, Toni I. Pallidal dysfunction drives a cerebellothalamic circuit into Parkinson tremor. Ann Neurol 2011; 69: 269–81.

Heo JH, Kim JW, Kwon Y, Lee SK, Eom GM, Kwon DY, et al. Sensory electrical stimulation for suppression of postural tremor in patients with essential tremor. Biomed Mater Eng 2015; 26: S803–9.

Hernandez-Martin E, Arguelles E, Zheng Y, Deshpande R, Sanger TD. High-fidelity transmission of high-frequency burst stimuli from peripheral nerve to thalamic nuclei in children with dystonia. Sci Rep 2021; 11: 8498.

Herrmann CS, Rach S, Neuling T, Strüber D. Transcranial alternating current stimulation: a review of the underlying mechanisms and modulation of cognitive processes. Front Hum Neurosci 2013; 7: 1–13.

Herron JA, Thompson MC, Brown T, Chizeck HJ, Ojemann JG, Ko AL. Chronic electrocorticography for sensing movement intention and closed-loop deep brain stimulation with wearable sensors in an essential tremor patient. J Neurosurg 2017; 127: 580–7.

Herz DM, Zavala BA, Bogacz R, Brown P. Neural Correlates of Decision Thresholds in the Human Subthalamic Nucleus. Curr Biol 2016; 26: 916–20.

Herzog J, Hamel W, Wenzelburger R, Pötter M, Pinsker MO, Bartussek J, et al. Kinematic analysis of thalamic versus subthalamic neurostimulation in postural and intention tremor. Brain 2007; 130: 1608–25.

Hikosaka O. GABAergic output of the basal ganglia. Prog Brain Res 2007; 160: 209–26.

Holgado AJN, Terry JR, Bogacz R. Conditions for the Generation of Beta Oscillations in the Subthalamic Nucleus-Globus Pallidus Network. J Neurosci 2010; 30: 12340–52.

Holt AB, Kormann E, Gulberti A, Pötter-Nerger M, McNamara CG, Cagnan H, et al. Phase-dependent suppression of beta oscillations in parkinson's disease patients. J Neurosci 2019; 39: 1119–34.

Holt AB, Netoff TI. Origins and suppression of oscillations in a computational model of Parkinson's disease. J Comput Neurosci 2014; 37: 505–21.

Holt AB, Wilson D, Shinn M, Moehlis J, Netoff TI. Phasic Burst Stimulation: A Closed-Loop Approach to Tuning Deep Brain Stimulation Parameters for Parkinson's Disease. PLoS Comput Biol 2016; 12: 1–14.

Holtzheimer PE, Husain MM, Lisanby SH, Taylor SF, Whitworth LA, McClintock S, et al. Subcallosal cingulate deep brain stimulation for treatment-resistant depression: a multisite, randomised, sham-controlled trial. The Lancet Psychiatry 2017; 4: 839–49.

Hooks BM, Mao T, Gutnisky DA, Yamawaki N, Svoboda K, Shepherd GMG. Organization of Cortical and Thalamic Input to Pyramidal Neurons in Mouse Motor Cortex. J Neurosci 2013; 33: 748–60.

Horn A, Kühn AA. Lead-DBS: A toolbox for deep brain stimulation electrode localizations and visualizations. Neuroimage 2015; 107: 127–35.

Hua SE, Lenz FA. Posture-Related Oscillations in Human Cerebellar Thalamus in Essential Tremor Are Enabled by Voluntary Motor Circuits. J Neurophysiol 2005; 93: 117–27.

Hutcheon B, Yarom Y. Resonance, oscillation and the intrinsic frequency preferences of neurons. Trends Neurosci 2000; 23: 216–22.

Inase M, Buford JA, Anderson ME. Changes in the control of arm position, movement, and thalamic discharge during local inactivation in the globus pallidus of the monkey. J Neurophysiol 1996; 75: 1087–104.

Ishikawa T, Tomatsu S, Tsunoda Y, Lee J, Hoffman DS, Kakei S. Releasing dentate nucleus cells from Purkinje cell inhibition generates output from the cerebrocerebellum. PLoS One 2014; 9: e108774.

Jackson A, Gee VJ, Baker SN, Lemon RN. Synchrony between Neurons with Similar Muscle Fields in Monkey Motor Cortex. Neuron 2003; 38: 115–25.

Jaeger D, Gilman S, Wayne Aldridge J. Neuronal activity in the striatum and pallidum of primates related to the execution of externally cued reaching movements. Brain Res 1995; 694: 111–27.

James SL, Abate D, Abate KH, Abay SM, Abbafati C, Abbasi N, et al. Global, regional, and national incidence, prevalence, and years lived with disability for 354 Diseases and Injuries for 195 countries and territories, 1990-2017: A systematic analysis for the Global Burden of Disease Study 2017. Lancet 2018; 392: 1789–858.

Jankovic J. Motor fluctuations and dyskinesias in Parkinson's disease: Clinical manifestations. Mov Disord 2005; 20

Jansen BH, Rit VG. Electroencephalogram and Visual-Evoked Potential Generation in a Mathematical-Model of Coupled Cortical Columns. Biol Cybern 1995; 73: 357–66.

Jenkinson and Brown. New insights into the relationship between dopamine, beta oscillations and motor function. Trends Neurosci 2011; 34: 611–8.

Jenkinson N, Brown P. New insights into the relationship between dopamine, beta oscillations and motor function. Trends Neurosci 2011; 34: 611–8.

Jenkinson N, Kühn AA, Brown P. Gamma oscillations in the human basal ganglia. Exp Neurol 2013;

245: 72–6.

Jensen O, Goel P, Kopell N, Pohja M, Hari R, Ermentrout B. On the human sensorimotor-cortex beta rhythm: Sources and modeling. Neuroimage 2005; 26: 347–55.

Johnson MD, Miocinovic S, McIntyre CC, Vitek JL. Mechanisms and Targets of Deep Brain Stimulation in Movement Disorders. Neurotherapeutics 2008; 5: 294–308.

Jones E. The Thalamus. Plenum; 1985

Jones EG. The thalamic matrix and thalamocortical synchrony. Trends Neurosci 2001; 24: 595–601.

Jones EG, Burton H, Porter R. Commissural and cortico-cortical 'columns' in the somatic sensory cortex of primates. Science (80- ) 1975; 190: 572–4.

Jourdain VA, Schechtmann G. Health Economics and Surgical Treatment for Parkinson's Disease in a World Perspective: Results from an International Survey. Stereotact Funct Neurosurg 2014; 92: 71–9.

Kahan J, Urner M, Moran R, Flandin G, Marreiros A, Mancini L, et al. Resting state functional MRI in Parkinson's disease: the impact of deep brain stimulation on 'effective' connectivity. Brain 2014; 137: 1130.

Kätzel D, Zemelman B V., Buetfering C, Wölfel M, Miesenböck G. The columnar and laminar organization of inhibitory connections to neocortical excitatory cells. Nat Neurosci 2011; 14: 100–9.

Kempf F, Brücke C, Salih F, Trottenberg T, Kupsch A, Schneider G-H, et al. Gamma activity and reactivity in human thalamic local field potentials. Eur J Neurosci 2009; 29: 943–53.

Kestenbaum M, Ford B, Louis ED. Estimating the Proportion of Essential Tremor and Parkinson's Disease Patients Undergoing Deep Brain Stimulation Surgery: Five-Year Data From Columbia University Medical Center (2009–2014). Mov Disord Clin Pract 2015; 2: 384–7.

Khanna P, Carmena JM. Neural oscillations: Beta band activity across motor networks. Curr Opin Neurobiol 2015; 32: 60–7.

Khanna P, Stanslaski S, Xiao Y, Ahrens T, Bourget D, Swann N, et al. Enabling closed-loop neurostimulation research with downloadable firmware upgrades. In: IEEE Biomedical Circuits and Systems Conference: Engineering for Healthy Minds and Able Bodies, BioCAS 2015 - Proceedings. Institute of Electrical and Electronics Engineers Inc.; 2015

Khawaldeh S, Tinkhauser G, Shah SA, Peterman K, Debove I, Nguyen TAK, et al. Subthalamic nucleus activity dynamics and limb movement prediction in Parkinson's disease. Brain 2020; 143: 582–96.

Kim J, Kim Y, Nakajima R, Shin A, Jeong M, Park AH, et al. Inhibitory Basal Ganglia Inputs Induce Excitatory Motor Signals in the Thalamus. Neuron 2017; 95: 1181-1196.e8.

Kim J, Wichmann T, Inan OT, De Weerth SP. A Wearable System For Attenuating Essential Tremor Based On Peripheral Nerve Stimulation [Internet]. IEEE J Transl Eng Heal Med 2020; 8[cited 2020 Jul 22] Available from: /pmc/articles/PMC7313727/?report=abstract

Kim JH, Chang WS, Jung HH, Chang JW. Effect of subthalamic deep brain stimulation on levodopa-induced dyskinesia in parkinson's disease. Yonsei Med J 2015; 56: 1316–21.

Kimberley TJ, Lewis SM, Auerbach EJ, Dorsey LL, Lojovich JM, Carey JR. Electrical stimulation driving functional improvements and cortical changes in subjects with stroke. Exp Brain Res 2004;

154: 450–60.

Kleiner-Fisman G, Fisman DN, Sime E, Saint-Cyr JA, Lozano AM, Lang AE. Long-term follow up of bilateral deep brain stimulation of the subthalamic nucleus in patients with advanced Parkinson disease. J Neurosurg 2003; 99: 489–95.

Klostermann F, Funk T, Vesper J, Curio G. Spatiotemporal characteristics of human intrathalamic high-frequency (> 400 Hz) SEP components. Neuroreport 1999; 10: 3627–31.

Kobayashi M, Pascual-Leone A. Transcranial magnetic stimulation in neurology. Lancet Neurol 2003; 2: 145–56.

Kohl S, Schönherr DM, Luigjes J, Denys D, Mueller UJ, Lenartz D, et al. Deep brain stimulation for treatment-refractory obsessive compulsive disorder: A systematic review [Internet]. BMC Psychiatry 2014; 14[cited 2021 May 26] Available from: https://pubmed.ncbi.nlm.nih.gov/25085317/

Koller WC, Lyons KE, Wilkinson SB, Troster AI, Pahwa R. Long-term safety and efficacy of unilateral deep brain stimulation of the thalamus in essential tremor. Mov Disord 2001; 16: 464–8.

Krack P, Hariz MI, Baunez C, Guridi J, Obeso JA. Deep brain stimulation: From neurology to psychiatry? Trends Neurosci 2010; 33: 474–84.

Krack P, Volkmann J, Tinkhauser G, Deuschl G. Deep Brain Stimulation in Movement Disorders: From Experimental Surgery to Evidence-Based Therapy. Mov Disord 2019; 34: 1795–810.

Kuhn A, Kempf F, Brucke C, Doyle L, Martinez-Torres I, Pogosyan A, et al. High-Frequency Stimulation of the Subthalamic Nucleus Suppresses Oscillatory β Activity in Patients with Parkinson's Disease in Parallel with Improvement in Motor Performance. J Neurosci 2008; 28: 6165–73.

Kühn AA, Kupsch A, Schneider GH, Brown P. Reduction in subthalamic 8-35 Hz oscillatory activity correlates with clinical improvement in Parkinson's disease. Eur J Neurosci 2006; 23: 1956–60.

Kühn AA, Tsui A, Aziz T, Ray N, Brücke C, Kupsch A, et al. Pathological synchronisation in the subthalamic nucleus of patients with Parkinson's disease relates to both bradykinesia and rigidity. Exp Neurol 2009; 215: 380–7.

Kühn AA, Williams D, Kupsch A, Limousin P, Hariz M, Schneider GH, et al. Event-related beta desynchronization in human subthalamic nucleus correlates with motor performance. Brain 2004; 127: 735–46.

Kunimatsu J, Tanaka M. Roles of the primate motor thalamus in the generation of antisaccades. J Neurosci 2010; 30: 5108–17.

Kuramoto E, Fujiyama F, Nakamura KC, Tanaka Y, Hioki H, Kaneko T. Complementary distribution of glutamatergic cerebellar and GABAergic basal ganglia afferents to the rat motor thalamic nuclei. Eur J Neurosci 2011; 33: 95–109.

Kuramoto E, Ohno S, Furuta T, Unzai T, Tanaka YR, Hioki H, et al. Ventral Medial Nucleus Neurons Send Thalamocortical Afferents More Widely and More Preferentially to Layer 1 than Neurons of the Ventral Anterior – Ventral Lateral Nuclear Complex in the Rat. 2015: 221–35.

Laxpati NG, Kasoff WS, Gross RE. Deep Brain Stimulation for the Treatment of Epilepsy: Circuits, Targets, and Trials. Neurotherapeutics 2014; 11: 508–26.

Leblois A, Bodor ÁL, Person AL, Perkel DJ. Millisecond timescale disinhibition mediates fast

information transmission through an avian basal ganglia loop. J Neurosci 2009; 29: 15420–33.

Lengyel M, Kwag J, Paulsen O, Dayan P. Matching storage and recall: Hippocampal spike timing-dependent plasticity and phase response curves. Nat Neurosci 2005; 8: 1677–83.

Lenz FA, Kwan HC, Martin RL, Tasker RR, Dostrovsky JO, Lenz YE. Single unit analysis of the human ventral thalamic nuclear group: Tremor-related activity in functionally identified cells. Brain 1994; 117: 531–43.

Lévy JP, Nguyen TAK, Lachenmayer L, Debove I, Tinkhauser G, Petermann K, et al. Structure-function relationship of the posterior subthalamic area with directional deep brain stimulation for essential tremor. NeuroImage Clin 2020; 28: 102486.

Levy R, Ashby P, Hutchison WD, Lang AE, Lozano AM, Dostrovsky JO. Dependence of subthalamic nucleus oscillations on movement and dopamine in Parkinson's disease. Brain 2002; 125: 1196–209.

Li S, Arbuthnott GW, Jutras MJ, Goldberg JA, Jaeger D. Resonant antidromic cortical circuit activation as a consequence of high-frequency subthalamic deep-brain stimulation. J Neurophysiol 2007; 98: 3525–37.

Little S, Beudel M, Zrinzo L, Foltynie T, Limousin P, Hariz M, et al. Bilateral adaptive deep brain stimulation is effective in Parkinson's disease. J Neurol Neurosurg Psychiatry 2016; 87: 717–21.

Little S, Bonaiuto J, Barnes G, Bestmann S. Human motor cortical beta bursts relate to movement planning and response errors. PLoS Biol 2019; 17: e3000479.

Little S, Brown P. What brain signals are suitable for feedback control of deep brain stimulation in Parkinson's disease? Ann N Y Acad Sci 2012; 1265: 9–24.

Little S, Pogosyan A, Kuhn AA, Brown P. Beta band stability over time correlates with Parkinsonian rigidity and bradykinesia. Exp Neurol 2012; 236: 383–8.

Little S, Pogosyan A, Neal S, Zavala B, Zrinzo L, Hariz M, et al. Adaptive deep brain stimulation in advanced Parkinson disease. Ann Neurol 2013: 449–57.

Little S, Tripoliti E, Beudel M, Pogosyan A, Cagnan H, Herz D, et al. Adaptive deep brain stimulation for Parkinson's disease demonstrates reduced speech side effects compared to conventional stimulation in the acute setting. J Neurol Neurosurg Psychiatry 2016; 87: 1388–9.

Litvak V, Jha A, Eusebio A, Oostenveld R, Foltynie T, Limousin P, et al. Resting oscillatory cortico-subthalamic connectivity in patients with Parkinson's disease. Brain 2011; 134: 359–74.

Llinás R, Jahnsen H. Electrophysiology of mammalian thalamic neurones in vitro. Nature 1982; 297: 406–8.

Lofredi R, Tan H, Neumann WJ, Yeh CH, Schneider GH, Kühn AA, et al. Beta bursts during continuous movements accompany the velocity decrement in Parkinson's disease patients. Neurobiol Dis 2019; 127: 462–71.

Lopez-Azcarate J, Tainta M, Rodriguez-Oroz MC, Valencia M, Gonzalez R, Guridi J, et al. Coupling between Beta and High-Frequency Activity in the Human Subthalamic Nucleus May Be a Pathophysiological Mechanism in Parkinson's Disease. J Neurosci 2010; 30: 6667–77.

Lorenz D, Frederiksen H, Moises H, Kopper F, Deuschl G, Christensen K. High concordance for essential tremor in monozygotic twins of old age. Neurology 2004; 62: 208–11.

Lorenz D, Poremba C, Papengut F, Schreiber S, Deuschl G. The psychosocial burden of essential tremor in an outpatient- and a community-based cohort. Eur J Neurol 2011; 18: 972–9.

Louis ED, Barnes L, Albert SM, Cote L, Schneier FR, Pulman SL, et al. Correlates of functional disability in essential tremor. Mov Disord 2001; 16: 914–20.

Louis ED, Faust PL, Vonsattel JPG, Honig LS, Rajput A, Robinson CA, et al. Neuropathological changes in essential tremor: 33 Cases compared with 21 controls. Brain 2007; 130: 3297–307.

Louis ED, Ferreira JJ. How common is the most common adult movement disorder? Update on the worldwide prevalence of essential tremor. Mov Disord 2010; 25: 534–41.

Louis ED, Ottman R. How familial is familial tremor? The genetic epidemiology of essential tremor. Neurology 1996; 46: 1200–5.

Louis ED, Ottman R, Allen Hauser W. How common is the most common adult movement disorder? Estimates of the prevalence of essential tremor throughout the world. Mov Disord 1998; 13: 5–10.

Lozano A, Hutchison W, Kiss Z, Tasker R, Davis K, Dostrovsky J. Methods for microelectrode-guided posteroventral pallidotomy. J Neurosurg 1996; 84: 194–202.

Lozano AM, Fosdick L, Chakravarty MM, Leoutsakos JM, Munro C, Oh E, et al. A Phase II Study of Fornix Deep Brain Stimulation in Mild Alzheimer's Disease. J Alzheimer's Dis 2016; 54: 777–87.

Lozano AM, Lipsman N, Bergman H, Brown P, Chabardes S, Chang JW, et al. Deep brain stimulation: current challenges and future directions. Nat Rev Neurol 2019; 15: 148–60.

Lundqvist M, Rose J, Herman P, Brincat SLL, Buschman TJJ, Miller EKK. Gamma and Beta Bursts Underlie Working Memory. Neuron 2016; 90: 152–64.

MacLeod NK, James TA, Kilpatrick IC, Starr MS. Evidence for a GABAergic nigrothalamic pathway in the rat - II. Electrophysiological studies. Exp Brain Res 1980; 40: 55–61.

Maendly R, Ruegg DG, Wiesendanger M, Lagowska J, Hess B. Thalamic relay for group I muscle afferents of forelimb nerves in the monkey. J Neurophysiol 1981; 46: 901–17.

Magnin M, Morel A, Jeanmonod D. Single-unit analysis of the pallidum, thalamus and subthalamic nucleus in parkinsonian patients. Neuroscience 2000; 96: 549–64.

Malekmohammadi M, Herron J, Velisar A, Blumenfeld Z, Trager MH, Chizeck HJ, et al. Kinematic Adaptive Deep Brain Stimulation for Resting Tremor in Parkinson's Disease. Mov Disord 2016; 31: 426–8.

Mallet N, Micklem BR, Henny P, Brown MT, Williams C, Bolam JP, et al. Dichotomous Organization of the External Globus Pallidus. Neuron 2012; 74: 1075–86.

Mallet N, Pogosyan A, Marton LF, Bolam JP, Brown P, Magill PJ. Parkinsonian Beta Oscillations in the External Globus Pallidus and Their Relationship with Subthalamic Nucleus Activity. J Neurosci 2008; 28: 14245–58.

Mallet N, Pogosyan A, Sharott A, Csicsvari J, Bolam JP, Brown P, et al. Disrupted Dopamine Transmission and the Emergence of Exaggerated Beta Oscillations in Subthalamic Nucleus and Cerebral Cortex. J Neurosci 2008; 28: 4795–806.

Maneski LP, Jorgovanović N, Ilić V, Došen S, Keller T, Popović MB, et al. Electrical stimulation for the suppression of pathological tremor. Med Biol Eng Comput 2011; 49: 1187–93.

Marreiros AC, Cagnan H, Moran RJ, Friston KJ, Brown P. Basal ganglia-cortical interactions in Parkinsonian patients. Neuroimage 2013; 66: 301–10.

Marsden JF, Ashby P, Limousin-Dowsey P, Rothwell JC, Brown P. Coherence between cerebellar thalamus, cortex and muscle in man Cerebellar thalamus interactions. 2000

Mauk MD, Steele PM, Medina JF. Cerebellar involvement in motor learning. Neuroscientist 1997; 3: 303–13.

Maurice N, Thierry AM, Glowinski J, Deniau JM. Spontaneous and Evoked Activity of Substantia Nigra Pars Reticulata Neurons during High-Frequency Stimulation of the Subthalamic Nucleus. J Neurosci 2003; 23: 9929–36.

Mayberg HS, Lozano AM, Voon V, McNeely HE, Seminowicz D, Hamani C, et al. Deep brain stimulation for treatment-resistant depression. Neuron 2005; 45: 651–60.

McCarthy MM, Moore-Kochlacs C, Gu X, Boyden ES, Han X, Kopell N. Striatal origin of the pathologic beta oscillations in Parkinson's disease. Proc Natl Acad Sci U S A 2011; 108: 11620–5.

McIntyre CC, Savasta M, Kerkerian-Le Goff L, Vitek JL. Uncovering the mechanism(s) of action of deep brain stimulation: Activation, inhibition, or both. Clin Neurophysiol 2004; 115: 1239–48.

McNamara C, Rothwell M, Sharott A. Phase-dependent closed-loop modulation of neural oscillations in vivo. bioRxiv 2020: 2020.05.21.102335.

Meidahl AC, Tinkhauser G, Herz DM, Cagnan H, Debarros J, Brown P. Adaptive Deep Brain Stimulation for Movement Disorders: The Long Road to Clinical Therapy. Mov Disord 2017; 32: 810–9.

Miller LC, Thompson CK, Negro F, Heckman CJ, Farina D, Dewald JPA. High-density surface EMG decomposition allows for recording of motor unit discharge from proximal and distal flexion synergy muscles simultaneously in individuals with stroke. In: 2014 36th Annual International Conference of the IEEE Engineering in Medicine and Biology Society, EMBC 2014. Institute of Electrical and Electronics Engineers Inc.; 2014. p. 5340–4

Milosevic L, Kalia SK, Hodaie M, Lozano AM, Popovic MR, Hutchison WD. Physiological mechanisms of thalamic ventral intermediate nucleus stimulation for tremor suppression. Brain 2018; 141: 2142–55.

Mink JW, Walkup J, Frey KA, Como P, Cath D, DeLong MR, et al. Patient selection and assessment recommendations for deep brain stimulation in Tourette syndrome. Mov Disord 2006; 21: 1831–8.

Mobbs RJ, Nair S, Blum P. Peripheral nerve stimulation for the treatment of chronic pain. J Clin Neurosci 2007; 14: 216–21.

Moran A, Bergman H, Israel Z, Bar-Gad I. Subthalamic nucleus functional organization revealed by parkinsonian neuronal oscillations and synchrony. Brain 2008; 131: 3395–409.

Moran RJ, Kiebel SJ, Stephan KE, Reilly RB, Daunizeau J, Friston KJ. A neural mass model of spectral responses in electrophysiology. Neuroimage 2007; 37: 706–20.

Moran RJ, Mallet N, Litvak V, Dolan RJ, Magill PJ, Friston KJ, et al. Alterations in brain connectivity underlying beta oscillations in parkinsonism. PLoS Comput Biol 2011; 7

Moran RJ, Stephan KE, Kiebel SJ, Rombach N, O'Connor WT, Murphy KJ, et al. Bayesian estimation of synaptic physiology from the spectral responses of neural masses. Neuroimage 2008;

42: 272–84.

Moran RJ, Stephan KE, Seidenbecher T, Pape HC, Dolan RJ, Friston KJ. Dynamic causal models of steady-state responses. Neuroimage 2009; 44: 796–811.

Müller UJ, Voges J, Steiner J, Galazky I, Heinze HJ, Möller M, et al. Deep brain stimulation of the nucleus accumbens for the treatment of addiction. Ann N Y Acad Sci 2013; 1282: 119–28.

Munhoz RP, Hanajima R, Ashby P, Lang AE. Acute effect of transcutaneous electrical nerve stimulation on tremor. Mov Disord 2003; 18: 191–4.

Murer MG, Tseng KY, Kasanetz F, Belluscio M, Riquelme LA. Brain oscillations, medium spiny neurons, and dopamine. Cell Mol Neurobiol 2002; 22: 611–32.

Muthuraman M, Heute U, Arning K, Anwar AR, Elble R, Deuschl G, et al. Oscillating central motor networks in pathological tremors and voluntary movements. What makes the difference? Neuroimage 2012; 60: 1331–9.

Muthuraman M, Raethjen J, Koirala N, Anwar AR, Mideksa KG, Elble R, et al. Cerebello-cortical network fingerprints differ between essential, Parkinson's and mimicked tremors. Brain 2018; 141: 1770–81.

Nakamura KC, Sharott A, Magill PJ. Temporal Coupling with Cortex Distinguishes Spontaneous Neuronal Activities in Identi fi ed Basal Ganglia-Recipient and Cerebellar-Recipient Zones of the Motor Thalamus. 2014: 81–97.

Nakamura KC, Sharott A, Tanaka T, Magill PJ. Input zone-selective dysrhythmia in motor thalamus after dopamine depletion. bioRxiv 2021: 2021.08.30.458172.

Nambu. A new dynamic model of the cortico-basal ganglia loop. Prog Brain Res 2004; 143: 461–6.

Nambu A, Tachibana Y. Mechanism of parkinsonian neuronal oscillations in the primate basal ganglia: some considerations based on our recent work. Front Syst Neurosci 2014; 8: 74.

Nambu A, Yoshida S, Jinnai K. Movement-related activity of thalamic neurons with input from the globus pallidus and projection to the motor cortex in the monkey. Exp Brain Res 1991; 84: 279–84.

Nevado-Holgado AJ, Mallet N, Magill PJ, Bogacz R. Effective connectivity of the subthalamic nucleus–globus pallidus network during Parkinsonian oscillations. J Physiol 2014; 592: 1429–55.

Nevet A, Morris G, Saban G, Arkadir D, Bergman H. Lack of spike-count and spike-time correlations in the substantia nigra reticulata despite overlap of neural responses. J Neurophysiol 2007; 98: 2232–43.

Nieuwhof F, Toni I, Buijink AWG, Rootselaar A-F van, Warrenburg BPC van de, Helmich RC. Phase-locked transcranial electrical brain stimulation for tremor suppression in dystonic tremor syndromes. medRxiv 2021: 2021.11.03.21265869.

Nuttin B, Cosyns P, Demeulemeester H, Gybels J, Meyerson B. Electrical stimulation in anterior limbs of internal capsules in patients with obsessive-compulsive disorder. Lancet 1999; 354: 1526.

Obeso JA, Olanow W, Nutt JG, Givup G. Levodopa motor complications in Parkinson's disease. 2000

Ohyama T, Mauk MD. Latent acquisition of timed responses in cerebellar cortex. J Neurosci 2001; 21: 682–90.

Ohye C, Narabayashi H. Physiological study of presumed ventralis intermedius neurons in the human thalamus. J Neurosurg 1979; 50: 290–7.

Ondo W. Essential tremor: What we can learn from current pharmacotherapy. Tremor and Other Hyperkinetic Movements 2016; 2016

Opri E, Cernera S, Molina R, Eisinger RS, Cagle JN, Almeida L, et al. Chronic embedded cortico-thalamic closed-loop deep brain stimulation for the treatment of essential tremor. Sci Transl Med 2020; 12: eaay7680.

Pagan FL, Butman JA, Dambrosia JM, Hallett M. Evaluation of essential tremor with multi-voxel magnetic resonance spectroscopy. Neurology 2003; 60: 1344 LP – 1347.

Pahwa R, Dhall R, Ostrem J, Gwinn R, Lyons K, Ro S, et al. An Acute Randomized Controlled Trial of Noninvasive Peripheral Nerve Stimulation in Essential Tremor. Neuromodulation 2019; 22: 537–45.

Pan LLH, Yang WW, Kao CL, Tsai MW, Wei SH, Fregni F, et al. Effects of 8-week sensory electrical stimulation combined with motor training on EEG-EMG coherence and motor function in individuals with stroke [Internet]. Sci Rep 2018; 8[cited 2021 May 31] Available from: https://pubmed.ncbi.nlm.nih.gov/29907780/

Panyakaew P, Cho HJ, Lee SW, Wu T, Hallett M. The Pathophysiology of Dystonic Tremors and Comparison With Essential Tremor. J Neurosci 2020; 40: 9317–26.

Paradiso G, Cunic D, Saint-Cyr JA, Hoque T, Lozano AM, Lang AE, et al. Involvement of human thalamus in the preparation of self-paced movement. Brain 2004; 127: 2717–31.

Pare D, Steriade M, Deschenes M, Oakson G. Physiological characteristics of anterior thalamic nuclei, a group devoid of inputs from reticular thalamic nucleus. J Neurophysiol 1987; 57: 1669–85.

Pascual-Valdunciel A, Hoo GW, Avrillon S, Barroso FO, Goldman JG, Hernandez-Pavon JC, et al. Peripheral electrical stimulation to reduce pathological tremor: a review. J Neuroeng Rehabil 2021; 18: 1–19.

Pedrosa DJ, Brown P, Cagnan H, Visser-Vandewalle V, Wirths J, Timmermann L, et al. A functional micro-electrode mapping of ventral thalamus in essential tremor. Brain 2018; 141: 2644–54.

Pedrosa DJ, Quatuor EL, Reck C, Pauls KAM, Huber CA, Visser-Vandewalle V, et al. Thalamomuscular coherence in essential tremor: Hen or egg in the emergence of tremor? J Neurosci 2014; 34: 14475–83.

Pedrosa DJ, Reck C, Florin E, Pauls KAM, Maarouf M, Wojtecki L, et al. Essential tremor and tremor in Parkinson's disease are associated with distinct 'tremor clusters' in the ventral thalamus. Exp Neurol 2012; 237: 435–43.

Peles O, Werner-Reiss U, Bergman H, Israel Z, Correspondence V. Phase-Specific Microstimulation Differentially Modulates Beta Oscillations and Affects Behavior [Internet]. 2020[cited 2021 Jan 27] Available from: https://doi.org/10.1016/j.celrep.2020.02.005

Person AL, Perkel DJ. Unitary IPSPs drive precise thalamic spiking in a circuit required for learning. Neuron 2005; 46: 129–40.

Pessiglione M, Guehl D, Rolland AS, François C, Hirsch EC, Féger J, et al. Thalamic neuronal activity in dopamine-depleted primates: Evidence for a loss of functional segregation within basal

ganglia circuits. J Neurosci 2005; 25: 1523–31.

Peurala SH, Pitkänen K, Sivenius J, Tarkka IM. Cutaneous electrical stimulation may enhance sensorimotor recovery in chronic stroke. Clin Rehabil 2002; 16: 709–16.

Pfeiffer RF. Non-motor symptoms in Parkinson's disease. Park Relat Disord 2016; 22: S119–22.

Pfurtscheller G, Lopes Da Silva FH. Event-related EEG/MEG synchronization and desynchronization: Basic principles. Clin Neurophysiol 1999; 110: 1842–57.

Piña-Fuentes D, Little S, Oterdoom M, Neal S, Pogosyan A, Tijssen MAJ, et al. Adaptive DBS in a Parkinson's patient with chronically implanted DBS: A proof of principle. Mov Disord 2017; 32: 1253–4.

Plaha P, Patel NK, Gill SS. Stimulation of the subthalamic region for essential tremor. J Neurosurg 2004; 101: 48–54.

Pollo C, Kaelin-Lang A, Oertel MF, Stieglitz L, Taub E, Fuhr P, et al. Directional deep brain stimulation: An intraoperative double-blind pilot study. Brain 2014; 137: 2015–26.

Porter R, Lewis MMD. Relationship of neuronal discharges in the precentral gyrus of monkeys to the performance of arm movements. Brain Res 1975; 98: 21–36.

Priori A, Foffani G, Pesenti A, Tamma F, Bianchi AM, Pellegrini M, et al. Rhythm-specific pharmacological modulation of subthalamic activity in Parkinson's disease. Exp Neurol 2004; 189: 369–79.

Prochazka A, Elek J, Javidan M. Attenuation of pathological tremors by functional electrical stimulation I: Method. Ann Biomed Eng 1992; 20: 205–24.

Raethjen J, Deuschl G. The oscillating central network of Essential tremor. Clin Neurophysiol 2012; 123: 61–4.

Raethjen J, Lindemann M, Schmaljohann H, Wenzelburger R, Pfister G, Deuschl G. Multiple oscillators are causing parkinsonian and essential tremor. Mov Disord 2000; 15: 84–94.

Rajput A, Robinson CA, Rajput AH. Essential tremor course and disability. Neurology 2004; 62: 932 LP – 936.

Raymond JL, Lisberger SG, Mauk MD. The cerebellum: A neuronal learning machine? Science (80- ) 1996; 272: 1126–31.

Reis C, Sharott A, Magill PJ, van Wijk BCM, Parr T, Zeidman P, et al. Thalamocortical dynamics underlying spontaneous transitions in beta power in Parkinsonism. Neuroimage 2019; 193: 103–14.

Reker P, Dembek TA, Becker J, Visser-Vandewalle V, Timmermann L. Directional deep brain stimulation: A case of avoiding dysarthria with bipolar directional current steering. Park Relat Disord 2016; 31: 156–8.

Ridding MC, Brouwer B, Miles TS, Pitcher JB, Thompson PD. Changes in muscle responses to stimulation of the motor cortex induced by peripheral nerve stimulation in human subjects. Exp Brain Res 2000; 131: 135–43.

Ridding MC, Rothwell JC, Inzelberg R. Changes in excitability of motor cortical circuitry in patients with parkinson's disease. Ann Neurol 1995; 37: 181–8.

Rodriguez-Oroz MC, Obeso JA, Lang AE, Houeto J-L, Pollak P, Rehncrona S, et al. Bilateral deep brain stimulation in Parkinson's disease: A multicentre study with 4 years follow-up. Brain 2005; 128: 2240–9.

Rosa M, Arlotti M, Ardolino G, Cogiamanian F, Marceglia S, Di Fonzo A, et al. Adaptive deep brain stimulation in a freely moving parkinsonian patient. Mov Disord 2015; 30: 1003–5.

Rosa M, Arlotti M, Marceglia S, Cogiamanian F, Ardolino G, Fonzo A Di, et al. Adaptive deep brain stimulation controls levodopa-induced side effects in Parkinsonian patients. Mov Disord 2017; 32: 628–9.

Rosin B, Slovik M, Mitelman R, Rivlin-Etzion M, Haber SN, Israel Z, et al. Closed-loop deep brain stimulation is superior in ameliorating parkinsonism. Neuron 2011; 72: 370–84.

Rousseeuw PJ. Silhouettes: A graphical aid to the interpretation and validation of cluster analysis. J Comput Appl Math 1987; 20: 53–65.

Sankar T, Chakravarty MM, Bescos A, Lara M, Obuchi T, Laxton AW, et al. Deep brain stimulation influences brain structure in Alzheimer's disease. Brain Stimul 2015; 8: 645–54.

Schnitzler A, Gross J. Normal and pathological oscillatory communication in the brain. Nat Rev Neurosci 2005; 6: 285–96.

Schnitzler A, Münks C, Butz M, Timmermann L, Gross J. Synchronized brain network associated with essential tremor as revealed by magnetoencephalography. Mov Disord 2009; 24: 1629–35.

Schultheiss NW, Edgerton JR, Jaeger D. Phase response curve analysis of a full morphological globus pallidus neuron model reveals distinct perisomatic and dendritic modes of synaptic integration. J Neurosci 2010; 30: 2767–82.

Schwab BC, Kase D, Zimnik A, Rosenbaum R, Codianni MG, Rubin JE, et al. Neural activity during a simple reaching task in macaques is counter to gating and rebound in basal ganglia–thalamic communication [Internet]. PLoS Biol 2020; 18[cited 2021 Jul 26] Available from: https://doi.org/10.1371/journal.pbio.3000829

Schwarting RKW, Huston JP. Unilateral 6-hydroxydopamine lesions of meso-striatal dopamine neurons and their physiological sequelae. Prog Neurobiol 1996; 49: 215–66.

Schwarting RKW, Huston JP. The unilateral 6-hydroxydopamine lesion model in behavioral brain research. Analysis of functional deficits, recovery and treatments. Prog Neurobiol 1996; 50: 275–331.

Shaikh AG, Jinnah HA, Tripp RM, Optican LM, Ramat S, Lenz FA, et al. Irregularity distinguishes limb tremor in cervical dystonia from essential tremor. J Neurol Neurosurg Psychiatry 2008; 79: 187.

Sharott A, Doig NM, Mallet N, Magill PJ. Relationships between the firing of identified striatal interneurons and spontaneous and driven cortical activities in vivo. J Neurosci 2012; 32: 13221–36.

Sharott A, Gulberti A, Hamel W, Köppen JA, Münchau A, Buhmann C, et al. Spatio-temporal dynamics of cortical drive to human subthalamic nucleus neurons in Parkinson's disease. Neurobiol Dis 2018; 112: 49–62.

Sharott A, Magill PJ, Harnack D, Kupsch A, Meissner W, Brown P. Dopamine depletion increases the power and coherence of β-oscillations in the cerebral cortex and subthalamic nucleus of the awake rat. Eur J Neurosci 2005; 21: 1413–22.

Sharott A, Vinciati F, Nakamura KC, Magill PJ. A population of indirect pathway striatal projection neurons is selectively entrained to parkinsonian beta oscillations. J Neurosci 2017; 37: 9977–98.

Shepherd GMG, Grillner S. Handbook of Brain Microcircuits [Internet]. Oxford UP,. 2010Available from: http://oxfordmedicine.com/view/10.1093/med/9780195389883.001.0001/med-9780195389883

Sherman MA, Lee S, Law R, Haegens S, Thorn CA, Hämäläinen MS, et al. Neural mechanisms of transient neocortical beta rhythms: Converging evidence from humans, computational modeling, monkeys, and mice. Proc Natl Acad Sci 2016; 113: E4885–94.

Sherman SM. Functioning of circuits connecting thalamus and cortex. Compr Physiol 2017; 7: 713–39.

Sherman SM, Guillery RW. Exploring the Thalamus and Its Role in Cortical Function. Massachusetts Institute of Technology Press; 2009

Shill HA, Adler CH, Sabbagh MN, Connor DJ, Caviness JN, Hentz JG, et al. Pathologic findings in prospectively ascertained essential tremor subjects. Neurology 2008; 70: 1452 LP – 1455.

Shu Y, McCormick DA. Inhibitory interactions between ferret thalamic reticular neurons. J Neurophysiol 2002; 87: 2571–6.

Siegle JH, Wilson MA. Enhancement of encoding and retrieval functions through theta phase-specific manipulation of hippocampus. Elife 2014; 2014

Silberstein P, Pogosyan A, Kühn AA, Hotton G, Tisch S, Kupsch A, et al. Cortico-cortical coupling in Parkinson's disease and its modulation by therapy. Brain 2005; 128: 1277–91.

Smeal RM, Bard Ermentrout G, White JA. Phase-response curves and synchronized neural networks. Philos Trans R Soc B Biol Sci 2010; 365: 2407–22.

Smith Y, Bevan MD, Shink E, Bolam JP. Microcircuitry of the direct and indirect pathways of the basal ganglia. Neuroscience 1998; 86: 353–87.

Soteropoulos DS, Baker SN. Cortico-cerebellar coherence during a precision grip task in the monkey. J Neurophysiol 2006; 95: 1194–206.

Starr PA, Rau GM, Davis V, Marks WJ, Ostrem JL, Simmons D, et al. Spontaneous pallidal neuronal activity in human dystonia: Comparison with Parkinson's disease and normal macaque. J Neurophysiol 2005; 93: 3165–76.

Stephan et al. Ten simple rules for dynamic causal modeling. Neuroimage 2010; 49: 3099–109.

Steriade M, McCormick DA, Sejnowski TJ. Thalamocortical oscillations in the sleeping and aroused brain. Science (80- ) 1993; 262: 679–85.

Strick PL. Activity of ventrolateral thalamic neurons during arm movement. J Neurophysiol 1976; 39: 1032–44.

Sulzer D, Surmeier DJ. Neuronal vulnerability, pathogenesis, and Parkinson's disease. Mov Disord 2013; 28: 41–50.

Sun FT, Morrell MJ. Closed-loop Neurostimulation: The Clinical Experience. Neurotherapeutics 2014; 11: 553–63.

Swann NC, De Hemptinne C, Miocinovic S, Qasim S, Wang SS, Ziman N, et al. Gamma oscillations

in the hyperkinetic state detected with chronic human brain recordings in parkinson's disease. J Neurosci 2016; 36: 6445–58.

Swann NC, De Hemptinne C, Thompson MC, Miocinovic S, Miller AM, Gilron R, et al. Adaptive deep brain stimulation for Parkinson's disease using motor cortex sensing [Internet]. J Neural Eng 2018; 15[cited 2021 Jun 10] Available from: https://pubmed.ncbi.nlm.nih.gov/29741160/

Tachibana Y, Iwamuro H, Kita H, Takada M, Nambu A. Subthalamo-pallidal interactions underlying parkinsonian neuronal oscillations in the primate basal ganglia. Eur J Neurosci 2011; 34: 1470–84.

Tan EK, Fook-Chong S, Lum SY, Gabriel C, Koh KK, Prakash KM, et al. Non-motor manifestations in essential tremor: Use of a validated instrument to evaluate a wide spectrum of symptoms. Park Relat Disord 2005; 11: 375–80.

Tanibuchi I, Kitano H, Jinnai K. Substantia nigra output to prefrontal cortex via thalamus in monkeys. I. Electrophysiological identification of thalamic relay neurons. J Neurophysiol 2009; 102: 2933–45.

Terman D, Rubin JE, Yew a C, Wilson CJ. Activity patterns in a model for the subthalamopallidal network of the basal ganglia. J Neurosci 2002; 22: 2963–76.

Thier P, Dicke PW, Haas R, Barash S. Encoding of movement time by populations of cerebellar Purkinje cells. Nature 2000; 405: 72–6.

Timmermann L, Gross J, Dirks M, Volkmann J, Freund H-J, Schnitzler A. The cerebral oscillatory network of parkinsonian resting tremor. Brain 2003; 126: 199–212.

Tinkhauser G, Pogosyan A, Little S, Beudel M, Herz DM, Tan H, et al. The modulatory effect of adaptive deep brain stimulation on beta bursts in Parkinson's disease. Brain 2017; 140: 1053–67.

Tinkhauser G, Pogosyan A, Tan H, Herz DM, Kühn AA, Brown P. Beta burst dynamics in Parkinson's disease OFF and ON dopaminergic medication. Brain 2017; 140: 2968–81.

Tinkhauser G, Torrecillos F, Duclos Y, Tan H, Pogosyan A, Fischer P, et al. Beta burst coupling across the motor circuit in Parkinson's disease. Neurobiol Dis 2018; 117: 217–25.

Toglia JU, Izzo K. Treatment of myoclonic dystonia with transcutaneous electrical nerve stimulation. Ital J Neurol Sci 1985; 6: 75–8.

Torrecillos F, Tinkhauser G, Fischer P, Green AL, Aziz TZ, Foltynie T, et al. Modulation of beta bursts in the subthalamic nucleus predicts motor performance. J Neurosci 2018; 38: 8905–17.

Tsang EW, Hamani C, Moro E, Mazzella F, Lozano AM, Hodaie M, et al. Movement related potentials and oscillatory activities in the human internal globus pallidus during voluntary movements. J Neurol Neurosurg Psychiatry 2012; 83: 91–7.

Turner RS, Anderson ME. Pallidal discharge related to the kinematics of reaching movements in two dimensions. J Neurophysiol 1997; 77: 1051–74.

Uhlhaas PJ, Singer W. Neural Synchrony in Brain Disorders: Relevance for Cognitive Dysfunctions and Pathophysiology. Neuron 2006; 52: 155–68.

Underwood CF, Parr-Brownlie LC. Primary motor cortex in Parkinson's disease: Functional changes and opportunities for neurostimulation. Neurobiol Dis 2021; 147: 105159.

Urasaki E, Wada S ichi, Kadoya C, Yokota A, Matsuoka S, Shima F. Origin of scalp far-field N18 of SSEPs in response to median nerve stimulation. Electroencephalogr Clin Neurophysiol Evoked

Potentials 1990; 77: 39–51.

Vandewalle V, Van Der Linden C, Groenewegen HJ, Caemaert J. Stereotactic treatment of Gilles de la Tourette syndrome by high frequency stimulation of thalamus. Lancet 1999; 353: 724.

Velisar A, Syrkin-Nikolau J, Blumenfeld Z, Trager MH, Afzal MF, Prabhakar V, et al. Dual threshold neural closed loop deep brain stimulation in Parkinson disease patients. Brain Stimul 2019; 12: 868–76.

Vidailhet M, Vercueil L, Houeto J-L, Krystkowiak P, Benabid A-L, Cornu P, et al. Bilateral Deep-Brain Stimulation of the Globus Pallidus in Primary Generalized Dystonia. N Engl J Med 2005; 352: 459–67.

Vidailhet M, Roze E, Jinnah HA. A simple way to distinguish essential tremor from tremulous Parkinson's disease. Brain 2017; 140: 1820–2.

Vinding MC, Tsitsi P, Waldthaler J, Oostenveld R, Ingvar M, Svenningsson P, et al. Reduction of spontaneous cortical beta bursts in Parkinson's disease is linked to symptom severity [Internet]. Brain Commun 2020; 2[cited 2021 Mar 22] Available from: https://academic.oup.com/braincomms/article/doi/10.1093/braincomms/fcaa052/5826350

Vitek JL, Ashe J, Kaneoke Y. Spontaneous neuronal activity in the motor thalamus: Alteration in pattern and rate in parkinsonism. In: Soc Neurosci. 1994. p. 561 (#237.4)

Volkmann J, Albanese A, Kulisevsky J, Tornqvist AL, Houeto JL, Pidoux B, et al. Long-term effects of pallidal or subthalamic deep brain stimulation on quality of life in Parkinson's disease. Mov Disord 2009; 24: 1154–61.

Wang DD, de Hemptinne C, Miocinovic S, Ostrem JL, Galifianakis NB, Luciano MS, et al. Pallidal deep-brain stimulation disrupts pallidal beta oscillations and coherence with primary motor cortex in Parkinson's disease. J Neurosci 2018; 38: 4556–68.

Wang XJ, Rinzel J, Rogawski MA. A model of the T-type calcium current and the low-threshold spike in thalamic neurons. https://doi.org/101152/jn1991663839 1991; 66: 839–50.

Weerasinghe G, Duchet B, Cagnan H, Brown P, Bick C, Bogacz R. Predicting the effects of deep brain stimulation using a reduced coupled oscillator model. PLoS Comput Biol 2019; 15: e1006575.

Weiler N, Wood L, Yu J, Solla SA, Shepherd GMG. Top-down laminar organization of the excitatory network in motor cortex. Nat Neurosci 2008; 11: 360–6.

Weinberger M, Mahant N, Hutchison WD, Lozano AM, Moro E, Hodaie M, et al. Beta oscillatory activity in the subthalamic nucleus and its relation to dopaminergic response in Parkinson's disease. J Neurophysiol 2006; 96: 3248–56.

Wessel JR. β-bursts reveal the trial-to-trial dynamics of movement initiation and cancellation. J Neurosci 2020; 40: 411–23.

West TO, Berthouze L, Farmer SF, Cagnan H, Litvak V. Inference of Brain Networks with Approximate Bayesian Computation – assessing face validity with an example application in Parkinsonism. Neuroimage 2021: 118020.

West TO, Farmer SF, Magill PJ, Sharott A, Litvak V, Cagnan H. State Dependency of Beta Oscillations in the Cortico-Basal-Ganglia Circuit and their Neuromodulation under Phase Locked Inputs. bioRxiv 2020: 2020.03.20.000711.

Wichmann T, Bergman H, Starr PA, Subramanian T, Watts RL, DeLong MR. Comparison of MPTP-induced changes in spontaneous neuronal discharge in the internal pallidal segment and in the substantia nigra pars reticulata in primates. Exp Brain Res 1999; 125: 397–409.

Wichmann T, Kliem MA. Neuronal Activity in the Primate Substantia Nigra Pars Reticulata during the Performance of Simple and Memory-Guided Elbow Movements. J Neurophysiol 2004; 91: 815–27.

Wijk BCM van, Beek PJ, Daffertshofer A. Differential modulations of ipsilateral and contralateral beta (de)synchronization during unimanual force production. Eur J Neurosci 2012; 36: 2088–97.

van Wijk BCM, Cagnan H, Litvak V, Kühn AA, Friston KJ. Generic dynamic causal modelling: An illustrative application to Parkinson's disease. Neuroimage 2018; 181: 818–30.

Wise SP, Donoghue JP. Motor Cortex of Rodents. In: Jones EG, Peters A, editor(s). Motor Cortex of Rodents. Boston, MA: Springer US; 1986. p. 243–70

Witjas T, Kaphan E, Azulay JP, Blin O, Ceccaldi M, Pouget J, et al. Nonmotor fluctuations in Parkinson's disease: Frequent and disabling. Neurology 2002; 59: 408–13.

Witt A, Palmigiano A, Neef A, El Hady A, Wolf F, Battaglia D. Controlling oscillation phase through precisely timed closed-loop optogenetic stimulation: A computational study. Front Neural Circuits 2013; 7: 49.

Wong JK, Cauraugh JH, Ho KWD, Broderick M, Ramirez-Zamora A, Almeida L, et al. STN vs. GPi deep brain stimulation for tremor suppression in Parkinson disease: A systematic review and meta-analysis. Park Relat Disord 2019; 58: 56–62.

Xie T, Bernard J, Warnke P. Post subthalamic area deep brain stimulation for tremors: a mini-review. Transl Neurodegener 2012 11 2012; 1: 1–8.

Yamawaki N, Borges K, Suter BA, Harris KD, Shepherd GMG. A genuine layer 4 in motor cortex with prototypical synaptic circuit connectivity. Elife 2014; 3: e05422.

Yamawaki N, Shepherd GMG. Synaptic Circuit Organization of Motor Corticothalamic Neurons. J Neurosci 2015; 35: 2293–307.

Yamawaki N, Stanford IM, Hall SD, Woodhall GL. Pharmacologically induced and stimulus evoked rhythmic neuronal oscillatory activity in the primary motor cortex in vitro. Neuroscience 2008; 151: 386–95.

Yoshimura Y, Callaway EM. Fine-scale specificity of cortical networks depends on inhibitory cell type and connectivity. Nat Neurosci 2005; 8: 1552–9.

Zaepffel M, Trachel R, Kilavik BE, Brochier T. Modulations of EEG Beta Power during Planning and Execution of Grasping Movements. PLoS One 2013; 8

Zanos S, Rembado I, Chen D, Fetz EE. Phase-Locked Stimulation during Cortical Beta Oscillations Produces Bidirectional Synaptic Plasticity in Awake Monkeys. Curr Biol 2018; 28: 2515-2526.e4.

Zhang J-R, Feng T, Hou Y-N, Chan P, Wu T. Functional Connectivity of Vim Nucleus in Tremor- and Akinetic-/Rigid-Dominant Parkinson's Disease. CNS Neurosci Ther 2016; 22: 378–86.

Zhang K, Bhatia S, Oh MY, Cohen D, Angle C, Whiting D. Long-term results of thalamic deep brain stimulation for essential tremor: Clinical article. J Neurosurg 2010; 112: 1271–6.

Zich C, Quinn AJ, Mardell LC, Ward NS, Bestmann S. Dissecting Transient Burst Events. Trends Cogn Sci 2020; 24: 784–8.

Zirh TA, Lenz FA, Reich SG, Dougherty PM. Patterns of bursting occurring in thalamic cells during parkinsonian tremor. Neuroscience 1998; 83: 107–21.

# Supplementary Materials

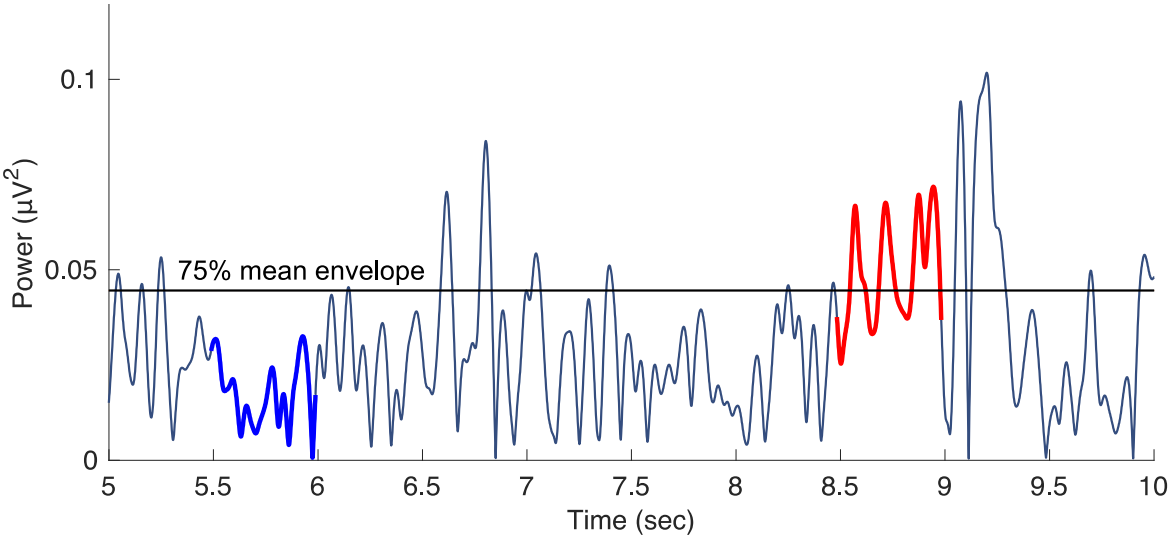


**Supplementary Figure S1 - Beta conditions and beta bursts. Example of beta bursts analysis in the low-power and high-power beta conditions.** In this example we can observe how LPβ (in blue) and HPβ (in red) have different levels of power and present different number of beta bursts. LPβ with no beta burst and HPβ with 3 beta bursts. Although we were unable to model beta bursts using CSD-DCM, we analysed the burst density in both low and high beta conditions a posteriori. Making use of the 75% percentile of the mean envelope as a threshold, the mean number of bursts in the LPβ condition (across trials and subjects) was 0.9 ± 0.3 and those bursts had the mean duration of 195 ± 106 msec. The mean number of bursts in the HPβ condition was 3.9 ± 0.7 and had the mean duration of 772 ± 188 msec. As expected, not only HPβ conditions show a higher density of beta bursts than LPβ conditions (approximately 4:1 in our data) but also its bursts show a longer duration. In both conditions, some trials showed incomplete bursts that were still included in the computation of average number of bursts and averaged duration of bursts per condition.

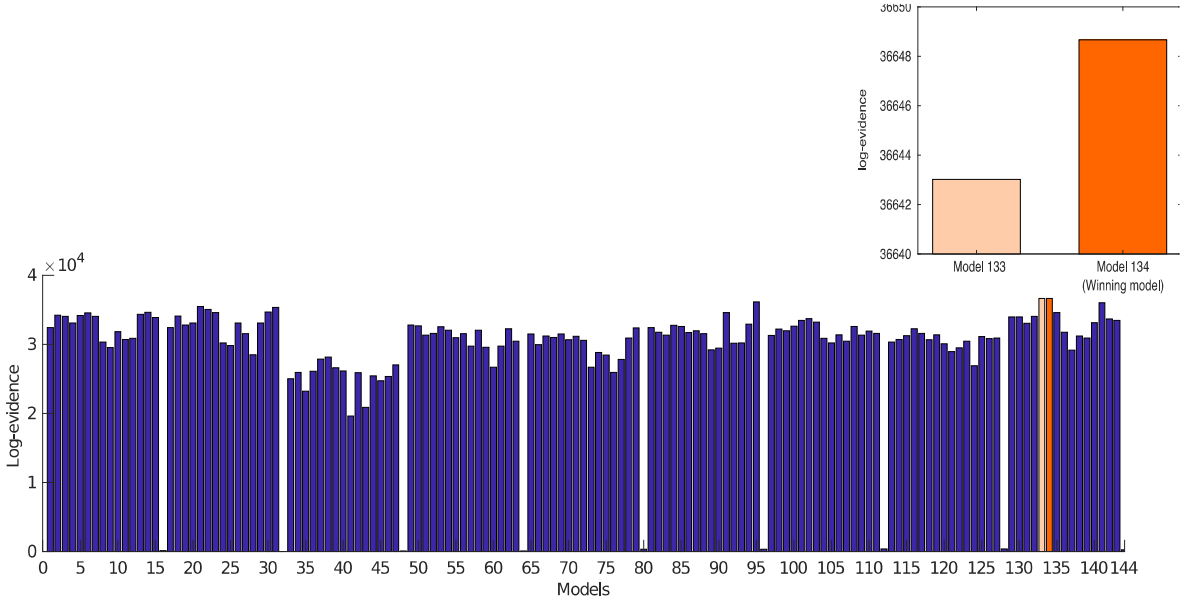


**Supplementary Figure S2 - FFX-BMC analysis of the 144 models. The bar chart shows normalised F values for each model.** From the 144 models (9 architectures x 16 modulatory configurations), model number 134 (orange) was the one with the higher log-evidence value ($3.6649x10^4$) showing a difference of approximately 6 from model 133 (beige) whose log-evidence was the second highest ($3.6643x10^4$). Second most plausible model being the model with changes in effective connectivity among the following subpopulations: superficial and deep pyramidal cells reciprocally, relay and reticular cells reciprocally, relay cells to deep pyramidal cells and inhibitory interneurons and deep (Illustrated in Figure **2.3** - Factor 1: Architecture, number 9; Factor 2: Modulatory configuration, number 5). Note that the above models are identical in their synaptic network except for the intracortical modulatory connections – while the winning model allows cortical modulatory dynamics between superficial and middle pyramidal populations, the alternative model shows intracortical connectivity changes between superficial and deep pyramidal cells. Nonetheless, both models highlight a change in glutamatergic inputs to the superficial pyramidal cells via intrinsic (and fast) interactions as a contributing factor for beta power enhancement.

$$\frac{di_{SP}}{dt} = \frac{\gamma_1 S(v_{MP}) + \gamma_{13} S(v_{DP}) - \gamma_5 S(v_{II}) - \gamma_3 S(v_{SP})}{\tau_{SP}} - \frac{2i_{SP}}{\tau_{SP}} - \frac{v_{SP}}{\tau_{SP}^2}$$

$$\frac{dv_{SP}}{dt} = i_{SP}$$

$$\frac{di_{MP}}{dt} = \frac{\gamma_2 S(v_{SP}) - \gamma_7 S(v_{II}) - \gamma_8 S(v_{MP})}{\tau_{MP}} - \frac{2i_{MP}}{\tau_{MP}} - \frac{v_{MP}}{\tau_{MP}^2}$$

$$\frac{dv_{MP}}{dt} = i_{MP}$$

$$\frac{di_{DP}}{dt} = \frac{\lambda_{REL-DP} S(v_{REL}) + \gamma_{14} S(v_{SP}) - \gamma_{10} S(v_{II}) - \gamma_{12} S(v_{DP})}{\tau_{DP}} - \frac{2i_{DP}}{\tau_{DP}} - \frac{v_{DP}}{\tau_{DP}^2}$$

$$\frac{dv_{DP}}{dt} = i_{DP}$$

$$\frac{di_{II}}{dt} = \frac{\lambda_{REL-II} S(v_{REL}) + \gamma_4 S(v_{SP}) + \gamma_9 S(v_{MP}) + \gamma_{11} S(v_{DP}) - \gamma_6 S(v_{II})}{\tau_{II}} - \frac{2i_{II}}{\tau_{II}} - \frac{v_{II}}{\tau_{II}^2}$$

$$\frac{dv_{II}}{dt} = i_{II}$$

$$\frac{di_{REL}}{dt} = \frac{\lambda_{DP-REL} S(v_{DP}) - \gamma_{16} S(v_{RET})}{\tau_{REL}} - \frac{2i_{REL}}{\tau_{REL}} - \frac{v_{REL}}{\tau_{REL}^2}$$

$$\frac{dv_{REL}}{dt} = i_{REL}$$

$$\frac{di_{RET}}{dt} = \frac{\lambda_{DP-REL} S(v_{DP}) + \gamma_{15} S(v_{REL}) - \gamma_{17} S(v_{RET})}{\tau_{RET}} - \frac{2i_{RET}}{\tau_{RET}} - \frac{v_{RET}}{\tau_{RET}^2}$$

$$\frac{dv_{RET}}{dt} = i_{RET}$$

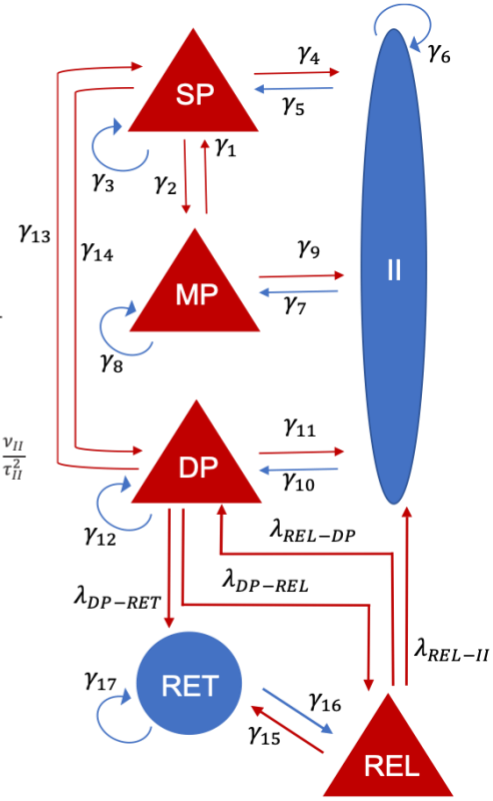


**Supplementary Figure S3- Differential equations of the winning model.** i -currents; v- voltages; SP/MP/DP- middle/superficial/deep pyramidal cells; II -inhibitory interneurons; REL – thalamic relay cells; RET – thalamic reticular cells; γ – synaptic coupling strength for intrinsic connections; $\boldsymbol{\lambda}$ - synaptic coupling strength for extrinsic connections; S– sigmoid function; τ – time constant. Blue coloured arrows denote GABAergic connections, while red arrows refer to Glutamatergic connections. Note that intralaminar coupling between pyramidal cells and local inhibitory interneurons (γ3, γ8, γ12) is parameterised with a single effective connectivity and should be contrasted with the interlaminar coupling with the common pool of inhibitory interneurons (γ5, γ7, γ10).

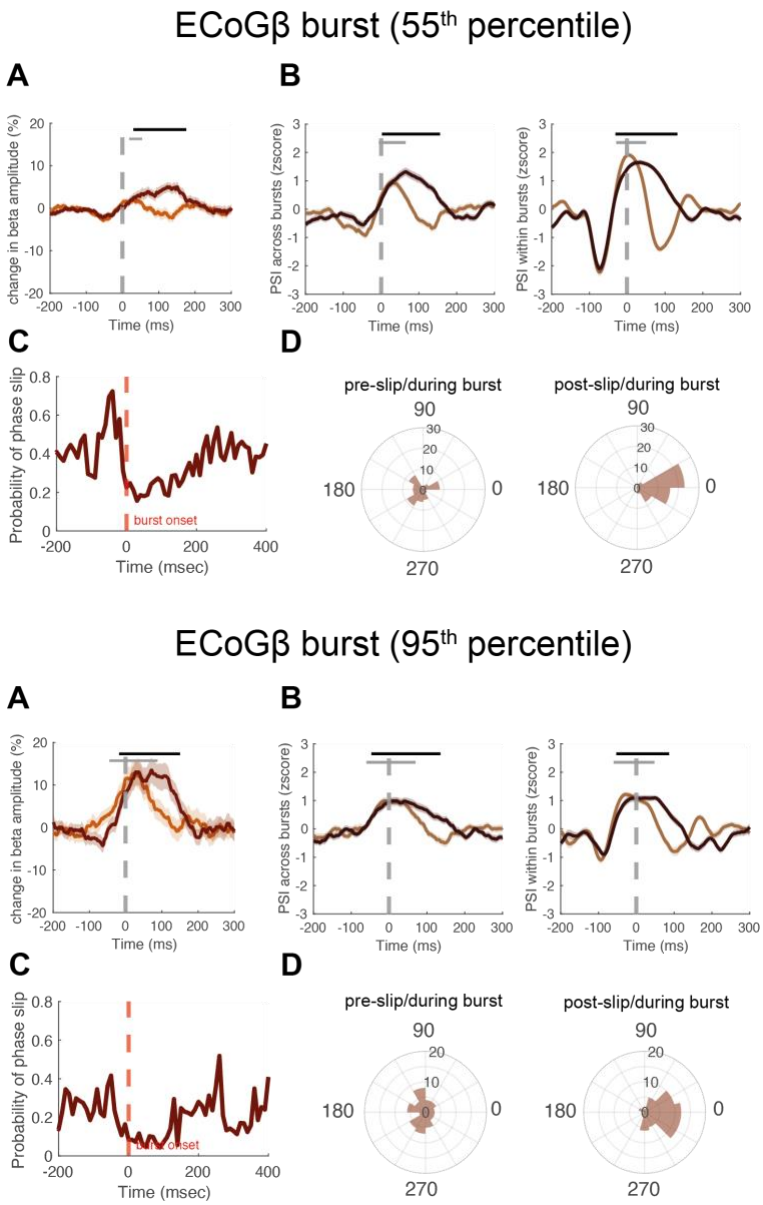


**Supplementary Figure S4 - Modulation of BZ BUAβ dynamics triggered by ECoG β-bursts derived from the 55th (top) and 95th (bottom) amplitude percentile threshold.** Panel A shows the change in subcortical BZ beta activity when data is aligned to the cortical burst onset. Panel B show changes in ECoGβ/BZ BUAβ phase coupling across (on the left-hand side) and within (on the right-hand side) cortical bursts. Shaded regions indicate mean±SEM. In panels A, and B two traces are shown per figure, one in a lighter and another in a darker tone to indicate whether data has been aligned to short (50ms<duration<median duration of all bursts) or long bursts (duration>median duration of all bursts), respectively. On those same figures significant periods of modulation were assessed via cluster-based non-parametric statistics ($p<0.025$). These are indicated by horizontal bars in a light or dark tone for short and long burst aligned data, respectively. Panel C shows the probability of phase slips across bursts. Using both amplitude percentile thresholds of 55$^{th}$ and 95$^{th}$ there is a higher probability of observing phase slips in the 200 ms prior to burst onset than in the 200 ms following burst onset ($p<0.0001$ for both thresholds). Dashed lines indicate the onset of ECoG β-bursts. Panel D shows that right after a phase slip (50 msec window), the established cortico-subcortical phase-alignment is

identical to that observed inside a burst ("post-slip/during burst", Rayleigh test p <0.0001). Conversely, the angular differences between the cortico-subcortical phase-alignment found right before a phase slip and inside a burst seems to diverge ("pre-slip/during burst", Rayleigh test, p>0.05 for the bursts defined according to the 95$^{th}$ envelope percentile threshold only).

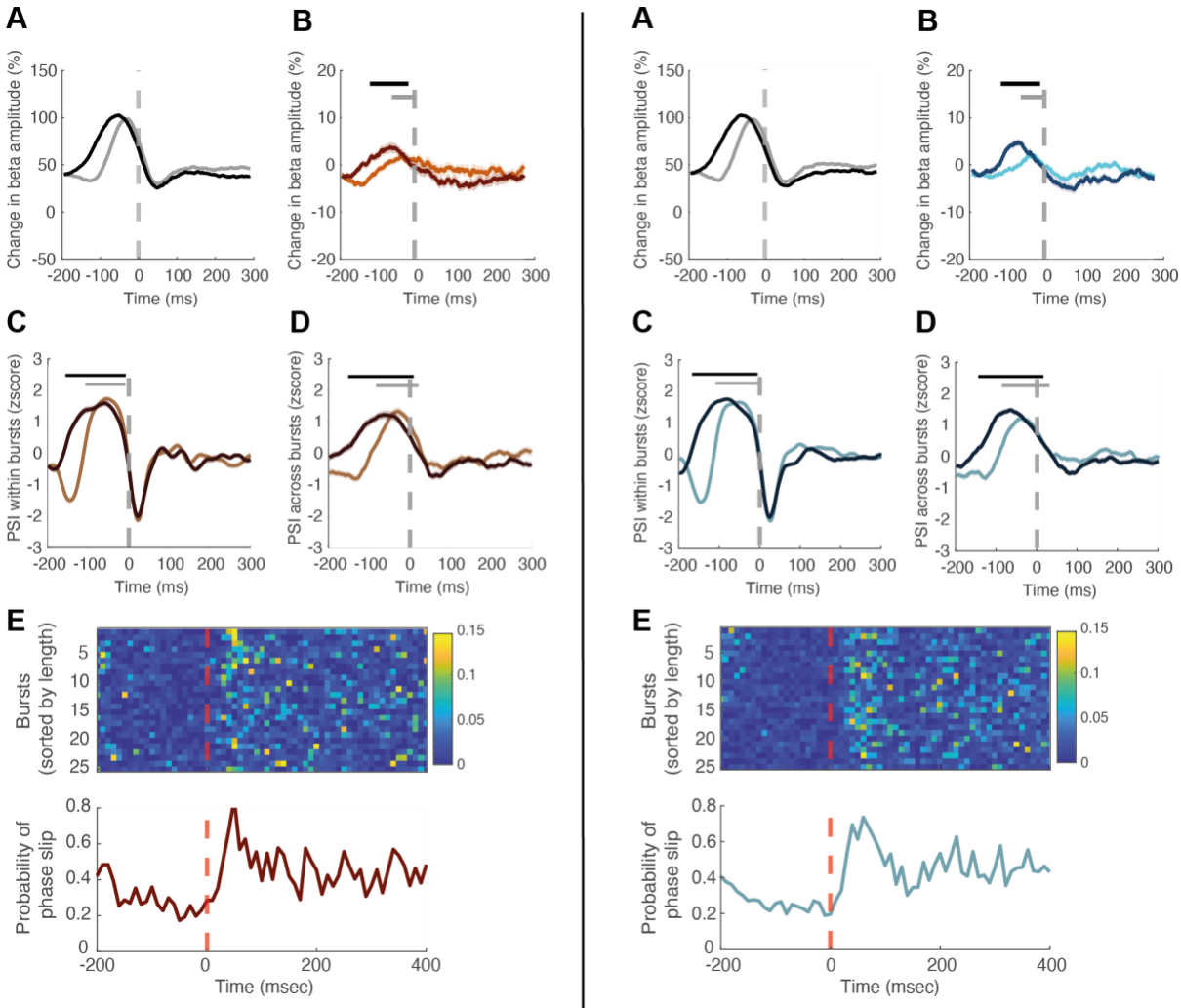


**Supplementary Figure S5 - Modulation of beta dynamics triggered by ECoG β-burst offset.** BZ results are shown on the left-hand side and results for SNr on the right-hand side. Grey, orange and blue lines denote the three different regions: cortex, BZ thalamus and SNr, respectively. Dashed lines represent the point of reference for data alignment, in this case the offset of ECoG β-bursts. Panel A shows the ECoGβ envelope during segments of data where it surpasses its 75$^{th}$ percentile. Panel B shows the change in subcortical beta activity when data is aligned to the cortical burst offset. Panel C and D show changes in cortico-subcortical phase coupling within and across cortical bursts, respectively. In panels B, C and D two traces are shown per figure, one in a lighter and another in a darker tone to indicate whether data has been aligned to short (50ms<duration<median duration of all bursts) or long bursts (duration>median duration of all bursts), respectively. On those same figures significant periods of modulation were assessed via cluster-based non-parametric statistics (p<0.025) and are indicated by horizontal bars in a light or dark tone for short and long burst aligned data, respectively. Shaded regions indicate mean±SEM. The heat maps on panel E shows the probability of

observing phase slips on the subcortico-cortical beta phase alignment during the 25 longest cortical beta bursts. Collapsing the probability of phase slips across bursts, the bottom panel shows how the probability of observing phase slips in the 200 ms prior to burst offset is inferior to that that in the 200 ms following burst offset ($p<0.0001$ for both BZβ/ECoGβ and SNrβ/ECoGβ phase-alignments).

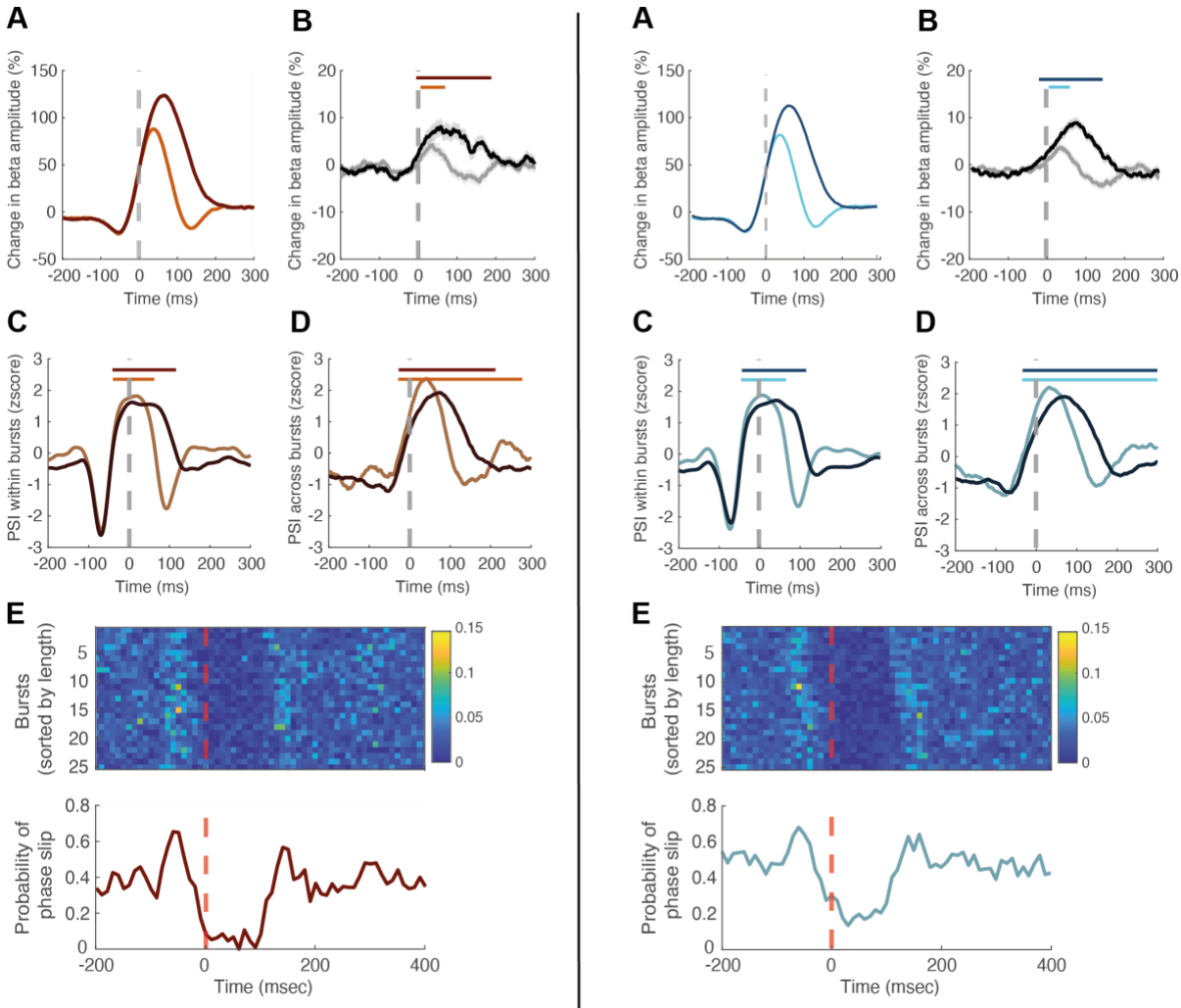


**Supplementary Figure S6 - Modulation of beta dynamics triggered by BUA β-burst onset.** BZ results are shown on the left-hand side and results for SNr on the right-hand side. Grey, orange and blue lines denote the three different regions: cortex, BZ thalamus and SNr, respectively. Dashed lines represent the point of reference for data alignment, in this case the onset of BUA β-bursts. Panel A shows the BUA β envelope during segments of data where it surpasses its 75$^{th}$ percentile. Panel B shows the change in cortical beta activity when data is aligned to the subcortical burst onset. Panel C and D show changes in cortico-subcortical phase coupling within and across subcortical bursts, respectively. In panels B, C and D two traces are shown per figure, one in a lighter and another in a darker tone to indicate whether data has been aligned to short (50ms<duration<median duration of all bursts) or long bursts (duration>median duration of all bursts), respectively. On those same figures significant periods of modulation were assessed via cluster-based non-parametric statistics ($p<0.025$) and are indicated by horizontal bars in a light or dark tone for short and long burst aligned data, respectively. Shaded regions indicate mean±SEM. The heat maps on panel E shows the probability of observing phase slips on the

subcortico-cortical beta phase alignment during the 25 longest BUA beta bursts. Collapsing the probability of phase slips across bursts, the bottom panel shows how the probability of observing phase slips in the 200 ms prior to burst offset is inferior to that that in the 200 ms following burst offset ($p<0.0001$ for both BZβ/ECoGβ and SNrβ/ECoGβ phase-alignments).

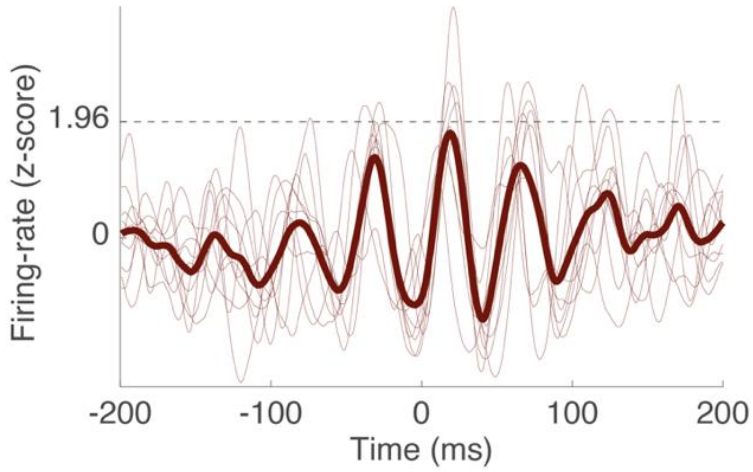


**Supplementary Figure S7 - Individual and group burst-triggered spiking activity of BZ neurons.** When inspecting the alignment of peaks and troughs across individual onset-triggered unit averages in a greater detail, a jitter of a few milliseconds can be visually observed. This suggests that within our pool neurons, the preferred ECoG β angle at which these neurons locked was not exactly the same.

## Cluster analysis

Peripheral manifestation of tremor is thought to reflect the neural dynamics of multiple central tremor oscillators (Pedrosa *et al.*, 2012). While for some patients, the weighted contribution of these oscillators is stable across tremor episodes affording a fixed peripheral tremor orientation (in the x, y and z coordinates), for others, such weighted contributions change spontaneously which peripherally is expressed as a change in the spatial manifestation of tremor. To ensure that measures of stimulation efficacy were not confounded by changes in tremor orientation and reflected the dominant tremor manifestation, we assessed how well contributions (i.e., coefficients) from different tremor axes to the first principal component could be segregated into two clusters at a given experimental task. To this end, coefficients of the first principal component were treated as a proxy for peripheral manifestation of tremor in three dimensions and cluster separation as an indication for two tremor orientations. Number of tremor orientations (i.e., clusters) was set to two, following a silhouette evaluation routine which evaluates the optimal number of clusters for a given data.

The PCA was performed on the tri-axial tremor data across merged NS and RSS conditions. Stimulated data consisted of *n* trials x 12 stimulated phases, while data from the non-stimulation condition consisted of 50,000 5- second segments randomly resampled from this condition (surrogate distribution described in section 0 and section and 5.2.5). Contributions from each axis to the first principal component were next allocated to one of the two clusters using the Ward's method, which performs cluster separation according to the Euclidean distance between objects. The average silhouette score was next separately calculated for the NS and RSS conditions. Silhouette scores range from -1 to 1 and represent points that are poorly and well matched to a cluster, respectively (Rousseeuw, 1987). A minimum average silhouette score of 0.75 for both NS and RSS conditions was set as a threshold to consider that there were two distinct tremor orientations.

This was the case for patient two (chapter 4) during both posture and spiral tasks. For this specific patient, the cluster with the most samples in from the RSS condition was selected, and RSS and NS data reduced to the data points found in that same cluster. Results from the cluster and PCA analyses of patient two are summarised in Supplementary Table S1.

| PATIENT 2 | Variance explained by first principal component: | Stimulation trials on cluster 2: | Averaged silhouette score: | Reduction of data point to: |
|---|---|---|---|---|
| Posture | 85% ± 12 SD | 82% | 0.95 NS<br>0.97 RSS | 48,929 NS<br>89 RSS |
| Spiral | 77% ± 10 SD | 73% | 0.92 NS<br>0.96 RSS | 48,929 NS<br>7 RSS |

**Supplementary Table S1– Summary of results from cluster and PCA on the data of patient 2.** STD = standard deviation; NS – No-Stimulation condition and RSS – Random-Search Stimulation condition.

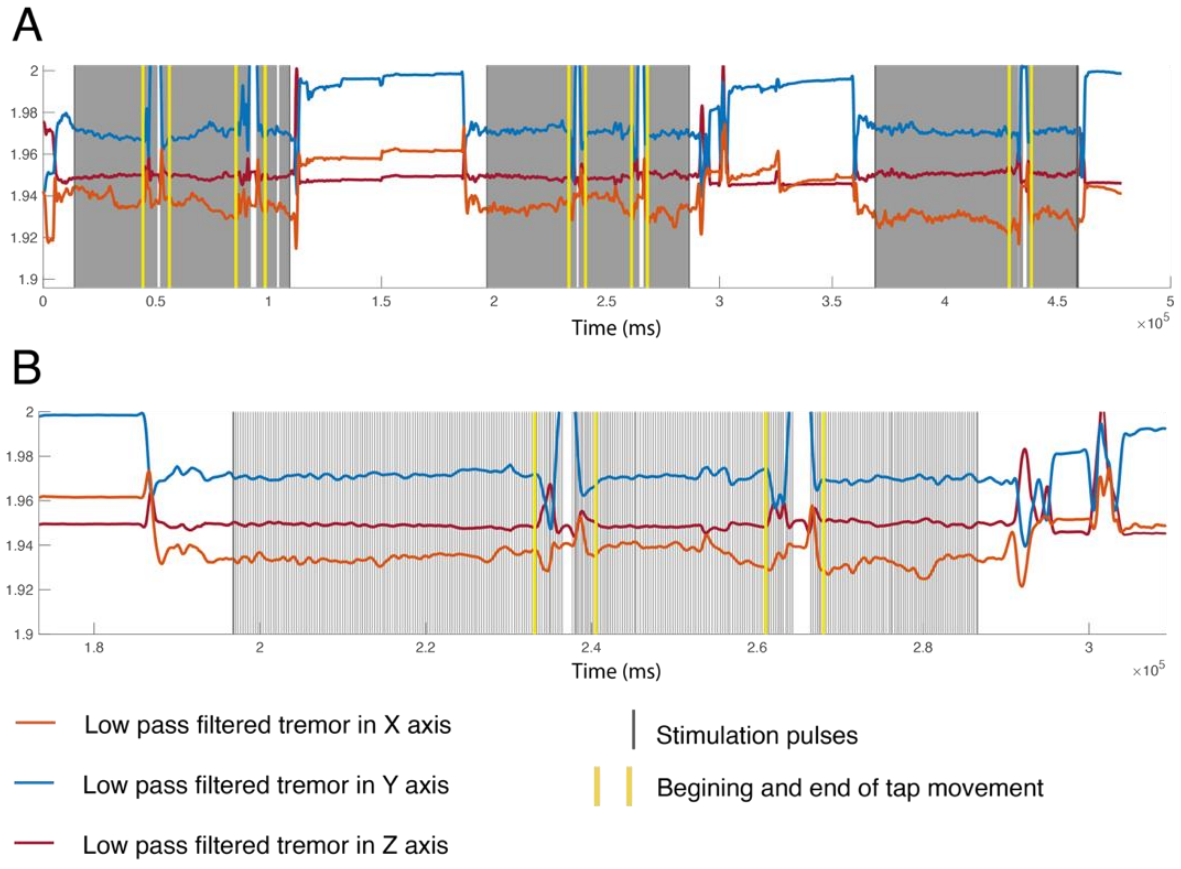


**Supplementary Figure S8 – Visual selection of tap segments in intermittent posture phase-specific stimulation (patient 4).** Beginning and end of tapping movements (vertical lines in yellow) were visually assessed by the DC offset present in the low pass filtered triaxial accelerometer signal (third order Butterworth filter cut-off frequency of 2Hz). Panel A shows the three phase-specific stimulation trials of patient 4 - the first one with two tapping movements and the last with a single one towards the end of the trial. Panel B zooms in the second trail for better visualisation of the DC offset.

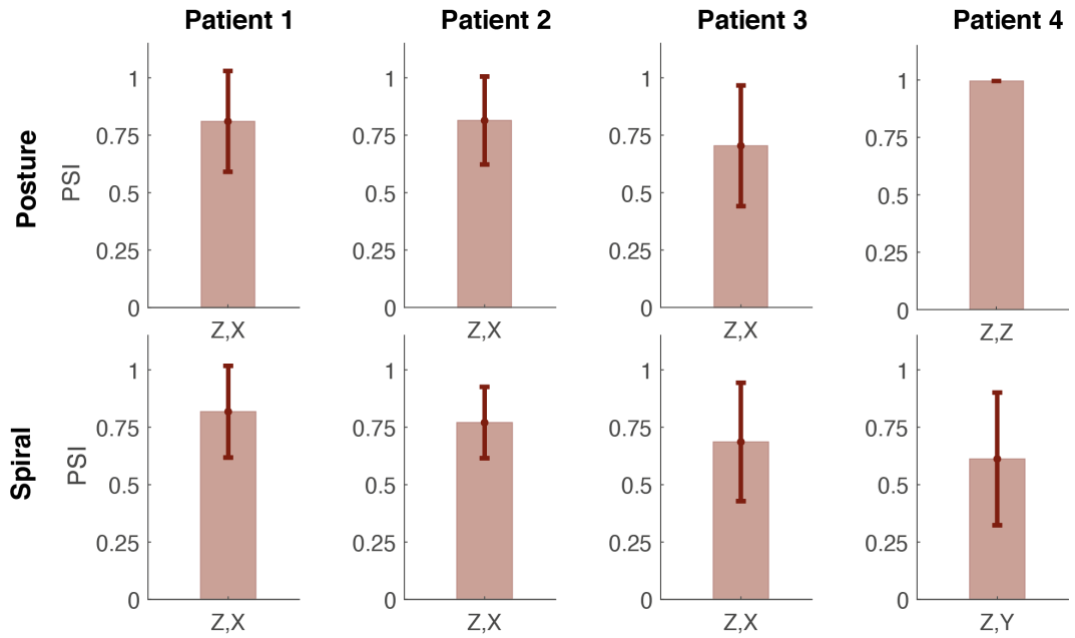


**Supplementary Figure S9 – Phase Synchrony Index between tracked and predominant tremor axes during Random-Search Stimulation posture holding and spiral drawing tasks.** To assess whether shifts of dominant tremor axes between NS and RSS conditions could have compromised the phase accuracy of stimulation effects, we have calculated the phase synchrony index (PSI) between phases differences of the tracked and predominant tremor axis for each patient during each task. For each individual patient, the tracked axis for posture and spiral RSS corresponded to that with the highest tremor peak while patients held a static posture during the NS condition. This was axis Z for all patients (shown in the X axis of each plot, first character). The dominant axis, now measured as the one with the highest envelope during the RSS condition was estimated separately for each task and is shown in the X axis, second character (cf. Figure **4.2**B and Figure **4.3**B). PSI of 1 indicates that phase difference between axes was always the same across the length of the recordings, while phase synchrony index of 0 indicates that phase difference between axes was randomly selected from a uniform distribution.

No-stimulation average tremor severity ($m/s^2$)

| Patients | Posture | Spiral |
|---|---|---|
| 1 | 1.42 ±1.38 SD | 1.62 ± 0.79 SD |
| 2 | 2.25± 0.94 SD | 1.88 ± 1.00 SD |
| 3 | 4.10 ± 2.69 SD | 5.25± 2.86 SD |
| 4 | 13.58 ± 2.67 SD | 1.77± 2.33 SD |

**Supplementary Table S2– Mean and standard deviation of tremor severity at the dominant tremor axis during the No-Stimulation condition.**

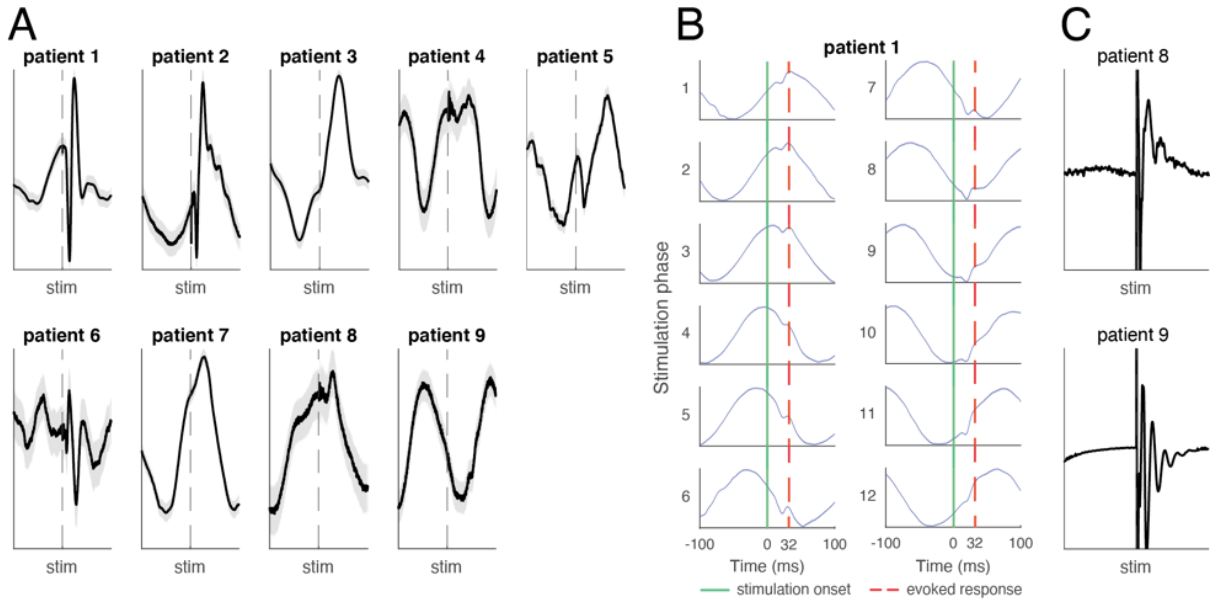


**Supplementary Figure S10– Peripheral confirmation of stimulation delivery at just above motor threshold.** Panel A shows the raw tremor signal in the Z coordinate centred at stimulation onset (with 250 msec each side), and averaged across all trials and stimulated phases, in a black line. Shaded grey areas show the SEM. Twitches can be seen locked to the stimulation onset (stim) in patients 1, 2, 4, 5, 6 and 8. Similarly, panel B shows for each stimulated phase, the raw tremor signal in the Z coordinate of patient 1 averaged across trials. The dashed red line depicts the visually identified evoked twitch (32msec). Panel C shows twitches in the EMG signal recorded from the thenar eminence averaged across all stimulation trials. Record centred at stimulation onset (with 250 msec each side).

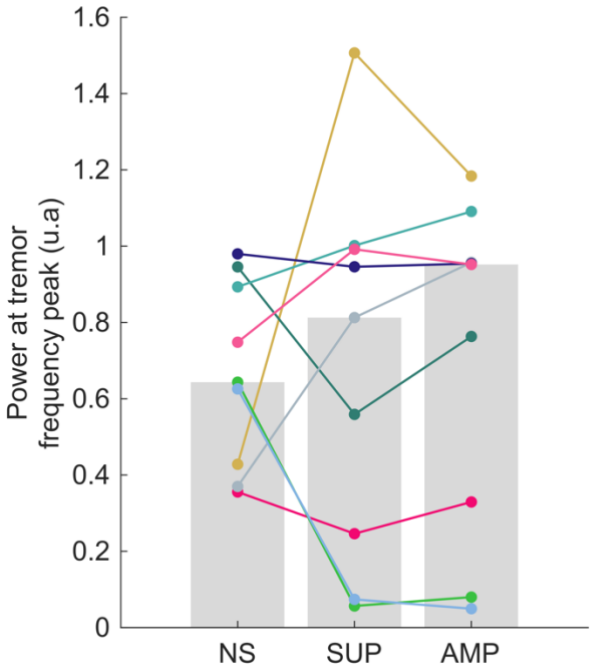


**Supplementary Figure S11- Power of tremor at peak frequency during stimulation versus no stimulation. The** light grey bar plots denote tremor median power at the tremor's peak frequency during instances where: 1) no stimulation was delivered (NS); 2) RSS was delivered and phase-dependent effects were suppressive (SUP) and 3) RSS was delivered and phase-dependent effects were amplifying (AMP). Individual average power at tremor's frequency peak under the above conditions is shown in different colours. Peripheral stimulation did not induce significant changes in tremor power. Specifically, while the power of tremor was not significantly different between suppressive and amplifying effects (p= 0.723), also none of the stimulation effects showed consistent differences in tremor power when compared to no stimulation (p= 0.901 suppression and p= 0.793 amplification).

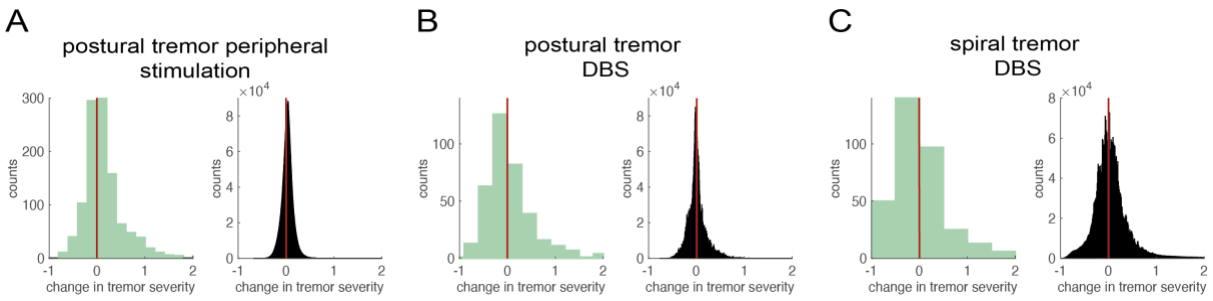


**Supplementary Figure S12– Amplifying versus suppressive effects during Random-Search Stimulation of chapter 4 and 5.** The figures above show the distribution of overall changes in tremor severity from cohorts of chapter 4 (panel A) and chapter 5 (panel B and C for postural and spiral task, respectively). In each panel the green histogram depicts the distribution of overall changes in tremor amplitude during the RSS condition. The black histogram combines the surrogate distributions of unstimulated data (sections 0 and 5.2.5) from all patients, which reflect spontaneous changes in tremor severity when no stimulation is being delivered. To test if there was a tendency towards amplification or suppression of tremor with stimulation versus no stimulation at each of the 3 contexts (RSS peripheral stimulation during postural tremor, RSS DBS during postural tremor and RSS DBS during spiral tremor) we have evaluated the symmetry of each patient's two distributions (stimulation and no-stimulation) and compared them at the group level with a t-test. We found that changes in postural tremor during RSS peripheral stimulation were significantly skewed towards amplification ($p=0.005$); changes in postural tremor during RSS DBS were significantly skewed towards a suppression ($p=0.011$), and changes in spiral tremor during RSS DBS did show a tendency towards suppression but this was not significantly different from the skewness of the surrogate distribution ($p=0.086$).